Synthesis of hydrophilic polymers with comb structure by free radical copolymerization for cementitious formulations

Iñaki Emaldi Galindo

Chemical Engineering Group
University of the Basque Country (UPV/EHU)
Donostia-San Sebastián
(2019)

POLYMAT

Ackowledgements

First of all, I would like to thank my supervisors Prof. Jose Ramon Leiza, Dr. Edurne Erkizia and Dr. Jorge Sanchez Dolado for giving the opportunity to develop this PhD and of course, for their tremendous help, guidance and patience during this PhD work, definitely this work could not be carried out without their help.

Secondly, I would like to thank EUSKAMPUS Foundation, Sustainable Construction Division from TECNALIA R&I, and the Polymerization Processes Group of POLYMAT Institute from UPV/EHU for funding and making possible to carry out the project.

I have only words of thanks for the professors that are part of the Polymerization Processes group; Prof. José M. Asua, Prof. Maria Paulis, Prof. Radmila Tomovska, Prof. Mariaje Barandiaran and Prof. José Carlos de la Cal. I have to say that I have learnt a lot from you and that it was my pleasure to be part of this extraordinary research group.

I cannot forget about all the people from Tecnalia that made me feel like home during my internships in Derio. Also, I would like to thank the scientist from SGIker (Servicios Generales de Investigación) from the UPV/EHU Dr. J.I. Miranda for his help with all the NMR experiments. I would like to acknowledge Prof. Agustin Etxeberria for the fruitful discussions with NMR analyses. Furthermore, I would like to especially acknowledge Dr. Shaghayegh Hamzehlou for

all her help during this PhD, definitely without your help it would not be possible to reach to this point.

Finally, I would like to all the PhDs and PostDocs that conform this wonderful group which is the Polymerization Processes group. I will not forget all the discussions, laughs and experiences that we have share during these four years. I wish the best for your future. Take care!

Para terminar, me gustaría agradecer a mi familia, especialmente a mis padres y a mi hermano Javier, todo el apoyo que me han dado durante estos años, solo puedo decir que sin ellos esto habría sido imposible. No me puedo olvidar tampoco de mi compañera de viajes que me ha aguantado todos estos años dándome todo su cariño, muchas gracias Maialen.

Table of Contents

Glossary

Cement Notation

Cement notation differs from conventional chemical notation, which is why the following notation for oxides was used:

Oxide	Cement Notation
CaO	C
SiO_2	S
Al_2O_3	A
H_2O	H
SO_3	$

The cement phases used in this work are defined in the following way:

Compound	Chemical Formula	Name
C_2S	$2CaO{\cdot}SiO_2$	Dicalcium Silicate (Belite)
C_3S	$3CaO{\cdot}SiO_2$	Tricalcium Silicate (Alite)
C_3A	$3CaO{\cdot}Al_2O_3$	Tricalcium Aluminate (Aluminate)
C_4AF	$4CaO{\cdot}Al_2O_3{\cdot}Fe_2O_3$	Ferrite

CSH	$CaO\text{-}SiO_2\text{-}H_2O$	Calcium Silicate Hydrate
CH	$Ca(OH)_2$	Calcium Hydroxide (Portlandite)
$C_6A\$_3H_{32}$	$3CaO\cdot Al_2O_3\cdot 3CaSO_4\cdot 32H_2O$	Ettringite (AFt)

Acronyms List

AA	Acrylic acid
AEA	Air-entraining admixture
AFt	Ettringite
AIBN	Azobisisobutyronitrile
AM	Acrylamide
bmom	by mol of monomer
bwom	by weight of monomer
BPO	Benzoyl peroxide
CEM	Cement
CFS	Cyclohexanone formaldehyde sulfide plasticizers
CH	Portlandite
^{13}C-NMR	Carbon Nuclear Magnetic Resonance
CO	Carbonyl
CTA	Chain Transfer Agent
C_3A	Aluminate
C_4AF	Ferrite

C_2S	Belite
C_3S	Alite
CSH	Calcium Silicate Hydrate
DP	Degree of Polymerization
Đ	Dispersity Index
EGu	Ethylene Glycol Units
FBS	Flexible Backbone Star
FBW	Flexible Backbone Worm
FDC	Flexible Decorated Chain
FMA	Furfuryl Methacrylate
f	Monomer fraction
F	Feeding rate
FRP	Free-radical polymerization
Ft	Feeding time
GHG	Greenhouse gases
GPC	Gel Permeation Chromatography
^{1}H-NMR	Proton Nuclear Magnetic Resonance
IBMA	Isobutyl Methacrylate
IC	Initial Charge
kp	Propagation rate coefficient
KPS	Potassium persulfate

LS	Lignosulfonates
MAA	Methacrylic Acid
MALS	Multi Angle Light Scatering
Mn	Number average molar mass
MMA	Methyl Methacrylate
MPEG	Methoxy Polyethylene Glycol
Mw	Weight average molar mass
MWD	Molar mass distribution
n-BMA	n Butyl Methacrylate
t-BMA	tert Butyl Methacrylate
η	Viscosity
NMR	Nuclear Magnetic Resonance
OMP	Organo-mineral phase
OPC	Ordinary Portland Cement
PCE	Polycarboxylic Ether
PEG	Polyethylene Glycol
PEGMA	Polyethylene Glycol Methacrylate
PMAA	Polymethacrylic acid
PLP	Pulsed laser polymerization
PMS	Sulfonated melamine formaldehyde condensates
PNS	Polynaphtalene sulfonates
RAFT	Reversible Addition Fragmentation chain Transfer
RG	Radius of gyration

RI	Refractive index
Rp	Polymerization Rate
RU	Repeating unit
r	Reactivity Ratio
SBS	Stretched Backbone Star
SBW	Stretched Backbone Worm
SC	Solids Content
SC_0	Initial Solids Content
SEM	Scanning Electron Microscopy
SP	Superplasticizer
SRA	Shrinkage Reducing Admixture
T	Temperature
TOC	Total Organic Carbon
W/C	Water to Cement Ratio
wt%	Total weight percent
X	Conversion
XRD	X-ray Diffraction
XRF	X-ray fluorescense
Y	Cumulative composition

Chapter 1. Introduction

1.1. Cementitious Materials

Concrete is a composite material composed by cement, water, sand and gravel and is the most widely used material worldwide also in construction. Another extensively used material in construction is mortar, which is composed by cement, water and sand. Cement is the binder of all these elements in both cases. It is produced by heating a mixture of raw materials such as limestone and clays, and it is composed by different phases that react in presence of water and harden with time. This characteristic feature is the key of its success in construction.

1.1.1. Historical Development

The first steps in construction came when buildings were constructed by placing heavy blocks of rock one on top of another, and they were firmly placed by friction forces. Development in construction brought the use of new materials called binders[1,2]. The first binders used were Nile slim and clays in the ancient Egypt and Sakkara. They were often used for decorative purpose, but also as mortar. The beginning of its application is not well establish but, it is known that it was already employed in the period 500-3400 B.C[2,3]. The use of lime as mortar was firstly applied by Greeks in Crete and later it was adopted by Romans. Those mortars were mixed very carefully and compacted, which ensured high densities and the preservation of buildings[1]. Both

Romans and Greeks knew the properties of some volcanic ashes that when mixed with lime and sand provided the mortars with increased properties of strength and durability. These mixtures were known as “pozzolans” because the firstly used ashes by Romans were from Puzzuoli, a village near Naples. However, Greeks used this combination of lime and volcanic ashes much before the finding of pozzolan[4].

A gradual decline in the quality of the mortar used in buildings set in after Roman times, and continued throughout the Middle Ages. Saxon and Norman buildings, for instance show evidence of badly mixed mortar, often prepared from imperfectly burnt lime. The conclusion appears certain, from the examination of French buildings, that in the period from 9th to 11th centuries the art of burning lime was almost completely lost. The quality of mortars started improving in the 12th century, but, it was not until the 15th century that they became outstanding[1,2].

The beginning of the history of modern cement can be established in 1754, when John Smeaton rediscovered the material in order to repair the lighthouse of Eddystone (England) in a durable manner. The next key event in the history of cement was the development of the patent of Portland cement in 1824 by Joseph Aspdin. Aspdin fixed the combination of limestone and clay and studied the manufacturing process[1,5]. However, the complexity of its production raised the price of the material and stopped its development, thus, it was not popularly used even though, it started to be fabricated in different places over Europe.

In 1885, Fedrerick Ransome patented the invention of the rotatory kiln, a rotatory oven that produced cement with more uniform properties. In this way, the heat necessary to cook the cement was reduced and it also provided time savings. This development allowed cement to

expand all over the world and to increase its production considerably. Nowadays, the production of cement is still carried out in a similar way to the early years of the 20th century.

1.1.2. Ordinary Portland Cement

Portland cement is the most common type of cement used around the world. It is a fine powder, composed mostly of clinker which is produced by heating limestone and clay minerals in a kiln. The clinker is composed of different phases which are called Alite, Belite, Aluminate and Ferrite. Alite phase is the main phase present in clinker. Then, the clinker is grinded and gypsum is added in dosages between 2-3% to obtain the cement powder.

Portland cement's (ordinary Portland cement - OPC) name is derived from its similarity to Portland stone, which was quarried on the Isle of Portland in Dorset, England.

The low cost and widespread availability of the limestone, clays, and other naturally-occurring materials used in the production of Portland cement make it one of the lowest-cost raw materials used over the last century. Concrete produced from Portland cement is one of the world's most versatile construction materials[6].

1.1.2.1. Cement Production

The location of cement works and production of cement is determined by the availability of raw materials within a reasonable distance between them[6]. Figure 1.1 shows an illustration of the cement production steps.

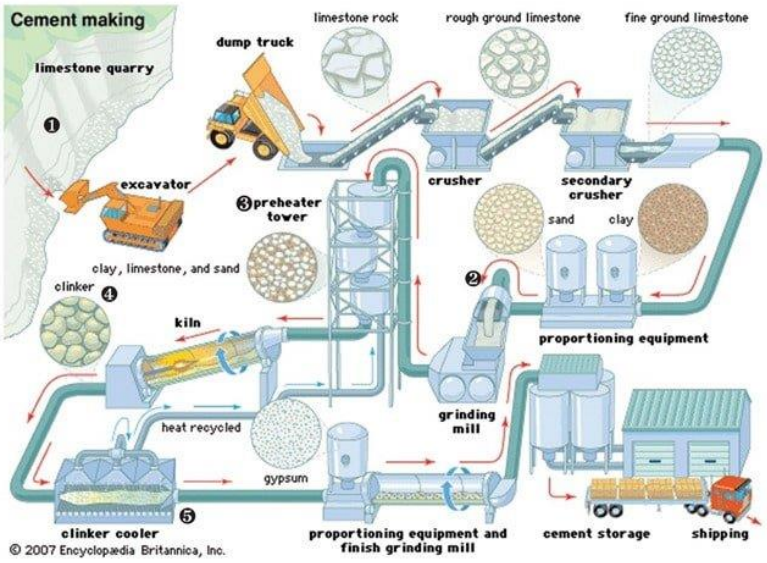

Figure 1.1: Illustration of the process of cement production obtained from www.theconstructor.org.

The raw materials are extracted from the quarry with explosives in the case of hard materials or with excavator in the case of soft materials. Once the materials are extracted and classified, they are crushed until the specified size is obtained, then, they are transported to the cement plant using a conveyor belt or trucks. The crushed material is kept in homogenous batches allowing a better dosage with less variability of the concentration of the materials. Before their use, these materials are milled in order to reduce their size and be able to cook more efficiently inside the oven. The milling process is generally carried out in vertical steamrollers and the materials are kept in a silo. Before inserting the materials in the oven, these are passed through a preheater in which the fumes from the oven go up through the chimney against the flow of the materials. Once the materials are in the oven the temperature rises up to 1500 ºC for

the complete clinkerization reaction to occur. According to Taylor[7], clinkerization reaction can be divided into three different stages according to the temperature:

1. Reactions taking place below 1300 ºC: Decomposition of calcite ($CaCO_3$), decomposition of clay minerals, reactions of calcite with products from the clay minerals to form belite, aluminate and ferrite. At the end of this stage the major phases present are belite, aluminate, lime and ferrite.
2. Reactions between 1300-1450 ºC: A melt is formed, mainly from aluminate and ferrite. Belite and lime react with the melt to give alite. The material nodulizes to form the clinker.
3. Reactions during the cooling stage: The melt crystallizes giving aluminate and ferrite. Polymorphic transitions of alite and belite occur.

Figure 1.2 shows a schematic diagram reported by Taylor[7] in which the clinkerization process is illustrated.

Once the clinker is obtained, it is mixed with gypsum and different mineral admixtures. The mixing is carried out in a grinder which consist of a rotatory tank with steel balls inside. These balls grind the clinker and homogenize it with the admixtures until a fine powder is obtained; this powder is called cement. The cement is then separated and stored for further packaging and transportation.

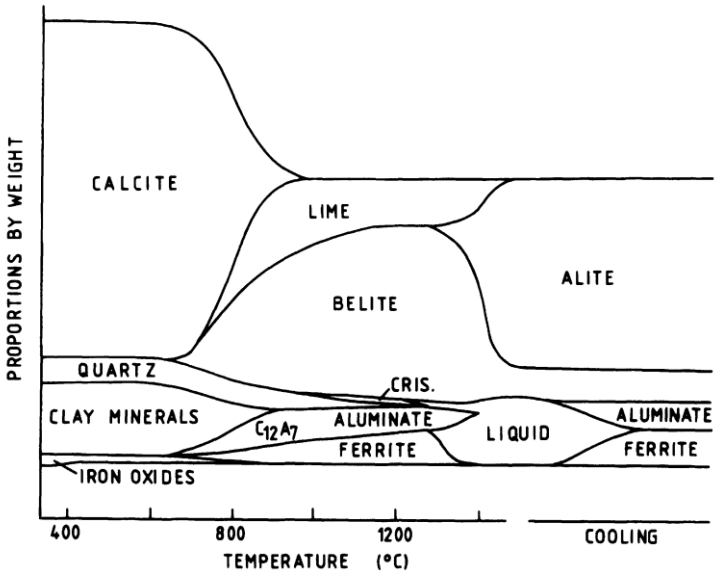

Figure 1.2: Temperature evolution of the clinkerization process[7].

1.1.2.2. Economic and Environmental Impact of Cement

Cement is still and will remain for a long time a key material to satisfy global housing and modern infrastructure needs. As a consequence, the cement industry worldwide is facing growing challenges in reducing the use of raw materials and energy resources, as well as reducing its CO_2 emissions. Today's annual global cement production has reached 2.8 billion tonnes, it is increasing about 2.5% per year and it is expected to increase up to some 4.4 billion tonnes by year 2050. Major growth is foreseen in countries such as China and India as well as in regions like the Middle East and Northern Africa[8].

Cement industry is an energy intensive industry, and it is one of the major contributors to greenhouse gases (GHG) emissions, specifically CO_2 emission. Emissions of CO_2 in cement industry mainly come directly from combustion of fossil fuels and from calcinations of the lime-stone into calcium oxide. An indirect amount of CO_2 comes from the consumption of electricity that is generated by burning fossil fuels[9]. The cement industry is responsible for nearly 6–8% of total carbon emission, and the cement subsector consumes approximately 12–15% of the total industrial energy, it thus becomes the second largest industry CO_2 contributor just after steel industry. However, transportation and electricity production are still larger CO_2 emmiter[9]. Nowadays, the cement is an important measure of the infrastructure degree of a society[8,10]. In the last 100 years, the world population has grown from 1.5 to 7 billion and nearly 3 billion people now live in or around cities[11], and the population and urbanization ratio keeps increasing in the developing countries. Consequently, the cement production increases bringing an increase in CO_2 emissions[12].

For the first time, the World Business Council for Sustainable Development and the Sustainable Cement Initiative, initiated the project “Getting Numbers Right” with the aim of developing a good database which includes global data of production, emission and energy consumption of cement industry[13].

Taking all these numbers into account it is expected that new research in methods of production, improvements or optimization of the energy consumption, the incorporation and development of new admixtures (organic and supplementary cementitious materials) in cement formulation, will be necessary in order to face the new challenges that cement industry has to tackle.

1.1.2.3. Composition of Ordinary Portland Cement

In the cement chemistry community, an abbreviated notation is used when writing the chemical compounds and crystalline phases that conform the cement and its hydration products. Table 1.1 shows the most widely used abbreviations in cement nomenclature[7].

Table 1.1: Abbreviation of oxides used in cement notation.

C = CaO	S = SiO_2	A = Al_2O_3	F = Fe_2O_3
M = MgO	K = K_2O	$\bar{S}$ = SO_3	N = Na_2O
T = TiO_2	P = P_2O_5	H = H_2O	$\bar{C}$ = CO_2

Generally, the main component of ordinary Portland cement is clinker, the product obtained after the clinkerization of the raw materials is composed of four main phases: C_3S – Alite, C_2S – Belite, C_3A – Aluminate and C_4AF – Ferrite. The four principal phases are normally present in the following proportions[14]:

- C_3S = 55 ± 5%
- C_2S = 25 ± 5%
- C_3A = 8 ± 2%
- C_4AF = 10 ± 2%

Alite is the main component of Portland cement. Its chemical formula is Ca_3SiO_5. In industrial clinkers alite phase can vary its composition by different ionic substitutions. Belite, which is dicalcium silicate (Ca_2SiO_4), also shows ionic substitutions and it generally presents β polymorph. Aluminate is tricalcium aluminate ($Ca_3Al_2O_6$) and it is substantially modified with ionic

substitutions, especially with K_2O. Finally, tretracalcium aluminoferrite (ferrite) ($2(Ca_2AlFeO_5)$) generally shows composition modification by the variation of the Al/Fe ratio and it also presents ionic substitutions[7,15].

1.1.2.4. Hydration of Ordinary Portland Cement

Understanding the reaction mechanisms of cement hydration is important from both academic and industrial points of view. The chemical and microstructural phenomena of cement hydration is quite complex due to its heterogeneity which makes it difficult to resolve individual mechanisms. Furthermore, the development of new type of cements, of lower environmental impact, such as cements with supplementary cementitious materials, calcium sulfoaluminate cements and the use of admixtures is introducing new challenges to the hydration mechanism analysis. This is why, several review works have been published which account the findings on the mechanisms that govern the hydration of cement[16,17]. However, there are still steps of the hydration mechanism that are not well understood. Furthermore, the interaction of the organic admixtures at the molecular level with each crystalline phase and the hydration compounds are not well characterized and studied either[18]. However, it is known that the reactivity of the individual clinker phases follows the following trend: $C_3A > C_3S > C_4AF > C_2S$[19]. In Table 1.2 the reactions of the main clinker phases with water are shown. As observed each clinker phase reacts in a different way with water (different amount of molecules of water) producing hydrated phases. Note, that in ordinary Portland cement gypsum is also added, and it modifies the reactions of C_3A and C_4AF. However, it is worth mentioning that the reaction presented in Table 1.2 are considered as tentative reactions because the exact stoichiometry of the calcium silicate

hydrate is still considered as unknown and in some cases more than one possible product could be formed.

Table 1.2: Hydration reactions of the main clinker phases[19].

Compound	Reaction	
C_3S	$2C_3S\ (Ca_3SiO_5) + 7H_2O \rightarrow 3CaO{\cdot}2SiO_2{\cdot}4H_2O\ (CSH) + 3Ca(OH)_2\ (CH)$	(eq: 1.1)
C_2S	$2C_2S\ (Ca_2SiO_4) + 5H_2O \rightarrow 3CaO{\cdot}2SiO_2{\cdot}4H_2O\ (CSH) + Ca(OH)_2\ (CH)$	(eq: 1.2)
C_3A	$2C_3A\ (Ca_3Al_2O_6) + 21H \rightarrow C_4AH_{13} + C_2AH_8$	(eq: 1.3)
Without Gypsum	$C_4AH_{13} + C_2AH_8 \rightarrow 2C_3AH_6 + 9H$	(eq: 1.4)
C_3A	$C_3A\ (Ca_3Al_2O_6) + 3C\bar{S}H_2 + 26H \rightarrow C_3A{\cdot}3C\bar{S}H_{32}$	(eq: 1.5)
With Gypsum	$C_3A{\cdot}3C\bar{S}H_2 + 2C_3A + 4H \rightarrow 3(C_3A{\cdot}C\bar{S}H_{12})$	(eq: 1.6)
C_4AF	$C_4AF\ (2(Ca_2AlFeO_5) + 16H \rightarrow 2C_2(AF)H_8$	(eq: 1.7)
Without Gypsum	$C_4AF\ (2(Ca_2AlFeO_5) + 16H \rightarrow C_4(AF)H_{13} + (AF)H_3$	(eq: 1.8)
C_4AF	$3C_4AF\ (2(Ca_2AlFeO_5) + 12C\bar{S}H_2 + 110H \rightarrow 4(C_6(AF)\bar{S}H_{32}) + 2(AF)H_3$	(eq: 1.9)
With Gypsum	$3C_4AF(2(Ca_2AlFeO_5) + 2(C_6(AF)\bar{S}H_32) \rightarrow 6(C_4(AF)\bar{S}H_{12}) + 2(AF)H_3$	(eq:1.10)

In order to gain mechanistic understanding at the molecular scale it is fundamental to analyze the individual kinetic steps of the hydration of Portland cement. These steps involved a collection of physico-chemical processes that fall into the following categories[20]:

- Dissolution / dissociation: Detachment of molecular units from the surface of a solid in contact with water.
- Diffusion: Transport of solution components through the pore volume of cement or along the surfaces of solids in the adsorption layer

- Growth: Surface attachment, incorporation of molecular units into the structure of crystalline or amorphous solids.
- Nucleation: Precipitation of solids heterogeneously on solid surfaces.
- Complexation: Reactions between simple ions to form ion complexes or adsorbed molecular complexes on solid surfaces.
- Adsorption: Accumulation of ions or other molecular units at an interface, such as the surface of a solid particle in a liquid.

However, these processes take place simultaneously in complex combinations, thus, it is very difficult to isolate the individual chemical processes for a detailed study. This task is already difficult for individual clinker phases so the difficulty increases exponentially if we are dealing with complex systems like Portland cement. Therefore, most experimental works have placed their attention on the evolution of heat flow of hydration with time.

We can have an idea of the rate at which the cement is hydrating by measuring the heat flow over time using calorimetry. In Figure 1.3 a typical heat flow curve of the hydration of cement is shown. The curve is divided into five different periods according to the rate of the heat evolved. Researchers have tried to explain the reaction mechanism of the hydration process based on these periods. Although, a general description of which reactions are occurring at each period has been established, there are periods that are not well understood yet[20].

When water is added to cement, a series of hydration reactions take place, leading to different hydration products. As can be seen in Figure 1.3 immediately after the water is added (Stage 1) a very exothermic reactions occurs, releasing a substantial amount of heat[16]. This stage is due to the dissolution of the different phases. Moreover, in this stage ettringite is formed

and precipitates. After the first peak there is a deceleration of the reaction which is followed by a period where there is almost no heat flow, called the induction period (Stage 2). Then the reaction goes into Stage 3 where the heat release rate increases fast again. This stage is called acceleration period and it is due to the formation and precipitation of the CSH, the main hydration product and portlandite (CH)[21]. After this stage, there is again a deceleration of the reaction where physical processes that induce particle arrangements are happening (Stage 4). This stage is called deceleration period and during this period two other small peaks occur. The first peak is due to the sulfate consumption point. This induces formation and precipitation of ettringite and dissolution of C_3A. The second peak is due to the reaction between ettringite and C_3A that produces aluminate ferrite monosulfate (AFm)[19]. In the last Stage the hydration reaction is happening very slowly and it may keep going for years.

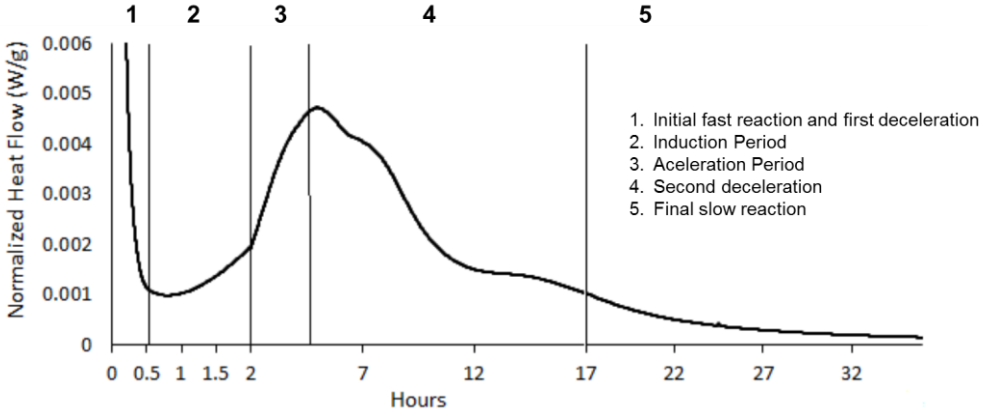

Figure 1.3: Hydration stages of the OPC employed in this work.

A schematic illustration of the development of the hydration process and the formation of CSH coating around the cement particles is shown in Figure 1.4, which was reproduced from Gatner et al.[16]. Mostly all cement particles are multi mineralic (more than one clinker phase is

present in each particle). As soon as the particles interact with water, early hydration reaction occurs, first two pictures which represent Stage 1 during the first minutes after water is added to cement. At this point mainly C_3A and C_3S react and an Aluminate rich coating form on the surface of the particles (initial formation of ettringite) and formation of the CSH gel can also be observed. The next pictures (3 and 4), represent the induction and acceleration periods (Stages 2 and 3) where the main hydration product CSH is formed. In picture 4, it can also be seen how the ettringite precipitates in needle like conformation that grows outward into the water filled space. Last pictures show the formation of monosulfate and the CSH product getting formed advancing inwards the cement particles which can correspong to the last stages of the hydration reaction of cement. As mentioned, these processes may take long periods of time.

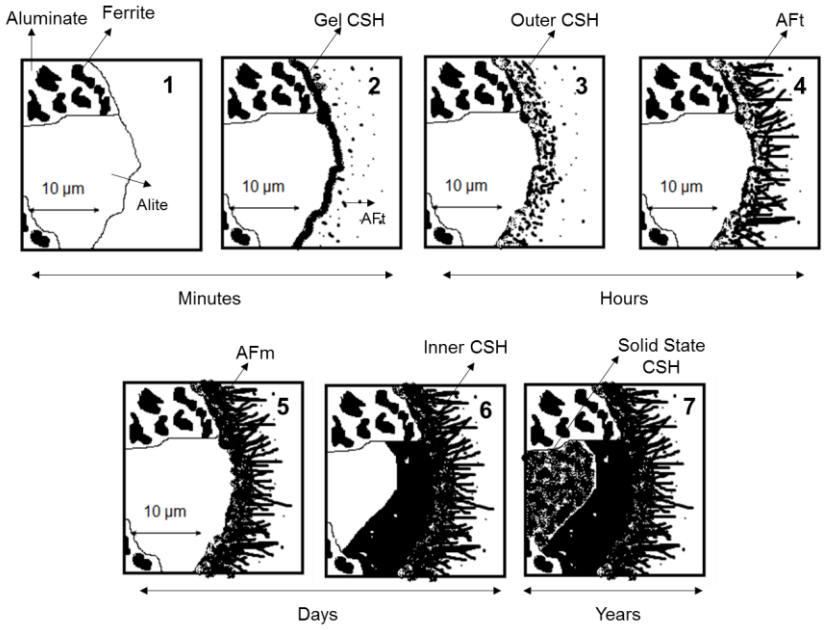

Figure 1.4: Illustration of the summary of the microstructural development of a cement particle hydration, reproduced from Gatner et al.[16].

1.1.2.5. Rheology of Cement Pastes

A feature of cementitious materials is that during the induction period the fresh cement can be molded and poured, thus mainly all rheological measurements of cement pastes are done during this time. Once the induction period is over a percolation threshold (particles flocculate and a long-range connectivity between particles forms) appears and the viscosity of the paste increases rapidly. The formation of this percolation threshold depends on many factors such as the type of cement or water to cement ratio among others.

The rheological behavior of cement-based materials can generally be explained by a Bingham model:

$$\tau = \tau_0 + \mu \cdot \dot{\gamma} \qquad \text{(eq: 1.11)}$$

Where τ is the shear stress, τ_0 the yield stress, μ the plastic viscosity and $\dot{\gamma}$ the shear rate[22]. Cement and concrete are considered complex and viscous fluids and it is difficult to characterize such a high viscosity material in the time available before setting. Accordingly, cement systems are yield stress fluids and the yield stress is a consequence of the interparticle forces.

Although the Bingham model is the most employed one there are also other models which take into account the yield stress of the material. In this work however, the Bingham model was used to describe the rheology of the pastes.

Depending on the application cement pastes, different rheological properties are sought, thus, the rheological behavior of cement pastes is a widely studied parameter and several

techniques are being used for its study. Feys et al.[23] listed the most common rheometers used by cement researchers. Concentric cylinders and parallel plates are referred as the most common ones despite their disadvantages at the time of defining the gaps for the measurements. However, a number of customize and different geometries are being promoted in order to overtake the drawbacks mentioned above.

Nevertheless, the necessity of measuring the rheology at the construction sites promoted the development of more simple ways of doing it. In this regard, the use of Abrams cone is widely spread and even researchers use it in their work. The cone is filled with the cement paste or concrete and is lifted afterwards on a table. A number bangs is given to the table spreading the cement pastes and afterwards the spread diameter of the slump is measured which gives an idea of the viscosity of the paste and by repeating the measurement over time the slump retention time is measured. The slump retention time is defined as the time that a cement pastes gives the maximum spread diameter. Due to its simplicity is a very easy to make measurement, which is why it has been widely implemented in laboratories as well as construction sites.

1.2. Polymeric Admixtures for Cementitious Materials

The development of the construction industry led to the employment of different admixtures that allowed the production of concrete of very specific properties. Chemical admixtures are generally organic molecules/macromolecules (some inorganic compounds are also used as admixtures) and they are nowadays very important as they can modify properties of fresh and hardened concrete, or in some cases both[24], so they are considered an important tool to develop tunable concretes. Furthermore, the addition of chemical admixtures allows the

production of higher amount of concrete with the same amount of binder (cement), in this way, they help to fulfill the sustainability requirements of the cement industry[25]. Besides the main effects produced by the admixtures, many have secondary effects, for example, most compounds used as water reducers can also produce retardation on the hydration of cement. In some cases, these effects can be beneficial but in others not.

Regarding the organic polymeric admixtures, several types can be found depending on their application. In some applications a combination of admixtures is also used.

Retarders: There is a large number of compounds that are used as retarders of the hydration. Many of them have water reducing capacity and sometimes they are also considered in water reducers category[26]. Carbohydrates are a common example of retarders, although inorganic salts can also be used but they are more expensive. If long retardation is sought phosphonates are utilized[27].

Viscosity Modifying Admixtures: This type of admixtures are employed to increase the stability and cohesion of concrete, underwater concrete and shotcrete (or sparayed concrete). Generally, they are hydrophilic organic polymers, although some inorganic compounds can also be used, such as nano-silica[28]. They are classified regarding their nature: Natural, semi-synthetic and synthetic polymers[29].

Air-entraining Admixtures (AEA): These molecules are surfactants, which are amphiphilic molecules that consist of a hydrophobic chain (generally long alkyl chains) and a hydrophilic head (ionic or polar groups). Air entraining admixtures (AEA) are employed to improve the properties of concrete at different environments. For example, they improve the durability of concrete under heat-freeze cycles as they create nano-pores which help to reduce

the cracking produced by the volume increase of water when it freezes. Furthermore, they are also used to decrease the viscosity of the cement suspension and increase the workability. Another application of these admixtures is the production of lightweight concrete.

Shrinkage Reducing Admixtures (SRA): These molecules are also surfactants but they differ from AEA in their mode of action. While adsorption of AEAs onto solids does in part support stabilization of air bubbles, SRA are efficient only by adsorbing at the liquid-vapour interface. Therefore, surfactants used as SRA are non-ionic so they do not strongly adsorb onto the charged surface of cement and its hydrates[29,30]. Shrinkage-reducing admixtures (SRAs) have become an interesting alternative to reduce cracks formed by autogenous shrinkage, especially when their use is combined with expansive agents[31].

Defoamers: Water reducers are invariably formulated with defoaming agents called defoamers. Especially PCEs present surfactancy due to the difference in polarity between polyethylene glycol side chains and the more hydrophobic polycarboxylate backbone. Therefore, defoamers are an essential component of PCE based admixtures. Defoamers or anti-foaming agents are chemical additives that hinder or reduce the formation of bubbles (foam) in various processes where air is mixed. Generally defoaming agents are highly hydrophobic and they have low solubility in aqueous chemical admixture products. Branched siloxanes, polyalkylene oxides or polyalkylene polyamines are some examples of the compounds used as defoamers[32].

Water reducers and superplasticizers: The use of this type of dispersants started in the 1930´s. These admixtures are used as dispersants to avoid particle segregation and to improve the flow characteristics (rheology) of suspensions in concrete applications. Their addition to concrete or mortar allows the reduction of the water to cement ratio without negatively

affecting the workability of the mixture, and enables the production of self-consolidating concrete and high performance concrete. They can be categorized into different groups: Natural polymers, synthetic linear polymers and superplasticizers (SPs) of new generation, namely polycarboxylic ethers (also known as comb-shaped copolymers)[29]. The latter ones are the main focus of this PhD thesis.

1.2.1. Superplasticizers

Among all type of admixtures employed in concrete and construction the superplasticizers are the ones that brought a significant development in the preparation of concretes with improved workability with the lowest water to cement ratios. They were already introduced in the market in the 1930's and since then different generations of products with improved properties have been produced. The last generation of superplasticizers, polycarboxylates, brought the most radical changes and they have provided substantial improvement and diversification of the sector[24]. For example, addition of polycarboxylates can reduce the water to cement ratio up to 0.20 (when usually in industry for high quality concrete no lower than 0.40 is used). This reduction in the use of water yielded concretes with very high mechanical properties (high performance concrete).

The first type of superplasticizers utilized was the lignosulfonates (LS), and they are used since the 1930´s. Their use have provided beneficial effect on the retarding of setting and water reduction as well as better workability of the concrete[24]. Despite their limited performance, since they cannot decrease the water to cement ratios as much as other superplasticizers, they are used in multiple applications due to their low price.

Lignosulfonates are highly branched macromolecules with molar masses between 10^3-10^6 g / mol and are formed from phenylpropane units connected in a non-regular manner by ether or C-C bonds. These macromolecules are obtained from by-products of the pulp industry. Figure 1.4. shows the chemical structure of a lignosulfonate. These admixtures adsorb on the surface of the particles of cement through their sulfonate groups and their deflocculating effect is due to electrostatic repulsion. Furthermore, their relatively big size creates a layer of adsorbate on the surface of cement preventing the cement particle to get close enough to stick[22]. Therefore, they reduce the viscosity of cement suspensions and the reduction can be correlated with the adsorbed amount[33]. Srinvasan et al.[34] proof the electrostatic repulsion effect of the LS by measuring the zeta potential evolution on OPC pastes reaching to potential minimums of -10 eV. Furthermore, Nathankuman et al.[35] besides electrostatic repulsion showed that non electrostatic interactions also contributed to the dispersion of the particles.

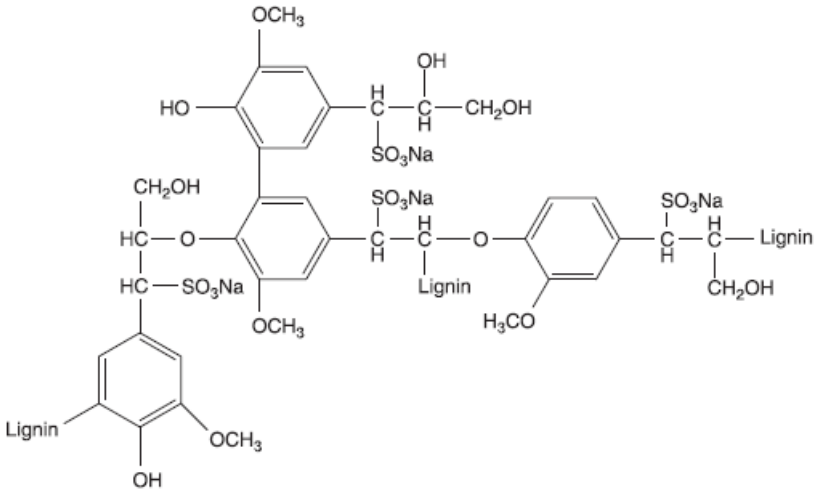

Figure 1.4: Chemical structure of main building block of a lignosulfonate molecule[24].

Polynaphtalene sulfonates (PNS) (see Figure 1.5A) were firstly introduced into the market in 1960´s and they are still widely used nowadays. They present higher dispersing ability than LS and therefore, higher water reduction is possible[24].

These polymers are synthesized in a two-step process: Firstly, the naphtalene is sulfonated with sulfuric acid, secondly, the condensation reaction is carried out in aqueous medium to form the linear anionic polymer[24]. Varying the reaction times, the molar masses of these polymers can be regulated. Generally, these polymers have average molar masses between $10^3 – 2 \cdot 10^3$ g /mol.

Sulfonated melamine formaldehyde condensates (PMS) (see Figure 1.5B) appeared later in the market in 1970's, and they are comparable to PNS dispersants. Similarly to PNS, these polymers are synthesized by condensation reaction and depending on the reaction conditions different linear polymers are obtained[24].

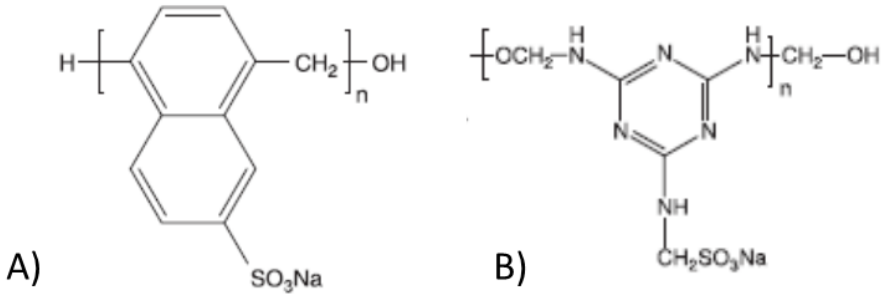

Figure 1.5: Chemical structure of polynaphtalane sulfonates A) and sulfonated melamine formaldehyde condensates B)[24].

Polynaphtalene sulfonates, PNS, and sulfonated melamine formaldehyde condensates, PMS, have been often compared. Plank and Hirsch[36] showed that both PNS and PMS disperse cement particles by electrostatic repulsion and that are adsorbed on higher amount than other type of superplasticizers, such as polycarboxylates. However between PNS and PMS the differences on adsorption amount were not high. Zhang and Kong[37] also demonstrated that PNS showed a typical mono-layer adsorption on much higher amount than the PCEs. On the other hand, Andersen and Roy[38] observed that commercial PMS showed slightly better dispersion than PNS.

After the discovery of the PNS and PMS, in the 1980´s Dr. T. Hirata[39] discovered what it is considered the greatest revolution on concrete admixtures, the polycarboxylate superplasticizers, also called PCEs or polycarboxylic ethers. Since their arrival to the market, their use grew rapidly and replaced the other type of superplasticizers like LS, PNS and PMS. While LS or PNS could reduce water in 20-30% the new PCEs achieved up to 40%. They can be used either to increase the strength of the concrete or to increase the workability[40]. These polymers, unlike LS or PNS, are not linear polymers with bulky groups. They consist of a polymer backbone with side chains distributed along the backbone. That is why they are also called comb-like copolymers. Figure 1.6 illustrates a typical comb-like copolymer.

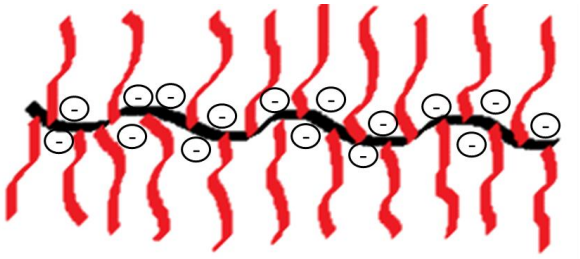

Figure 1.6: Illustration of a typical structure of PCE comb-like copolymer.

Generally, the backbone of these polymers is formed by anionic carboxylic groups and branches are composed by non-ionic polyethylene glycol (PEG) units. The negatively charged carboxylic groups adsorb on the surface of cement particles while the non-ionic side chains create steric repulsion[24]. Their success is mostly due to their great versatility to obtain different molecular structures and the possibility to tune their microstructure. However, understanding the structure-property relationship is still a great challenge in this field. There are several micrsotructural parameters that determine the performance of the PCEs[40]:

- Chemistry of the backbone[41,42]
- Length of the backbone[43]
- Amount of anionic groups[44]
- Number of side chains[45]
- Length of side chains[46,47]
- Linkage between side chain and the backbone[44]
- Overall charge density[48]

The versatility of the PCEs allow them to have a great impact on the market and this type of superplasticizers started to be used in Europe in 2005. After some years, in 2016, 80% of the European construction market uses this type of superplasticizers. Furthermore, the constant improvements in product performance, and the steady trend of lower cost made possible the PCEs to reach to such numbers. Actually, the global volume of PCE produced surpasses 4 million tons (dry polymer-based numbers) and to this it has to be added another 125000 tons of powder PCE production which are used for dry-mix mortar formulations. Still, in some regions of Central Asia and Africa do not use PCEs at all[49]. The market has grown especially in China,

where in 2004 PCEs were considered brand new, wheras in 2017 China was producing 2.25 million tons, which corresponds to more than the 50% of the global market.

1.2.1.1. Chemistry of Polycarboxylate PCE Superplasticizers

Several chemistries have been investigated and implemented in the field of PCEs, each of them with specific characteristics. In the following section a short description of the most employed monomers is briefly presented. The chemical structure of some of the PCEs used is shown in Figure 1.7.

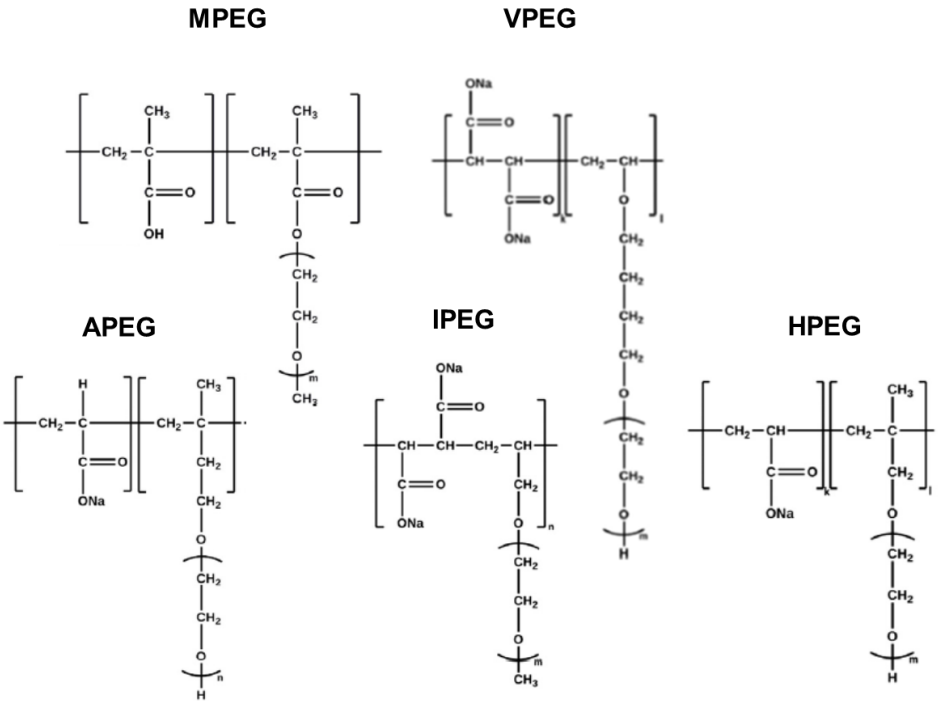

Figure 1.7: Chemical structure of the most common PCEs employed nowadays[41]

MPEG-type PCEs: The synthesis routes will be explained in more detail in the next section. These copolymers consist of a methacrylic acid backbone and methyl ether polyethylene glycol methacrylate as the monomer producing the side chain. This type of PCEs was the first type that was introduced into the Japanese market by Nippon Shokubai[39]. It can be synthesized by two different routes: Esterification of the side chain into the main backbone and (controlled) free radical copolymerization.

APEG-type PCEs: This type of PCEs is prepared from α-allyl-ω-methoxy or ω-hydroxy poly(ethylene glycol) ether and maleic anhydride or acrylic acid by free radical copolymerization in aqueous solution or in bulk[41,50]. This type of polymers possess ABAB monomer sequence due to the mesomeric stabilization, thus they are considered alternate copolymers. Generally, they are synthesized in bulk where viscous mixtures are obtained which are diluted to 60% solids content afterwards. They can be also synthesized in aqueous solution, but it requires longer reactions times. When the copolymer is synthesized in bulk, benzoyl peroxide (BPO) is used as initiator, the monomers are added previously into the reactor and the initiator is added continuously as powder[51]. On the other hand, if the synthesis is carried out in aqueous phase, star-like copolymers are obtained; namely, copolymers with very short backbone or degree of polymerization (DP). The APEG-type of PCEs produce better flowability in concrete than other types of PCEs. Plank et al.[51–54] also showed that the terminal group of the side chain can also produce different effects. If the terminal group is a hydroxyl group instead of a methoxy group the flow speed of the cement is enhanced as shown by Plank et al.[52].

VPEG-type PCEs: This type of PCEs is synthesized by free radical copolymerization at low temperatures (T < 30 ºC) with specific low temperature initiators and using maleic anhydride or acrylic acid and polyethylene glycol vinyl ethers. The advantage of the vinyl ether over the allyl

ether is that they possess much higher reactivity and therefore, it allows to polymerize them with a broader range of monomers and thus tailor the PCE backbones. Low temperatures are used to avoid monomer degradation[41,55].

HPEG-type PCEs: In this case, α-methallyl-ω-methoxy or ω-hydroxy poly(ethylene glycol) is used as macromonomer in the copolymerization with acrylic acid. These PCEs are synthesized by many companies in China and the copolymerization can be carried out at room temperature or at conventional free radical reaction temperatures depending on the initiator systems used.

This type of PCE stands above the other kinds due to their facile synthesis and stability, but especially due to their usual superior dispersion performance. Generally, HPEG type PCEs outperform other types of PCEs except IPEG type and their variability on different characteristics such as side chain length or molar mass made them to be number 1 type of PCE in Chinese market[49].

IPEG-type PCEs: This type of PCE (also known as TPEG-PCE) is synthesized from isoprenyl oxy poly(ethylene glycol) ethers and unsaturated carboxylic acids such as acrylic acid via free radical copolymerization. In recent years, this PCEs have become highly popular, especially in China, because of its excellent performance, which often exceeds that of MPEG and APEG, and its simple preparation utilizing free radical copolymerization. However, several disadvantages such as isoprenol availability and decomposition of the pure macromonomer limit their use worldwide[49].

The mentioned types of PCEs are the most commonly employed ones, although the industrial and academic research is still developing new products with more versatile properties.

Below some of recently developed PCE's are listed and Figure 1.8 shows their molecular structures.

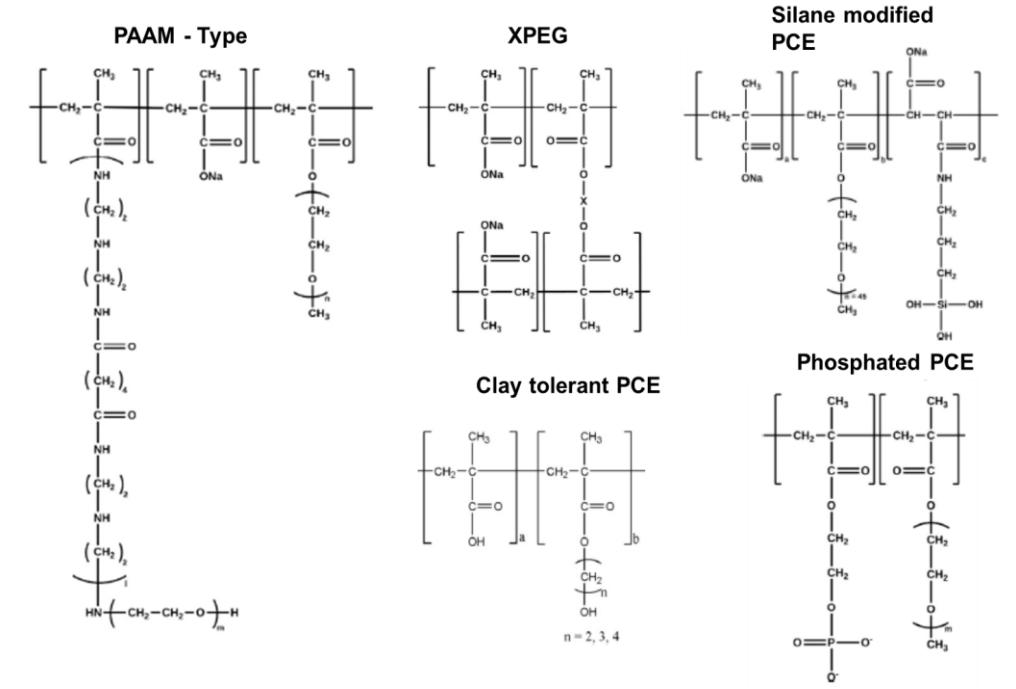

Figure 1.8: Chemical structure of novel PCEs and PCEs with especial characteristics[41].

- PAAM-type (polyamidoamine) PCEs[56]. They possess mixed side chains composed of polyamidoamine (PAAM) and polyethylene oxide (PEO) segments. This structural feature distinguishes them fundamentally from all other PCEs which exclusively contain polyethylene oxide / polypropylene oxide (PEO/PPO) side chains.
- Silane modified PCEs[57]: 3-trimethoxysilylpropyl methacrylate (MAPTMS) and N-maleic ɣ-amidopropyl triethoxy silane (MAPS) monomers were incorporated to the

conventional synthesis of MPEG type PCEs in order to provide them of silanol groups that are able to react with silicate groups present in cement particles.

- XPEG-type PCEs (Crosslinked PCEs)[58,59]: Slightly crosslinked PCEs formed by diesters from PEG or maleic anhydride were synthesized and shown to provide enhance dispersion in comparison to other PCEs.
- Phosphated PCEs[60–63]: By having stronger adsorbing groups (phosphates) than the conventional carboxylic acid, this PCEs are said to adsorb almost immediately onto cement particles and provide major advantages in specific applications.
- Clay tolerant PCEs[64–66]: The most commonly used side chain for PCEs is poly(ethylene glycol). However, PEG side chains intercalate easily between layers of clays diminishing the fluidizing effect of the PCE. The MAA-co-HEMA copolymers possess hydroxyl alkyl side chains which differ from PEG and result in clay tolerance.

1.2.1.2. Effect of PCE Microstructure on the Cement Paste Properties

MPEG-type PCEs are the focus of the study of this work. As previously mentioned they were discovered in the 1980´s, but how their molecular microstructure affects the interaction mechanism with cement particles is not well understood yet. Nevertheless, several studies have been performed to optimize their performance[18,67–69].

Charged backbones formed of methacrylic acid (MAA) are chosen to induce adsorption on cement particles via electrostatic interactions while the side chains composed of poly(ehtylene glycol) methacrylate (PEGMA) induce steric hindrance.

Although a great number of research studies exist on the effect of the PCEs, most of them did not investigate the effect of the chemical structure of the PCEs on the interaction with cement particles and were only focused on the optimization of the dosages. Winnefeld et al.[47], in an attempt of closing the gap between the molecular structure and its effect on the properties of cement paste, studied a series of MPEG-PCEs with systematic variations on the molecular structure. They found that when the quantity of PEG side chains is decreased workability increased and hydration was delayed, although the length of the side chains and the molar masses had minor effects.

Zingg et al.[70] showed that the presence of MPEG-PCEs leads to retarding effects on the start of the acceleration period on cement pastes. A higher charge density and dosage of PCE resulted in a stronger delay. They also found that the workability was influenced by the charge density of the PCE and the charge density was also the key factor that controlled the adsorption behavior in agreement with previous investigations. Furthermore, they suggested that steric stabilization was the mechanism governing the flow behavior of the cement pastes.

In another study, Ran et al.[71] found that the amount of PCE adsorbed was controlled by the COO^- content in the polymer backbone and by the length of the side chains as well as the copolymer conformation because the side chains are coiled rather than stretched[72]. The adsorption of the PCEs controlled the dispersion of the particles and the rheological behavior of the cement pastes. They also stated that although the dispersion effect increased as the adsorbed amount increased, the dispersion ability of the PCEs depended mostly on the side chain length, where the long side chains produced stronger dispersion than short side chains. Furthermore, the zeta potential was especially influenced by the length of the side chains, being the PCEs with short side chains the ones producing the largest potentials.

In an attempt to rationalize the structure-property relationship measured by several researches Flatt et al.[73] described the microstructure of comb-like PCE's by defining 3 parameters of the repeating units of these macromolecules as illustrated in Figure 1.9.

- n: Number of segments that represent the polymer backbone
- N: Number of monomers in each segment "n"
- P: Number of monomer units in the side chain

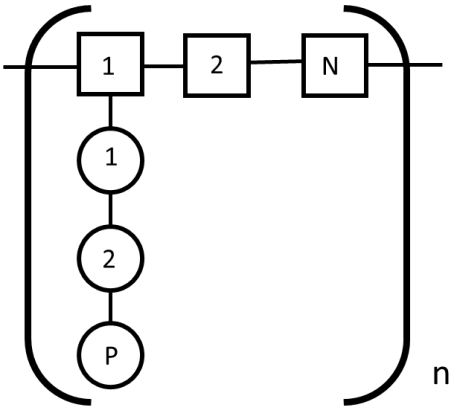

Figure 1.9: Schematic illustration of the comb copolymer considered by Flatt et al.[73] The comb copolymer contains n segments, each containing N backbone monomers and a side chain of P monomers.

Flatt et al.[73] adapted the model of Gay and Raphael[74] in order to define the conformation of PCEs in solution depending on their microstructural parameters, n, N and P. Five different conformations were defined: decorated chain (DC), flexible backbone worm (FBW), stretched backbone worm (SBW), stretched backbone star (SBS), and flexible backbone star (FBS). The five different conformations were assembled into the following phase diagram.

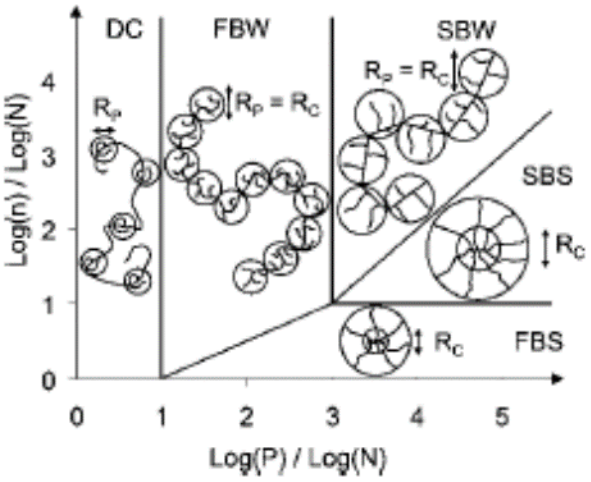

Figure 1.10: Phase diagram for comb copolymers adapted by Flatt et al.[73] based on the proposed scheme of Gay and Raphael[74]. DC: Decorated chain; FBW: Flexible backbone worm; SBW: Stretched backbone worm; SBS: Stretched backbone star; FBS: Flexible backbone star.

In that study, Flatt et al.[73] mentioned that FBW was the most common conformation for PCEs and it was defined as a chain of cores, each having a radius of gyration of (actually average end-to-end distance) R_C, and the overall polymer radius of gyration R_G that it shown in the following equation:

$$RG = \left(\left(\frac{a_N}{a_p}\right)^2 \frac{(1-2\chi)}{2}\right)^{1/5} a_P P^{2/5} N^{1/5} n^{3/5} \qquad \text{(eq: 1.12)}$$

where, a_N and a_P are the sizes of the monomers, χ is interaction parameter of PEO and P, N and n the microstructural parameters.

They assumed that when PCEs adsorb onto the surface of cement particles they can be treated similarly to the FBW in solution (they do not change their conformation), using a chain of hemispheres on a surface. The size and number of these hemispheres are derived in an analogous way to the size and number of cores in solution and they defined the radius of the hemispheres and the surface occupied by each molecule (S).

$$S_A = \frac{\pi}{\sqrt{2}} a_N a_P \left(2\sqrt{2}(1-2\chi)\frac{a_P}{a_N}\right)^{2/5} P^{9/10} N^{3/10} n \qquad \text{(eq: 1.13)}$$

The surface occupation of the PCEs on cement particles is an important aspect of the dispersive efficiency as it controls the adsorbed layer thickness together with the steric repulsion forces. Very importantly, for a sufficient surface coverage, the attractive van der Waals force is quickly overcome by steric repulsion[18]. The adsorption efficiency of PCEs depends on the polymer structure and its affinity for the surface as well as on the possible presence of competing species. Therefore, to be able to define PCEs adsorption ability in relation to their molecular structure, an adsorption equilibrium constant building upon the adsorption conformation relation given above was derived by Marchon et al.[18] by making several assumptions.

In a first step, they assumed that both adsorption and desorption rate constants depend on the polymer charge density per unit surface that they occupy. The adsorption and desorption rates are taken to be, respectively, proportional and inversely proportional to this charge density: $(n \cdot (N-1) \cdot z)/S_A$.

It is also assumed that the adsorption rate constant is inversely proportional to the number of repeat units n (or number of side chains) due to polymer rearrangement. Therefore, the adsorption equilibrium constant was defined with the following equation:

$$K_A^* \propto \frac{z^2(N-1)^2}{nP^{9/5}N^{3/5}} \cdot 10^5 \qquad \text{(eq: 1.14)}$$

where z is the number of charges carried by each monomer in the backbone. The higher the adsorption equilibrium constant of a PCE, the better its adsorption ability and the lower is its sensitivity to competitive adsorption.

Marchon et al.[69] also related the dispersion efficiency of the PCEs with their microstructural parameters. They reported that the dispersion efficiency increases with the thickness of the adsorbed layer, which depends mainly on the side chain length and scales up according to $P^{7/10}N^{-1/10}$ if full coverage of the PCE is produced. However, most practical situations involve incomplete surface coverage; in such cases, the surface fraction occupied can be assessed from the amount of PCE adsorbed per unit of area and scales up as follows: $P^{9/10}N^{3/10}n$. Furthermore, previously, they have did relate the structural parameters of PCEs with the retardation on the hydration of model cements[18]. The retardation can be expressed as follows[69]:

$$\Delta t \propto \frac{c_{PCE}}{M_{RU}}\left(\frac{N-1}{N}\right)^{3/2} \qquad \text{(eq: 1.15)}$$

where, Δt is the retardation of the maximum of the main hydration peak, c_{PCE} is the dosage in mass, and M_{RU} the molecular mass of the repeating unit.

$$M_{RU} = Mw_{m,BB} \cdot N + Mw_{m,SC} \cdot P \qquad \text{(eq: 1.16)}$$

where $Mw_{m,BB}$ and $Mw_{m,SC}$ are the molecular weight of one monomer in the backbone and side chain, respectively. This can be considered one of the first studies that combined the mastering of rheological properties of model cement pastes and hydration delay. Their work

presented a molecular structure optimization chart based on a set of empirical equations that accounted for the rheological impact in relation to the structure and dosage of the PCEs.

1.2.1.3. Synthesis Routes of MPEG type PCEs

MPEG-type PCEs can be synthesized following two different methods. The first method is the esterification of the PEG side chains on the polymer backbone.

Prior to the process of esterification it is necessary to synthesize the poly(methacrylic acid) (PMAA) backbone, which can be done using different polymerization methods. Polymethacrylic acid can be synthesized by free radical polymerization in aqueous phase employing batch or semibatch reactors[75]. This method will yield polymethacrylic acid homopolymers with generally broad molar mass distributions (MWD) (dispersity index higher than 2). In some academic works[68] PMAA with narrower MWDs have been synthesized by controlled free radical polymerization using RAFT agents (reagents for controlled free-radical polymerization). For that, tert-butyl methacrylate is polymerized in organic solvent and once the t-BMA polymer is obtained it is hydrolyzed with concentrated hydrochloric acid (HCl) under reflux. After evaporation of the solvent and dissolution in water, PMAA is freeze dried for one day.

For the esterification of the PMAA, methoxy poly (ethylene glycol) is used with an acid catalyst (p-toluene sulfonic acid) while using vacuum to remove the water formed from the process. This esterification reaction is conducted at high temperatures (175 ºC) and the reaction lasts for 5 hours according to Guicquero et al.[76]. It is claimed by Flatt et al.[24,29] that this method leads to uniformly distributed side chains along the backbone.

The second method to synthesize MPEG-type PCEs is by aqueous phase free radical copolymerization of methacrylic acid (MAA) and methyl ether poly(ethylene glycol) methacrylate (PEGMA) comonomers. This approach is the most common method as it is considered a simple experimental process and is cost-effective[41]. The molar masses of these PCEs can be controlled during the synthesis by adjusting initiator concentration, solids content, chain transfer agent concentration or monomer flow rates. On the other hand, the monomer sequence distribution depends on the reactivity ratios of the comonomers and general polymer chemistr[77,78]. This is the method used in this work and in the following section the most important aspects of the aqueous free radical copolymerization will be briefly described.

1.2.1.4. Free Radical Copolymerization in Aqueous Phase

Free radical polymerization (FRP) is a chain-growth polymerization method. In FRP, polymer chains are produced by addition of monomer units to an active center which is a free-radical. Free radical copolymerization is attractive because of the huge number of monomers that can be polymerized and different media that can be used (organic, aqueous or dispersed media)[77].

Many products for our everyday life are synthesized by free-radical polymerization and an important set of materials are produced in aqueous solution, where both the monomers and the polymers are soluble in water[79]. This is also the case of MPEG-type PCEs.

Despite the fact that free radical copolymerization has been used in several works for the production of MPEG-type PCEs[42,43,48,51,73–78], very few works have discussed the kinetics of the

reaction or the effect of process variables on the molar mass distribution of the copolymers produced. Also, few works discuss the especial characteristics of aqueous phase free-radical polymerization[45,87]. In this section the most important aspects will be summarized.

The kinetics of aqueous phase free-radical polymerization presents unusual (as compared to the behavior on organic solvents) dependence with the reaction medium such as, pH, monomer weight fraction and electrolyte concentration to mention a few. Several works have addressed the specific features of the aqueous FRP of MAA and PEGMA monomers. Beuermann et al.[88] determined by pulsed-laser-polymerization couple with SEC measurements (PLP/ SEC) the propagation rate coefficient of non-ionized MAA in aqueous solution. They found that the kp (propagation rate coefficient) of MAA decreased when increasing the solids content (concentration of MAA). Later, Lacík et al.[89] found that the ionization degree also has substantial effect on the kp of MAA, thus, pH of the medium is crucial. These authors provided a semi-empirical equation to determine the propagation rate coefficient of MAA in aqueous phase as a function of temperature, MAA concentration and ionization degree. More recently, Cuccatto et al.[90] have found that electrolyte concentration has a strong effect on the propagation rate coefficient and extended the equation to account for this effect and MAA concentrations below 5 wt% of MAA.

On the other hand, Smolne et al.[91] found that PEGylated monomers behave similarly to water soluble monomers. Especially the kp of these monomers varies largely with monomer concentration, in particular it decreases by a factor of seven between highly diluted solution to bulk conditions.

1.3. Motivation and Main Objectives

Superplasticizers are nowadays one of the most important constituents of modern concrete. They have generally been used to decrease the viscosity of the cement suspension or/and to reduce the amount of mixing water necessary, achieving concretes with high mechanical properties. Due to the high amount of concrete used in construction, superplasticizers have become one of the most important polymeric admixtures for the cement industry. However, the knowledge of the interaction between these materials and cementitious materials is still not fully understood and most of the optimization of product and dosages is performed based on trial and error. Furthermore, in several works the microstructure of the PCEs is unknown or only partially known, which makes very difficult to obtain relevant conclusions on how the PCEs work. Nevertheless, in the last decade Flatt et al.[18,67–69,73] have devoted a great deal of research on the field of MPEG-type PCE microstructure and OPC fresh and hardened properties with the aim of optimizing the microstructure and mastering the fluidity and retardation of the hydration. Despite the extensive work developed by Flatt et al. the interaction of the PCEs with different clinker phases and the effect on their hydration retardation is still unknown.

The main objective of this thesis is to study the fundamental effects of the interaction of the model MPEG-PCE macromolecules and the cement particles. Therefore, the project will consist mainly of two different parts. The first part (chapters 2 and 3), will be devoted to the controlled synthesis by free radical copolymerization of MAA and PEGMA macromonomers and characterization of their microstructure. Microstructure of the PCE's macromolecules will be defined by the backbone length, the side chain length or the amount of side chain or anionic carboxylic groups in the backbone.

The second task of the thesis (chapter 4, and 5) will be devoted to analyzing the interaction of the model macromolecules synthesized in the first part with the aim of establishing fundamental knowledge on the structure-property relationship. For this purpose ordinary Portland cements and different clinker phases present in OPC will be used.

1.4. Outline of the Thesis

In Chapter 2, the synthesis of MAA-co-PEGMA5 copolymers in aqueous phase is presented. The main objective in this chapter is to obtain MAA/PEGMA5 copolymers of homogeneous composition with controlled molar masses and comonomer ratios. Due to the fact that MAA-co-PEGMA5 copolymers are not hydrophilic enough as to be soluble in water at acidic pH, polymerizations are carried out at basic pH. Under this condition the reactivity of PEGMA is much greater than that of MAA and hence starved monomer addition strategies are not sufficient to produce copolymers with homogeneous copolymer composition. In order to produce homogeneous copolymers advanced monomer addition policies are implemented. For this purpose a mathematical model of the copolymerization of the MAA and PEGMA5 in alkali aqueous media was developed.

In Chapter 3, homogeneous copolymers with longer side chains were synthesized (PEGMA20, PEGMA45, PEGMA113 were used) with the same composition (MAA/PEGMA = 3/1) and different molar masses. Longer PEGMA macromonomers are more hydrophilic and hence acidic conditions can be used in the polymerization, where the reactivity ratios of the comonomers are very close and hence starved semibatch strategies are sufficient to produce homogenenous copolymers. Furthermore, in this chapter all the MPEG-type PCEs were

determined and the study of the architecture and conformation of the copolymers in aqueous solution was also analyzed, and the MPEG-type PCEs were classified according to the three microstructural parameters proposed by Flatt et al.[73] and this information was used in chapter 4 and 5.

In Chapter 4, the interactions of the synthesized copolymers with different structural parameters (n, N and P) with ordinary Portland cements were investigated in depth by the conventional cement analysis techniques. Furthermore, the effect on the hydration and rheology of the cement was also studied as well as the effect of the microstructural parameters (n, P, N) on adsorption, dispersion viscosity and retardation assessed and compared with the theoretical predictions proposed by Flatt et al.[69]

Chapter 5 studied the effect of the copolymers on the individual clinker phases. Three of the main phases were used for the study, C_2S, C_3S and C_3A. As in chapter 4 the effect of microstructural parameters (n, P, N) on the adsorption, zeta potential and hydration retardation was analyzed.

In Chapter 6, the most relevant conclusions of this thesis are summarized and based on the conclusions and the results obtained through this thesis, future work and perspectives in the field of the interactions of polymeric macromolecules with cementitious materials are also presented.

With the aim of avoiding the repetition of the experimental procedures and technical information of the techniques employed, a detailed description of them is given in Appendix I (Polymeric material, processes and characterization methods) and in Appendix IV (Cementitious materials and characterization methods). Appendix II and III show relevant information regarding

the measurement of the reactivity ratios of the different monomers and the development of the mathematical model for the design of the optimal addition strategies.

1.5. References

(1) Lea, F. M. *The Chemistry of Cement and Concrete*, 3rd Editio.; Chemical Publishing Company: New York, USA, 1971.

(2) Kurdowski, W. *Cement and Concrete Chemistry*; Springer: Krakow, Poland, 2014.

(3) Jaworski, Z. *The History of Binder Materials*; Akademii Nauk SSSR: Moskow, Russia, 1963.

(4) Malhorta, V. M.; Mehta, P. K. *Pozzolanic and Cementitious Materials*; CRC Press: Boca Raton, US, 1996.

(5) Manzano, H. *Atomistic Simulation Studies of the Cement Paste Components PhD Thesis by Hegoi Manzano*; 2009.

(6) Bye, G. C. *Portland Cement: Composition, Production and Properties*, Second Edi.; Thomas Telford Publishing LTD: London UK, 1999.

(7) Taylor, H. F. W. The Chemistry of Portland Cement Manufacture. In *Cement Chemistry*; Thomas Telford Publishing LTD: London UK, 1997; pp 55–87.

(8) Schneider, M.; Romer, M.; Tschudin, M.; Bolio, H. Cement and Concrete Research Sustainable Cement Production — Present and Future. *Cem. Concr. Res.* **2011**, *41* (7), 642–650.

(9) Ali, M. B.; Saidur, R.; Hossain, M. S. A Review on Emission Analysis in Cement Industries. *Renew. Sustain. Energy Rev.* **2011**, *15* (5), 2252–2261.

(10) Aïtcin, P. Cements of Yesterday and Today Concrete of Tomorrow. *Cem. Concr. Res.* **2000**, *30*, 1349–1359.

(11) Cleland, J. World Population Growth ; Past , Present and Future. **2013**, No. May, 543–554.

(12) Shen, W.; Liu, Y.; Yan, B.; Wang, J.; He, P.; Zhou, C.; Huo, X. Cement Industry of China : Driving Force , Environment Impact and Sustainable Development. *Renew. Sustain. Energy Rev.* **2017**, *75* (July 2016), 618–628.

(13) Sustainable Cement Initiative. *Getting Numbers Right*; 2016.

(14) Chatterjee, A. K. *Cement Production Technology: Principles and Practice*; CRC Press:

Boca Raton, US, 2018.

(15) Lei, L. A Comprehensive Study of Interactions Occurring Between Superplasticizers and Clays, and Superplasticizers and Cement, TUM Technischen Universität München, 2016.

(16) Gartner, E. M.; Young, J. F.; Damidot, D. A.; Jawed, I. Hydration of Portland Cement. In *Structure and Performace of Cements*; CRC Press: London UK, 2001.

(17) Taylor, H. S. W.; Barret, P.; Brown, P. W.; Double, D. D.; Frohnsdorff, G.; Johansen, V.; Smidth, F. L.; Odler, I.; Parrott, L. J.; Pommersheim, J. M.; et al. The Hydration of Tricalcium Silicate. *Mater. Struct.* **1984**, *17* (6), 457–468.

(18) Marchon, D.; Juilland, P.; Gallucci, E.; Frunz, L.; Flatt, R. J. Molecular and Submolecular Scale Effects of Comb-Copolymers on Tri-Calcium Silicate Reactivity: Toward Molecular Design. *J. Am. Ceram. Soc.* **2017**, *100* (3), 817–841.

(19) Ramachandran, V. S.; Feldman, R. F. 1. Concrete Science. In *Concrete Admixture Handbook*; 1996; pp 1–66.

(20) Bullard, J. W.; Jennings, H. M.; Livingston, R. A.; Nonat, A.; Scherer, G. W.; Schweitzer, J. S.; Scrivener, K. L.; Thomas, J. J. Mechanisms of Cement Hydration. *Cem. Concr. Res.* **2011**, *41*, 1208–1223.

(21) Vazquez, A.; Pique, T. M. 5 - Biotech Admixtures for Enhancing Portland Cement Hydration. In *Biopolymer and Biotech Admixtures for Eco-Efficient Construction Materials*; Elsevier Ltd, 2016; pp 81–98.

(22) Banfill, P. F. G. Rheology of Fresh Cement and Concrete. *Rheol. Rev.* **2006**, 61–130.

(23) Feys, D.; Cepuritis, R.; Jacobsen, S.; Lesage, K.; Secrieru, E.; Yahia, A. Measuring Rheological Properties of Cement Pastes : Most Common Techniques , Procedures and Challenges. **2017**, 129–135.

(24) Flatt, R.; Schober, I. *Superplasticizers and the Rheology of Concrete 7. Understanding the Rheology of Concrete*; Roussel, N., Ed.; Woodhead Publishing Limited: Oxford, 2011.

(25) Whitney, D. P. 3. Chemical Admixtures. In *Concrete Construction Engineering Handbook*; Nawy, E. G., Ed.; CRC Press: Boca Raton, US, 1998; pp 301–320.

(26) Ramachandran, V. S. 6. Water Reducers/Retarders. In *Concrete Admixture Handbook*; Ramachandran, V. S., Ed.; William Andrew Publishing: Pork Ridje, NJ, US, 1996; pp 286–409.

(27) Ramachandran, V. S.; Lowery, M. S.; Wise, T.; Polomark, G. M. The Role of Phosphonates in the Hydration of Portland Cement. *Mater. Struct.* **1993**, *26* (7), 425–432.

(28) Plank, J. Application of Biopolymers in Construction Engineering. *Biopolym. Online* **2005**.

(29) Gelardi, G.; Mantellato, S.; Marchon, D.; Palacios, M.; Eberhardt, A. B.; Flatt, R. 9. Chemistry of Chemical Admixture. In *Science and Technology of Concrete Admixture*; Aïtchin, P.-C., Flatt, R., Eds.; Woodhead Publishing Limited: Cambridge UK, 2016; pp 149–219.

(30) Eberhardt, A. B. On the Mechanism of Shrinkage Reducing Admixtures in Self Consolidating Mortars and Concrete, Bauhaus Universität Weimar, 2010.

(31) Gagné, R. 23. Shrinkage Reducing Amixtures. In *Science and Technology of Concrete Admixture*; 2016; pp 457–470.

(32) Jeknavorian, A. Overview of Defoming Technologies for Polycarboxylate-Based Superplasticizers. In *2nd International Conference on Polycarboxylate Superplasticizers*; 2017; pp 97–110.

(33) Björnström, J.; Chandra, S. Effect of Superplasticizers on the Rheological Properties of Cements. *Mater. Struct.* **2003**, *36* (10), 685–692.

(34) Srinivasan, S.; Barbhuiya, S. A.; Charan, D.; Pandey, S. P. Characterising Cement – Superplasticiser Interaction Using Zeta Potential Measurements. *Constr. Build. Mater.* **2010**, *24* (12), 2517–2521.

(35) Nanthakumar, B.; Arinaitwe, E. Adsorption of Sodium Lignosulfonates on Hematite. *Adsorption* **2010**, *16* (4), 447–455.

(36) Plank, J.; Hirsch, C. Impact of Zeta Potential of Early Cement Hydration Phases on Superplasticizer Adsorption. *Cem. Concr. Res.* **2007**, *37* (4), 537–542.

(37) Zhang, Y.; Kong, X. Correlations of the Dispersing Capability of NSF and PCE Types of Superplasticizer and Their Impacts on Cement Hydration with the Adsorption in Fresh Cement Pastes. *Cem. Concr. Res.* **2015**, *69*, 1–9.

(38) Andersen, P. J.; Roy, D. M.; Gaidis, J. M.; W.R. Grace and Co. The Effects of Adsorption of Superplasticizers on the Surface of Cement. *Cem. Concr. Res.* **1987**, *17* (5), 805–813.

(39) Hirata, T. Cement Dispersant. JP 842,022 (S59-018338), 1981.

(40) Nkinamubanzi, P. C.; Mantellato, S.; Flatt, R. 16. Superplasticizers in Practice. In *Science and Technology of Concrete Admixture*; Woodhead Publishing Limited: Cambridge UK, 2016; pp 353–377.

(41) Plank, J.; Sakai, E.; Miao, C. W.; Yu, C.; Hong, J. X. Chemical Admixtures - Chemistry, Applications and Their Impact on Concrete Microstructure and Durability. *Cem. Concr. Res.* **2015**, *78*, 81–99.

(42) Plank, J.; Schroefl, C.; Gruber, M.; Lesti, M.; Sieber, R. Effectiveness of Polycarboxylate Superplasticizers in Ultra-High Strength Concrete : The Importance of PCE Compatibility with Silica Fume. *J. Adv. Concr. Technol.* **2009**, *7* (1), 5–12.

(43) Yamada, K.; Takahashi, T.; Hanehara, S.; Matsuhisa, M. Effects of the Chemical Structure on the Properties of Polycarboxylate-Type Superplasticizer. *Cem. Concr. Res.* **2000**, *30* (2), 197–207.

(44) Sarıkahya, H. Effect of Chemical Structure of Polycarboxylate-Based Superplasticizers on Workability Retention of Self-Compacting Concrete. **2008**, *22*, 1972–1980.

(45) Pourchet, S.; Liautaud, S.; Rinaldi, D.; Pochard, I. Effect of the Repartition of the PEG Side Chains on the Adsorption and Dispersion Behaviors of PCP in Presence of Sulfate. *Cem. Concr. Res.* **2012**, *42* (2), 431–439.

(46) Li, C. Z.; Feng, N. Q.; Li, Y. De; Chen, R. J. Effects of Polyethlene Oxide Chains on the Performance of Polycarboxylate-Type Water-Reducers. *Cem. Concr. Res.* **2005**, *35* (5), 867–873.

(47) Winnefeld, F.; Becker, S.; Pakusch, J.; Götz, T. Effects of the Molecular Architecture of Comb-Shaped Superplasticizers on Their Performance in Cementitious Systems. *Cem. Concr. Compos.* **2007**, *29* (4), 251–262.

(48) Vickers, T. M.; Farrington, S. A.; Bury, J. R.; Brower, L. E. Influence of Dispersant Structure and Mixing Speed on Concrete Slump Retention. **2005**, *35*, 1882–1890.

(49) Lei, L.; Plank, J. Future Perspective of PCE Technology. In *2nd International Conference on Polycarboxylate Superplasticizers*; 2017; pp 19–61.

(50) Akimoto, S.; Honda, S.; Yasucohchi, T. Additives for Cement. EP0291073, 1992.

(51) Habbaba, A.; Lange, A.; Plank, J. Synthesis and Performance of a Modified Polycarboxylate Dispersant for Concrete Possessing Enhanced Cement Compatibility. *J. Appl. Polym. Sci.* **2013**, *129* (1), 346–353.

(52) Lange, A.; Hirata, T.; Plank, J. Influence of the HLB Value of Polycarboxylate

Superplasticizers on the Flow Behavior of Mortar and Concrete. *Cem. Concr. Res.* **2014**, *60*, 45–50.

(53) Lange, A.; Plank, J. Optimization of Comb-Shaped Polycarboxylate Cement Dispersants to Achieve Fast-Flowing Mortar and Concrete. *J. Appl. Polym. Sci.* **2015**, *132* (37), 1–9.

(54) Lange, A.; Plank, J. Study on the Foaming Behaviour of Allyl Ether-Based Polycarboxylate Superplasticizers. *Cem. Concr. Res.* **2012**, *42* (2), 484–489.

(55) Albrecht, G.; Weichmann, J.; Penkner, J.; Kern, A. Copolymers Based on Oxyalkylene Glycol Alkenyl Ethers and Derivatives of Unsaturated Dicarboxylic Acids. EP 0.736.553, 1996.

(56) Amaya, T.; Ikeda, A.; Inamura, J.; Kobayashi, A.; Saito, K.; Danzinger, W.; Tomoyose, T. Cement Dispersant and Cement Composition Containing the Dispersant. WO 0.039.045, 2000.

(57) Fan, W.; Stoffelbach, F.; Rieger, J.; Regnaud, L.; Vichot, A.; Bresson, B.; Lequeux, N. Cement and Concrete Research A New Class of Organosilane-Modi Fi Ed Polycarboxylate Superplasticizers with Low Sulfate Sensitivity. *Cem. Concr. Res.* **2012**, *42* (1), 166–172.

(58) Tahara, H.; Ito, H.; Mizushima, M. Cement Additive, Method for Producing the Same, and Concrete Composition. US 5.476.885, 1995.

(59) Miao, C.; Qiao, M.; Ran, Q.; Liu, J.; Zhou, D.; Yang, Y.; Mao, Y. Preparation Method of Hyperbranched Polycarboxylic Acid Type Copolymer Cement Dispersant. US 2013.0102.749, 2013.

(60) Yoshioka, K.; Tazawa, E. I.; Kawai, K.; Enohata, T. Adsorption Characteristics of Superplasticizers on Cement Component Minerals. *Cem. Concr. Res.* **2002**, *32* (10), 1507–1513.

(61) Mosquet, M.; Chevalier, Y.; Brunel, S.; Guicquero, J. P.; Perchec, P. L. E. Polyoxyethylene Di-Phosphonates as Efficient Dispersing Polymers for Aqueous Suspensions. **1997**, *65*, 2545–2555.

(62) Dalas, F.; Nonat, A.; Pourchet, S.; Mosquet, M.; Rinaldi, D.; Sabio, S. Tailoring the Anionic Function and the Side Chains of Comb-like Superplasticizers to Improve Their Adsorption. *Cem. Concr. Res.* **2015**, *67*, 21–30.

(63) Kraus, A.; Dierschke, F.; Becker, F.; Schuhbeck, T.; Grassl, H.; Groess, K. Method for Producing Phosphate Polycondensation Products and the Use Threof. US 2011.0281975, 2011.

(64) Lei, L.; Plank, J. Synthesis and Properties of a Vinyl Ether-Based Polycarboxylate Superplasticizer for Concrete Possessing Clay Tolerance. *Ind. Eng. Chem. Res.* **2014**, *53* (3), 1048–1055.

(65) Lei, L.; Plank, J. Cement and Concrete Research A Concept for a Polycarboxylate Superplasticizer Possessing Enhanced Clay Tolerance. *Cem. Concr. Res.* **2012**, *42* (10), 1299–1306.

(66) Lei, L.; Plank, J. Cement and Concrete Research A Study on the Impact of Different Clay Minerals on the Dispersing Force of Conventional and Modi Fi Ed Vinyl Ether Based Polycarboxylate Superplasticizers. *Cem. Concr. Res.* **2014**, *60*, 1–10.

(67) Marchon, D.; Sulser, U.; Eberhardt, A.; Flatt, R. J. Molecular Design of Comb-Shaped Polycarboxylate Dispersants for Environmentally Friendly Concrete. *Soft Matter* **2013**, *9* (45), 10719.

(68) Gelardi, G.; Sanson, N.; Nagy, G.; Flatt, R. J. Characterization of Comb-Shaped Copolymers by Multidetection SEC, DLS and SANS. *Polymers (Basel).* **2017**, *9* (2).

(69) Marchon, D.; Boscaro, F.; Flatt, R. J. Cement and Concrete Research First Steps to the Molecular Structure Optimization of Polycarboxylate Ether Superplasticizers : Mastering Fluidity and Retardation. *Cem. Concr. Res.* **2019**, *115* (October 2018), 116–123.

(70) Zingg, A.; Winnefeld, F.; Holzer, L.; Pakusch, J.; Becker, S.; Figi, R.; Gauckler, L. Interaction of Polycarboxylate-Based Superplasticizers with Cements Containing Different C3A Amounts. *Cem. Concr. Compos.* **2009**, *31* (3), 153–162.

(71) Ran, Q.; Somasundaran, P.; Miao, C.; Liu, J.; Wu, S.; Shen, J. Journal of Colloid and Interface Science Effect of the Length of the Side Chains of Comb-like Copolymer Dispersants on Dispersion and Rheological Properties of Concentrated Cement Suspensions. *J. Colloid Interface Sci.* **2009**, *336* (2), 624–633.

(72) Kauppi, A.; Andersson, K. M.; Bergstr, L. Probing the Effect of Superplasticizer Adsorption on the Surface Forces Using the Colloidal Probe AFM Technique. **2005**, *35*, 133–140.

(73) Flatt, R. J.; Schober, I.; Raphael, E.; Plassard, C.; Lesniewska, E. Conformation of Adsorbed Comb Copolymer Dispersants. *Langmuir* **2009**, *25* (2), 845–855.

(74) Gay, C.; Raphaël, E. Comb-like Polymers inside Nanoscale Pores. *Adv. Colloid Interface Sci.* **2001**, *94* (1–3), 229–236.

(75) Kroner, M.; Perner, J.; Büchner, K.-H.; Wild, J.; Pfister, J. Method for Modifying Acid Group Cantaining Polymer. WO 01/72853 A1, 2001.

(76) Guicquero, J. P.; Maitrasse, P.; Mosquet, M. A.; Sers, A. A Water Soluble or Water Dispersible Dispersing Agent. FR 2.776.285, 1999.

(77) Asúa, J. M. *Polymer Reaction Engineering*; Blackwell Publishing, 2007.

(78) Odian, G. *Principles of Polymerization*, 4th ed.; Odian, G., Ed.; John Wiley and Sons Ltd.: New York, USA, 1970.

(79) Preusser, C.; Hutchinson, R. A. Measuring and Modelling the Peculiarities of Aqueous-Phase Radical Polymerization. **2016**, *94* (November), 2045–2051.

(80) Ferrari, L.; Kaufmann, J.; Winnefeld, F.; Plank, J. Multi-Method Approach to Study Influence of Superplasticizers on Cement Suspensions. *Cem. Concr. Res.* **2011**, *41* (10), 1058–1066.

(81) Plank, J.; Sachsenhauser, B. Experimental Determination of the Effective Anionic Charge Density of Polycarboxylate Superplasticizers in Cement Pore Solution. *Cem. Concr. Res.* **2009**, *39* (1), 1–5.

(82) Ferrari, L.; Kaufmann, J.; Winnefeld, F.; Plank, J. Interaction of Cement Model Systems with Superplasticizers Investigated by Atomic Force Microscopy, Zeta Potential, and Adsorption Measurements. *J. Colloid Interface Sci.* **2010**, *347* (1), 15–24.

(83) Zhang, Y. R.; Kong, X. M.; Lu, Z. B.; Lu, Z. C.; Hou, S. S. Effects of the Charge Characteristics of Polycarboxylate Superplasticizers on the Adsorption and the Retardation in Cement Pastes. *Cem. Concr. Res.* **2015**, *67*, 184–196.

(84) Zhang, Y.; Cai, X.; Kong, X.; Gao, L. Effects of Comb-Shaped Superplasticizers with Different Charge Characteristics on the Microstructure and Properties of Fresh Cement Pastes. **2017**, *155*, 441–450.

(85) Plank, J.; Pöllmann, K.; Zouaoui, N.; Andres, P. R.; Schaefer, C. Synthesis and Performance of Methacrylic Ester Based Polycarboxylate Superplasticizers Possessing Hydroxy Terminated Poly(Ethylene Glycol) Side Chains. *Cem. Concr. Res.* **2008**, *38* (10), 1210–1216.

(86) Han, S.; Plank, J. Mechanistic Study on the Effect of Sulfate Ions on Polycarboxylate Superplasticisers in Cement. *Adv. Cem. Res.* **2013**, *25* (4), 200–207.

(87) Rinaldi, D.; Hamaide, T.; Graillat, C.; Agosto, F. D.; Spitz, R.; Georges, B.; Mosquet, M.; Maitrasse, P. RAFT Copolymerization of Methacrylic Acid and Poly (Ethylene Glycol) Methyl Ether Methacrylate in the Presence of a Hydrophobic Chain Transfer Agent in Organic Solution and in Water. *J. Polym. Sci. Part A Polym. Chem.* **2009**, *47*, 3045–3055.

(88) Beuermann, S.; Buback, M.; Hesse, P.; Lacík, I. Free-Radical Propagation Rate Coefficient of Nonionized Methacrylic Acid in Aqueous Solution from Low Monomer Concentrations to Bulk Polymerization. *Macromolecules* **2006**, *39* (1), 184–193.

(89) Lacík, I.; Učňová, L.; Kukučková, S.; Buback, M.; Hesse, P.; Beuermann, S. Propagation Rate Coefficient of Free-Radical Polymerization of Partially and Fully Ionized Methacrylic Acid in Aqueous Solution. *Macromolecules* **2009**, *42* (20), 7753–7761.

(90) Fischer, E. J.; Storti, G.; Cuccato, D. Aqueous Free-Radical Polymerization of Non-Ionized and Fully Ionized Methacrylic Acid. *Processes* **2017**, *5*, 23.

(91) Smolne, S.; Weber, S.; Buback, M. Propagation and Termination Kinetics of Poly(Ethylene Glycol) Methyl Ether Methacrylate in Aqueous Solution. *Macromol. Chem. Phys.* **2016**, *217* (21), 2391–2401.

Chapter 2: Synthesis of MPEG Type of Superplasticizers with Short Lateral Chains

2.1. Introduction

Water soluble poly(MAA-co-PEGMA) copolymers present comb-like structure, where the size of the lateral chains can be tuned by using PEGMA macromonomers with different number of ethylene glycol units. This type of macromolecules under basic conditions present an anionic backbone due to the ionization of the carboxylic monomers, and uncharged side chains. These type of copolymers are widely used in construction as Superplasticizers for cementitious formulations.

In this chapter, the aim is to synthesize comb like copolymers (MAA-co-PEGMA) with short lateral chains (4-5 ethylene glycol units) and controlled microstructure; namely, copolymer composition and molar mass, to study the effect of the microstructure of these copolymers on the hydration and rheology of cements.

Part of this chapter has been published in:

1. Processes, ***2017**, 5, 19*
2. Polymer Chemistry, ***2019**,10, 1000-1009*

In this work, the comb-like copolymers will be synthesized by free-radical copolymerization of MAA and PEGMA5 comonomers. Semibatch operation is considered to control copolymer properties like copolymer composition and molar mass and to better cope the exothermicity of the reaction and hence better temperature control.

In order to produce copolymers with the required copolymer composition (note that the composition of MAA in the chains will allow to tune the charge density of the chains) the concentration of the comonomers (MAA and PEGMA5) has to be controlled. To do so the feeding of the comonomers to the reactor must be controlled. The most common and easy way to achieve this control is by feeding the two monomers under starved conditions in the ratio desired in the copolymer. This implies long feeding rates and a fraction of the copolymer will not have the desired composition[1]. A more demanding, yet more robust and accurate strategy is the one that feeds the two monomers to the reactor to maintain the ratio of the comonomer concentrations, in the value that ensures the required copolymer composition, that can be calculated from the Mayo-Lewis instantaneous composition equation[2]. For the second strategy open-loop[3–5] and closed-loop[6–8] strategies can be used. Both strategies require a mathematical model of the process and the later on-line measurement to determine the state of the process (i.e. the concentration of the monomers in the reactor)[3] to take the necessary correction actions.

In this chapter, monomer starved strategies and open-loop strategies will be used to produce copolymers of MAA-co-PEGMA5 with the desired composition. The molar mass of the copolymers will be controlled by the feeding of the chain transfer agents.

2.2. Estimation of the Reactivity Ratios of MAA-PEGMA Monomers

The composition and sequence distribution of the comonomers in the chain is expected to have an impact on the performance of the comb copolymer chains in the cementitious formulations. Therefore, in order to produce homogenous copolymers with a given composition and hence be able to understand their adsorption behavior when applied in cementitious formulations as SPs, it is of paramount importance to control the copolymer composition of the chains during the polymerization reaction

MAA and PEGMA monomers belong to the family of methacrylates. Generally, monomers of the same family tend to have similar reactivity ratios and produce copolymers with little composition drift. Bevington et al.[9] estimated the reactivity ratios of methyl methacrylate (MMA) with other monomers of the methacrylate family in organic solvent (see Table 2.1). It can be observed that for all monomer pairs the reactivity ratios are very close and hence very small composition drift is expected in their copolymerization.

Table 2.1: Reactivity ratios of different monomers of the methacrylate family.

M1	M2	r_1	r_2
MMA	FMA	0.75	1.19
MMA	n-BMA	0.79	1.27
MMA	IBMA	0.91	1.09

FMA: Furfuryl Methacrylate n-BMA: n-Butyl Methacrylate IBMA: Isobutyl Methacrylate

MMA: Methyl Methacrylate

Unfortunately, the information about the reactivity ratios of MAA/PEGMA5 comonomer pair in aqueous solution is scarce[10,11] and reports for conditions where the MAA is fully ionized (basic conditions) are not available.

Smith and Klier[10] found that the reactivity ratios measured in deuterated water (D_2O) for the non-ionized MAA were very close to 1 for both monomers (r_{MAA} = 1.03 and r_{PEGMA} = 1.02); however, by changing 50% of D_2O by ethanol (D_2O/Ethanol = 50/50, a continuous phase used in dispersion polymerization), the reactivity ratios measured for the monomers increased (r_{MAA} = 2.0 and r_{PEGMA} = 3.6). Obviously, this has an impact on the distribution of the monomer sequence in the chain that is random in water and more “blocky” in the case of water/ethanol.

Krivorotova et al.[11] have recently analyzed the copolymerization of MAA and PEGMA macromonomers carried out by conventional and controlled free-radical polymerization (RAFT, reversible addition fragmentation chain transfer) in the mixture D_2O/dioxane initiated by azobisisobutyronitrile (AIBN). MAA was also non-ionized in the experimental conditions investigated in this work. Interestingly, the authors considered two PEGMA macromonomers differing in the number of ethylene glycol units (EGu) in the side chain (PEGMA 5 and PEGMA 45). The authors found that for PEGMA5, the reactivity ratios for conventional free-radical copolymerization and for controlled free-radical copolymerization were close from each other. On the other hand, for PEGMA 45 macromonomer the polymerization technique employed had substantial effect on the reactivity ratios.

From batchwise experiments conducted during this work (at neutral pH; that is MAA fully ionized) it was observed that substantial composition drift was obtained (see Figure 2.1a and 2.1b), because of PEGMA5 being more reactive than MAA. In addition, the polymerization rates

were found to be a function of the solids content. This indicates that water soluble monomers under ionized conditions present features with regard to their reactivity ratios that are not found in organic solvents.

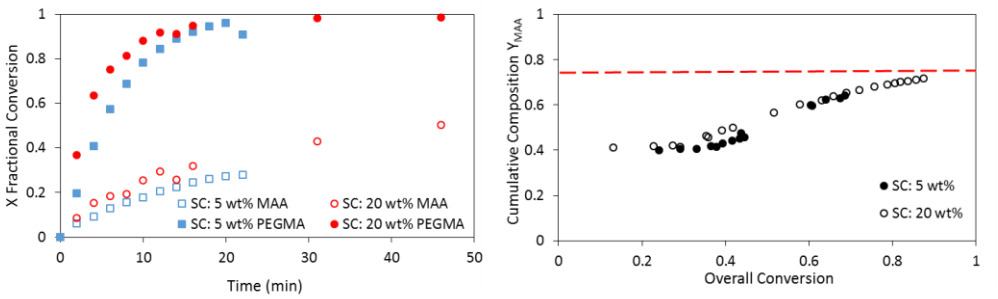

Figure 2.1: Fractional conversion evolution with time and cumulative composition evolution over overall conversion of two different batch experiments with a comonomer ration of MAA/PEGMA5: 3/1 (pH = 7; T = 70 ºC; KPS: 1% bwom).

This section aims at determining the reactivity ratios of the comonomer system under fully ionized conditions of the MAA and at varying initial monomer concentrations (solids content) in order to use this information in the mathematical model needed for open loop control strategies to control copolymer composition that will be developed later in the chapter.

The reactivity ratios were estimated considering that the reactivity of the propagation reaction is governed by the nature of the monomer and the terminal unit of the polymer radical (terminal model). For that, the method developed by De la Cal et al.[12,13] was used in this work to estimate the reactivity ratios, (see Appendix II for the detailed procedure).

2.2.1. Experimental Part

Aqueous phase (H_2O/D_2O) copolymerizations of MAA and PEGMA5 were carried out in NMR tubes and the concentration of the unreacted monomers was in-situ monitored by ^{1}H-NMR.

Comonomer solutions were prepared at different solids contents (5-20 wt%) with different molar ratios. The comonomer molar ratios are the following: (MAA/PEGMA5: 3/1, 2/1, 1/1). Comonomer mixture solutions were neutralized with NaOH solutions and kept at pH between 7 and 9 to ensure total ionization of the carboxylic monomer in all cases. All reactions were initiated with KPS (1% bwom). Reactions were performed at 70 ºC.

Figure 2.2 presents the in-situ acquired spectra during one of the copolymerizations that clearly shows the disappearance of the vinyl double bonds of PEGMA5 and MAA (this comonomer is not completely consumed in this experiment) in the δ 5.25-5.75 ppm region.

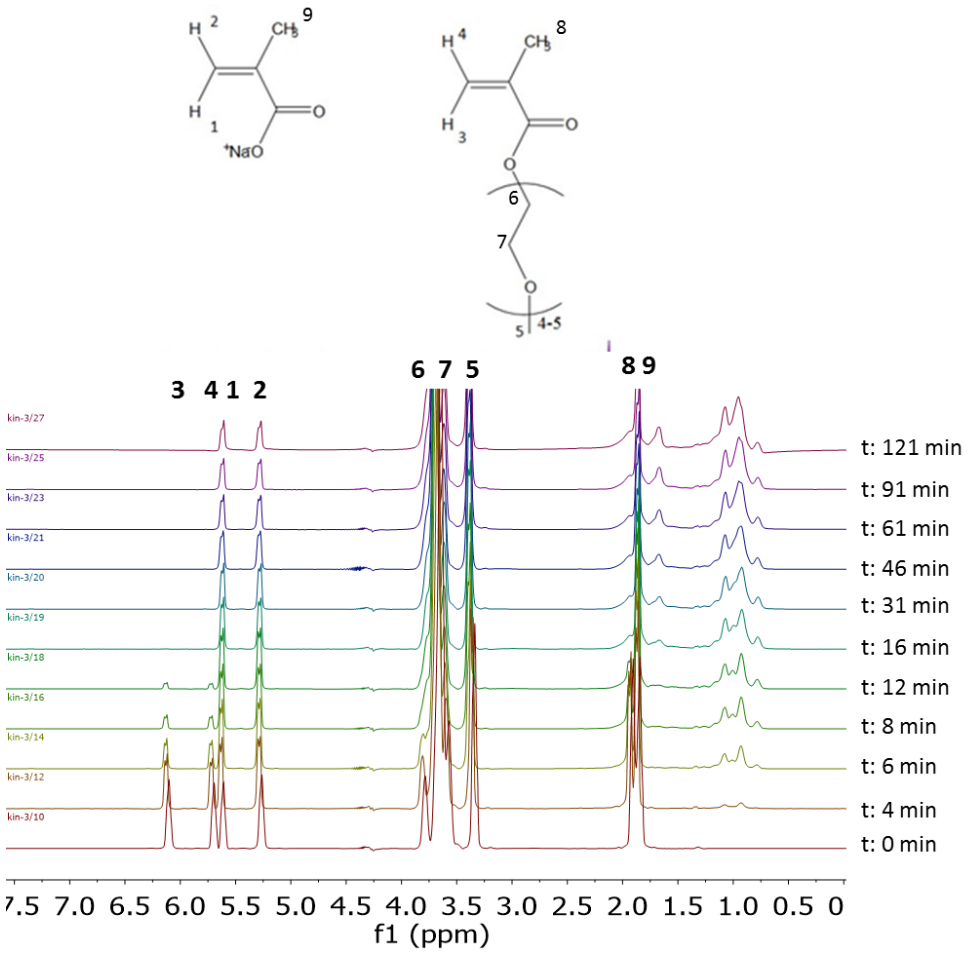

Figure 2.2: Time evolution of the proton nuclear magnetic resonance (^{1}H-NMR) spectra of the aqueous-solution copolymerization of MAA and PEGMA5 carried out at 70 ºC (SC = 10 wt % MAA/PEGMA5 = 1/1).

2.2.2. Influence of Solids Content

Copolymerizations of MAA and PEGMA5 were carried out in NMR tubes at different comonomer ratios (MAA/PEGMA: 3/1, 2/1 and 1/1) and different solids content (SC: 5, 10, 15 and 20 wt%).

For the sake of brevity, only the individual conversions of MAA and PEGMA as a function of time for a representative (e.g. Monomer ratio 1/1 and the four SC studied) is presented here; the rest are included in Appendix II.

Figure 2.3 shows that conversions of both comonomers increase with solids content (for MAA the effect is clearer at higher MAA/PEGMA ratios; see Appendix II) and that PEGMA5 is more reactive than MAA at fully ionized conditions. The effect of solids content on the conversion indicates that the dependence of the polymerization rate on the monomer conversion is not of first order for any of the two monomers. If the polymerization rate had a first order dependence with the conversion, the fractional conversion of each of the comonomers would have been the same for the different solids content. This behavior has been also reported for the aqueous solution homopolymerization of MAA[14–18]. It has been found that the propagation rate coefficient of MAA was a function of the concentration of the monomers in the aqueous phase, the ionization degree and electrolyte concentration. Under fully ionized conditions the propagation rate coefficient of MAA increases with monomer weight fraction, but under non-ionized and partially ionized conditions the propagation rate coefficients decrease with increasing monomer fraction.

Similar to other water soluble monomers, the kinetics of the polymerization of PEG methacrylates is affected by the monomer weight fraction in aqueous solution[19]. The propagation

rate coefficient increased as the solids content decreased which follows the same trend as the polymerization of non-ionized or partially ionized MAA.

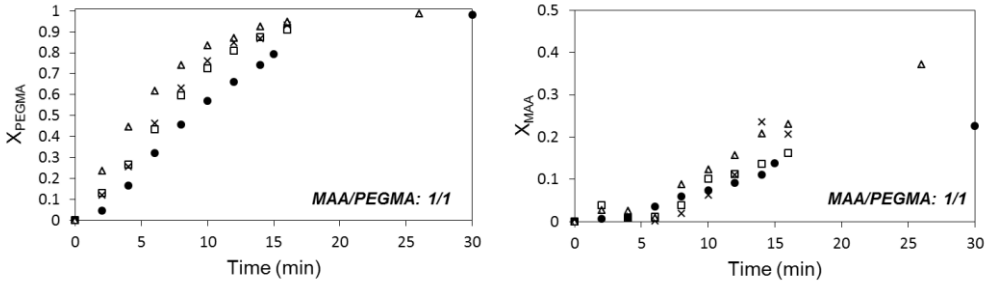

Figure 2.3: Time evolution of the conversion of MAA (right) and PEGMA 5 (left) for monomer ratio 1/1 at different solids content. (SC: ● – 5 wt%; □ – 10 wt%; x – 15 wt %; Δ - 20 wt%).

From this data the cumulative composition referred to MAA as a function of the overall conversion is plotted and used in the estimation algorithm. Note that in contrast with other methods to estimate the reactivity ratios, in this work we used the data of the whole experiment for each composition[20,21].

Figure 2.4 shows the comparison between the cumulative compositions of MAA determined experimentally from the NMR data (dots) and the estimated one (lines) for the estimated reactivity ratios at each solids content.

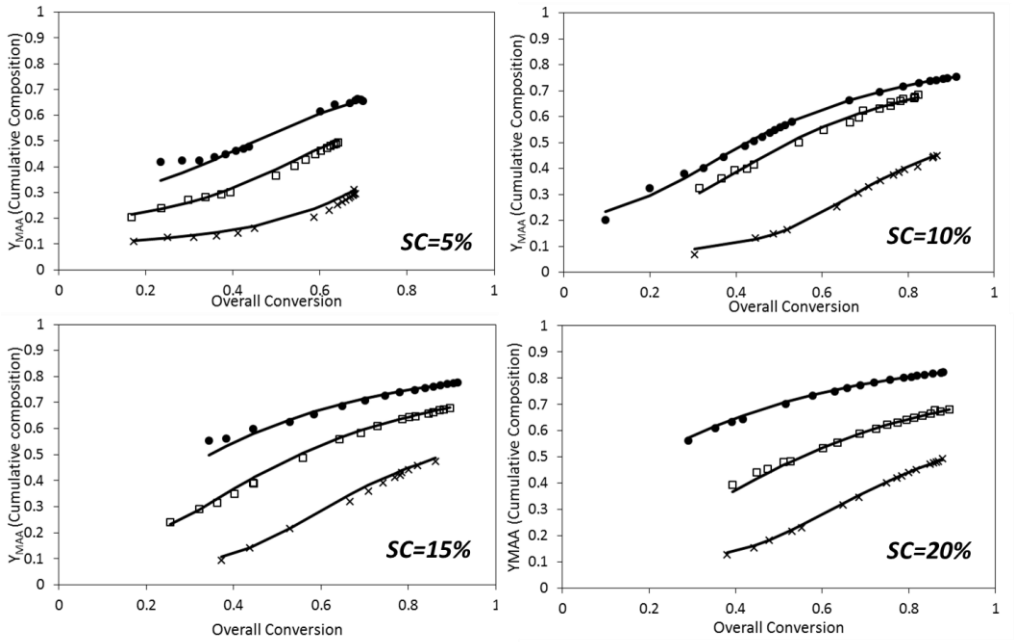

Figure 2.4: Conversion evolution of the cumulative composition of MAA for the in-situ NMR experiments. (Dots) experimental results, (lines) model predictions for the estimated reactivity ratios at each solids content. Molar ratios: x – 1/1, □ – 2/1, ● – 3/1.

Figure 2.5 shows the estimated reactivity ratios at each solids content. It can be seen that the reactivity ratios of each comonomer increases with solids content. This unexpected dependence of the reactivity ratios with solids content has been recently found for the aqueous-phase copolymerization of AA (acrylic acid) and AM (acrylamide) [22], a comonomer system that shares similar features with the analyzed one in this work. A linear dependency of the reactivity ratios of PEGMA5 and MAA with solids content was found to fit reasonably well the experimental data:

$$r_{MAA} = 0.07 + 1.89 \cdot SC_0 \quad \text{(eq: 2.1)}$$

$$r_{PEGMA} = 9.89 + 117.21 \cdot SC_0 \quad \text{(eq: 2.2)}$$

Where SC_0 is the initial weight fraction of comonomers in the copolymerization formulation ($0 < SC_0 < 1$).

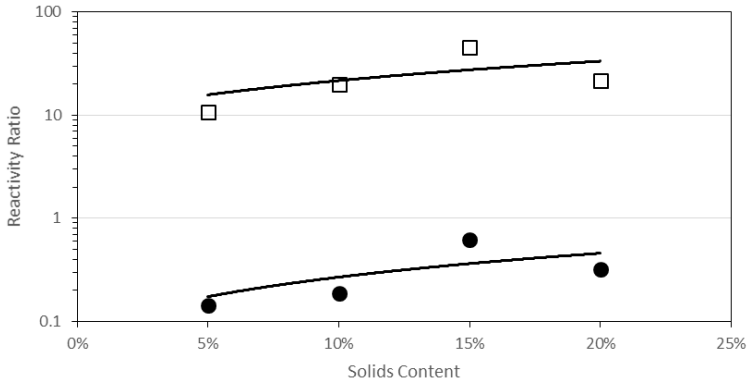

Figure 2.5: Reactivity ratios for the copolymerization of fully ionized (pH = 7) MAA and PEGMA5 as determined by fitting data at each initial solids content (squares and circles). A linear fit of the reactivity ratios estimated at each solids content is included (solid line) □ – r_{PEGMA}, ● – r_{MAA}.

2.3. Synthesis of MAA-co-PEGMA5 Copolymers with Homogeneous Composition

In view of the widely different reactivity ratios of MAA and PEGMA5 and in order to synthesize copolymers with homogeneous compositions semibatch operation was implemented. It is well known[1] that to produce homogeneous copolymers in the copolymerization of monomers

with widely different reactivity ratios by semibatch operation, one of the easiest way is to feed the monomer under starved conditions. Under starved conditions the following condition must be fullfilled:

$$\frac{F_{MAA}}{F_{PEGMA}} \cong \frac{Rp_{MAA}}{Rp_{PEGMA}} \qquad \text{(eq: 2.3)}$$

Namely, the ratio of the feeding rate of the comonomers should be very close to the ratio of the polymerization rate of the comonomers. In order to achieve this condition during semibatch operation one needs to feed the comonomer mixture to the reactor at very slow feeding rate and must achieve high instantaneous conversions (X_{inst} > 85%), which requires high polymerization rates.

2.3.1. Results and Discussion

2.3.1.1. Assessment of Starved Conditions

As discussed above to achieve true starved conditions high polymerization rates are needed. The optimal initiator concentration, reaction temperature and feeding rates (or time) were first assessed by measuring the evolution of the cumulative copolymer composition during the experiments. Figure 2.6 and 2.7 show that reasonable starved conditions (high overall instantaneous conversions and homogeneous copolymer composition) were achieved when running the reaction at 90 ºC with 2 wt% (bwom) of initiator and at solids content of 30 %. These conditions were considered to produce comb-like copolymers with given copolymer composition and molar masses as it is discussed in the following sections.

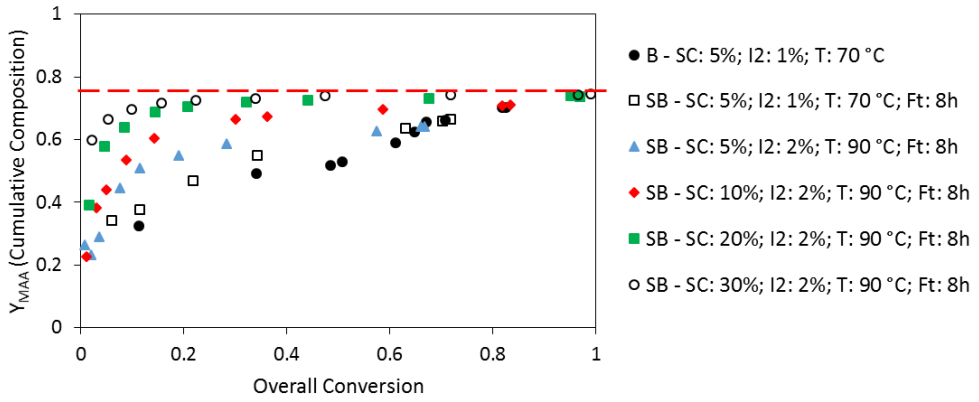

Figure 2.6: Evolution of the copolymer cumulative composition when varying the experiment conditions of semibatch copolymerizations of MAA and PEGMA5. Legend: B-Batch, SB-Semibatch, SC-Solids content, I2-Inititator concentration (bwom), T-Temperature, Ft-Feeding time.

In Figure 2.7 it can be observed that the increase of initiator concentration and the increase in the temperature from 70 ºC to 90 ºC had only minor increase in the instantaneous conversion. On the other hand, the increase of solids content had more pronounce increase on the instantaneous conversion and polymerization rate. When experiments were run at 10 wt% solids content high instantaneous conversion (Xi_{nst} > 85%) was not achieved. At 20 wt% SC the reaction achieved starved condition at 70% of overall conversion. Finally, as previously mentioned reasonable starved conditions (instantaneous conversions higher than 85-90% in almost 80% of the process) were achieved at 30 wt% SC, 2% initiator concentration (bwom), and at 90 ºC with 8h of feeding.

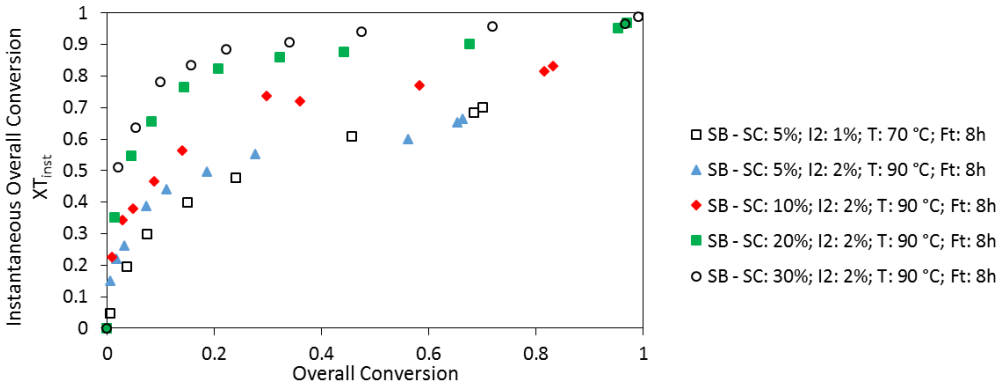

Figure 2.7: Evolution of the copolymer instantaneous overall conversion when reactions of semibatch copolymerizations of MAA and PEGMA5 at different conditions were performed. Legend: B-Batch, SB-Semibatch, SC-Solids content, I2-Inititator concentration (bwom), T-Temperature, Ft-Feeding time.

2.3.1.2. Effect of Comonomer Ratio in Monomer Starved Semibatch Copolymerizations

Three different comonomer ratios were employed: 2/1, 3/1, 4/1 in the monomer starved semibatch conditions optimized in the previous section. Conversions were measured by ^{1}H-NMR using the watergate sequence. Figure 2.8 shows the fractional partial and overall conversions.

The overall fractional conversion was below 90% during the first 2 hours of reaction and hence starved conditions were not achieved in this period and as shown by the individual fractional conversion the PEGMA5 comonomer reacted faster and hence the copolymer composition was richer in PEGMA5 during a substantial part of the process. Almost full conversion was achieved in the three cases.

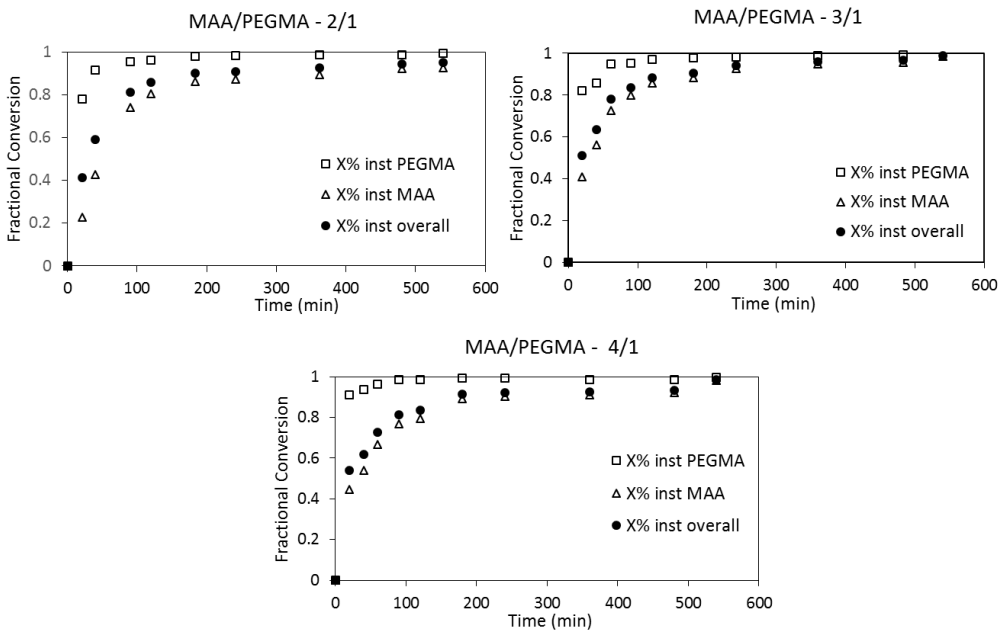

Figure 2.8: Time evolution of individual and overall conversion for the copolymerization of MAA and PEGMA at different comonomer ratios.

In order to analyze the homogeneity of the polymer chains the cumulative copolymer composition was determined from the individual monomer fractional conversions and plotted over the total conversion.

In comparison with the cumulative copolymer composition obtained in a batch process, (see Figure 2.1) the starved semibatch processes yield substantially more homogeneous copolymers for each comonomer ratio. Nevertheless, as discussed above starved conditions were not achieved during the first 120 minutes (approximately 15-20 % conversion) and hence there is a fraction of chains which have a composition richer in PEGMA5 than the desired value.

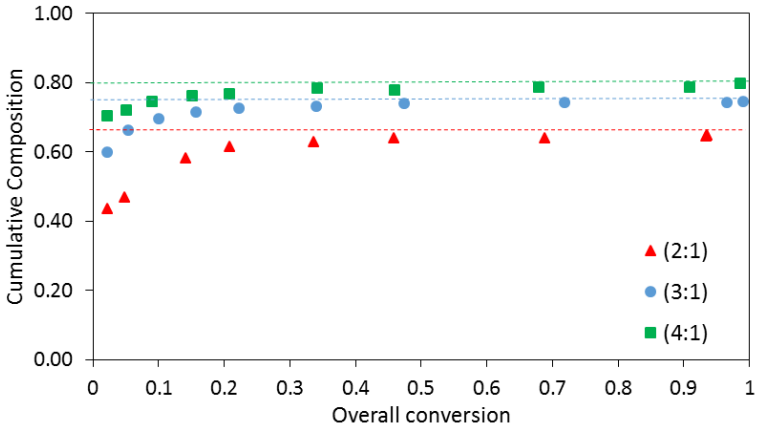

Figure 2.9: Conversion evolution of the cumulative copolymer composition referred to MAA comonomer for the different comonomer ratios.

In addition to the cumulative copolymer composition of the copolymer chains, the sequence distribution of the comonomers in the chain is an important parameter because it can directly affect the interaction of the copolymer chains with the cementitious materials and their adsorption behavior.

High resolution ^{13}C-NMR is a powerful tool to analyze the comonomer distribution along the chains in copolymers[23]. In methacrylate copolymers it is well known that the carboxyl peaks are especially sensitive to the changes in the microstructure. MAA-co-PEGMA5 copolymers display two well differentiated signals: one referred to carboxylic monomer and other corresponding to the ester monomer. The carbonyl signal in itself displays a complex pattern but by performing a Lorentzian deconvolution into triad and pentads a more detailed understanding

of the microstructure can be obtained[24]. The intensities of each triad have been correlated to the sum of the intensities of the corresponding pentads:

- (AAA) = (AAAAA) + (AAAAB) + (BAAAB) (eq: 2.4)
- (AAB) = (AAABA) + (AAABB) + (BAABA) + (BAABB) (eq: 2.5)
- (BAB) = (ABABA) + (ABABB) + (BBABB) (eq: 2.6)

Figure 2.10 shows the carbonyl region of the MAA comonomer in the copolymer. As it can be seen the C=O peak pattern is not a single peak, but multiple peaks that is a consequence of neighboring units to MAA in the chain. The higher the resolution of the NMR equipment the better the resolution of the comonomer sequence distribution. As can be seen by increasing the fraction of MAA in the copolymer the first peak increases prominently whereas the other decrease. Table 2.2 shows the calculated fraction of each triad for the different cases. The values for the ideal triads were calculated based on the Bernoullian model[25] in which the probability of incorporation of one comonomer unit to the growing copolymer chain depends on the fraction of monomers in the mixture (e.g., $r_1=r_2=1$, random copolymerization). Thus, the triad values for random copolymerization can be calculated as follows:

- (AAA): Y_{MAA}^3 (eq: 2.7)
- (AAB): $Y_{MAA}^2 \cdot (1 - Y_{MAA})$ (eq: 2.8)
- (BAB): $(1 - Y_{MAA})^2 \cdot Y_{MAA}$ (eq: 2.9)

where YMAA is the copolymer composition referred to MAA

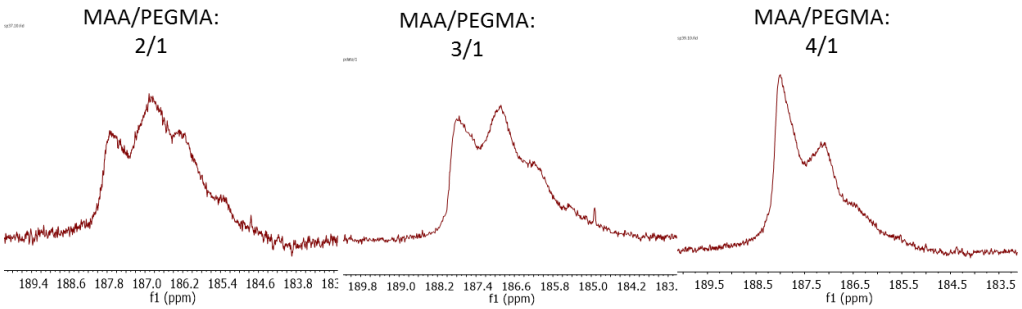

Figure 2.10: ^{13}C-NMR pattern of the carbonyl area corresponding to the carboxylic monomer of the synthesized copolymers with different comonomer ratios.

Table 2.2. Fraction of the triads obtained from ^{13}C-NMR measurements and the ideal fraction of triads (random copolymerization). A is MAA unit and B is PEGMA5 unit.

	Experimental			***Ideal***		
	Triad			***Triad****		
Comonomer Ratio	***(AAA)***	***(AAB)***	***(BAB)***	***(AAA)***	***(AAB)***	***(BAB)***
2/1 – S2	0.228	0.353	0.068	0.273	0.296	0.080
3/1 – S1	0.353	0.337	0.057	0.417	0.282	0.048
4/1 – S3	0.439	0.316	0.043	0.506	0.258	0.033

*Calculated using Bernouillian model: (AAA): Y_{MAA}^3; (AAB): $2 \cdot Y_{MAA}^2 \cdot (1-Y_{MAA})$; (BAB): $(1-Y_{MAA})^2 \cdot Y_{MAA}$; Y_{MAA} is the copolymer composition referred to MAA monomer.

As expected the contribution of the triad (AAA) increased substantially when changing the comonomer ratio from 2/1 to 4/1 in the copolymerization. However, the change in the triads (AAB) and (BAB) is less significant. Note that in all cases the value of the triad (AAA) is substantially smaller than the value corresponding to ideal random copolymerization.

Furthermore, triad (AAB) is higher than the ideal values. The smaller values of the experimental (AAA) triad is due to the fact that true starved conditions are not achieved at the beginning of the process, and hence copolymer chains are richer in PEGMA5 comonomer (see Figure 2.9).

Absolute molar masses and dispersities of the synthesized copolymers were measured by means of GPC (SEC/MALS/RI). An alkaline (pH>10) $NaNO_3$ 0.1M solution was employed as eluent. In literature[26], the dn/dc values of PEG (dn/dc=0.135 ml/g) has been generally used to obtain the absolute molar mass of this type of copolymers. In this work, the dn/dc values for each copolymer were determined using the refraction index instrument. It is worth mentioning that since the copolymers obtained are not fully homogenous in composition an average (apparent) value of the dn/dc is obtained. Table 2.3 presents the values measured for the three copolymers that are substantially different to the value of pure PEG used in the literature; namely the higher the MAA content the higher the dn/dc.

Table 2.3: dn/dc values obtained for the synthesized copolymers in starved semibatch operation with different comonomer ratio.

Comonomer Ratio	***dn/dc (ml/g)***
2/1 – S2	0.181
3/1 – S1	0.191
4/1 – S3	0.207

Figure 2.11 and Table 2.4 present the results of the MWD analysis. The weight average molar mass (and degree of polymerization) are similar for the copolymerizations with 2/1 and 3/1 and decreased for the 4/1 ratio. Dispersity also decreased for 4/1 comonomer ratio. It is not clear

the reason for this decrease of the molar masses because the overall polymerization rates are very close for the three copolymerization experiments (see Figure 2.8).

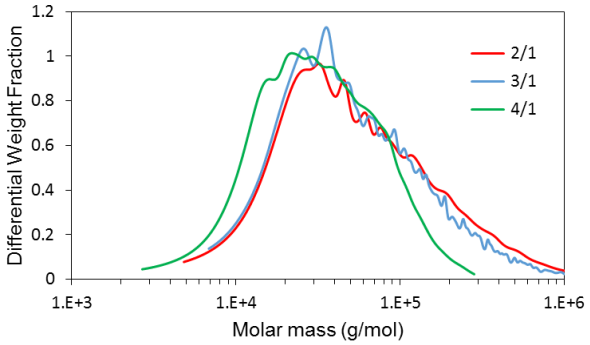

Figure 2.11: Molar mass distribution of the synthesized copolymers.

Table 2.4: Molar mass, dispersity index and degree of polymerization of the synthesized copolymers.

Comonomer Ratio	*Mw (kg/mol)*	*Đ*	*DP**
2/1 – S2	100.2 ± 0.7	3.0	211
3/1 – S1	88.0 ± 1.4	3.0	206
4/1 – S3	43.3 ± 0.3	2.2	156

*DP is calculated from Mn using an average molar mass of the repeating unit based on the copolymer composition of each experiment.

2.3.1.3. Effect of Chain Transfer Agent

As discussed above homogeneous copolymers of MAA/PEGMA5 with well-defined composition and molar mass are sought to study the effect of this microstructural features of the copolymer chains on their interaction with the cement particles and hence on their effect on the

cement hydration. In this section, copolymer chains with 3/1 composition and molar masses smaller than those produced in the previous section were targeted by using a chain transfer agent in the semibatch copolymerization. The CTA chosen for the synthesis of the copolymers was 3-mercaptopropionic acid, which is water soluble. Four different concentrations were employed for the copolymer with MAA/PEGMA5 3/1 comonomer ratio: 0%, 0.5%, 1% and 1.5% by mol of monomer (bmom).

Table 2.5 and Figure 2.12 present the molar mass distribution and the average values and dispersities for the experiments carried out with different concentrations of the CTA. The GPC traces show that the distribution shifted to lower molar masses increasing the CTA concentration and the dispersity of the distribution was narrowed and approached the minimum value achievable in free radical polymerization with termination controlled by a chain transfer reaction (Đ = 2). Copolymers with molar masses in the range 88-32 KDa were synthesized successfully.

Table 2.5: Molar mass, dispersity index and degree of polymerization of the synthesized copolymers. The dn/dc value employed is the previous reported for the copolymer with a comonomer ratio of 3/1 (dn/dc=0.191).

CTA Concentration	***Mw (kg/mol)***	**Đ**	***DP***
0.0% - S1	88.0 ± 1.4	3.0	206
0.5% - S4	51.4 ± 0.5	2.2	166
1.0% - S5	40.8 ± 0.6	2.0	146
1.5% - S6	32.8 ± 0.3	2.0	112

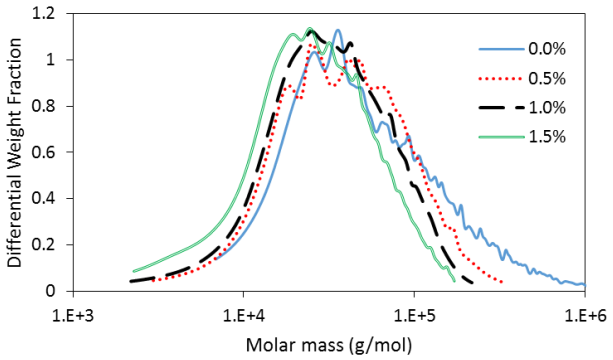

Figure 2.12: Molar mass distribution of the synthesized copolymers with a 3/1 MAA/PEGMA5 ratio and different amounts of CTA as indicated in the legend.

However, the addition of the CTA had an unexpected impact on the kinetics of the copolymerization (see Figure 2.13). The reactivity of the MAA comonomer decreased (the rate of consumption of MAA slowed down) as the concentration of the CTA increased and unreacted amount of MAA was present after 600 minutes of polymerization; the unreacted MAA increased with the amount of CTA used in the formulation. This effect is reflected in the cumulative composition of the chains which are richer in PEGMA5 than the copolymers synthesized without CTA, and in addition the higher is the CTA, the higher is the drift as shown in Figure 2.14. The reason for this behavior is not clear, but it is likely related to the presence of additional charges in the reaction medium (3-MPA is also deprotonated at pH = 7) that preferentially affect to the addition of the MAA comonomer to the growing chains. As it has been reported by Cuccato et al. [27,28] this effect can substantially affect some relevant kinetic steps. Monomer-monomer association, hindrance of the internal motions and electrostatic forces producing diffusion limitations, are some of the relevant phenomena which may have affected the propagation reaction of these water soluble ionizable species.

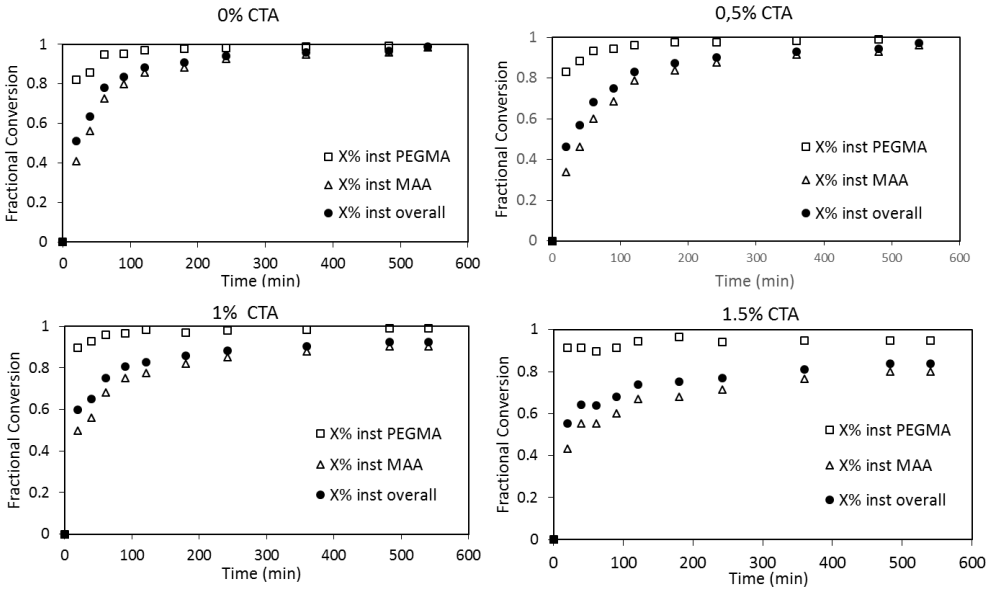

Figure 2.13: Time evolution of individual and overall instantaneous conversions for the copolymerization of MAA and PEGMA with different CTA concentrations for 3/1 comonomer ratio.

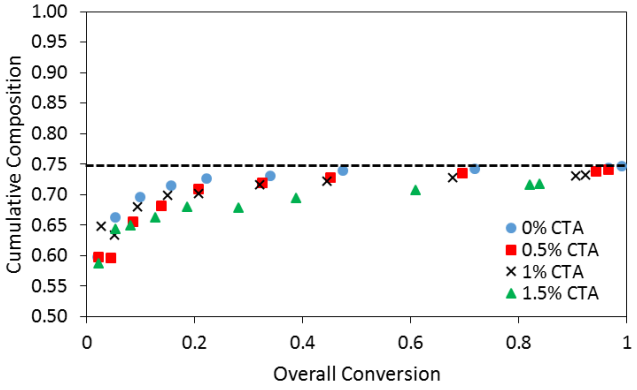

Figure 2.14: Conversion evolution of the cumulative composition for the MAA/PEGMA5 copolymers synthesized in starved semibatch copolymerization (ratio 3/1) with different CTA concentration.

The higher composition drift and the lower incorporation of MAA is also reflected in the ^{13}C-NMR region of the carbonyl signal shown in Figure 2.15. As can be seen the intensity of the first peak which is characteristic of (AAA) triads decreased by increasing the concentration of CTA because less MAA was incorporate into the chains. Furthermore, there is also an increase in the intensity of the second and third peaks that are mainly associated with (AAB) and (BAB) triads at higher CTA concentrations. It can also be observed that the higher the CTA concentration the bigger the difference between experimental and theoretical value (corresponding to random copolymerization) of the (AAA) triad, showing the unexpected low incorporation of the MAA comonomer to copolymer chains.

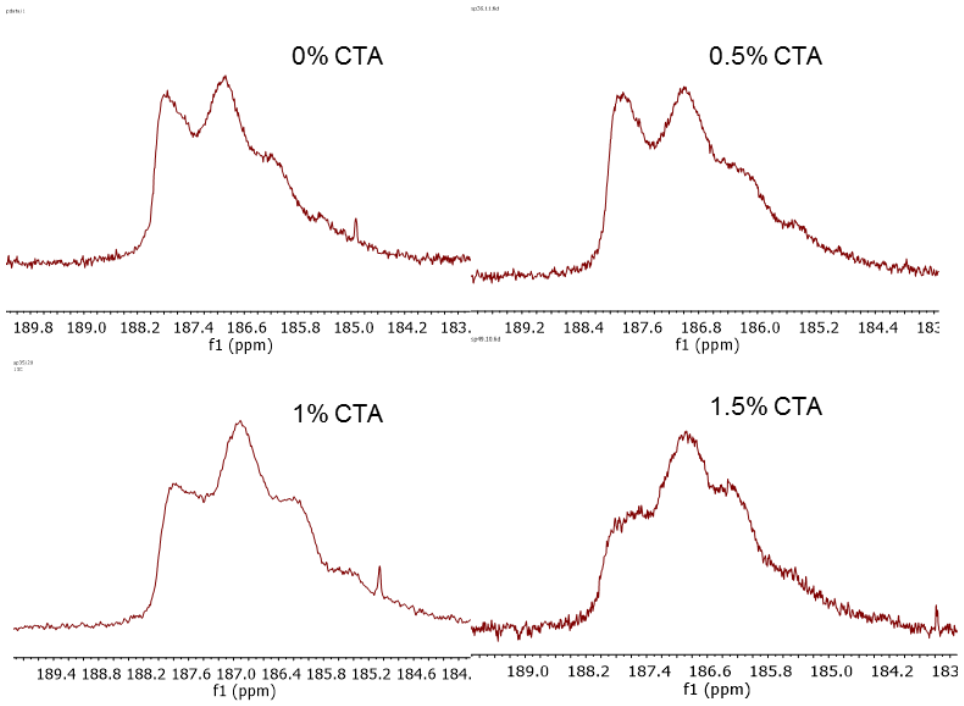

Figure 2.15: ^{13}C-NMR pattern of the carbonyl area of the synthesized copolymers with different CTA concentration.

To sum up, copolymers of MAA/PEGMA5 with different molar masses were synthesized, but unfortunately the composition of the chains, although it was targeted to be MAA/PEGMA = 3/1 was slightly different in each copolymer. The lower the molar mass the lower the incorporation of MAA and the higher the composition drift. These features will be considered when analyzing the effect of the copolymers in the hydration of cement in chapter 4.

Table 2.6.: Fraction of the triads obtained from ^{13}C-NMR measurements and the ideal fraction of triads (random copolymerization). A is MAA unit and B is PEGMA5 unit.

	Experimental			***Ideal***		
	Triad			***Triad****		
CTA Concentration	***(AAA)***	***(AAB)***	***(BAB)***	***(AAA)***	***(AAB)***	***(BAB)***
0.0% - S1	0.353	0.337	0.057	0.417	0.282	0.048
0.5% - S4	0.323	0.329	0.090	0.409	0.284	0.049
1.0% - S5	0.307	0.340	0.086	0.392	0.287	0.053
1.5% - S6	0.267	0.370	0.080	0.369	0.291	0.057

*Calculated using Bernouillian model: (AAA): Y_{MAA}^3; (AAB): $2 \cdot Y_{MAA}^2 \cdot (1-Y_{MAA})$; (BAB): $(1-Y_{MAA})^2 \cdot Y_{MAA}$; Y_{MAA} is the copolymer composition referred to MAA monomer.

2.4. Copolymer Composition Control Strategies

2.4.1. Open-Loop Optimal Addition Policies

Batch processes lead to copolymers with a gradual change in the incorporation of the monomers to the polymer chains copolymerizing with monomers with widely different reactivity ratios, referred as composition drift, as it has been observed previously in this chapter. Thus, this

type of processes are not suitable to obtain copolymers with a homogeneous copolymer composition[29]. Semibatch processes are more versatile for this aim due to its flexibility of operation. The versatility of semibatch reactors allows to produce copolymers with a given composition. For that, the comonomer concentration ratio in the reactor must be kept constant at the value which ensures the desired composition. The value can be easily determine from the Mayo-Lewis equation[2,30].

$$y_i = \frac{Rp_i}{Rp_i + Rp_j} = \frac{r_i \cdot f_i^2 + f_i \cdot f_j}{r_i \cdot f_i^2 + 2 \cdot f_i \cdot f_j + r_j \cdot f_j^2} \qquad \text{(eq: 2.10)}$$

Where r_i is the reactivity ratio of monomer i, f_i is the fraction of monomer i, and Rp_i is the polymerization rate of monomer i.

$$f_i = \frac{[M_i]}{[M_i]+[M_j]} \qquad \text{(eq: 2.11)}$$

As discussed in the introduction there are several feeding strategies that can be implemented to maintain fi or fi/fj in the desired value provided by the Mayo-Lewis equation. The monomer starved feeding strategy is the easiest and more straightforward one and it is likely the most used in industrial environment. However, as it has been shown in the previous section it presents some drawbacks: the copolymer composition is not controlled during the whole process (15-20% of the copolymer chains present lower composition referred to MAA than the targeted one) and the process time is too long (for this particular copolymer system monomer additions of 8 hours are employed).

Open-loop[3–5,31] and closed-loop[6–8] control strategies have been proposed in the literature to overcome these drawbacks of the starved addition strategies. Both strategies required a mathematical model of the copolymerization process and in addition closed-loop strategies required on-line measurements of the properties to be controlled; in this particular case the concentration of the monomers in the reactor.

In this work, open-loop control strategies have been considered and the optimal addition strategies developed by Arzamendi et al.[3–5] for the copolymer composition control in emulsion polymerization systems have been adapted for the free-radical aqueous solution copolymerization of MAA and PEGMA5.

The most efficient strategy is to maximize the concentration of the least reactive monomer in the reactor (considering the maximum heat removal capacity of the reactor) and feeding the most reactive monomer in such a way that the ratio of the comonomer concentrations is kept at the value that yields the desired copolymer composition[5]. Using the Mayo-Lewis copolymerization equation[2], the ratio of the concentrations of the comonomers [MAA]/[PEGMA5] needed to obtain a copolymer composition Y_{MAA} is given by:

$$R = \frac{[MAA]}{[PEGMA5]} = \frac{K - 1 + \sqrt{(K-1)2 + 4r_1 r_2 K}}{2r_1 r_2} \qquad \text{(eq: 2.12)}$$

Where $K = Rp_{MAA}/Rp_{PEGMA5} = Y_{MAA}/(1-Y_{MAA})$ and r_1 and r_2 are the reactivity ratios of monomer 1 (MAA) and monomer 2 (PEGMA5). The rate at which the most reactive monomer (PEGMA5) must be fed to maintain this ratio can be calculated from the material balances.

$$\frac{dMAA}{dt} = F_{MAA} - Rp_{MAA} \cdot V \qquad \text{(eq: 2.13)}$$

$$\frac{dPEGMA5}{dt} = F_{PEGMA5} - Rp_{PEGMA5} \cdot V \qquad \text{(eq: 2.14)}$$

and equation (2.12) as follows:

$$F_{PEGMA5} = \frac{Rp_{MAA}}{K} + \frac{1}{R}(F_{MAA} - Rp_{MAA}) \qquad \text{(eq: 2.15)}$$

Equation (2.15) gives the feed rate of the PEGMA5 (the most reactive monomer) as a function of the feed rate of the least reactive monomer, the desired copolymer composition and the polymerization rate of the MAA (the least reactive monomer). If heat removal rate is high (lab scale reactors) one can charge initially all the MAA (F_{MAA} = 0) in the reactor. For reactors with limited heat removal capacity (large scale reactors) only a fraction of MAA can be initially loaded and the rest should be fed maintaining the heat removal rate constraints[5].

In both cases to calculate the feed rate of PEGMA5, F_{PEGMA5}, the rate of consumption of MAA must be known. This requires having a predictive mathematical model of the copolymerization of MAA and PEGMA5, which is not available in the literature and it was developed in this work.

In order to calculate the optimal addition profiles from equation 2.12 and 2.15 the parameters of the kinetic model must be known. This includes the homopropagation rate constant of MAA and PEGMA5, the reactivity ratios, and the termination rate coefficients, among others. The better the accuracy of this kinetic parameters the better will be the prediction of the

optimal addition profile to produce homogeneous copolymers. Note that since this is an open-loop control strategy if there is any model mismatch (or non-modelled perturbation) the calculated monomer addition profile may not lead to the desired composition control.

To ensure that the model represents well the reality the kinetic parameters of the model were adjusted to fit batch and starved feed semibatch experiments. For the sake of readability of the chapter the description of the full mathematical model and the parameter estimation procedure and the obtained estimated parameters is presented and discussed in Appendix III. Here only the optimal trajectories calculated for PEGMA5 for each copolymer composition sought and the properties of the copolymers produced will be presented.

2.4.2. Implementation of Optimal Addition Policies to Produce MAA-co-PEGMA5 Copolymers with Homogeneous Composition

Optimal addition profiles for the production of MAA/PEGMA5 copolymers with homogenous composition 2/1, 3/1 and 4/1 were calculated based on the procedure described in the previous section and the kinetics estimated parameters (in Appendix II and III).

The experimental procedure for running these experiments was as follows:

The reactor is initially charged with an aqueous solution which contains part of both monomers (30% of the total amount of MAA and the calculated amount of PEGMA5 to ensure the initial composition sought) and which is neutralized to pH=7. Then, a fully ionized MAA water solution with a constant feeding rate was added to the reactor while PEGMA5 monomer was fed with a variable feeding rate (calculated as explained in the previous section). All the reactions

were performed at 90 ºC and initiated with the water soluble thermal initiator KPS. Three different reactions were performed in order to obtain copolymers with homogenous composition of (Y_{MAA} = 0.66, 0.75 and 0.8) with respect to MAA.

Table 2.7 presents the formulation used for the 3 targeted copolymers with the values of the initial amounts (in weight fraction) of MAA (30 wt% of total MAA amount) and PEGMA5 calculated according to the strategy discussed in the previous section.

Table 2.7: Formulations to prepare MAA/PEGMA5 copolymers with variable comonomer ratios employing the optimal addition policy.

Reaction	***MAA/PEGMA5 (2/1)***			***MAA/PEGMA5 (3/1)***			***MAA/PEGMA5 (4/1)***		
Ingredients	IC (wt%)	FMAA (wt%)	FPEGMA (wt%)	IC (wt%)	FMAA (wt%)	FPEGMA (wt%)	IC (wt%)	FMAA (wt%)	FPEGMA (wt%)
MAA	3.28	7.66		4.16	9.71		4.82	11.24	
PEGMA	1.47		17.59	1.37		14.76	1.47		12.48
H_2O	56.80	8.06		52.85	10.22		50.29	11.83	
NaOH	1.02	3.34		1.91	4.23		2.19	4.90	
$NaHCO_3$	0.18			0.19			0.18		
KPS	0.60			0.60			0.60		
Total	63.35	19.06	17.59	61.08	24.16	14.76	59.55	27.97	12.48

The addition of the rest of the less reactive monomer (70 wt% of MAA) was done in the three cases for 90 minutes.

Figure 2.16 presents the optimal addition profiles calculated for PEGMA5 (the total mass to be added is plotted for each polymerization). Also Figure 2.16 includes the constant flow rate

used for MAA in each experiment. The polymerizations were maintained for one hour more at the same temperature upon finishing the stream of PEGMA5.

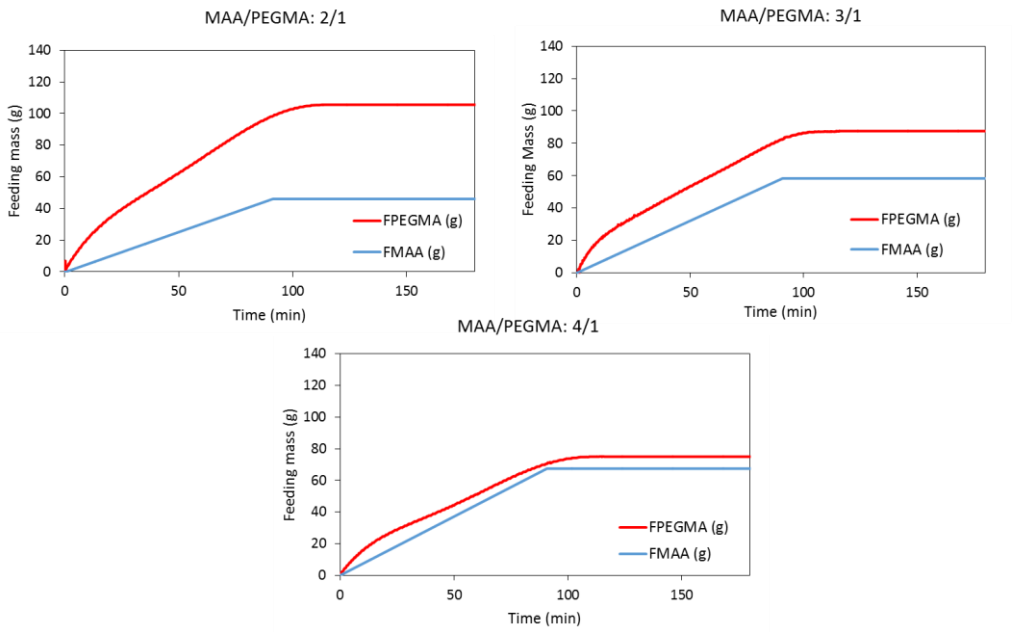

Figure 2.16: Optimal monomer addition profiles (total mass fed vs time) calculated for the production of MAA/PEGMA5 copolymers with homogeneous composition 2/1, 3/1 and 4/1.

Figure 2.17 presents the evolution of the individual and overall instantaneous conversion measured during the three optimal experiments. From this data the cumulative copolymer composition was calculated for each experiment and it is plotted in Figure 2.18.

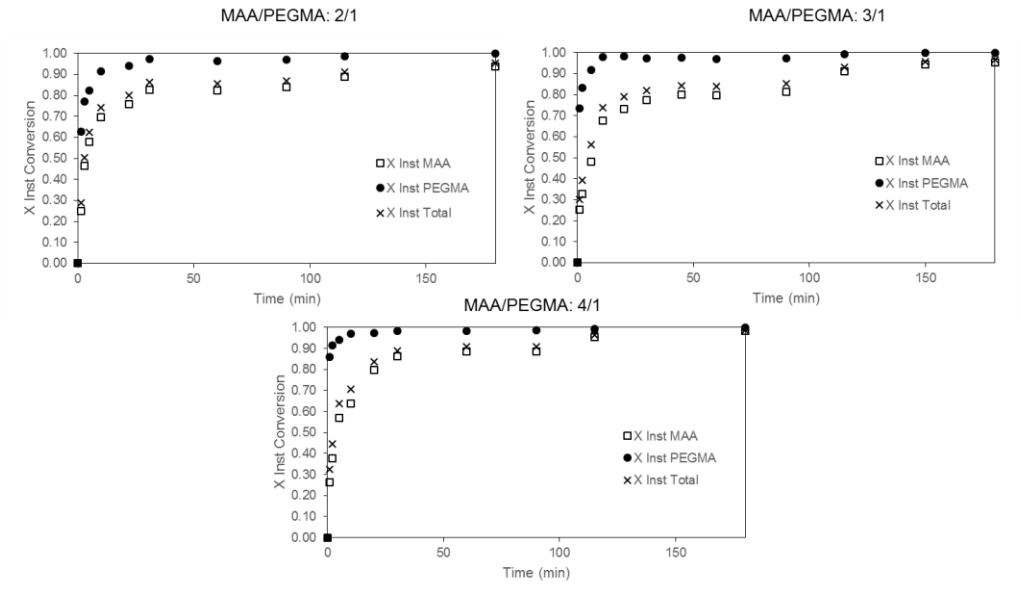

Figure 2.17: Time evolution of individual and overall instantaneous conversion for the copolymerizations of MAA and PEGMA5 with different comonomer ratios using the calculated optimal monomer addition profiles.

Figure 2.18 shows that the required copolymer composition has been produced during the whole process in substantially shorter time than that used in the semibatch monomer starved strategy. In other words, homogenous composition copolymers have been produced in shorter time.

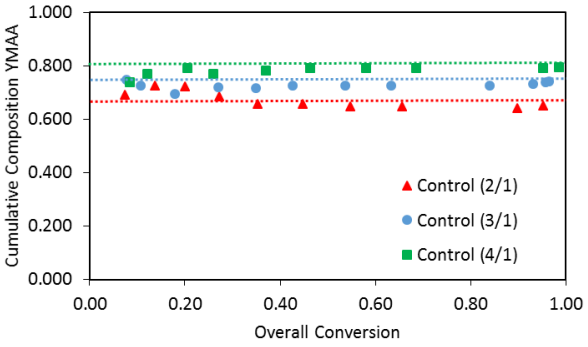

Figure 2.18: Conversion evolution of the cumulative copolymer composition of the poly(MAA-co-PEGMA5) copolymers with different comonomer ratios synthesized employing optimal monomer addition policies.

As can be observed in figure 2.19 the pattern of the carbonyl area of the copolymers is sufficiently well resolved and deconvolution into pentads was performed with ease. As it can be seen, the fraction of (AAA) triad increases substantially by increasing the MAA comonomer ratio. On the other hand, the fraction of (AAB) triad is similar in the three cases while the fraction of (BAB) triads decreases.

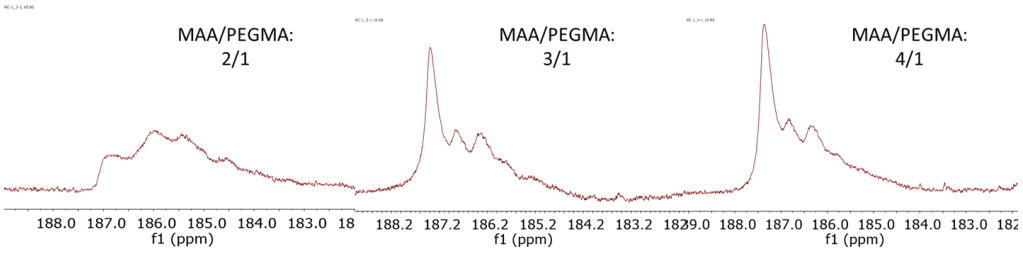

Figure 2.19: ^{13}C-NMR pattern of the carbonyl area corresponding to the carboxylic monomer of the synthesized copolymers with different comonomer ratios.

Table 2.8: Fraction of the triads obtained from the ^{13}C-NMR measurements and the ideal fractions of triads (random copolymerization) for the optimal addition experiments.

	Experimental			***Ideal****		
	Triad			***Triad***		
Reaction	***(AAA)***	***(AAB)***	***(BAB)***	***(AAA)***	***(AAB)***	***(BAB)***
MAA/PEGMA: 2/1 – C2	0.267	0.296	0.088	0.273	0.296	0.080
MAA/PEGMA: 3/1 – C1	0.417	0.292	0.032	0.417	0.282	0.048
MAA/PEGMA: 4/1 – C3	0.475	0.276	0.046	0.506	0.258	0.033

*Calculated using a Bernoullian model. Y_{MAA} is the composition referred to MAA monomer.

It can be observed that the experimental and ideal values of the triads are very close between them. This is an additional confirmation that homogeneous copolymer with the desired composition have been produced.

Molar masses of the synthesized copolymers were measured via aqueous GPC (SEC/MALS/RI) with a $NaNO_3$ 0.1M alkaline solution (pH>10) as eluent. The dn/dc values were also measured for each copolymer and they were compared with the values obtained for the copolymers produced under starved conditions (see Table 2.11). The differences in the measured dn/dc values can be attributed to the heterogeneity (15-20% of the overall) of the copolymers synthesized via starved conditions (see Figure 2.9).

Table 2.9: dn/dc values of the copolymers synthesized via optimal addition policies. The values of the copolymers synthesized via starved condition are included for the sake of comparison.

	Starved Conditions	***Optimal Addition Policies***
Comonomer Ratio	***dn/dc (ml/g)***	***dn/dc (ml/g)***
2/1	0.181	0.175
3/1	0.191	0.184
4/1	0.207	0.210

As can be observed in figure 2.20, there are not remarkable differences on the molar mass distributions of the three optimal experiments with different composition. Copolymers with 3/1 and 4/1 comonomer ratios tend to have slightly broader distribution and a bit higher Mw. Besides, the degree of polymerization obtained in the three cases is very similar.

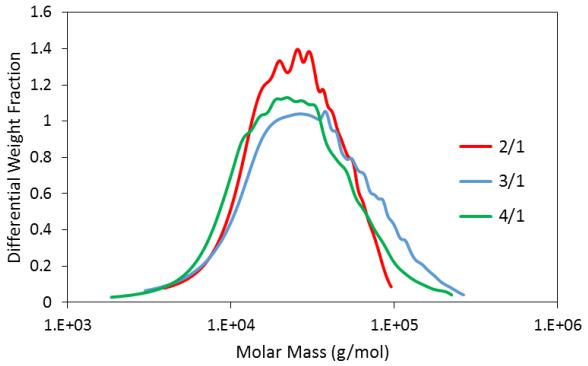

Figure 2.20: Molar mass distribution of the MAA/PEGMA5 copolymers synthesized using the optimal addition policies.

If the molar mass of the copolymers synthesized by optimal addition policies are compared with those synthesized under starved condition (see Table 2.4) it can be observed that

the molar mass and the degree of polymerization obtained under starved condition was substantially higher. One of the main differences between the two processes is the addition of the initiator. In the monomer starved experiments, the initiator was fed during 8h, while in the optimal addition policies the initiator was added in a shot at the start of the process. Hence, the radical concentration in the optimal addition experiments is much higher than in the monomer starved experiments. Note that one important characteristic of free-radical polymerization is that the size of the macromolecules produced is inversely proportional to the square root of the initiator concentration. Thus, higher initiator concentrations will lead to polymers with lower molar masses.

Table 2.11: Molar mass distribution, dispersity index and degree of polymerization of the MAA/PEGMA5 copolymers synthesized via optimal addition policies.

Comonomer Ratio	***Mw (kg/mol)***	**Đ**	***DP***
2/1 – C2	28.2 ± 0.6	1.6	116
3/1 – C1	41.3 ± 0.5	2.2	136
4/1 – C3	32.3 ± 0.3	2.0	126

2.5. Conclusions

In this chapter, the synthesis of MAA-co-PEGMA5 copolymers in neutral-alkaline conditions was studied. Firstly, the reactivity ratios of the comonomer pair when MAA was fully ionized were determined by a combination of in-situ ^{1}H-NMR measurements of copolymerization of MAA and PEGMA5 and a parameter estimation algorithm. It was found that PEGMA5 was

much more reactive than MAA and that the reactivity ratios depend on the monomer concentration (solids content).

Semibatch copolymerization is a route to produce homogeneous copolymers of widely different reactivity ratios, like in this case, MAA and PEGMA5 under fully ionized conditions of MAA in aqueous phase. One way is to employ starved monomer addition strategy, in which high polymerization rates are required. In order to reach to high polymerization rates 30 wt% SC, 2 wt% bwom of initiator, 90 ºC and 8 hours of feeding were employed. However, in this work we have demonstrated that industrially common starved feed strategy cannot guarantee the production of homogeneous copolymers of MAA-co-PEGMA5. From an industrial point of view this strategy is not very demanding due to its long process times and approximately 20% of the total polymer deviated from the desired composition. Furthermore, when water soluble CTAs were employed higher deviation from the expected value was observed due to a lower incorporation of the MAA.

In an attempt to improve the homogeneity of the copolymer chains advanced open-loop control strategies were developed. This strategy required the development of a mathematical model of the aqueous phase copolymerization of MAA and PEGMA5. The model took into account all the kinetic parameters such as the propagation rate coefficients and the reactivity ratios of the pair of monomers among others. Model details are presented in the Appendix III. Based on this model optimal addition strategies that allowed the production of homogeneous poly(MAA-co-PEGMA5) with 2/1, 3/1, and 4/1 copolymer compositions in substantially shorter times and with improved homogeneity of the copolymer composition have been developed. The robustness of the model and the strategy was verified by the determination of the comonomer sequence distribution.

2.6. References

(1) Doremaele, G. H. J. Van; Schoonbrood, H. A. S.; Kurja, J.; German, A. L. Copolymer Composition Control by Means of Semicontinuous Emulsion Copolymerization. *J. Appl. Polym. Sci.* **1992**, *45*, 957–966.

(2) Mayo, F. R.; Lewis, F. M. Copolymerization I. A Basis for Comparing the Behavior of Monomers in Copolymerization. The Copolymerization of Styrene and Methyl Methacryate. *J. Am. Chem. Soc.* **1944**, *66* (9), 1594–1601.

(3) Arzamendi, G.; Asua, J. M. Monomer Addition Policies for Copolymer Composition Control in Semicontinous Emulsion Copolymerization. *J. Appl. Polym. Sci.* **1989**, *38*, 2019–2036.

(4) Arzamendi, G.; Asua, J. M. Copolymer Composition Control During the Seed Emulsion Copolymerization of Vinyl Acetate and Methyl Acrylate. *Macromol. Symp.* **1990**, *35* (36), 249–268.

(5) Arzamendi, G.; Asua, J. M. Copolymer Composition Control of Emulsion Copolymers in Reactors with Limited Capacity for Heat Removal. *Ind. Eng. Chem. Res.* **1991**, *30* (6), 1342–1350.

(6) Leiza, J. R.; De La Cal, J. C.; Asúa, J. M. On-Line Copolymer Composition Control in the Semicontinious Emulsion Copolymerization of Ethyl Acrylate and Methyl Methacrylate. *Polym. React. Eng.* **1992**, *1* (4), 461–498.

(7) Urretabizkaia, A.; Leiza, J. R.; Asúa, J. M. On-Line Terpolymer Composition Control in Semicontinious Emulsion Polymerization. *AIChE J.* **1994**, *40* (11), 1850–1864.

(8) Asúa, J. M.; Sáenz de Buruaga, I.; Arotçarena, M.; Urretabizkaia, A.; Armitage, P. D.; Gugliota, L. M.; Leiza, J. R. On-Line Control of Emulsion Polymerization Reactors. *Dechema Monogr.* **1995**, *131*, 655–671.

(9) Bevington, J. C.; Harris, D. O. Reactivities of Acrylates and Methacrylates. *Polym. Lett.* **1967**, *5*, 799–802.

(10) Smith, B. L.; Klier, J. Determination of Monomer Reactivity Ratios for Copolymerizations of Methacrylic Acid with Poly (Ethylene Glycol) Monomethacrylate. *J. Appl. Polym. Sci.* **1998**, *68* (6), 1019–1025.

(11) Krivorotova, T.; Vareikis, A.; Gromadzki, D.; Netopilík, M.; Makuška, R. Conventional Free-Radical and RAFT Copolymerization of Poly(Ethylene Oxide) Containing Macromonomers. *Eur. Polym. J.* **2010**, *46* (3), 546–556.

(12) De La Cal, J.C., Leiza, J.R., Asúa, J. M. Estimation of Reactivity Ratios Using Emulsion Copolymerization Data. Journal of Polymer Science: Part A: Polymer Chemistry 1991, pp 155–167.

(13) García, G.; Cal, J. C. D. la. Síntesis de Floculantes Catiónicos En Reactores Continuos, PhD Thesis, University of Basque Country (UPV/EHU), Donostia-San Sebastián, 2009.

(14) Beuermann, S.; Buback, M.; Hesse, P.; Lacík, I. Free-Radical Propagation Rate Coefficient of Nonionized Methacrylic Acid in Aqueous Solution from Low Monomer Concentrations to Bulk Polymerization. *Macromolecules* **2006**, *39* (1), 184–193.

(15) Beuermann, S.; Buback, M.; Hesse, P.; Kukućková, S.; Lacík, I. Propagation Rate Coefficient of Non-Ionized Methacrylic Acid Radical Polymerization in Aqueous Solution. The Effect of Monomer Conversion. *Macromol. Symp.* **2007**, *248*, 41–49.

(16) Buback, M.; Hesse, P.; Hutchinson, R. A.; Lacík, I.; Kasák, P.; Stach, M.; Utz, I. Kinetics and Modeling of Free-Radical Batch Poymerization of Nonionized Methacrylic Acid in Aqueous Solution. *Ind. Eng. Chem. Res.* **2008**, *47* (21), 8197–8204.

(17) Lacık, I.; Lucia, U.; Beuermann, S. Propagation Rate Coefficient of Free-Radical Polymerization of Partially and Fully Ionized Methacrylic Acid in Aqueous Solution. *Macromolecules* **2009**, *42* (20), 7753–7761.

(18) Beuermann, S.; Buback, M.; Hesse, P.; Kukuc, S.; Lacik, I.; Hutchinson, R. A. Termination Kinetics of the Free-Radical Polymerization of Nonionized Methacrylic Acid in Aqueous Solution Termination Kinetics of the Free-Radical Polymerization of Nonionized Methacrylic Acid in Aqueous Solution. *Macromolecules* **2008**, *41* (10), 3513–3520.

(19) Smolne, S.; Weber, S.; Buback, M. Propagation and Termination Kinetics of Poly(Ethylene Glycol) Methyl Ether Methacrylate in Aqueous Solution. *Macromol. Chem. Phys.* **2016**, *217* (21), 2391–2401.

(20) Kazemi, N.; Duever, T. A.; Penlidis, A. Reactivity Ratio Estimation from Cumulative Copolymer Composition Data. *Macromol. React. Eng.* **2011**, *5* (9–10), 385–403.

(21) Cummings, S.; Zhang, Y.; Kazemi, N.; Penlidis, A.; Dubé, M. A. Determination of Reactivity Ratios for the Copolymerization of Poly(Acrylic Acid-Co-Itaconic Acid). *J. Appl. Polym. Sci.* **2016**, *133* (40), 6–11.

(22) Preusser, C.; Ezenwajiaku, I. H.; Hutchinson, R. A. The Combined Influence of Monomer Concentration and Ionization on Acrylamide/Acrylic Acid Composition in Aqueous Solution Radical Batch Copolymerization. *Macromolecules* **2016**, *49* (13), 4746–4756.

(23) Halverson, F.; Lancaster, J. E.; O'Connor, M. N. Sequence Distribution of Carboxyl Groups in Hydrolyzed Polyacrylamide. *Macromolecules* **1985**, *18* (6), 1139–1144.

(24) Borget, P.; Galmiche, L.; Le Meins, J. F.; Lafuma, F. Microstructural Characterisation and Behaviour in Different Salt Solutions of Sodium Polymethacrylate-g-PEO Comb Copolymers. *Colloids Surfaces A Physicochem. Eng. Asp.* **2005**, *260* (1–3), 173–182.

(25) Herbert, I. R. *Statistical Analysis of Copolymer Sequence Distribution. NMR Spectroscopy of Polymers*, 1 st.; Ibbett, R. N., Ed.; Springer: Coventry, UK, 1993.

(26) Plank, J.; Pöllmann, K.; Zouaoui, N.; Andres, P. R.; Schaefer, C. Synthesis and Performance of Methacrylic Ester Based Polycarboxylate Superplasticizers Possessing Hydroxy Terminated Poly (Ethylene Glycol) Side Chains. **2008**, *38*, 1210–1216.

(27) Fischer, E. J.; Storti, G.; Cuccato, D. Aqueous Free-Radical Polymerization of Non-Ionized and Fully Ionized Methacrylic Acid. *Processes* **2017**, *5* (2), 23.

(28) Cuccato, D.; Storti, G.; Morbidelli, M. Experimental and Modeling Study of Acrylamide Copolymerization with Quaternary Ammonium Salt in Aqueous Solution. *Macromolecules* **2015**, *48* (15), 5076–5087.

(29) Lacík, I.; Beuermann, S.; Buback, M. PLP-SEC Study into Free-Radical Propagation Rate of Nonionized Acrylic Acid in Aqueous Solution. *Macromolecules* **2003**, *36* (25), 9355–9363.

(30) Cutie, S. S.; Smith, P. B.; Henton, D. E.; Staples, T. L.; Powell, C. Acrylic Acid Polymerization Kinetics. *J. Polym. Sci. Part A Polym. Chem.* **1997**, *35*, 2029–2047.

(31) Arzamendi, G.; Asua, J. M. Strategies for Composition Control of Emulsion (CO/TER) Polymers. *Trends Polym. Sci.* **1991**, *2*, 27–46.

Chapter 3: Synthesis and Conformation of MPEG-type PCE Superplasticizers with Long Lateral Chains

3.1. Introduction

As explained in Chapter 2 poly(MAA-co-PEGMA) copolymers present a comb structure, where the backbone is anionically charged at alkali conditions but the side chains remain uncharged. In addition, the microstructural properties of the copolymers (MWD, backbone charge density or side chain length) may have a substantial effects on the hydration and rheological properties of the cementitous formulations[1–5]. Therefore, in this chapter, the aim is to synthesize copolymers with different side chain length and molar mass but keeping constant the comonomer ratio during the synthesis.

In this case, the PEGMA macromonomers which are employed for the synthesis of the copolymers contain 20, 45 and 113 ethylene glycol units (Mn = 950, 2000 and 5000 g/mol).

For all the copolymers synthesized the microstructure (cumulative copolymer composition, monomer sequential distribution and absolute molar masses) and the copolymerization kinetics, will be determined.

3.2. Experimental Part

Contrary to the MAA-co-PEGMA5 copolymers, the counterparts with larger side chain length are soluble in water under acidic and basic conditions (due to the increase of hydrophilicity of the copolymers by increasing the number of EG groups in the side chain[6]). Thus, for the synthesis of MAA-co-PEGMA copolymers with the larger units sought in this chapter, acidic conditions can be employed, which makes the synthesis of homogeneous composition copolymers easier because the reactivity ratios of MAA and PEGMA are similar (close to 1 for both monomers[7]) and hence monomer starved addition strategies will ensure the control of the copolymer composition. Therefore, semibatch free-radical solution copolymerization with constant feeding rates of the two monomers in the desired ratio in the copolymer should ensure the synthesis of copolymers with homogeneous composition.

The aqueous solution copolymerization reactions were carried out semibatchwise in a 1 L glass jacketed reactor with a mechanical stirrer rotating at 250 rpm. In a typical reaction a fraction (20 wt%) of the total amount of water of the formulation was initially loaded in the reactor. Then, the reactor was heated to 90ºC and a monomer aqueous solution and the initiator solution were fed into the reactor in two separate streams for 8 hours; the reaction was left one more hour for postpolymerization in order to get rid of the unreacted monomer. During the reaction nitrogen was bubbled in the reactor with a flow rate of 15 ml/min. The solids content of the copolymerizations were adjusted to produce copolymer solutions with reasonable viscosities. For some PEGMA's chain transfer agents were also included in the formulation with the same purpose of controlling the viscosity of the aqueous solution by reducing the molar mass. 3-mercaptopropionic acid (3-MPA) was used as CTA and all reactions were initiated by a water soluble thermal initiator KPS. Tables 3.1 and 3.2 summarize the characteristics and compositions

of the synthesized copolymers. Samples were withdrawn from the reactor at different times in order to analyze the evolution of the individual monomer conversions, cumulative copolymer compositions and molar mass distributions

Selected copolymers synthesized in this section were used as Superplasticizers for cementitious formulations prepared in next chapters.

Table 3.1: Characteristics of the synthesized copolymers.

PCE	Macromonomer	MAA/PEGMA	SC %	CTA %	pH	η (Pa·s) at $\dot{\gamma}$ = 10 s^{-1}
M1	PEGMA 20	3/1	20.26	0	2.2	0.013
M2		3/1	30.49	0	1.8	0.083
L1	PEGMA 45	3/1	20.80	0	2.1	0.055
L2		3/1	20.55	1	2.0	0.034
L3		3/1	20.64	2	2.1	0.020
XL1	PEGMA 113	3/1	10.89	4	2.1	0.023

Table 3.2: Formulations to prepare MAA/PEGMA copolymers with PEGMA macromonomers of different side chain lengths by semicontinuous aqueous solution copolymerization.

PCE	**M1**		**M2**		**L1**		**L2**		**L3**		**XL1**	
Ingredients	**IC* wt%**	**F** wt%**	**IC wt%**	**F wt%**	**IC wt%**	**F wt%**	**IC wt%**	**F wt%**	**IC wt%**	**F wt%**	**IC wt%**	**F wt%**
MAA	0.00	4.20	0.00	6.30	0.00	2.31	0.00	2.28	0.00	2.3	0.00	0.52
PEGMA	0.00	15.37	0.00	23.14	0.00	17.74	0.00	17.63	0.00	17.74	0.00	10.12
$NaHCO_3$	0.00	0.12	0.00	0.13	0.00	0.13	0.00	0.13	0.00	0.13	0.00	0.08
3-MPA	0.00	0.00	0.00	0.00	0.00	0.00	0.00	0.04	0.00	0.08	0.00	0.04
H_2O	20.02	59.88	20.06	49.80	20.00	59.42	20.01	59.51	20.01	59.35	20.09	68.93
KPS	0.00	0.41	0.00	0.60	0.00	0.40	0.00	0.40	0.00	0.39	0.00	0.21

* IC - Initial Charge
**F - Feeding

3.3. Copolymerization Kinetics and Cumulative Copolymer Composition

Kinetics was monitored by ^{1}H-NMR analysis of the samples withdrawn from the reactor by employing the watergate sequence. Figures 3.1-3.3 show the instantaneous individual and overall conversions for the experiments listed in Table 3.2.

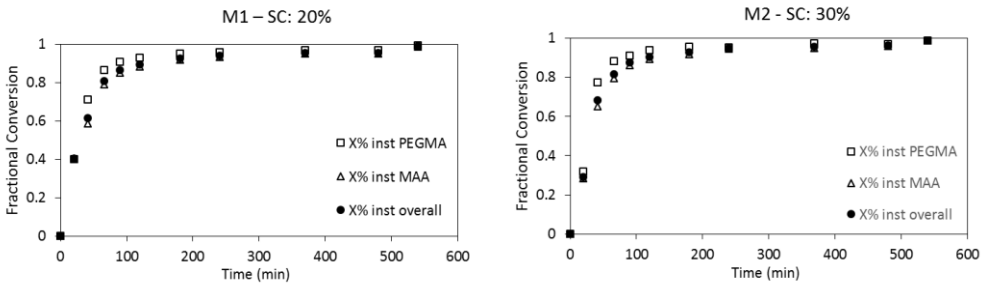

Figure 3.1: Time evolution of individual and overall conversions for the copolymerizations of MAA and PEGMA20 (20 EGu) with different SC.

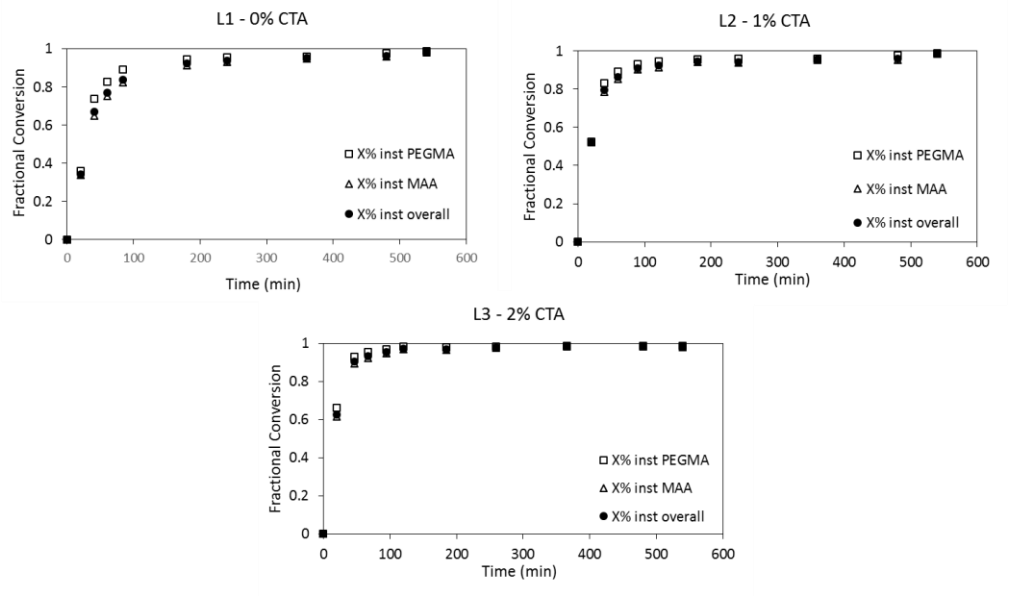

Figure 3.2: Time evolution of individual and overall conversions for the copolymerizations of MAA and PEGMA45 (45 EGu) with 20 wt% solids content and with different CTA content.

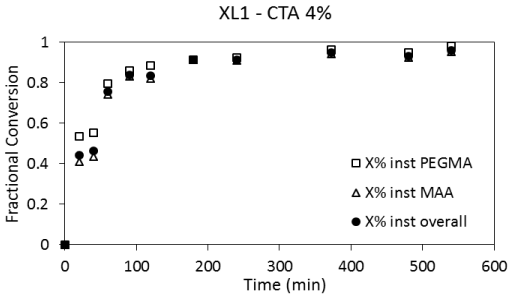

Figure 3.3: Time evolution of individual and overall conversion for the copolymerization of MAA and PEGMA113 (113 EGu) at 10 wt% solids content with 4% bmom of CTA.

As it can be seen, the conversion of both monomers is very similar even though PEGMA monomer conversion is slightly higher in all the copolymerizations. The similarity in the conversion is expected since the reactivity ratios in acid conditions are close to the unity for both monomers (r_{MAA}: 1.02, r_{PEGMA}: 1.03)[7]. Consequently, minimum composition drift was obtained and copolymers with homogeneous cumulative composition during the whole process were synthesized as shown in Figure 3.4. High instantaneous conversions (> 90%) were achieved in 120 minutes in all reactions except for XL1 that required around 180 minutes. This is mainly due to the lower SC employed. Full conversion was reached in all polymerizations except for the case XL1 (97% conversion).

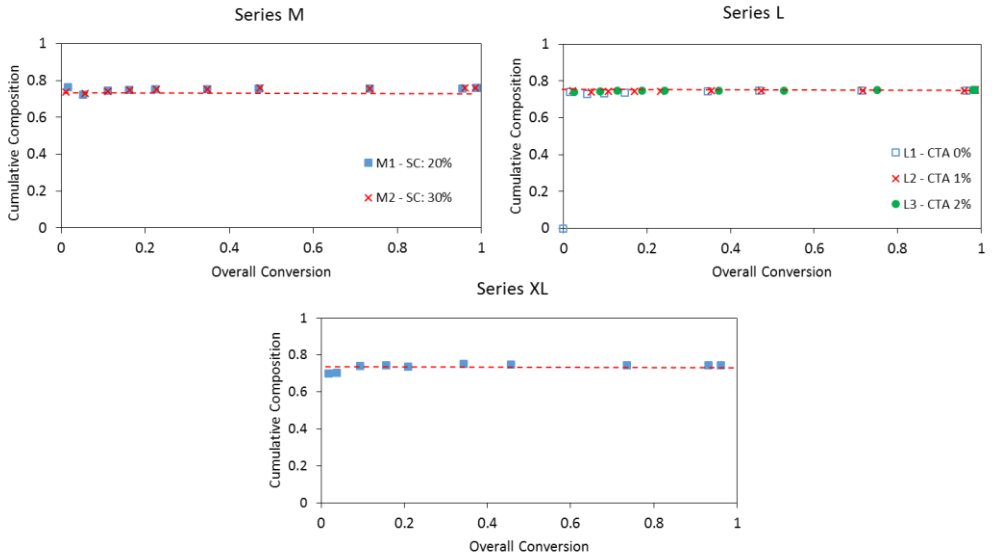

Figure 3.4: Conversion evolution of the cumulative copolymer composition referred to MAA comonomer for the MAA/PEGMA copolymers synthesized in semibatch conditions.

3.4. Monomer Sequence Distribution

From the analysis of the cumulative composition it can be expected that comonomers in the chains are homogeneously distributed. To verify it, ^{13}C-NMR was employed to analyze the monomer sequence distribution of the chains. The carbonyl peaks were analyzed performing a Lorentzian deconvolution. In the previous chapter, a deconvolution into pentads was performed, in order to later relate the intensities of the pentads with the triads[8]. In this case, the resolution of the pentads is not good enough and, hence the deconvolution of the spectra was done into triads[9]. The low resolution of the spectra is because of the high intensity of the polyethylene glycol group of the lateral chains (the same comonomer molar ratio was used and hence the number of EG units substantially increases as the side chain length of the PEGMA increases), that makes the intensity of the carbonyl peaks too low. Figure 3.5 presents the full spectrum of reaction (L1) in which the shift of the (CH_2-CH_2-O) group (δ: 69.5 ppm) shows the highest intensity. Therefore, the ^{13}C-NMR analyses were performed with a selected pulse to increase the resolution of the carbonyl peaks.

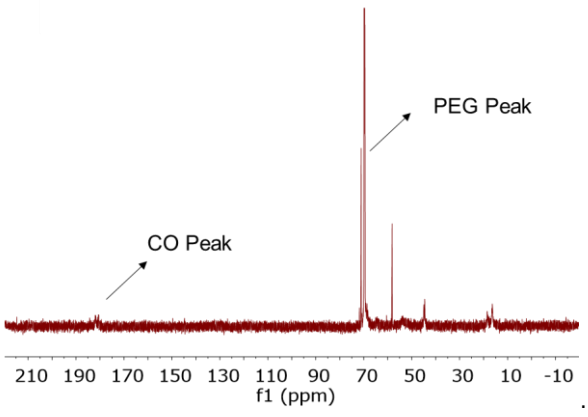

Figure 3.5: ^{13}C-NMR full spectrum of the L1 reaction.

As can be seen in figures 3.6-3.8 the resolution of the spectra decreases as the length of the side chain of the PEGMA comonomer increases. However, the shape of the carbonyl pattern is more defined than in the case of series S copolymers (see chapter 2.3.2); thus, more homogeneous monomer sequence distribution can be expected. Table 3.3 summarizes the experimental and theoretical values of the different triads.

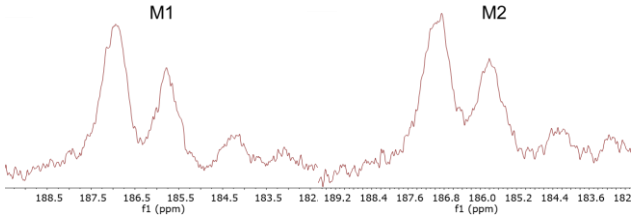

Figure 3.6: ^{13}C-NMR pattern of the carbonyl area corresponding to the carboxylic monomer of the series M copolymers.

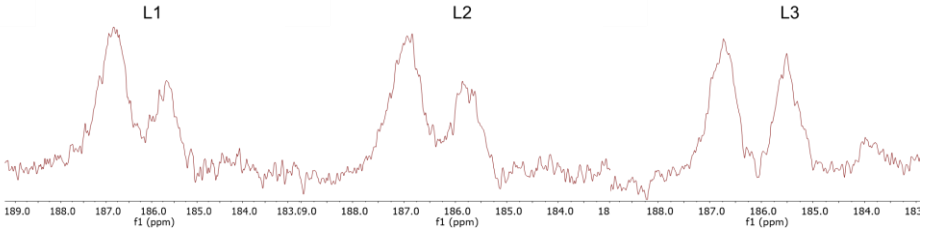

Figure 3.7: ^{13}C-NMR pattern of the carbonyl area corresponding to the carboxylic monomer of the series L copolymers.

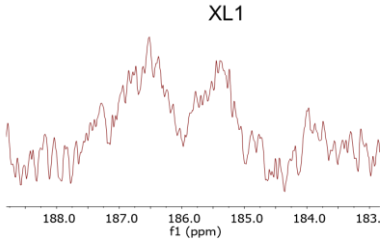

Figure 3.8: ^{13}C-NMR pattern of the carbonyl area corresponding to the carboxylic monomer of the series XL copolymers.

Table 3.3: Fraction of the triads obtained from the Lorentzian deconvolution for each copolymer. Experimental and theoretical values are included for the sake of comparison.

	Experimental			***Ideal***		
	Triad			***Triad****		
PCE	***(AAA)***	***(AAB)***	***(BAB)***	***(AAA)***	***(AAB)***	***(BAB)***
M1	0.447	0.243	0.068	0.436	0.278	0.044
M2	0.439	0.263	0.058	0.438	0.278	0.044
L1	0.440	0.247	0.064	0.422	0.281	0.047
L2	0.446	0.248	0.056	0.422	0.281	0.047
L3	0.409	0.265	0.076	0.420	0.282	0.047
XL1	0.424	0.252	0.070	0.412	0.283	0.049

A letter represents the carboxylic monomer MAA and B represents the PEGMA macromonomer. *Calculated using the Bernoullian model: (AAA): Y_{MAA}^3; (AAB): $2 \cdot Y_{MAA}^2 \cdot (1-Y_{MAA})$; (BAB): $(1-Y_{MAA})^2 \cdot Y_{MAA}$

It is remarkable the good agreement existing between the experimentally determined triad fractions and those corresponding to a random copolymerization ($r_1=r_2=1$). The small discrepancies observed, more noticeable for (BAB) triad, are likely due to low resolution of the

shift in the range δ: 183.8-185 ppm. The sequence distribution further confirms the homogeneity of the composition of all the copolymer synthesized with large number of EG units in the lateral chains, and very close reactivity ratios (and close to 1) of the comonomers. Note that copolymers with homogeneous composition like these ones were also produced with the short PEGMA in neutral-alkali conditions when using the optimal addition profiles.

3.5. Molar Mass Distributions and Radius of Gyration

Molar masses, dispersities and radius of gyration of the synthesized copolymers were analyzed by means of GPC (SEC/RI/MALS), details of the equipment employed can be found in Appendix I. As for the MAA/PEGMA5 copolymer the dn/dc values were determined for each copolymer.

Table 3.4: dn/dc values for MAA/PEGMA (3/1 ratio) copolymers with different number of EG units in the PEGMA monomer.

PEGMA Side Chain Length	***dn/dc (ml/g)***
5 EGu	0.191
20 EGu	0.154
45 EGu	0.124
113 EGu	0.116

Most of the literature reports for these type of copolymers either use the molar masses referred to PEO standards, which leads to a substantial deviation from the actual values as recently reported by Flatt et al.[10] or calculate on-line[10] the dn/dc assuming 100% recovery of the injected sample, which is not always the case or used directly the dn/dc of PEO (0.135 ml/g)[11–13] which as shown above might lead to wrong values with implication on the elucidation of the

conformation of these comb like copolymers and their adsorption mechanism in cementitious particles[14,15].

Table 3.5 and Figures 3.9-3.11 show the weight-average molar mass, dispersity and the MWDs for all the copolymers synthesized. For series M, PEGMA with 20 EGu in the lateral chain, the molar mass increases with the solids content. Note that in the experiment at 30% solids content the initiator concentration was also increased (the same percentage based on monomer was used; see Table 3.2) and hence the increase of the polymerization rate by the increase of the monomer concentration can be compensated by the increased radical concentration, (increased radical termination rate) and this might compensate the expected increase of the molar mass by an increase on the solids content. However, molar mass increases and according to Figure 3.9 a shoulder at molar masses above 10^5 g/mol is produced at 30% SC. This shoulder is likely caused by the higher viscosity of the reaction in the 30% SC experiment that yield and enhanced gel effect and the increase of the molar mass.

Table 3.5: Molecular characteristics of the synthesized PCEs.

PCE	$\overline{Mw}$ (kg/mol)	Mn Side Chain (g/mol)	Đ	$\overline{DP}$*
M1	46.2 ± 0.2	950	2.0	75
M2	81.6 ± 0.3	950	3.0	88
L1	794.9 ± 8.2	2000	11.5	122
L2	184.7 ± 0.8	2000	4.1	79
L3	88.5 ± 0.4	2000	2.4	64
XL1	1303.5 ± 14.6	5000	12.3	80

* DP is calculated from Mn using an average molar mass of the repeating unit based on the copolymer composition of each experiment. DP = Mn/RU

The repeating unit can be defined as follows:

$$RU = f_{MAA} \cdot Mw_{MAA} + f_{PEGMA} \cdot Mw_{PEGMA}$$

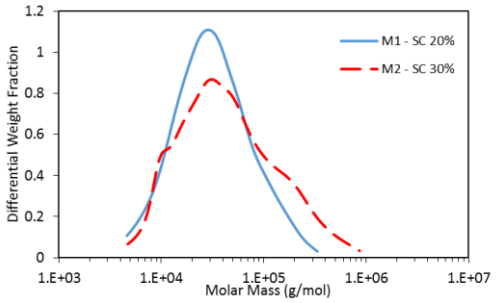

Figure 3.9: Molar mass distribution of the M (MAA/PEGMA20) series copolymers.

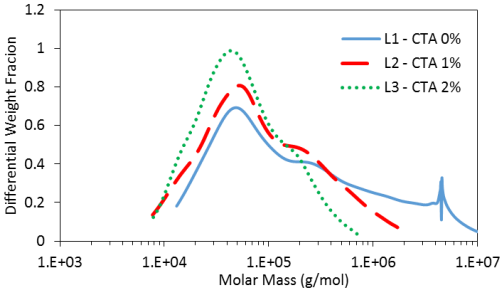

Figure 3.10: Molar mass distribution of the L (MAA/PEGMA45) series copolymers.

For series L, PEGMA with 45 EGu in the lateral chain, increasing the concentration of CTA decreased the average molar masses and narrowed the dispersity. The MWD for the PEGMA 45 shows a clear shoulder in all the copolymers, but the shoulder at high molar masses achieved in absence of CTA ($3 \cdot 10^5$-$1 \cdot 10^7$ g/mol) is substantially reduced by the addition of CTA. This is an indication that by shifting the termination of chains from a bimolecular mechanism (termination by combination or disproportionation of growing chains) to a homomolecular mechanism where only a single growing chain and the CTA molecules are involved, has a

tremendous impact on the molar masses. This is a clear indication that gel effect is partially suppressed by the addition of CTA.

For series XL, PEGMA with 113 EG units in the lateral chains, the copolymerization was carried out at lower solids content, 10 wt%, and with high CTA amount (4 mol % based on monomer) in order to get aqueous solutions with manageable viscosity. The absolute average molar mass obtained is of about 1.3 $\cdot 10^6$ g/mol and with a very broad dispersity, although the degree of polymerization is in the order of those obtained for shorter PEGMAs.

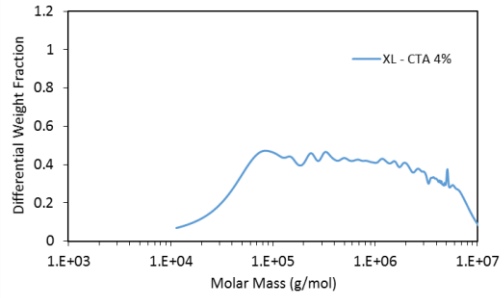

Figure 3.11: Molar mass distribution of the XL (MAA/PEGMA113) series copolymer.

Figures 3.12 and 3.13 show the distribution of the radius of gyration distributions for the synthesized copolymers (series S, M, L and XL). It is worth noting that the multi-angle light scattering detector used does not allow to measure macromolecules with radius of gyration below 10 nm. This means that for the copolymers with low molar masses, the distribution of radius of gyration will not correspond to the whole polymer. Unfortunately, the copolymer of series S synthesized using the optimum addition profiles (named as C1, C2 and C3) the amount of copolymer chains with radius of gyration higher than 10 nm is low, and they are not representative of the whole sample and therefore, were not represented in the here.

Figure 3.12 shows the distribution of radius of gyration for series S. For the copolymers with a MAA/PEGMA = 3/1 ratio and different molar masses (see chapter 2) the distributions are in agreement with the molar mass distributions and are narrower for the experiments with CTA. For the experiments with different MAA/PEGMA ratios (Figure 3.12 B) the result is interesting because the molar mass distributions for cases 3/1 and 2/1 are very similar (indeed the molar mass for copolymer with ratio 2/1 is higher than for copolymer with ratio 3/1 (see Figure 2.11 and Table 2.4) but the radius of gyration show the opposite trend; namely, the radius of gyration for 3/1 are higher than for 2/1.

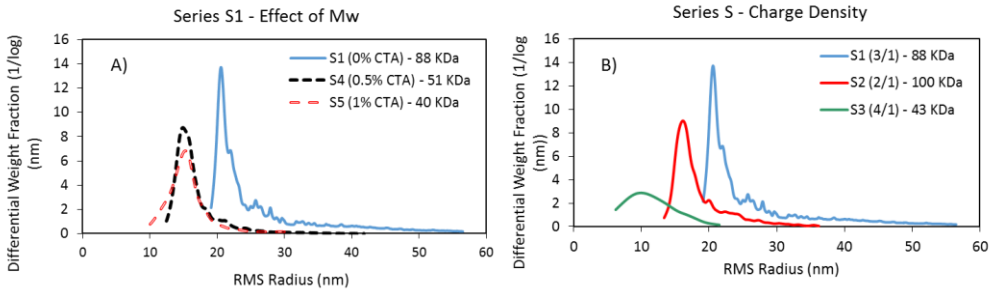

Figure 3.12: RMS radius distribution for series S copolymers. A) Comparison of copolymers with variable degree of polymerization. B) Comparison of copolymers with variable monomer ratio.

Figure 3.13 shows the distributions of radius of gyration for the copolymers of series M, L and XL. The distributions are in good agreement with the molar mass distributions. Thus, the copolymer with higher molar masses and broader distributions also led to higher radius of gyration and broader distributions. This is clearly illustrated in Figure 3.13B for series L that correspond to copolymers with 3/1 composition produced with increasing amount of CTA.

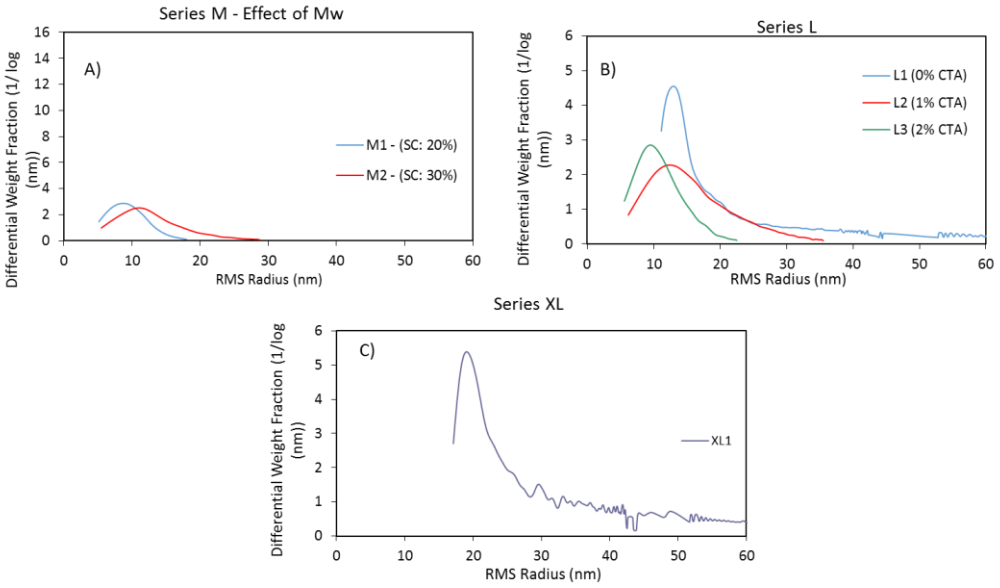

Figure 3.13: RMS radius distribution for Series M, L and XL copolymers.

3.6. Architecture and Conformation in Solution of Comb Copolymers

3.6.1. Theory for Linear and Comb-Like Polymers

In order to understand the microstructure-property relationship between the comb-like macromolecules (used as superplasticizers) and cement or other inorganic particles, the knowledge of their conformation in solution is a must[14]. For that, in this last part of the chapter the conformation of the macromolecules synthesized were determined using recently developed models for comb-like copolymers with similar compositions to these synthesized in this work[10,14].

The models used to describe the conformation of comb-like copolymers in solution are based on the scaling law developed by Flory[16]. This law was developed for linear polymers in a

good solvent for which the average end-to-end distance, R, can be calculated, minimizing the Flory free energy A_F. This energy can be written as a sum of the elastic energy and the excluded volume energy term[14]:

$$\frac{A_F}{k_B T} = \frac{3R^2}{2Pa^2} + Pv\frac{P}{R^3} \qquad \text{(eq: 3.1)}$$

$$v = a^3(1 - 2\chi) \qquad \text{(eq: 3.2)}$$

a is the monomer size, *P* the number of monomer in the chain and *v* the excluded volume that depends on the Flory parameter χ (eq. 3.2). Minimization of eq 3.1 leads to:

$$R = (1 - 2\chi)^{1/5} a P^{3/5} \qquad \text{(eq: 3.3)}$$

that shows that the power dependence of the radius of gyration and the molar mass of linear chains is 3/5.

Gay and Raphael extended the model to comb-like homopolymers using the approach of Brochard and de Gennes[17,18] for star polymers that is based on permeation studies using nanoscale pores. More recently, this model was adapted by Flatt et al.[14] to the comb-like copolymers used as superplasticizers, PCE's. In this upgraded model, the polymer backbone is defined as the assemblage of n repeating structural units, each containing N monomers and one side chain of P monomers (see Figure 3.14). Five different type of conformations were then defined: flexible decorated chains (FDC), flexible backbone worm (FBW), stretched backbone worm (SBW), stretched backbone star (SBS), and flexible backbone star (FBS).

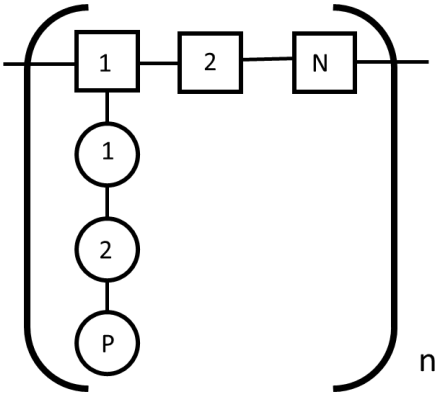

Figure 3.14: Description of a segment (bluiding block) in a comb copolymer chain as proposed in references[14,15]. The copolymer chain contains n segments (building blocks), with N monomer units in each segment (building block) and P repeating units in the side chains.

Thus, if P < N namely the side chain is short, the whole chain behaves like a simple chain of n x N monomer units decorated with swollen side chains. The regime of the backbone conformation is flexible and hence copolymers with this structure have a Flexible Decorated Chain (FDC) conformation.

If P is very long, that is very long side chains, the overall conformation is of a star with n arms each of length P. Two regimes can be distinguished in this case: I) If the number of monomer units in the backbone between side chains is small; N < n, then the backbone is completely stretched and this conformation is known as stretched backbone star, SBS. II) If N is large the backbone is weakly stretched and hence this conformation is called Flexible backbone star, FBS. In the two conformations the central region of the star contains the backbone.

If P is reduced (side chain length reduced) at some point the side chains do not extend beyond the core region. This occurs when P is equal to the number of monomer units in the core region. In this case the molecules develop into self-avoiding wall of each core and hence resembles a wiggling worm that can show stretched (SBW) or flexible (FBW) conformation regimes.

These regimes were conveniently assembled into a phase diagram by Gay and Raphael as shown in Figure 3.15.

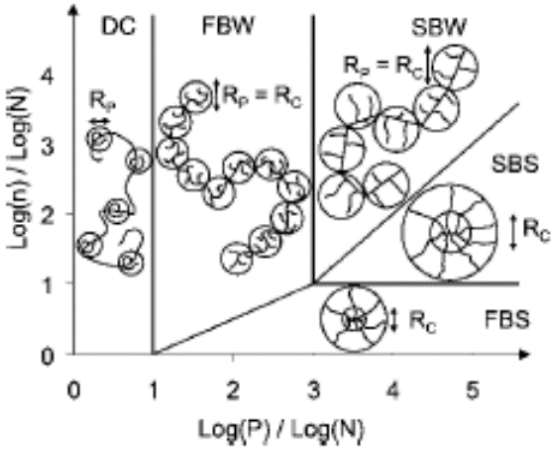

Figure 3.15: Phase diagram for comb copolymers adapted by Flatt et al.[14] based on the proposed scheme of Gay and Raphael[15]. DC: Decorated chain; FBW: Flexible backbone worm; SBW: Stretched backbone worm; SBS: Stretched backbone star; FBS: Flexible backbone star.

For the FBW conformation, which is the most likely for comb-like copolymers used as PCEs in cementitious formulations[14], this type of conformation can be viewed as a chain of cores,

each having a radius of gyration of (actually average end-to-end distance) Rc, and the overall polymers radius of gyration, R, following the Flory scaling law[16]

$$R = Rc\left(\frac{n}{n_c}\right)^{3/5} \qquad \text{(eq: 3.4)}$$

where, n_c is the number of side chains in a core. Each core can be viewed as borderline case between the FBW and FBS conformations. This imposes the condition that for each core:

$$n_c{}^2 = P/N \qquad \text{(eq: 3.5)}$$

which implies that the elastic energy of the side chains and the backbone section in the core are equal in a core.

The size of a core is obtained by minimizing its Flory energy:

$$\frac{A_F}{k_B T} = \frac{3}{2}\frac{R_c^2}{N_a^2} + \frac{3}{2}n_c\frac{R_c^2}{P_a^2} + n_c P_v\frac{n_c P}{R_c^3} \qquad \text{(eq: 3.6)}$$

This energy includes an elastic energy for both the backbone segment (first term) and one for the side chains (second term). The third term corresponds to the excluded volume energy of the side chain segments in a core. Indeed, each of the $n_c P$ monomers feels an average concentration of the order of $n_c P/R_c^3$, hence having an excluded volume energy of the order of $v n_c P/R_c^3$. Multiplying the latter expression by the number of monomers, $n_c P$, leads to the expression in eq. 3.6.

Minimization of eq. 3.6 and the use of 3.5 and 3.4 fields yields the polymer radius of gyration[14].

$$R = (1-2\chi)^{1/5} a P^{2/5} N^{1/5} n^{3/5} \qquad \text{(eq: 3.7)}$$

By using different sizes of monomers in the backbone and in the side-chain Flatt et al.[14] adapted the equation developed by Gay and Raphael[15] (eq. 3.7) to be used in comb-like copolymers. Thus, the Flory equation can be written as:

$$\frac{A_F}{k_B T} = \frac{3}{2}\frac{R_c^2}{n_c N_{a_N}^2} + \frac{3}{2} n_c \frac{R_c^2}{P_{a_p}^2} + n_c P_{a_p}^3 (1-2\chi)\frac{n_c P}{R_c^3} \qquad \text{(eq: 3.8)}$$

where a_N is the backbone monomer size, a_P the side-chain monomer size and the number of side chains in a core is given by:

$$n_c{}^2 = \frac{P}{N}\left(\frac{a_p}{a_N}\right)^2 \qquad \text{(eq: 3.9)}$$

which leads to the following equation for the radius of gyration of the polymer:

$$RG = \left(\left(\frac{a_N}{a_p}\right)^2 \frac{(1-2\chi)}{2}\right)^{1/5} a_P P^{2/5} N^{1/5} n^{3/5} \qquad \text{(eq: 3.10)}$$

For the comb-like copolymers synthesized in this work that contain methacrylate monomers in the backbone and poly(ethylene oxide) side chains the values for the sizes of the

monomers units are known; a_P = 0.25 nm and a_N = 0.36 nm[14]. The interaction parameter χ for PEO was also recently reported to be 0.37 at 25 ºC[19].

3.6.2. Conformation of Comb-like Copolymers of Series S, M, L and XL

According to the model developed by Flatt et al.[14] it is possible to determine the type of conformation of the PCE's synthesized in this work and to predict the radius of gyration (eq. 3.10) provided that the values of n, P and N can be determined.

The number of segments, n, can be determined as the degree of polymerization of the copolymer chain (DP) divided by the number of monomer units in each segment, N (number of MAA and PEGMA monomer units in a segment), and P is equal to the number of EG repeating units in the PEGMA macromonomer.

These values were obtained as follows: P is known from the PEGMA macromonomer supplier. In addition, the macromonomers were analyzed by MALDI-TOF and the average values of the absolute molar mass obtained did match reasonably well with the values reported by the suppliers (see Appendix I) and hence P values of 5, 20, 45 and 113 were used.

The values of N can be determined from the ratio MAA/PEGMA used in the formulation provided that homogeneous copolymers were produced along the polymerization. As shown in chapter 2 were comb-like copolymers with PEGMA5 were synthesized this condition was not fulfilled for the PCE's synthesized using the monomer starved semibatch polymerization which produced at least 20% of the polymer with a composition drift with respect to the target values. This inhomogeneity was further confirmed by the ^{13}C-NMR measurements of the monomer

sequence distribution that showed a lower amount of AAA triads than the corresponding to an ideal random copolymerization. Therefore, using the MAA/PEGMA ratio will overestimate the actual value for the PCE's synthesized in chapter 2. Otherwise, in this chapter (series M, L and XL with longer PEGMA macromonomers) homogeneous copolymers were produced and hence the value of N can be safely taken as the ratio of MAA/PEGMA used in the formulation. For series S the ratio MAA/PEGMA is only accurate for the experiments carried out with optimal addition profiles that yield homogeneous copolymer compositions.

To calculate the value of n for each PCE the degree of polymerization is needed. Gelardi et al.[10] have very recently discussed about the appropriateness of SEC measurements to determine the value of n. They claimed that the values of n cannot be accurately determined using SEC (even using MALS detectors that yield absolute molar masses) if the PCE's are synthesized by free-radical copolymerization. According to them, they can only be accurately determined if the PCE's are produced by esterification and provided that the backbone is previously characterized by SEC (MALS) and the value of N known (measuring grafting by NMR). Nevertheless, in this work, we have calculated n using SEC/MALS data to determine the degree of polymerization (with accurate values of dn/dc measured independently for each copolymer instead of determining on-line the dn/dc assuming 100% of mass recovery as done by Gelardi et al.[10]).

First, the conformation of the comb-like copolymers synthesized in this work was determined based on the criteria described above using the experimentally determined values of n, P and N listed in Table 3.6. Figure 3.16 displays the conformation of the copolymer in the phase diagram proposed by Gay and Raphael[15].

As can be seen in table 3.6 and Figure 3.16 most of the copolymers synthesized present a flexible backbone worm like conformation except for the XL1. Note that the copolymers that contain short lateral chains (synthesized in chapter 2 named as S1 to S6 the ones synthesized by starved semibatch method and name C1 to C3 the ones synthesized by optimal addition method) have a very linear structure and are at the boundary of being considered as decorated chains. In these cases, the higher the ratio of MAA to PEGMA monomer the closer to the decorated chain conformation. On the other hand, XL1 presents a stretched backbone worm like conformation, but it is worth noting that the MWD for this copolymer has a very broad dispersity (Đ = 12). Thus, there are chains that do not present SBW conformation. Chains with Mn < 40 kg/mol will present a stretched backbone star structure (SBS), however, the population of these chains will be relatively small.

Second, the scaling laws proposed by the group of Flatt to relate the model microstructure of comb-like PCE's (namely the values n, P and N) with the radius of gyration of the macromolecules in a good solvent were also assessed in this work by comparing the predictions of eq. 3.10 for the radius of gyration (using the values of n, P and N listed in Table 3.6 calculated and described above) with measurements of the radius of gyration (SEC/MALS). Gelardi et al.[10] have recently concluded that the scaling law models developed for comb-like copolymer PCE's (synthesized by esterification process) captured relatively well the dependencies on the molecular structure properties, although the absolute values were not in full agreement. In this work, they also claimed that the value of n of the PCE's cannot be calculated by SEC when the PCE's are produced by free radical copolymerization. The same exercise was done here for the PCE's synthesized in chapter 2 and 3 by free radical copolymerization and with the values of n calculated by SEC/MALS as explained above.

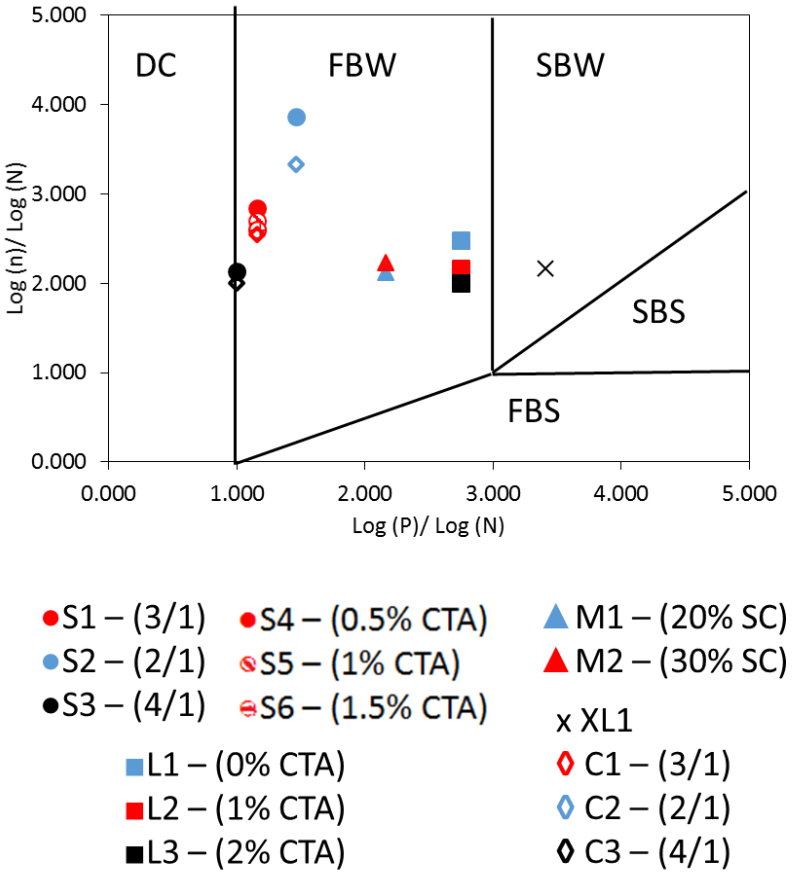

Figure 3.16: Phase diagram for comb copolymers synthesized in this work.

Table 3.6: Characteristics and classification of the selected PCEs synthesized in chapters 2 and 3 based on the conformation proposed by Gay and Raphael and adapted by Flatt.

PCE	*P*	*N*	*n*	*Calculated Rc (nm)*	*log (n)/log (N)*	*log (P)/log (N)*	*Classification*
S1 - (3/1 - 0% CTA)	5	4	51	0.692	2.836	1.161	FBW-DC
S2 - (2/1)	5	3	70	0.712	3.867	1.465	FBW
S3 - (4/1)	5	5	31	0.676	2.134	1.000	FBW - DC
S4 - (0.5% CTA)	5	4	42	0.692	2.696	1.161	FBW - DC
S5 - (1% CTA)	5	4	37	0.692	2.605	1.161	FBW - DC
S6 - (1.5% CTA)	5	4	28	0.692	2.404	1.161	FBW - DC
M1 - (20% SC)	20	4	19	1.825	2.124	2.161	FBW
M2 - (30% SC)	20	4	22	1.825	2.230	2.161	FBW
L1 - (0% CTA)	45	4	31	3.220	2.477	2.746	FBW
L2 - (1% CTA)	45	4	20	3.220	2.161	2.746	FBW
L3 - (2% CTA)	45	4	16	3.220	2.000	2.746	FBW
XL1	113	4	20	6.134	2.161	3.410	SBW
C1 (3/1)	5	4	34	0.692	2.544	1.161	FBW - DC
C2 (2/1)	5	3	39	0.712	3.335	1.465	FBW
C3 (4/1)	5	5	25	0.676	2.000	1.000	FBW - DC

Table 3.7 presents the experimental weight average radius of gyration and those calculated from the scaling law model (eq. 3.10 using the parameters of Table 3.6) for all the PCE's. RGz and RGw of the synthesized PCEs were determined by SEC/MALS analysis as shown above (see section 3.5). The theoretical values of RG required the value of P, N and n. The value of n is determined from the z average degree of polymerization ($n_z = DP_z/N$). For consistency the average values of polymerization used here were recalculated considering only the chains with radius of gyration calculated by MALS with an error below 10% (chains with radius of gyration higher than 10 nm do generally fulfill this requirement).

Table 3.7: Radius of gyration determined by MALS and theoretically employing equation 3.10 developed by Flatt et al.[10].

PCE	RGz_{MALS}	RGz_{THEO}
S1 (3/1 – 0% CTA)	30.23 ± 1.21	37.52
S2 (2/1 – 0% CTA)	24.15 ± 1.01	32.18
S3 (4/1 – 0% CTA)	14.66 ± 1.37	15.09
S4 (3/1 – 0.5% CTA)	17.97 ± 1.33	11.98
S5(3/1 – 1% CTA)	15.86 ± 2.19	8.61
S6 (3/1 – 1.5% CTA)	-	-
M1 (SC: 20%)	11.38 ± 1.14	19.81
M2 (SC: 30%)	16.72 ± 0.87	29.22
L1 (0% CTA)	50.51 ± 0.92	122.72
L2 (1%CTA)	20.02 ± 0.80	41.56
L3 (2% CTA)	12.99 ± 1.04	26.28
XL1	48.48 ± 0.77	104.91
C1 (3/1)	-	-
C2 (2/1)	-	-
C3 (4/1)	-	-

Figure 3.17 plot the experimental radius of gyration z average versus the theoretically calculated ones (using the parameters of the copolymer n, P and N and the scaling law developed by Gay and Raphael[15] and upgraded by Flatt et al.[14] for comb like copolymers used as superplasticizers).

A good linear correlation would indicate that the power laws which relate the radius of gyration of the macromolecules in solution with the characteristic properties of the macromolecules (n, P and N) represent well the conformation of these comb copolymers in solution. Figure 3.17 shows that the linear fitting is good for copolymers of series M, L and XL, but it is not as good for the short PEGMA, copolymer series S. The discrepancy for the short series can be due to several reasons. On one hand, the conformation of the copolymers is at the boundary between a decorated chain and a flexible backbone worm (see Figure 3.16) for which the power law was built and hence the prediction of the model might not be accurate. On the other hand, the value of N used in the theoretical calculation of the radius of gyration is uncertain because of the composition drift of almost 20% of the chains and this can also justify the poor fitting between the model and experimental predictions for the RG_z. The good fitting obtained between the model predictions and the experimental radius of gyration for the series with the longer PEGMAs (series M, L and XL) demonstrates that the value of n (measured as DP_z/N, with DP_z measured from SEC/MALS using dn/dc values calculated independently for each copolymer) was accurate and that therefore, PCE's synthesized by FRP can also be characterized by structural parameters n, P and N as opposed to the claim of Gelardi et al.[10].

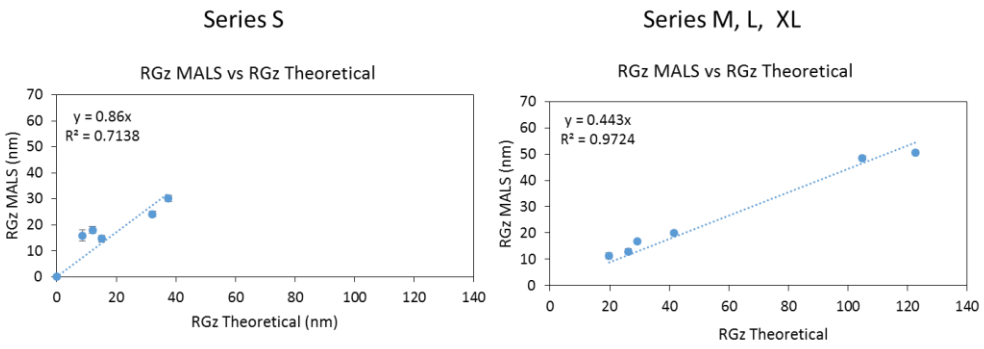

Figure 3.17: Experimental RGz as determined by MALS as a function of the theoretical weight average RG. A) Series S PCEs B) Series M, L and XL PCEs.

As a summary, it can be said that the PCEs of series M, L, XL behave as FBW type comb copolymers while the PCEs of the series S despite of being classified as FBW theoretically it could not be proven experimentally because the value of n cannot be determined with complete accuracy. Also, it has to be mentioned that equation 3.10 captures well the changes in size of the PCEs with FBW conformation, but it cannot provide quantitative values of those sizes.

3.7. Conclusions

MAA-co-PEGMA copolymers with different side chain lengths were synthesized by semibatch free-radical aqueous copolymerization carried out under monomer starved conditions. The synthesis was performed under acidic conditions because of the similar reactivity ratios of the comonomers in this condition.

As expected homogeneous copolymers in terms of composition were obtained as it has been proved by the kinetics and the microstructure analysis performed by ^{13}C-NMR. In terms of MWD, the longer the side chain length (longer PEGMAs) the more complicated it is to control the

viscosity of the medium and hence gel content leads to copolymers with broad MWD (a clear shoulder/tail at the high molar mass end). To reduce viscosity and narrow the dispersity of the copolymers, experiments were carried out using CTA and lower solids content.

The conformation of the synthesized copolymers in a good solvent was estimated following the theoretical approach described by Gay and Raphael[15] and Flatt et al.[14] The conformation of the synthesized copolymers fits into the so-called Flexible Backbone Worm (FBW) based on the structural characteristics of the comb-copolymers n, P and N determined by SEC/MALS, ^{1}H and ^{13}C-NMR and MALDI-TOF. Only the copolymer XL1, produced with the PEGMA with 113 EG groups in the lateral chain, falls in the conformation called Stretched Backbone Worm (SBW) and some PCEs of series S are in the borderline between decorated chain (DC) and FBW conformation.

In addition, the experimentally determined structural characteristics of the comb-copolymers PCEs were used to validate the power law model for the prediction of the radius of gyration developed by Gay and Raphael[15] and adapted by Flatt et al.[14] for FBW type of PCEs. It was found that for the PCEs synthesized with the long PEGMAs the model captured well the power law dependencies on molecular structure parameters of solution conformation. However, as also found by Gelardi et al[10] the numerical prefactor is not accurate, which means that, although the relative effect of changes in molecular structure can be well predicted, the absolute values are not.

3.8. References

(1) Winnefeld, F.; Becker, S.; Pakusch, J.; Götz, T. Effects of the Molecular Architecture of Comb-Shaped Superplasticizers on Their Performance in Cementitious Systems. *Cem. Concr. Compos.* **2007**, *29* (4), 251–262.

(2) Zingg, A.; Winnefeld, F.; Holzer, L.; Pakusch, J.; Becker, S.; Gauckler, L. Adsorption of Polyelectrolytes and Its Influence on the Rheology, Zeta Potential, and Microstructure of Various Cement and Hydrate Phases. *J. Colloid Interface Sci.* **2008**, *323* (2), 301–312.

(3) Zingg, A.; Winnefeld, F.; Holzer, L.; Pakusch, J.; Becker, S.; Figi, R.; Gauckler, L. Interaction of Polycarboxylate-Based Superplasticizers with Cements Containing Different C3A Amounts. *Cem. Concr. Compos.* **2009**, *31* (3), 153–162.

(4) Plank, J.; Sachsenhauser, B. Impact of Molecular Structure on Zeta Potential and Adsorbed Conformation of α-Allyl-ω-Methoxypolyethylene Glycol -Maleic Anhydride Superplasticizers. *J. Adv. Concr. Technol.* **2006**, *4* (2), 233–239.

(5) Kong, F. R.; Pan, L. S.; Wang, C. M.; Zhang, D. La; Xu, N. Effects of Polycarboxylate Superplasticizers with Different Molecular Structure on the Hydration Behavior of Cement Paste. *Constr. Build. Mater.* **2016**, *105*, 545–553.

(6) Lutz, J. F. Polymerization of Oligo(Ethylene Glycol) (Meth)Acrylates: Toward New Generations of Smart Biocompatible Materials. *J. Polym. Sci. Part A Polym. Chem.* **2008**, *46* (11), 3459–3470.

(7) Smith, B. L.; Klier, J. Determination of Monomer Reactivity Ratios for Copolymerizations of Methacrylic Acid with Poly (Ethylene Glycol) Monomethacrylate. *J. Appl. Polym. Sci.* **1998**, *68* (6), 1019–1025.

(8) Borget, P.; Galmiche, L.; Le Meins, J. F.; Lafuma, F. Microstructural Characterisation and Behaviour in Different Salt Solutions of Sodium Polymethacrylate-g-PEO Comb Copolymers. *Colloids Surfaces A Physicochem. Eng. Asp.* **2005**, *260* (1–3), 173–182.

(9) Magny, B.; Lafuma, F.; Iliopoulos, I. Determination of Microstructure of Hydrophobically Modified Water-Soluble Polymers by 13C n.m.R. *Polymer (Guildf).* **1992**, *33* (15), 3151–3154.

(10) Gelardi, G.; Sanson, N.; Nagy, G.; Flatt, R. J. Characterization of Comb-Shaped Copolymers by Multidetection SEC, DLS and SANS. *Polymers (Basel).* **2017**, *9* (2).

(11) Plank, J.; Sakai, E.; Miao, C. W.; Yu, C.; Hong, J. X. Chemical Admixtures - Chemistry, Applications and Their Impact on Concrete Microstructure and Durability. *Cem. Concr.*

Res. **2015**, *78*, 81–99.

(12) Habbaba, A.; Lange, A.; Plank, J. Synthesis and Performance of a Modified Polycarboxylate Dispersant for Concrete Possessing Enhanced Cement Compatibility. *J. Appl. Polym. Sci.* **2013**, *129* (1), 346–353.

(13) Plank, J.; Pöllmann, K.; Zouaoui, N.; Andres, P. R.; Schaefer, C. Synthesis and Performance of Methacrylic Ester Based Polycarboxylate Superplasticizers Possessing Hydroxy Terminated Poly (Ethylene Glycol) Side Chains. **2008**, *38*, 1210–1216.

(14) Flatt, R. J.; Schober, I.; Raphael, E.; Plassard, C.; Lesniewska, E. Conformation of Adsorbed Comb Copolymer Dispersants. *Langmuir* **2009**, *25* (2), 845–855.

(15) Gay, C.; Raphaël, E. Comb-like Polymers inside Nanoscale Pores. *Adv. Colloid Interface Sci.* **2001**, *94* (1–3), 229–236.

(16) Flory, J. P. *Principles of Polmyer Chemistry*; Cornell University Press: Ithaca, NY, USA, 1953.

(17) Brochard, F.; de Gennes, P. G. Injection Threshold for a Star Polymer inside a Nanopore. *C.R. Acad. Sci. Paris* **1996**, *323* (II), 473–479.

(18) Gennes, P. G. de. *Advances in Polymer Science*; 1999.

(19) Pedersen, J. S.; Sommer, C. *Progress in Colloid and Polymer Science*, 130th ed.; Springer: Berlin, Germany, 2005.

Chapter 4: Effect of MPEG Superplasticizers on Ordinary Portland Cement: Understanding the Effect of the Microstructure

4.1. Introduction

Construction industry have been working on the improvement of the fresh and hardened properties of cement paste for long time since the very first admixture appeared in the 1930's. The main improvement of the twentieth century came when Hirata[1] discovered in 1981 what now are called the polycarboxylic ethers or polycarboxylates (PCE) compounds. These PCEs act as efficient cement lubricants or dispersers of inorganic particles. Since then, several groups have been studying how the microstructure of PCEs affect the final properties on cement and concrete and hence, from that research PCEs based on different chemistries have been developed[2]. However, understanding the relation between PCE´s microstructure and the cement properties has been elusive. In literature there is a lack of the synthesis procedures (especially regarding the polymerization processes and molecular characteristics of the macromolecules), which make this task even more complicated. It is obvious that without a complete understanding of the microstructure and the synthesis of these macromolecules, molecular design of targeted structures for developing concretes and mortars with especial characteristics would be a

challenging task[3], and therefore industry generally has opted for a trial and error approach to optimize the performance of the PCE superplasticizers in cementitious formulations.

Prior to the analysis of PCEs on the properties of cement pastes it is important to understand the behavior of cement pastes without admixtures. OPC in dry conditions is a heterogeneous material which is composed in its majority of 4 different crystalline phases (C_3S – Alite, C_2S – Belite, C_3A – Aluminates and C_4AF – Ferroaluminates and a small amount of $CaSO_4$ –Gypsum (added to the clinker) (complete cement nomenclature can be found in chapter 1, Introduction)). Each phase reacts in a different manner when water is added to the OPC and have also an effect in the reactivity of the other crystalline phases, thus, understanding the kinetic mechanisms of cement hydration has been one of the main topics in cement science, but still numerous issues remain unresolved[4]. When water is added to cement, a series of hydration reactions takes place, leading to different hydration products. Heat is released in these reactions and a common tool to monitor these reactions is calorimetry. Figure 4.1 shows a typical calorimetric curve of an ordinary Portland cement hydration where different periods can be observed. In the first minutes, the reaction is exothermic, releasing a substantial amount of heat, afterwards, the heat flow (or the rate of the heat release) remains constant for a period of time which is called induction period. After this period the rate of heat released increases and it is when the main reaction occurs, the formation of CSH. This period is called the acceleration period. This acceleration period starts at about 2-3 hours after the mixing process. Once the heat release reaches to its maximum, heat rate starts slowing down. At this period physical processes of arrangement starts happening, this latter periods is called deceleration period. However, the reaction may last for years, and the evolving microstructure is the one which determines the long-term mechanical properties. In this work the focus was placed on the early stages of the cement pastes (< 24 h).

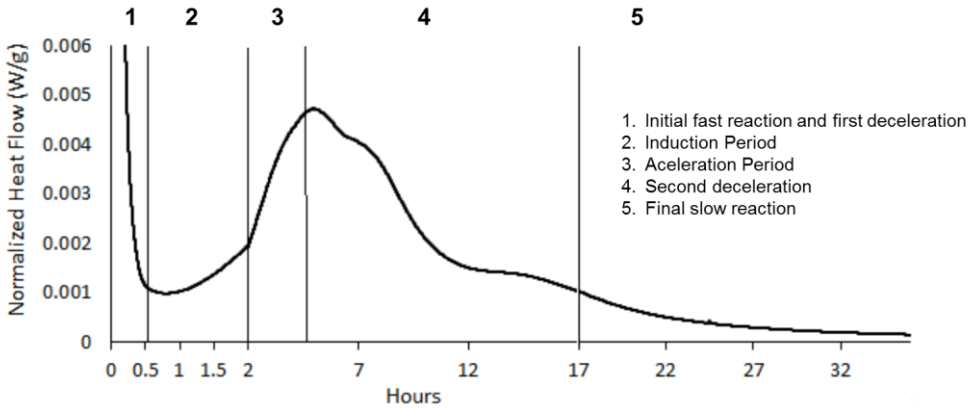

Figure 4.1: Hydration stages of an OPC.

A feature of the cementitious materials is that after mixing with water, for a period of time, the fresh cement can be molded and poured, this period is coincide with the induction period. Thus, all rheological measurements of cement pastes are mainly done during this time. Once the induction period is the viscosity of the pastes increases rapidly because a percolation threshold is formed in the material. The formation of this percolation threshold depends on many factors, such as the type of cement and water to cement ratio among others.

The rheological behavior of cement based materials can generally be explained by a Bingham model:

$$\tau = \tau_0 + \mu \cdot \gamma \qquad \text{(eq: 4.1)}$$

Where τ is the shear stress, τ_0 the yield stress, μ the plastic viscosity and ɣ the shear rate[5]. Cement and concrete are considered complex and viscous fluids and despite the Bingham model is the most employed one to characterize their viscosity, other rheological models have

also been proposed to describe the behavior of cement pastes[5]. Nevertheless, in this work Bingham model was used to characterize the cement pastes.

Setting is a term used to describe the stiffness of a cement paste. In principle, the setting of cement is a percolation process in which isolated or weakly bound particles are connected by the formation of hydration products so that solid paths are formed in the hardening pastes[6]. The setting of the cement paste depends on many factors but water to cement ratio (W/C) is one of the most important ones[7]. The addition of superplasticizers substantially affects the setting and especially PCEs offer the possibility of tailoring their structure depending on the setting performance sought in the cement paste[8]. The setting of the cement pastes is substantially retarded with the addition of the PCEs, which is due to the dispersive effect produced by steric hindrance or electrostatic dispersion that retards the formation of a 3D structure.

Generally, a Langmuir type adsorption isotherm is used to explain the adsorption of PCEs, in which the surface (in this case cement particle surface) has certain number of sites and PCEs stick on them by physisorption or chemisorption. This adsorption mode assumes that:

I) The surface is completely flat and it is complete homogeneous.

II) There is no desorption from the adsorbed compound.

III) All adsorbing sites are equivalent.

IV) The adsorption is monolayer[9].

Hence, PCEs adsorb linearly until the saturation point where an adsorption plateau appears. When the molecules are adsorbed on the surface of particles the non-adsorbing side chains that induce steric repulsion are responsible for the dispersive effect preventing the agglomeration of particles[10].

In this chapter, the aim is to study the interaction of synthesized homogeneous comb-like copolymers (see chapters 2 and 3) with the cement. In those chapters, the aim was to obtain PCEs with controlled microstructural parameters (n, N and P) (see section 3.6.2, Figure 3.16 and Table 3.6). In chapter 2, PCEs with short side chains, (low P), were synthesized, thus comb copolymers with variable backbone length (variable n) and variable comonomer ratio (variable N) were synthesized. In chapter 3, PCEs with long side chains (larger and variable P) were synthesized maintaining the comonomer ratio fixed (N was maintained invariable). All these PCEs were added into cementitious formulations (Ordinary Porland Cement, OPC) in order to better understand the effect that the microstructure of the polymers have on the cement particles and therefore on the hydration and rheological properties of the formed pastes.

Fundamental studies addressing the relationship between the microstructural parameters of the PCE's (recently described by the group of Flatt with the parameters n, N and P) for a building block of a comb like copolymer that represents well the PCE macromolecules and cement (OPC or individual phases) are scarce[3]. Theoretical models that relate fundamental aspects of the PCE's to their interaction with cement particles have been presented very recently by Flatt's group[11]. They proposed that adsorption affinity of PCEs represented by the adsorption equilibrium constant $\boldsymbol{K_A^*}$ depends on the molecular structure as follows:

$$K_A^* \propto \frac{z^2(N-1)^2}{nP^{9/5}N^{3/5}} \cdot 10^5 \qquad \text{(eq: 4.2)}$$

where z is the number of charges carried by each monomer in the backbone. The higher the adsorption equilibrium constant of a PCE[11]. This equation offers the possibility to rank the

crucial property of adsorption respect to molecular structure parameters and it will be assess in this chapter for the MPEG superplasticizers synthesized in chapter 2 and 3.

Marchon et al.[11] also related the dispersion efficiency of the PCEs with their microstructural parameters. The dispersion efficiency increases in respect to the thickness of the adsorbed layer and scales up with the microstructural parameters: $P^{7/10}N^{-1/10}$ if full coverage of the surface by PCEs is produced.

On the other hand, conventional situations do not fulfill full surface coverage, in such cases, the surface fraction occupied is assessed from the amount of PCE adsorbed per unit of area and scales up as follows: $P^{9/10}N^{3/10}n$.

Furthermore, they related the structural parameters of PCEs with the retardation on the hydration of model cement[3]. The retardation can be expressed as follows[11]:

$$\Delta t \propto \frac{c_{PCE}}{M_{RU}}\left(\frac{N-1}{N}\right)^{3/2} \qquad \text{(eq: 4.3)}$$

where, Δt is the retardation of the maximum of the main hydration peak, c_{PCE} is the dosage in mass, and M_{RU} the molar mass of the repeating unit.

$$M_{RU} = Mw_{m,BB} \cdot N + Mw_{m,SC} \cdot P \qquad \text{(eq: 4.4)}$$

where $Mw_{m,BB}$ and $Mw_{m,SC}$ are the molar mass of one monomer in the backbone and side chain respectively.

Generally, MPEG type PCEs with relatively short chains (Series S - 5 EGu, low P) have are not used for the dispersion of cementitious materials thus, the knowledge of how this type of PCEs influence the properties of cement pastes is limited. Some few works can be found where, PCEs with lateral chains of 6[12] and 8-9 EGu were used[5], while there are a number of studies where a combination of short and long lateral chains in the same polymeric chain (terpolymers) were used[14]. Kirby et al[15] studied PCEs of very short lateral chains (2 EGu) although, in this case, the backbone was acrylic acid (AA) based and the lateral chains were based on imide linkages.

The typical range of the molar mass of the side chains is between 500 and 10000 g/mol which corresponds to 11-230 EGu. However, most of the commercial products have lateral chain lengths between 17 and 113 EGu (750-5000 g/mol)[16]. In this work, side chains of 5, 20, 45 and 113 EGu were used, which are within typical commercial lengths.

The mentioned features are of paramount importance to understand the relation between the microstructure of PCEs and the properties and performance of cement pastes. This chapter is composed of two main parts: In the first one, the characterization of the cement (OPC) used in the study was carried out. In the second one, the interaction of the PCEs with the cementitious particles was analyzed measuring the consumption of the PCE's and zeta potential of the dispersions. Moreover, rheological properties, hydration studies and setting studies were performed and are discussed.

4.2. Experimental Part

The cement used was CEM Type I 52.5R (OPC) which was kindly supplied by Lemona Cements S.A. Firstly, this material was characterized employing conventional characterization techniques for cementitious materials. After, cement pastes were prepared using the synthesized superplasticizers and several characterization techniques were employed to determine the interaction between the superplasticizers and the OPC.

4.2.1. Characterization of Cement

- ***Scanning Electron Microscopy (SEM)***

Scanning electron microscopy (SEM) was employed to observe the morphology of the raw material and the dispersion of the particle size. In this case, in order to obtain a better contrast of the material the surface was coated with a thin gold film.

- ***X-Ray Diffraction – Rietvelda analysis***

X-ray diffraction (XRD) was used for the identification of the crystalline phases. The X-ray diffractometer used was X-Pert Pro from Philips. Rietveld quantitative XRD was used to quantify the phases and elemental analysis was performed by X-ray Fluorescence. These analyses were done in the Servicios Centralizados de Apoyo a la Investigación (SCAI) of the Universidad de Málaga, using the UniQuant instrument.

- ***Density measurements and surface area***

The measurement of the density of the material was performed employing the Le Chatellier flask method. Based on the obtained measurements Blaine fineness was also determined in order to know the surface area of cement.

- ***Particle size measurements***

Particle size distribution of the cement particles was measured by Mastersize 2000 instrument in iso-propanol. Number and volume distributions were determined.

4.2.2. Characterization of Cement Pastes

- ***Consumption of PCEs***

In order to determine the consumption of the synthesized PCEs in the OPC, 20 g of cement were mixed with 40 grams of water (PCE aqueous solutions) for 25 minutes and after the solid was filtered through a Buchner funnel. Different dosages varying from 0-6 mg PCE/ g OPC were used. The liquid phase extracted was then analyzed using Total Organic Carbon (TOC) analysis[17] at constant temperature. The total mass consumed was calculated subtracting the measured quantity by TOC to the total mass added. These analyses were conducted by SGIker in the Faculty of the Science and Technology of the University of the Basque Country UPV/EHU in Leioa (Bizkaia-Spain).

There are three different ways PCE's can interact with cementitious materials[17]:

1. A fraction of the PCE is adsorbed on the surface of the cementitious materials.

2. A fraction remains in the aqueous phase (the fraction measured by TOC measurements).
3. A fraction reacts with the forming mineral phases (e.g. CSH, CH).

It is known that when admixtures are added to cement pastes they interact with the cement particles. Flatt and Houst[18] concluded that the total admixture present in cement pastes is either adsorbed onto cement particles or consumed in the formation of an organo-mineral phase (OMP). When superplasticizers are added to cement suspensions they interact with the ongoing chemical reactions[19] and an organo-mineral phase can be formed around the particles at early stages of the hydration consuming the superplasticizers in an unproductive way. However, the extent of how much this affects the consumption and its effects on viscosity, and workability retention is still unclear[18].Still some part of the added PCEs remains in the aqueous phase of the cement paste[18,20]. Consequently, given that the method used is not able to distinguish between these two forms the most accurate term for the fraction calculated from the TOC measurement is “consumed” admixture[17].

- ***Zeta Potential measurements***

The zeta potential of a cement suspension as a function of the dosage of the PCE was analyzed using Colloidal Dynamics Acoustosizer IIs. For the measurements, 30 g of cement and 160 g of water were mixed (w/c: 5.33 – water to cement ratio). The PCEs were added with an automatic titrator and the concentration of PCEs used was between 0-8 mg PCE/ g OPC[17].

- ***Sample preparation for hydration and rheological measurements***

The rheology, hydration kinetics, and setting studies were done just after the mixing process of the cement pastes. The mixing was carried out at w/c: 0.33. A reference measurement of just cement without any admixture was carried out for the sake of comparison. The concentration of PCE added to the cement pastes was 3 mg PCE/ g OPC. This concentration was fixed for all the test carried out throughout the PhD.

The preparation of the cement pastes (for rheological measurements and hydration kinetics) was done following a procedure developed by the Materials Group of the Sustainable Construction Division in Tecnalia in which 50 grams of OPC for the mixing were used. For that, a glass mixing bowl of a particular design was used. Figure 4.2 shows the mixing equipment. After the water is added, the mixing procedure is the following:

1. 90 seconds mixing at 750 rpm
2. Stop for 60 seconds
3. 90 seconds mixing at 750 rpm

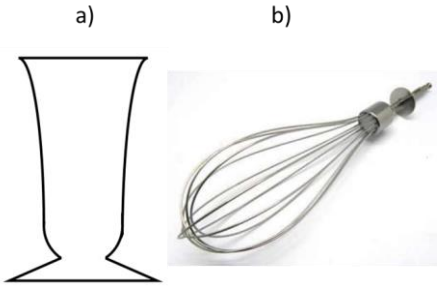

Figure 4.2: Equipment used for mixing the cement pastes. a) Geometry of the mixing bowl. b) Skimmer used for the mixing.

The setting time tests were done based on the UNE-EN 196-3 standard. The amount of cement used was 500 g and the mixing was carried out in an automatic mortar mixer following the procedure described below. The concentration of PCE added to the cement pastes was 3 mg PCE/ g CEM.

1. 30 seconds mixing, 140 rpm – 62 rpm (Planetary movement)
2. Stop for 15 seconds
3. 60 seconds mixing, 285 rpm – 140 rpm (Planetary movement)

- ***Rheological measurements***

Apparent viscosity of cement pastes was measured using a TA Instruments-Discovery Hybrid Rheometer HR-3. The measurements were carried out in a continuous ramp from 1 to 1000 s^{-1}. In order to measure the time evolution of the apparent viscosity, flow peak hold experiments were carried out at 0.01 s^{-1} shear rate in the same rheometer. For time evolution studies, special geometry (helix) with the cylinders was employed.

- ***Hydration studies***

Hydration reactions were recorded in a TAM air conduction calorimeter at 25 ºC with water as reference material.

- ***Setting studies***

Setting time was determined using Vicat needle with the Autovicat instrument (Ibertest). The test was carried out based on the UNE-EN 196-3 standard procedure. In these measurements, the initial setting is considered when the needle penetrates below 35 mm and the final setting is considered when the penetration does not exceed 5 mm.

4.3. Results and Discussion

4.3.1. Cement Characterization

- ***Scanning Electron Microscopy (SEM)***

The morphology of the cement particles was analyzed by SEM and as expected, there is a great dispersity of sizes and of shapes. Most of the particles have irregular shapes and many small particles are agglomerated onto the bigger ones.

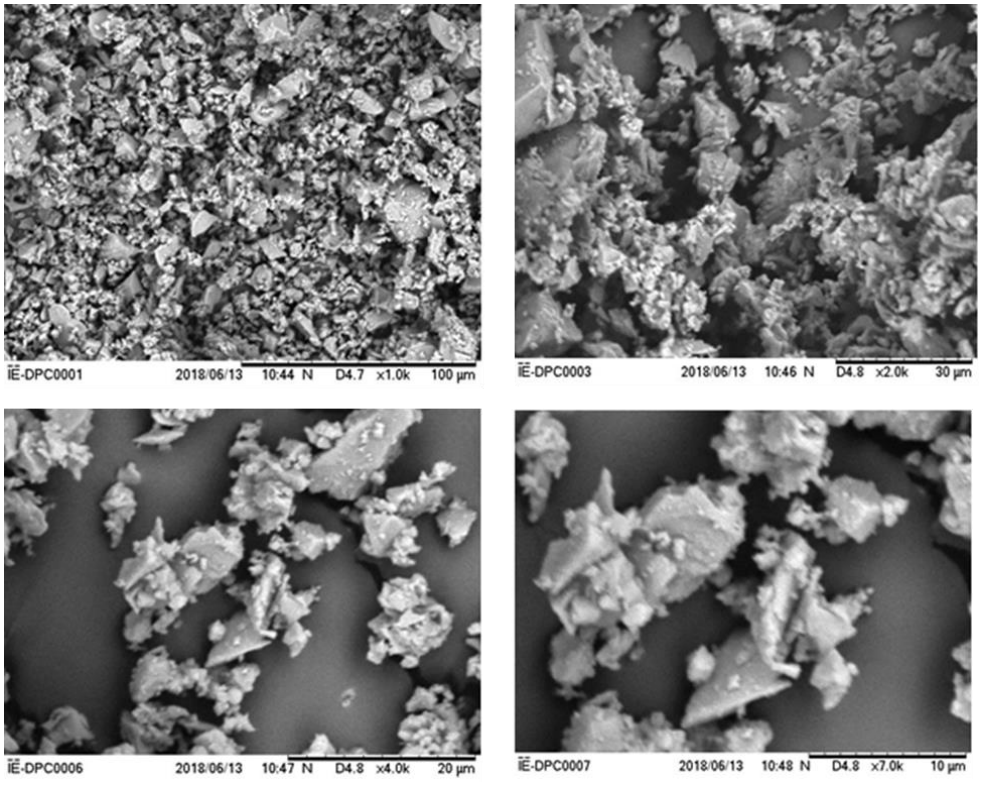

Figure 4.3: SEM images of the OPC employed in this work.

- ***X-Ray Diffraction – Rietveld – X-Ray Fluorescence***

Figure 4.4 shows the XRD diffractogram of the employed OPC. The crystalline phases shown in the diffractogram are assigned to alite (Ca_3SiO_5 or C_3S), belite (Ca_2SiO_4 or C_2S), tricalcium aluminate ($Ca_3Al_2O_3$ or C_3A), calcium aluminium iron oxide (calcium aluminoferrite Ca_4AF), quartz (SiO_2) and calcium sulfate dihydrate or gypsum.

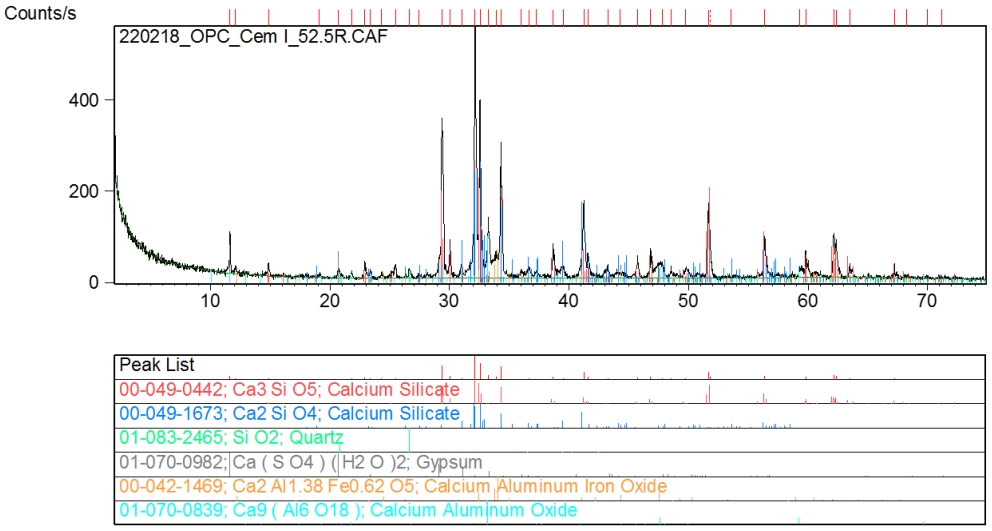

Figure 4.4: X-ray diffractogram of the OPC employed, and the corresponding assignment of the crystalline phases.

The quantitative composition was determined by Rietveld analysis shown in Table 4.1

Table 4.1: Composition of the OPC (in wt %) used in this study quantified by Rietveld analysis and the typical composition of an OPC type I.

Rietveld Analysis		***General composition Type I OPC***[21]	
Phases	***wt %***	***Phases***	***wt %***
Amorphous	10.8		
C_3S	48.1	C_3S	55
β-C_2S	17	β-C_2S	19
Cubic C_3A	6.8	Cubic C_3A	7
C_4AF	5.9	C_4AF	2.8
Calcite	6.1		
Akermanite	2.1		
Portlandite	1		
Gypsum	0.9		
Quartz	0.6		
Bassanite	0.6		
Dolomite	-		

The composition of the cement used in this work is atypical composition for a type I cement although it shows a slightly higher amount of amorphous material. This could be due to the fact that some of the cement reacted with humidity during storage.

The elemental analysis of the OPC by X-ray fluorescence was also carried out (see Table 4.2). From the values obtained it can be said that the OPC employed in this work is in the range of conventional OPC.

Table 4.2: Composition of oxides of the OPC employed in this work and the average values of the composition of 125 samples.

Oxide	Lemona Cements (wt %)	Range (wt %)	Average (wt %)
CaO	61.13	60.2 – 66.3	63.81
SiO_2	18.94	18.6 – 23.4	21.45
Al_2O_3	4.92	2.4 – 6.3	4.45
Fe_2O_3	2.84	1.3 – 6.1	3.07
MgO	1.24	0.6 – 4.8	2.42
P_2O_5	0.19	--	0.11
TiO_2	0.21	--	0.22
Na_2O	0.23	0.05 – 1.2	0.20
K_2O	0.92	0.05 - 1.2	0.83
SO_3	3.82	1.7 – 4.6	2.46

- ***Density measurements and surface area***

Characterizing cements in terms of density and surface area by Blaine fineness is also an important parameter, which can help to understand better the interaction of PCEs with the surface of the cement particles. The surface area has an effect on the rate at which the cement reacts with water, the smaller the size of the particle the higher the surface per volume ratio, thus, the smallest particles react at higher rate than bigger ones. The surface area of a typical OPC measured by Blaine fineness is in the range of 3000-5000 cm^2/g[22]. On the other hand, the average density of cement is considered as 3.15 g/cm^3 even though there might be differences between batches. In this case, the OPC used had a density of 3.10 g/cm^3 and a surface area of 4523 cm^2/g (see Table 4.3).

Table 4.3: Density and Blaine fineness obtained for the OPC employed in this work.

Material	Density (g/cm^3)	Surface Area (cm^2/g)
OPC Type I 52.5R Cementos Lemona	3.1039	4523

- ***Particle size measurements***

Particle size distribution measurements were carried out dispersing cement particles in isopropanol. A Mastersize 2000 instrument was used and the number and volume distributions were calculated. As it was observed in Figure 4.3 (SEM images) the particle size distribution was very broad; bimodal. Figure 4.5 shows the number and volume particle size distributions. A bi-modal distribution of particle sizes is identified with a large number of small (in the range of 1 μm) and a substantially smaller number of much larger particles (in the range 2-80 μm). The number average and the volume average particle sizes are 0.61 μm and 13.69 μm, respectively. This result is in good agreement with the SEM images that show the majority of the particles to be smaller than 1 μm, but with a population of big particles (> 10 μm).

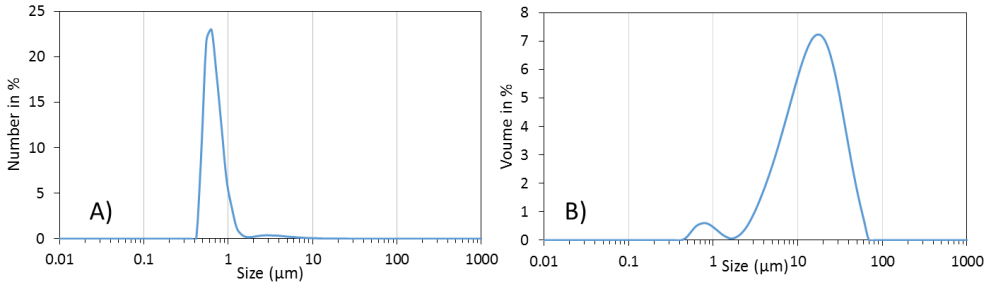

Figure 4.5: Particle size distribution of the OPC cement dispersion in isopropanol used in this work. A) Number distribution. B) Volume distribution.

4.3.2. Effect of Superplasticizers

In this section, superplasticizers with different microstructure will be added to cement suspensions in order to analyze the interaction between the macromolecules and the OPC. The three characteristic parameters that define the microstructure of the comb like MPEG superplasticizers defined in chapter 3 will be used to analyze the effect of the microstructure with the cement particles and its properties. The effect of backbone length or “n” parameter of the SPs, the charge density of the backbone or “N” parameter, and finally the effect of the side chain length or “P” will be evaluated.

Firstly, the interaction with the cement particles will be investigated by analyzing adsorption isotherms and zeta potential measurements, because adsorption is the key to achieve an optimal dispersion of the particles. The dispersion of the particles will have an effect on properties like rheology, hydration and setting of the cement paste.

4.3.2.1. Effect of the Superplasticizer Backbone Chain Length, n, and Side Chain Length, P

The superplasticizers employed for studying the effect of the backbone chain length, n were prepared under starved semibatch conditions (see Chapter 2 and Chapter 3) with a fixed ratio of MAA/ PEGMA, or “N” parameter. Table 4.4 shows the main characteristics of the synthesized superplasticizers.

Table 4.4: Main characteristics of the synthesized SPs used in the analysis of the effect of n.

PCE	*Mw (kg/mol)*	*Đ*	*DP*	*n*	*P*	*N*
S1	88.0 ± 1.4	3.0	206	51.7	5	*4.0*
S4	51.4 ± 0.5	2.2	166	42.1	5	*3.9*
S5	40.8 ± 0.6	2.0	146	37.5	5	*3.9*
S6	32.8 ± 0.3	2.0	112	29.4	5	*3.8*
M1	46.2 ± 0.2	2.0	75	18.6	20	*4.0*
M2	81.6 ± 0.3	3.0	88	21.7	20	*4.0*
L1	794.9 ± 8.2	11.5	122	30.5	45	*4.0*
L2	184.7 ± 0.8	4.1	78	19.5	45	*4.0*
L3	88.5 ± 0.4	2.4	64	16.0	45	*4.0*
XL1	1303.5 ± 14.6	12.3	80	20.0	113	*4.0*

- ***Consumption of PCEs***

Figure 4.6 shows the consumption of PCE's plotted as the total mass consumed for the different PCE series.

Substantial differences in the consumption of PCE's can be observed. Thus, for short lateral chains (P=5) saturation is not reached and the typical Langmuir type isotherms is not achieved. However, for longer lateral chains, P=20 and 45 the curves resemble better this behavior and saturation is reached; clearly consumption of the PCE's is lower for the longer lateral chain PCE's, but there are not big differences between P=20, P=45 and P=113 (see Figure 4.6 right bottom).

For all the PCEs assessed the consumption is high at low dosages, but it decreases as the dosage is increased except for PCE's with P=5 where consumed fraction is more or less maintained at high dosages. Hirata et al. [23] using atomistic dynamic simulations showed that the side chains of the PCE's shrunk in the pore solution and that this conformation affected the interaction with the cement particle. Shrinking of long lateral chains can shield the charge present in the backbone and hence reduce the overall charge density and the adsorption of the PCEs reaching a saturation value. This could explain the difference observed between the PCEs with P=5 and those with P=20 and 45.

The effect of the backbone length, n, can be compared for PCEs with equal P values. Thus, for series S (P=5) PCEs with n values ranging between 51 and 29 can be compared (see Figure 4.6 top left). At a dosage of 3 mg PCE/ g CEM (taken as reference) when increasing the chain length the, consumed mass of the PCE increases. For P=45, PCEs with values between 30 and 16 were analyzed and a higher consumption was also obtained for longer n values.

Interestingly, there is good agreement between the experimentally determined and consumed number of PCE chain per unit of area and the theoretical expression proposed by Marchon et al.[11] for the adsorption constant K_A^* (equation 4.2) that depends on n, N and P. Note that the experimental data considers all the PCE's consumption (adsorbed PCE and consumed in the formation of the OMP) and not only the adsorbed PCE like the theoretical expression. Hence, the fact that the trends of microstructural parameters are well captured by the model can be considered as an indication that adsorption is likely the main part of the consumption results. The experimental results indicate that the number of PCE chains consumed per unit of area decreases by increasing the size of the lateral side chain, P, and also decreases by increasing the chain length of the backbone for a constant P, that is, increasing n.

Table 4.5 shows the consumed amount of PCEs by weight, by unit of area calculated considering the average surface area measured for the OPC (Table 4.3), and the consumed number of chains at 3 mg PCE addition / g CEM based on the Mn of the PCEs. Table 4.5 also includes the adsorption constant calculated from equation 4.2[3,24], using the microstructure parameters n, N and P and these values can be compared with the experimentally determined number of chain per unit of area.

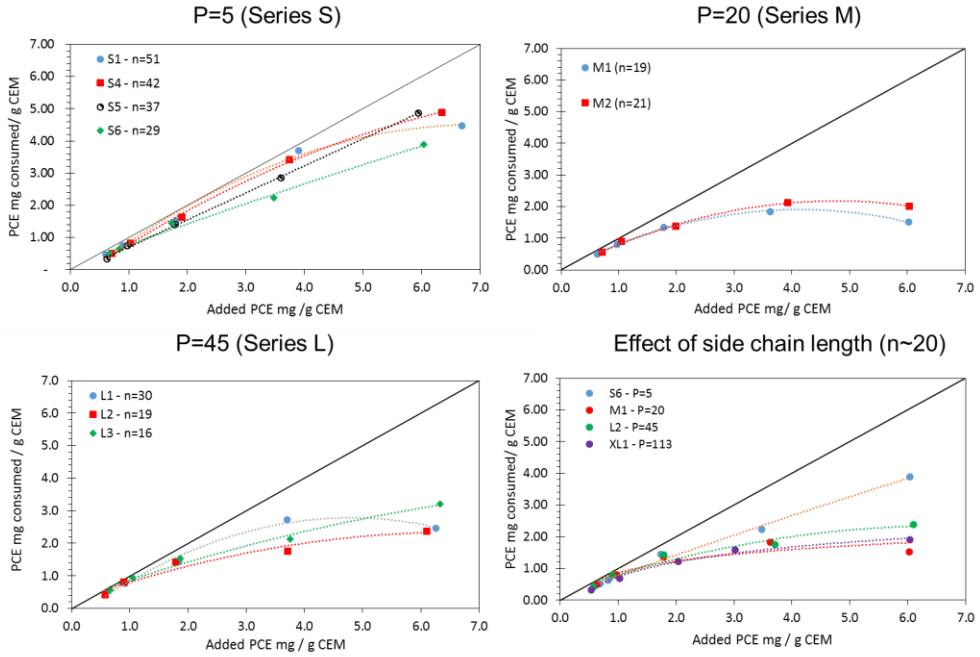

Figure 4.6: Consumption of PCEs with variable n parameter for different side chain length (P=5, 20 and 45) and with variable P parameter for similar backbone length (n ~ 20).

Table 4.5: Consumed amount of the different PCEs per unit of weight, area and number of chains adsorbed per area[25].

	Surface Area - Blaine Fineness (m^2/g)	*PCE /P/ n*	*Consumed amount at (3 mg Pol/ g CEM)*		*Consumed number of PCE chains per unit area (chains/100 nm^2)*	K_A^* *Adsorption equilibrium constant*[11]*
			per unit weight (mg/g)	*per unit area (mg/m^2)*		
Cement (OPC)	0.4523	S1/ 5/ 51	2.80	6.190	4.23	414.7
		S4/ 5/ 42	2.65	5.860	6.86	499.9
		S5/ 5/ 37	2.35	5.196	7.66	545.0
		S6/ 5/ 29	2.00	4.422	8.11	666.2
		M1/ 20/ 18	1.65	3.648	4.75	98.2
		M2/ 20/ 21	1.75	3.869	2.85	84.1
		L1/ 45/ 30	2.30	5.085	0.39	13.6
		L2/ 45/ 19	1.65	3.648	1.19	21.2
		L3/ 45/ 16	1.85	4.090	2.78	25.8
		XL1/ 113/ 20	1.40	3.095	0.14	3.9

* Calculated using equation 4.2.

In an attempt to quantitatively compare the theoretical prediction and the experimental data, K_A^* and the consumed number of PCE chains per unit of area are plotted in Figure 4.7 as a function of n parameter. Note, that the synthesized PCEs are limited, therefore, only series S and L are used in the comparison. The power dependencies of each case, are compared. The theoretical expression for K_A^* only considered the adsorption by electrostatic adsorption, while the number of consumed chains involves adsorption and consumption during the formation of organo-mineral phase. Figure 4.7 shows that the trends are reasonably well predicted by the expression proposed by Marchon et al.[11].

For example the consumed PCE chains per unit of area depends more strongly on the backbone-chain length of the PCE's, n, than theoretically predicted. For PCE's with P=5 and P=45 the inverse dependence is proportional to the power of 1.12 and 2.95 respectively, whereas, the theoretical predicts a power of 1.

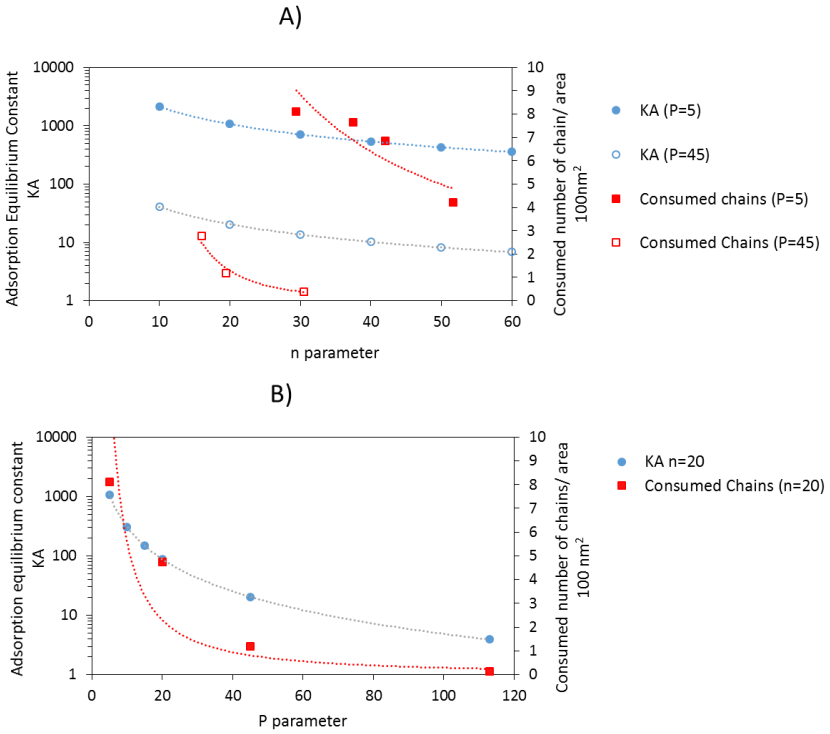

Figure 4.7: Comparison of theoretical prediction (blue dots and lines) for K_A and the experimental data (red squares and lines) of the consumed chains per area. A) Comparison in respect to n parameter of the PCEs. B) Comparison in respect to P parameter of the PCEs.

On the other hand, the theoretical approach (eq: 4.2) shows that the adsorption equilibrium constant is inversely proportional to the power of 1.8 with P parameter. Comparing

the experimental data with this approach it can be observed that in this case the dependency is higher in the theoretical prediction than in the experimental data, in fact, the experimental dependency obtained is inversely proportional to P to the power of 1.28. This comparison is also included in Figure 4.7 B). The dependence obtained in all cases are summarize in Table 4.6.

Table 4.6: Dependencies obtained (theoretical K_A and experimental consumed chains) for the different PCEs.

PCE	Equation
Series S (P=5)	Theoretical Prediction: $K_A^* \propto 21442 \cdot n^{-1}$ Experimental Result: $Consumed\ Chains \propto 395.98 \cdot n^{-1.12}$
Series L (P=45)	Theoretical Prediction: $K_A^* \propto 410.79 \cdot n^{-1}$ Experimental Result: $Consumed\ Chains \propto 8911 \cdot n^{-2.95}$
Effect of side chain length (n ~20)	Theoretical Prediction: $K_A^* \propto 19426 \cdot P^{-1.8}$ Experimental Result: $Consumed\ Chains \propto 106 \cdot P^{-1.28}$

- ***Zeta Potential measurements***

As it is known, there is a strong correlation between the adsorption of the PCEs and the zeta potential of the surface of the particles. Flatt[26] compared the variation of zeta potential induced by the addition of different PCEs to a $Mg(OH)_2$ water dispersion. For that case, he observed that the minimum on the zeta potential measurement could be correlated to a saturation point of PCE. Thus, the measurement of the zeta potential could help to understand how the PCEs interact with the surface of the cement particles.

Figure 4.8 shows that raw cement paste (OPC) without any admixture have a slightly positive zeta potential; this value derives from the surface composition of the different clinker phases C_3S, C_2S, C_3A and C_4AF[27]. When adding PCEs with short side chain (P=5) it decreases to values around -10 mV at the smallest dosage (1 mg PCE / g CEM) and further addition did not affect the zeta potential. This means that over this dosage the adsorption of PCEs with short side chains (P=5) did not occur on the surface of the particles, but during the formation of the organo-mineral phase. Furthermore, the measured negative ζ-potential indicates that for low P (P=5), the lateral chains do not shield the charges of the backbone or that the conformation of the adsorbed chains are in the loop configuration rather than in the train conformation[28] (see Figure 4.9) since the latter conformation would lead to a value close to zero. These conformations were introduced by Andersen et al.[28] in 1987 with the aim of explaining the differences observed between two admixtures in cement pastes, but they were not based on microstructural parameters n, N and P as the admixtures they employed were not PCEs.

Nevertheless, variation of n for PCEs with short side chains (P=5) has little effect on the zeta potential of the cement suspension.

For PCE's with longer values of P (equal values of N and varying values of n; P=20 and 45) the ζ-potential remained similar to the OPC dispersion without admixtures and close to zero. This reveals that the negative charges of the backbone are shielded by the lateral chain; namely the adsorption occurs in a train-conformation (20 EG units are enough to shield the negative charges) and hence the stability of the dispersion is achieved by steric repulsion rather than by electrostatic repulsion achieved when P was short. Furthermore, at 1 mg/ g CEM a saturation point was reached (see Figure 4.6) thus, over this dosage the PCEs remained in the pore solution

or were captured during the organo-mineral phase formation[29]. Similar to PCEs with P=5 in the case of PCEs with longer Ps, the n parameter has no effect on the zeta potential either.

Increasing the side chain length to P=113, has negligible effect on the zeta potential of the suspension and the adsorption may occur as train conformation like in the case of PCEs with P=20 and 45. Figure 4.8 also shows a comparison of PCEs with similar n but with variable P (P=5, 20, 45 and 113).

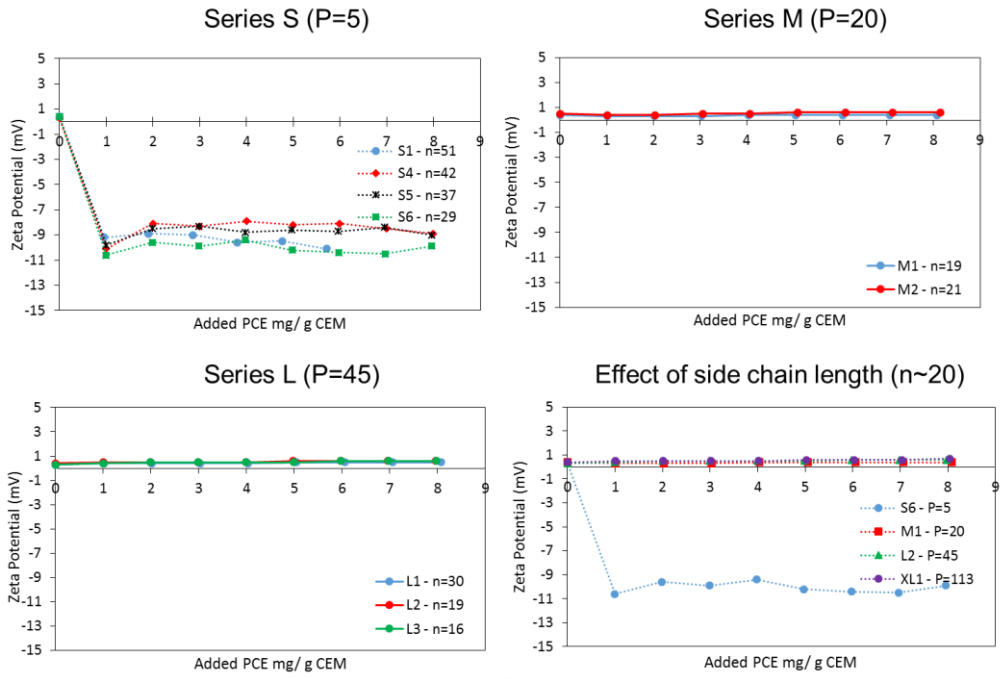

Figure 4.8: Evolution of the Zeta potential values as a function of the added amount of PCE (in mg PCE/ g CEM).

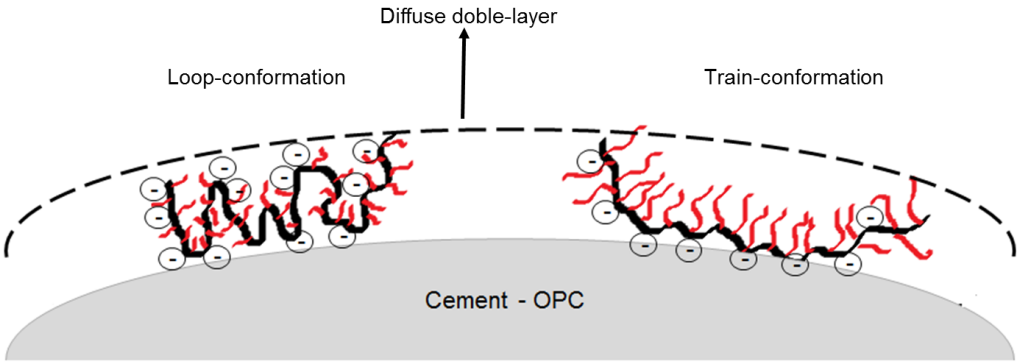

Figure 4.9: Schematic illustration of the different types of conformations[28].

- ***Rheological measurements***

The rheological parameters of the cement pastes (with and without PCEs) were determined by rotational rheometer. In this work, the apparent viscosity as a function of shear rate was studied. For this analysis a quantity of 3 mg PCE/ g Cem was used. Figure 4.10 shows the effect in the viscosity of the cement pastes that PCEs with different side chain length (P = 5, 20 and 45) equal N and different values of n have. The addition of PCEs of series S (P = 5) reduced the viscosity by one order of magnitude, but there is not noticeable effect of the backbone length (n parameter) on the achieved viscosities.

Increasing P from 5 (series S) to 20-45 (series M and L), substantially decreased the viscosity; steric hindrance produced by side chains or the train adsorption conformation being mainly the reason to yield a lower viscosity. When increasing P from 20 to 45 (for N=4 and different n values) viscosity was not affected. Increasing n (for equal N and different P values) has little or no effect on viscosity. The fact that molar mass (in the 60-200 kg/mol range) does

not seem to affect in either type of adsorption, nor the ζ-pontential it might indicate that n is not an important parameter (in this range) for the initial rheology of the dispersions.

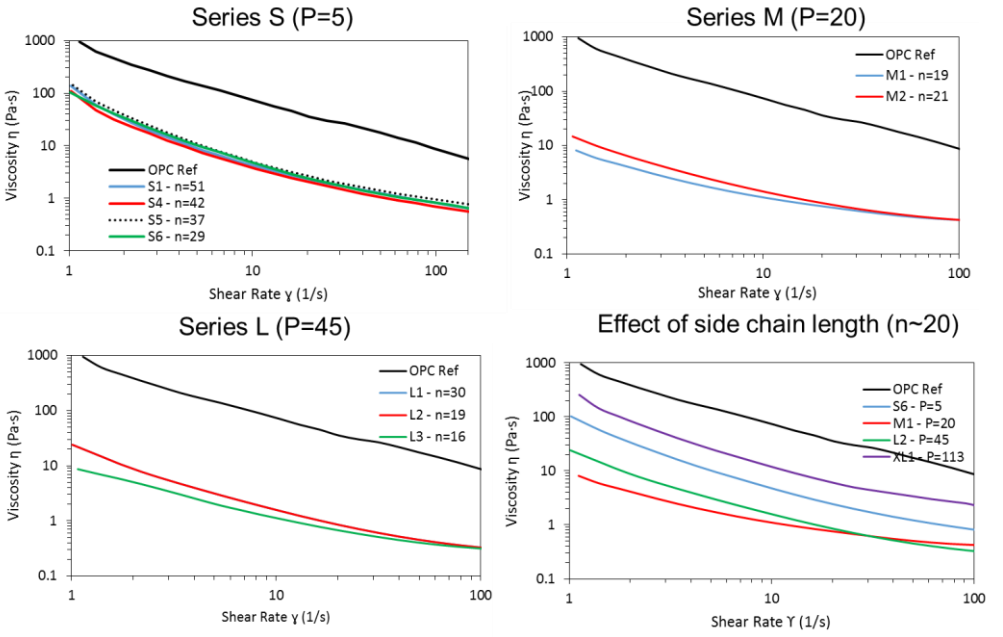

Figure 4.10: Evolution of the viscosity of the cement pastes with different PCEs as a function of shear rate.

Marchon et al.[11] reported that adsorbed polymer keeps particles further apart than in the case that if there is no polymer present, because it reduces the Van der Walls forces between particles and hence viscosity of the dispersion. This effect increases with the thickness of the adsorbed layer, which scales up with molecular structure according to: Dispersion $\propto P^{9/10} \cdot N^{3/10} \cdot n$. Therefore, the results of this work are in reasonable qualitative agreement with the predictions of this equation although the decrease on the viscosity by increasing the side chains from 5 to 20 is under-estimated. This underestimation is likely due to the fact that in the case of the short side chains the repulsion is governed by electrostatic forces rather than steric ones. On the other

hand, the PCE with the longest side chains (P=113) presents lower dispersion efficiency than the rest of the PCEs. However, as it was shown in chapter 3, its conformation in solution differs from the rest (XL1 – SBW; M and L – FBW) and its dispersion mechanism could be different.

- ***Time evolution of the rheological measurements***

In addition to rheological measurements of fresh paste the time evolution of the apparent viscosity is extremely interesting for constructors and industry in general. The time length for which the cement is manageable is known as the workability window. In this work, it would be defined as the time when a change in the slope of the apparent viscosity appears. The workability window will be the parameter that determines how to treat the paste and it would determine which application for the cement is more suitable. To determine the workability of a cement paste the flow test (Abrams cone)[12,17,30,31] is used, especially in industry because of its simplicity and because it can be performed next to the construction place. Nevertheless, reproducibility of the measurements is poor and in this work a rheometer with especial geometry was used to obtain this property. This method has also been used previously[32]. Figure 4.11 shows the measured time evolution of the apparent viscosity with the rotational rheometer using a special geometry (helix) for a 3 mg PCE / g CEM dosage. It has to be mentioned that, only cement pastes with PCEs of series S (P=5) have been compared when studying the effect of the backbone length (Figure 4.11).

Figure 4.11 shows that when PCEs are added the workability window is extended, the reference paste (without admixture) only maintained the workability for around 30 minutes while the cement pastes with PCEs extended the workability window beyond those 30 minutes. As a general trend it can be said that the PCEs with higher n kept the workability for longer time. It

should be also noted that the PCEs with higher n value tend to have higher consumption (in mass) and also PCEs with higher n produce a higher surface coverage (at 3 mg PCE/ g CEM dosage), most probably, this can be the reason of extending the workability window of cement suspensions (in the case of PCEs with low P, series S).

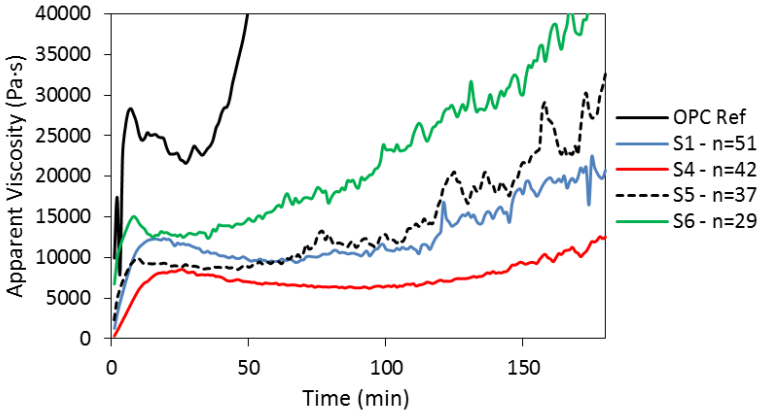

Figure 4.11: Time evolution of apparent viscosity of the OPC cement pastes when different PCEs of Series S (P=5) were used.

Figure 4.12 shows the time evolution of the apparent viscosity of cement pastes with the PCE's of different P values. PCE's with a medium P value (P = 20 and 45) maintained the fluidity of the paste for almost three hours. On the other hand, in the case of the PCE with low P value (P=5, series S), the fluidity decreased after 60 minutes approximately. Note that the dispersion effect of this PCE is different from PCEs with medium P value (P=20 and 45, series M and L), where the longer side chains provide a strong steric hindrance. PCEs with low P disperse the particles by electrostatic effect as it was inferred by the zeta potential measurements. The PCE with the highest P values (P=113, series XL) showed very low fluidity retention, probably due to its low adsorption capacity.

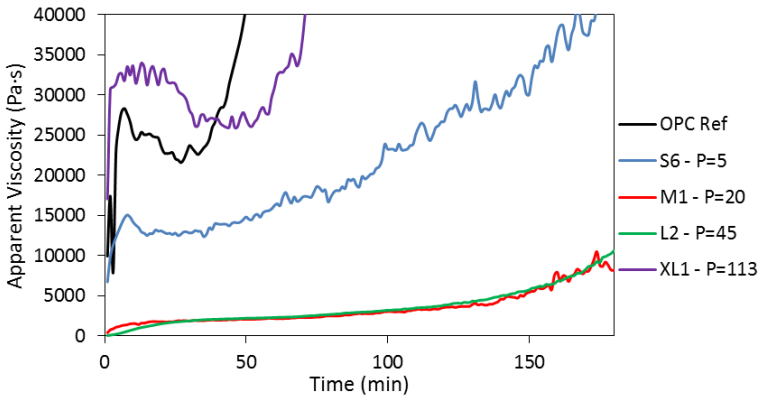

Figure 4.12: Time evolution of apparent viscosity of the OPC cement pastes when PCEs with different side chain lengths were used.

- ***Hydration kinetics by calorimetry***

Hydration of cementitious materials is one of the most determinant property and it has also been one of the most studied. The hydration of OPC is a sequence of reactions between clinker (individual phases) water and sulfates from gypsum leading to setting and hardening of the cement paste. The setting of the cement paste occurs when the particles form a 3D solid skeleton, and this reaction can be monitored by different techniques that include rheological measurements, hydration calorimetry and setting studies[32]. In this part especial attention will be placed on the hydration monitored by calorimetry. As it has been previously mentioned and shown in Figure 4.1, hydration of cementitious materials consists of 5 different stages and it can last for months, even years, however, in this work special focus has been placed on the early stages of the hydration (< 48h).

OPC is composed of different constituents being C_3S the main one (50-70%) and the one most studied[33,34]. Furthermore, C_3S is responsible of the main heat released peak when following the hydration kinetics of Portland cements, but it is not the only peak that appears. It was shown[4] that a secondary peak appears after the alite peak due to the hydration of the aluminate phases.

In addition to the evolution of the heat release from the calorimetric curves the time at which the main peak appears and the total heat released after 30 hours was also measured. Figure 4.13 shows the time evolution of the normalized heat flow of cement pastes without admixture and with different PCEs (fixed N=4, different P values 5, 20 and 45 (series S, M and L respectively, and variable n; listed in Table 4.4). Table 4.7 shows the values of the peak time, the Δt in hours (difference respect to the reference, without PCE) and the normalized heat released. For this experiment the PCE dosage was 3 mg PCE/ g CEM in all the cases.

As can be observed in Figure 4.13, there is retardation on the hydration when PCEs are added to the cement paste, the main peak appears substantially later. The normalized heat released after 30h is slightly higher for the hydration in presence of the PCE's, but no clear trends were observed (Table 4.7). Mollah et al.[35] explained the retardation action of the PCEs on the hydration of the cement as a consequence of the following aspects:

- The PCEs are adsorbed onto the surface of the cement particles creating an impermeable coating and thus, retarding the dissolution of Ca^{2+} ions to the pore solution. (The pore solution is defined as the liquid phase of cement paste[36]). The composition of the aqueous phase of hydrating cementitious materials strongly affects the chemical processes and the interactions between solid and liquid phases.

- The PCEs present in the pore solution could form chelates with the Ca^{2+} ions and reduce the concentration of these ions in the aqueous solution retarding their precipitation.
- The dispersive action of the PCEs affects the kinetics of the process and changes the morphology of the hydrated phases.

Furthermore, according to Marchon et al.[3] the retardation on the hydration is due to local interactions between the adsorbed polymer and the mineral surfaces leading to the block of hydration mechanism. Also, it was shown[3] that ettringite acts as sink for PCEs limiting the retardation of the hydration of silicate phases unless a sufficient amount of PCE is added to completely cover the ettringite surface.

It can be seen in Figure 4.13 that the heat released profiles present a main peak and a secondary peak (in some cases higher than the main peak, when PCEs of low P are used (series S, P=5)). In other cases (when PCEs with higher P are used (series M and L, P=20 and 45)) is more or less a shoulder, right after the first maximum. The secondary peak, (aluminate peak) represents the sulfate depletion point and corresponds to a faster ettringite precipitation and faster tricalcium aluminate dissolution[3]. Plank and Hirsch[27] demonstrated that PCEs are especially prone to be adsorbed onto ettringite. This observation of the increase of the secondary peak might be because the adsorption of the PCEs on the ettringite promotes its precipitation and the dissolution of the aluminate. The adsorption of PCEs with high P (series M and L) might be less favored than PCEs with low P (series S) and therefore the peak observed is lower.

The effect of n on the hydration process is negligible for all the PCE's with the same side chain length, used in this work. Only in the case of L1, which has a high dispersity (Đ=11) the

hydration peak obtained is lower in height than in the other cases although the delay shown is similar to the one shown by L2 and L3. On the other hand, the longer the value of P, PCEs with longer side chains (except of P=5), the earlier the start of the hydration reaction as can be seen also in Figure 4.13. This coincides with the amount of chains adsorbed on the cement particles (see Table 4.5) and the adsorption equilibrium constant. These results are in agreement with the ones observed by Winnefeld et al. [31].

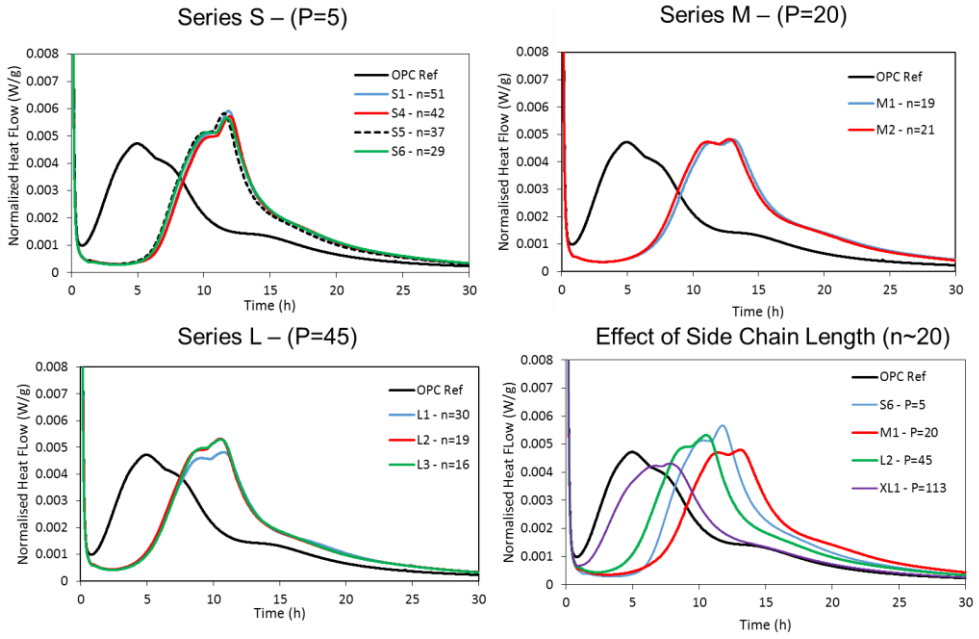

Figure 4.13: A) Time evolution of the normalized heat flow when different PCEs are used.

Table 4.7 presents the Δt values obtained based on the results shown in Figure 4.13 and defined as the difference of the main peak time between the cement paste with PCE and the reference without superplasticizers.

Table 4.7: Main peak time, Δt in hours and the normalized heat released at 30h for the different PCEs.

PCE/ n/ P	*Main Peak Time (h)*	*Δt (h)**	*Normalized heat 30h (J/g)*
OPC Ref	5.18	-	190.86
S1/ 51/ 5	10.69	5.51	192.95
S4/ 42/ 5	10.58	5.40	191.31
S5/ 37/ 5	10.07	4.89	194.88
S6/ 29/ 5	10.27	5.09	195.45
M1/ 19/ 20	11.50	6.32	195.74
M2/ 21/ 20	11.14	5.96	191.46
L1/ 30/ 45	9.08	3.90	195.07
L2/ 19/ 45	9.09	3.91	197.79
L3/ 16/ 45	9.30	4.12	192.78
XL1/ 20/ 113	6.74	1.56	186.91

* Δt is difference of the main peak time between the cement paste with PCE and the reference without superplasticizers

As in the case of consumption of PCEs, Marchon et al.[11] attempted to predict theoretically the retardation of the hydration respect to the molecular structure. They defined Δt with the following dependency:

$$\Delta t \propto \frac{c_{PCE}}{M_{RU}}\left(\frac{N-1}{N}\right)^{3/2} \qquad \text{(eq: 4.3)}$$

where, Δt is the retardation of the maximum of the main hydration peak repect to the reference main peak, c_{PCE} is the dosage in mass, and M_{RU} the molar mass of the repeating unit that is calculated as:

$$M_{RU} = Mw_{m,BB} \cdot N + Mw_{m,SC} \cdot P \qquad \text{(eq: 4.4)}$$

where $Mw_{m,BB}$ and $Mw_{m,SC}$ are the molar mass of one monomer in the backbone and side chain, respectively. Taking this prediction into account, retardation should be independent of the chain length of PCEs, n, and inversely proportional to P or to the side chin length. In Figure 4.14, a comparison between experimental data obtained in this work and the theoretical prediction is presented. For a direct comparison, and easiness of visualization all the values are normalized taking as reference M1. It can be observed that as predicted by the model (eq: 4.3) Δt is independent of n. However, the absolute values do not fully agree. The discrepancy between the model prediction and the experimental values was found mostly for the PCEs with the shortest side chains. The PCEs with the short chains are the ones that less satisfy the assumptions made to derive the theoretical equation. The prediction of retardation for the PCEs with P=20 and 45 is reasonably good.

When P parameter is analyzed it can be observed that there is good correlation between the theoretical prediction formulated by Marchon et al.[11] and the experimental results obtained in this work. However, the agreement is substantially worse at low P values, likely because this PCE's adsorb and perform in a different manner than the rest. Indeed, PCEs with P=5 are at the boundary between FBW and DC conformation (see section 3.6.2), therefore, the theoretical prediction might not be totally accurate for PCEs that do not fit into FBW conformation. Furthermore, note that PCEs with P=5 disperse the cement particles by electrostatic interaction while the other PCEs disperse them by steric hindrance. This difference might also be the reason for the discrepancies observed between the experimental results and theoretical predictions.

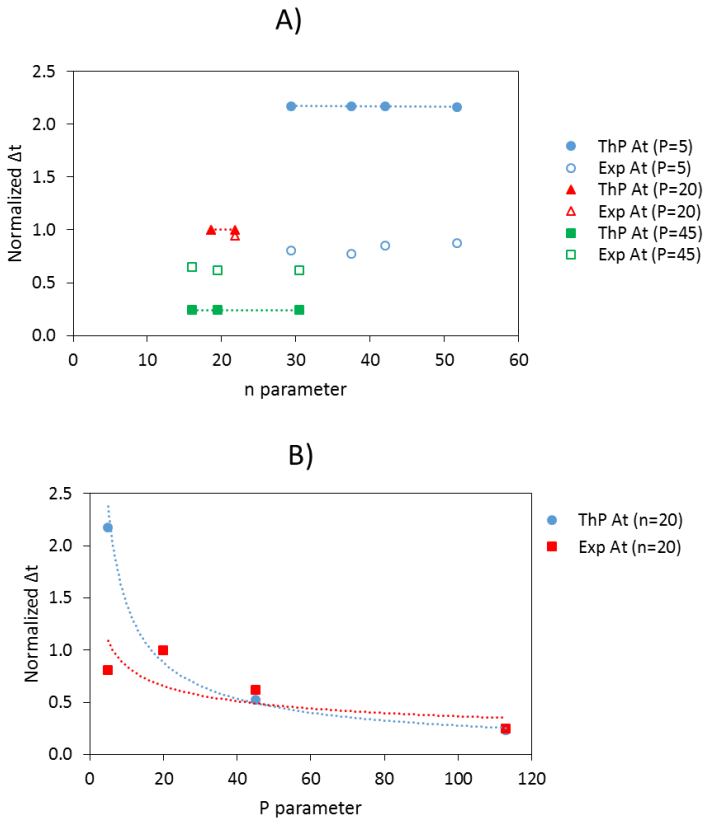

Figure 4.14: Retardation of the hydration of the OPC, Δt, as a function of the chain length, n, and the side chain length, P, of the PCE's. All values have been normalized to M1

- ***Setting time measurements***

The effect of the PCE structure on the setting of the cement pastes has also been studied in this work. The setting studies provide very useful information as they can be correlated with the hydration kinetics of the cement. Figure 4.15 shows the penetration depth time evolution of

the Vicat needle for OPC cement pastes without (reference) and with the PCEs synthesized in this work (see Table 4.4).

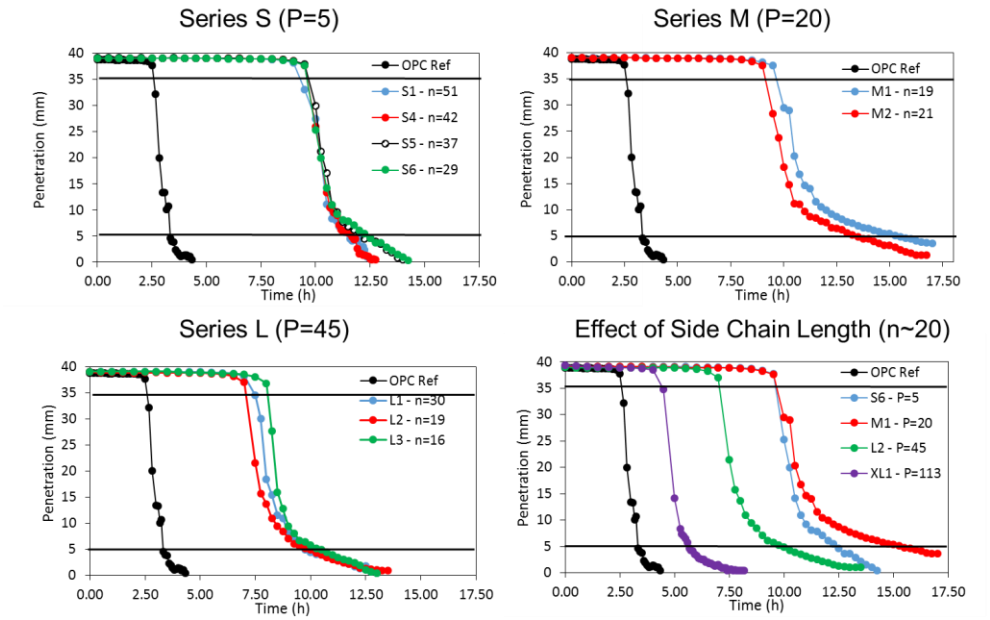

Figure 4.15: Penetration depth comparison of cement pastes with different PCEs.

The addition of PCEs have substantial effect on the delay of the setting time; a similar effect was observed in calorimetry experiments. The n value has a slight effect on the final setting time (it increases when n decreases) and it has almost no effect on the initial setting time when PCEs with short side chains are used (series S, P=5). In the case of M and L series (P=20 and 45) the values of n have also a slight effect in the setting time. Lower value of n provided longer initial and final setting time, however the differences are not large.

Table 4.8: Initial setting time, final setting time and setting duration of the pastes with different PCEs.

PCE/ n/ P	*Initial Setting Time (h)*	*Final Setting Time (h)*	*Setting Time (h)**
OPC Ref	2.60	3.30	0.70
S1/ 51/ 5	9.30	11.55	2.25
S4/ 42/ 5	9.55	11.65	2.10
S5/ 37/ 5	9.55	12.15	2.60
S6/ 29/ 5	9.55	12.35	2.80
M1/ 19/ 20	9.55	15.30	5.75
M2/ 21/ 20	9.10	13.30	4.20
L1/ 30/ 45	7.45	9.75	2.30
L2/ 19/ 45	7.00	9.95	2.95
L3/ 16/ 45	8.05	10.50	2.45
XL1/ 20/ 113	4.45	5.65	1.20

*Setting time is defined as the difference in hours between the final and the initial setting time.

Figure 4.16 shows a correlation between the setting time measurements and the hydration kinetics followed by calorimetry. It can be observed that when PCEs are added to the cementitious system the setting process does not start until the acceleration period is almost finished (see Figure 4.1) while in the reference paste the setting process starts at the middle of the acceleration period. From this finding it can be suggested that when PCEs are added the agglomeration of cement particles, which are formed in the process have smaller sizes and so it takes longer time to achieve a percolation threshold which is the point where a 3D structure is formed in the pastes and the setting starts. Furthermore, the theoretical prediction on the delay of the hydration reaction suggest that Δt can be correlated with the initial setting time and that the latter also should be independent of the n parameter. As seen previously, n has shown almost no effect on the setting measurements.

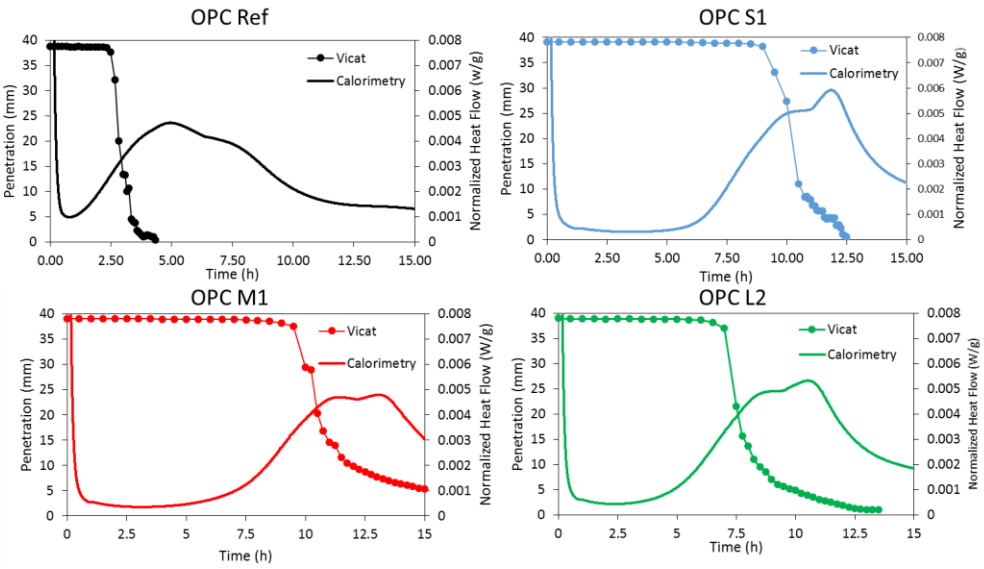

Figure 4.16: Setting time studies in comparison with hydration kinetics of different cement pastes.

4.3.2.2. Effect of the MAA/PEGMA Ratio or N parameter (Backbone Charge Density)

In this part of the chapter the effect of the ratio between the methacrylic acid and PEGMA macromonomers in the repeating unit or N parameter (charge density of the backbone) in different properties will be analyzed. Table 4.9 shows the main characteristics of the PCEs employed for this purpose. Note that only PCE's with short lateral chains (P=5) have been synthesized in this work having different N values.

Table 4.9: Main characteristics of the SPs employed in the analysis of the N parameter.

PCE	*Mw (kg/mol)*	*Đ*	*DP*	*n*	*P*	*N*
S2	100.2 ± 0.7	3.0	211	71.5	5	*3.0*
S1	88.0 ± 1.4	3.0	206	51.7	5	*4.0*
S3	40.8 ± 0.6	2.0	156	31.2	5	*5.0*

- ***Consumption of PCE's***

Figure 4.17 shows the mass of PCE consumed at different dosages. It can be observed that there is not a clear saturation point and relatively high consumption amounts are obtained in the whole range. As discussed in the previous section, when P is short (P=5), a saturation point is not achieved and increasing the charge density does not have clear trend in this narrow range of N.

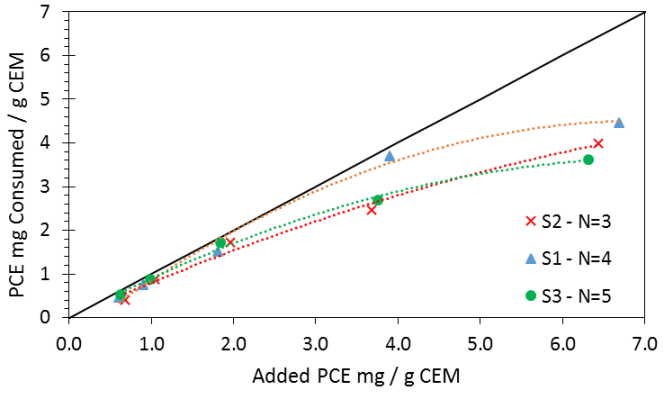

Figure 4.17: Consumption of the series S PCEs (short lateral chain P=5) with variable N parameter.

Table 4.10 shows the consumed amount of PCEs by weight, extracted from Figure 4.17, by unit of area considering the average of the surface area measured for the OPC (Table 4.3) and the consumed number of chains at 3 mg PCE addition / g CEM based on the Mn of the PCEs. The adsorption equilibrium constant has also been calculated.

As it can be observed, the consumed number of chains per unit of area increases with the charge density of the backbone (higher N) and this trend is in good agreement with the calculated trend for the adsorption constant (equation 4.2) based on the parameters n, P and N for these PCEs.

Table 4.10: Consumed amount of the different PCEs in terms of per unit weight, area and number of chains consumed per area[25].

Cement (OPC)	*Surface Area - Blaine Fineness (m2/g)*	*PCE/ N*	*Consumed amount at (3 mg Pol/ g CEM)*		*Consumed number of PCE chains per unit area (chains/100 nm2)*	K_A^* * Adsorption equilibrium constant
			per unit weight (mg/g)	*per unit area (mg/m2)*		
	0.4523	S2/ 3	2.16	4.776	2.87	153.3
		S1/ 4	2.80	6.190	4.23	414.7
		S3/ 5	2.30	5.085	7.07	1065.9

* Calculated from equation 4.2

Figure 4.18 plots the dependency of the theorecial adsorption constant (eq. 4.2) and the experimentally determined consumed nuber of chains per unit of area as a function of the N value (ratio MAA/PEGMA). Although the trends are in agreement the potential factor of the dependence is higher for the theoretical values than for the experimental results (2.17 vs 1.75) as shown in Table 4.11. The difference can be attributed to the lack of consideration in the theoretical prediction to the chains consumed during the formation of the OMP.

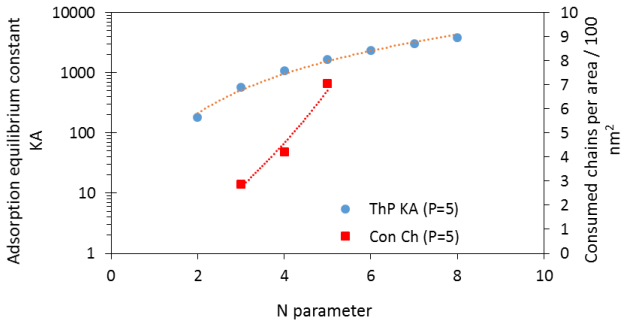

Figure 4.18: Comparison of theoretical prediction for K_A and the experimental data of the consumed chains per area respect to N parameter.

Table 4.11: Dependence of the adsorption equilibrium constant (theoretical K_A and experimental consumed chains) on N for the different PCEs.

PCE	Equation
Series S (P=5)	Theoretical Prediction: $K_A^* \propto 46.26 \cdot N^{2.17}$ Experimental Result: $Consumed\ Chains \propto 0.4075 \cdot N^{1.75}$

- ***Zeta Potential measurements***

Figure 4.19 shows the zeta potential of the cement pastes as a function of the PCE addition dosage. It can be seen that the addition of the PCEs produced a minimum value on the zeta potential of the cement suspension. As previously mentioned, negative zeta potential on cement pastes are attributed to the electrostatic dispersion of the cement particles and due to the loop conformation of this type of PCEs (see Figure 4.9). Polycondensates (type of superplasticizers based on aromatic rings and sulfonate groups, see Chapter 1.2.1) and this type of PCEs (with short side chains, low P values, P=5) produce a similar dispersion mechanism

which is electrostatic repulsion, causing the decrease of the zeta potential to negative values[27], however polycondensates require much higher addition dosages. The minimum value observed in zeta potential measurements has been correlated with the saturation dosages in previous works[37], although in this case is not that clear.

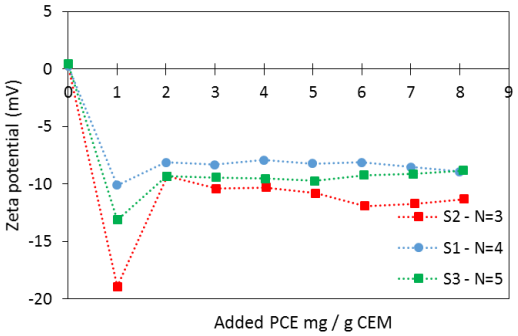

Figure 4.19: Evolution of the Zeta potential values as a function of the amount of PCE (in mg PCE/ g CEM).

- ***Rheological measurements***

The variation of N (variation of the charge density) have a slight effect on the decrease of the viscosity of the cement paste. Figure 4.20 shows the evolution of viscosity of the cement paste as a function of the shear rate. As it can be observed, PCEs S1 and S2 (N=3 and N=4) reduced more the viscosity although the difference is modest. Furthermore, Winnefeld et al.[31] found that for PCEs with side chain lengths of 9 EGu the workability did not depend on the charge density. These results are in good agreement with the results of Figure 4.20.

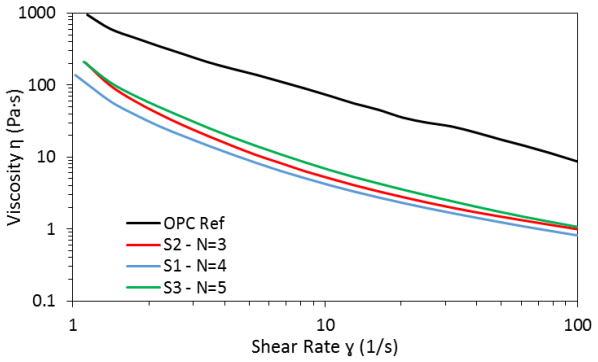

Figure 4.20: Evolution of the viscosity of the cement pastes with PCEs of different value of N (different charge density) over the applied shear rate.

Time evolution of rheological measurements

Figure 4.21 shows that increasing the charge density of the backbone increases the workability retention of the cement paste from N=3 to N=4, but a further increase (to N=5) does not show any noticeable increase although the apparent viscosities are lower.

We showed (Table 4.10) that increasing the charge density of the backbone of the PCEs (higher N) led to a higher number of consumed chains per unit of area of cement particles. As discussed above the consumed chains are the contribution of the adsorbed PCE chains and those reacting in the pore solution producing organo-minerals[18]. Therefore, it cannot be directly linked the effect of N in the consumed number of PCE chains with the effect of N on the workability of the cement pastes even though the increase of the charge density increases the consumed PCEs and the workability.

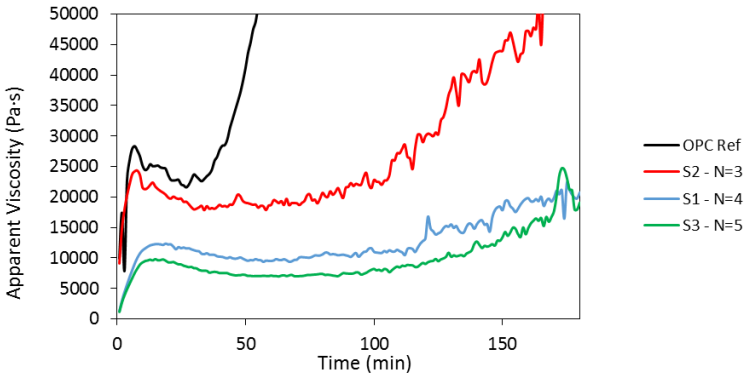

Figure 4.21: Apparent viscosity time evolution of OPC cement paste with PCEs of different N value (charge density).

- ***Hydration kinetics by calorimetry***

Figure 4.22 shows the time evolution of the normalized heat flow. In this case, no trend with respect to N value is observed for the retardation of the hydration of the cement paste. The PCE with the lowest N value (S2, N=3) delay the least the hydration, followed by the PCE with the highest N value (S3, N=5) and the N=4 PCEs delay the most the hydration. However, Winnefeld et al.[31] reported that increasing the N value (higher charge density) higher retardation is observed, however they used PCEs with longer side chains (P=23). From the literature reports it could be expected a higher retardation of S3 (N=5) PCE than the S1 (N=4).

On the other hand, it is observed that the formation of monosulphates is enhanced when PCEs with higher N value (higher charge density) are added to the cement pastes (Figure 4.22 secondary peaks between 10-12h). The increase of the secondary peak might be because the adsorption of the PCEs on the ettringite (because of its positively charged surface[27,38]) promote

the reaction between tricalciumaluminate (C_3A) and sulfate monosulphate. Plank et al.[39] proved that when PCEs of higher N value (higher charge density) are employed the formed crystals of ettringite are of smaller size, which enhances the hydration of monosulphates as it is observed in this case.

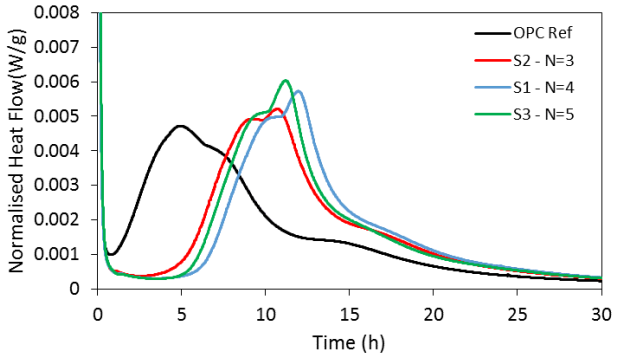

Figure 4.22: Time evolution of the normalized heat flow of PCEs with variable N value.

Table 4.12: Peak time on normalized heat flow of the hydration kinetics and the normalized heat released at that peak time.

PCE/ N	***Main Peak Time (h)***	***Δt (h)***	***Normalized heat at 30h (J/g)***
OPC Ref	5.18	-	190.86
S2/ 3	9.09	3.91	198.16
S1/ 4	10.69	5.51	192.95
S3/ 5	9.98	4.80	195.46

Figure 4.23 presents the effect of N on the normalized Δt for both theoretical prediction and experimental results. The normalization has been done respect to the PCE with N=5. Interestingly, both theoretical prediction and experimental results shown the maximum

retardation for the values of N=4. However, the experimental results show a more noticeable decrease on Δt from N=4 to N=3 than the theoretical calculations.

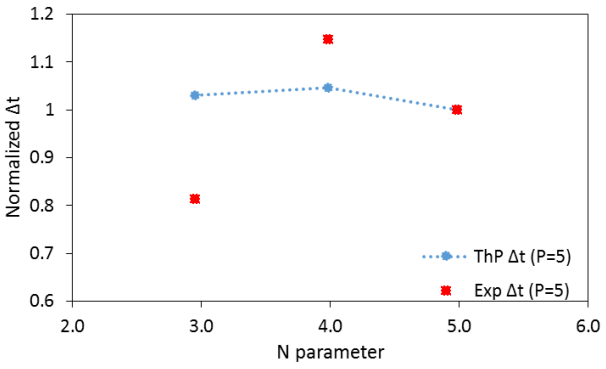

Figure 4.23: Retardation of the hydration of OPC cement, Δt, as a function of the ratio MAA/PEGMA (N parameter) of the PCE's. All the values normalized to the retardation of S3 (N=5).

- ***Setting measurements***

Figure 4.24 shows the penetration depth time evolution of the Vicat needle for cement pastes with PCEs with variable N and same P (P=5). As can be seen, there is a delay of the initial setting time when PCEs are used and the trend observed is the same as the one observed in the calorimetric curves (Δt). The final setting however, does not follow the same trend as the initial one. In this case the higher the N value the earlier the final setting time. The results suggest that the amount of charges in the backbone affects the speed of rigidification of the cement suspension.

Table 4.13: Initial, final setting time and setting duration of the cement pastes with different PCEs.

PCE/ N	*Initial Setting Time (h)*	*Final Setting Time (h)*	*Setting Time (h)**
OPC Ref	2.60	3.30	0.70
S2/ 3	8.15	11.60	3.45
S1/ 4	9.30	11.55	2.25
S3/ 5	8.75	10.10	1.35

*Setting time is defined as the difference in hours between the final and the initial setting time.

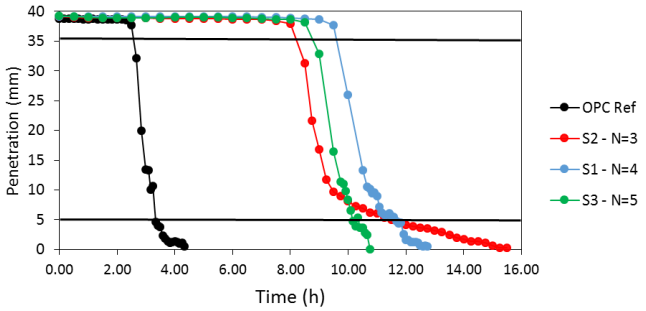

Figure 4.23: Penetration depth comparison of cement pastes with PCEs with different N value for P=5.

4.4. Conclusions

The objective of this chapter was shed light on the effect of the microstructure of the MPEG type PCE's synthesize in chapters 2 and 3 (summarized in the parameters n, N and P recently defined by Flatt et al.[11]) on the performance of OPC pastes.

Firstly, the cement material was characterized by several techniques which showed that the employed material was in accordance with characteristics of a typical Cem I 52.5R type OPC.

One specific feature of the OPC was that it had a bi-modal particle size distribution. It was shown that most of the particles had size below 1 μm but most of the volume was occupied by particles of around 10 μm.

Effect of n: The consumption measurements showed that the higher the n parameter (higher backbone length) the higher the consumption by mass when PCEs with short side chains (P=5) were used. On the other hand, the n parameter did not have substantial effect on the zeta potential results. The rheological measurements over time showed an improvement on the workability when PCEs with higher n parameter were used. Despite the fact that addition of PCEs provided retardation on hydration, the effect of n parameter was negligible, as it was also shown in the theoretical predictions. However, the setting time of the material was slightly altered by n parameter. In this case, the lower the n parameter the longer the setting time of the cementitous suspension.

Effect of P: PCEs with short side chains (low P values, series S) showed high consumption on OPC, however the adsorption was not in accordance with a Langmuir shape, probably because they did not reach to a saturation point. Their adsorption behavior could be comparable to the one of polycondensates which require very high dosages to reach to the plateau. On the other hand, PCEs with medium and long lateral chains (P = 20, 45, 113) showed clear Langmuir shape curves on their adsorption isotherms providing a clear saturation point at 1 mg PCE/ g CEM dosage. From the analysis of the side chain length it can be said that the PCEs with the shortest side chains (P = 5, Series S) showed the highest consumption. The consumption tendency was also compared with the theoretical predictions and it showed a good correlation in this case as well. However, the theoretical prediction overestimated the consumed amount of PCE.

PCEs with short side chains (low P, P=5) generally adsorb onto the surface of the particles in a loop-type conformation decreasing the zeta potential of the OPC, and they disperse the particle by electrostatic repulsion, while it was shown that PCEs with longer side chains (P=20, 45 and 113) provided a train type adsorption as they did not alter the zeta potential of the particles, thus, their main dispersion mechanism is the steric hindrance produced by the side chains.

The dispersion effect produced by PCEs with medium side chain lengths (P=20 and 45) was stronger than the one produced by PCEs with short chains (P = 5, series S) because the viscosity was decreased to a larger extent. Furthermore, it was shown that PCEs with extremely long side chains (P=113) are not as effective as PCEs with medium side chain chains (P=20 and 45). One explanation for this behaviour could be that extremely long side chains could tend to shrink therefore, they could not produce an effective steric hindrance

The study of the hydration reaction showed that when comparing series of PCEs with medium or long side chains (P = 20, 45 and 113) the shorter the side chain length the longer the retardation of the hydration and it correlates with the theoretical predictions. Finally, setting time studies showed that they correlate with hydration studies and in the same way the shorter the side chain (lower P value) the longer the delayed on the setting of the pastes.

Effect of N: The N parameter (charge density) of PCEs with short side chains (P = 5, series S) showed that PCEs with higher N values (higher charge density) showed higher consumption. However, this tendency was not kept when the dosage was increased. The zeta potential also changed with the N parameter but there was not a clear trend. Rheological measurements showed that PCE's with higher N value presented better workability retention of

the cement pastes. The effect on the hydration kinetic is not large when the N value is changed but there is an increase on the production of the monosulphate phase when PCEs of higher N parameter were used. Theoretical predictions developed by Marchon et al.[11] do not show a trend on the retardation of the hydration with respect to N parameter and experimental results correlate with this tendency. Furthermore, the setting time was also reduced when PCEs of high N value were used.

4.5. References

(1) Hirata, T. Cement Dispersant. JP 842,022 (S59-018338), 1981.

(2) Plank, J.; Sakai, E.; Miao, C. W.; Yu, C.; Hong, J. X. Chemical Admixtures - Chemistry, Applications and Their Impact on Concrete Microstructure and Durability. *Cem. Concr. Res.* **2015**, *78*, 81–99.

(3) Marchon, D.; Juilland, P.; Gallucci, E.; Frunz, L.; Flatt, R. J. Molecular and Submolecular Scale Effects of Comb-Copolymers on Tri-Calcium Silicate Reactivity: Toward Molecular Design. *J. Am. Ceram. Soc.* **2017**, *100* (3), 817–841.

(4) Bullard, J. W.; Jennings, H. M.; Livingston, R. A.; Nonat, A.; Scherer, G. W.; Schweitzer, J. S.; Scrivener, K. L.; Thomas, J. J. Mechanisms of Cement Hydration. *Cem. Concr. Res.* **2011**, *41*, 1208–1223.

(5) Banfill, P. F. G. Rheology of Fresh Cement and Concrete. *Rheol. Rev.* **2006**, 61–130.

(6) Jiang, S. P.; Mutin, J. C.; Nonat, A. Studies on Mechanism and Physico-Chemical Parameters at the Origin of the Cement Setting. 1. The Fundamental Proceses Involved during the Cement Setting. *Cem. Concr. Res.* **1995**, *25* (4), 779–789.

(7) Zhang, M. H.; Sisomphon, K.; Ng, T. S.; Sun, D. J. Effect of Superplasticizers on Workability Retention and Initial Setting Time of Cement Pastes. *Constr. Build. Mater.* **2010**, *24* (9), 1700–1707.

(8) Aitcin, P. C.; Jolicoeur, C.; MacGregor, J. G. Superplasticizers. How They Work and Why They Occasionally Don't. *Concr. Int.* **1994**, *16* (5), 45–52.

(9) Masel, R. I. *Principles of Adsorption and Reaction on Solid Surfaces*; Wiley: Chicago, US, 1996.

(10) Gelardi, G.; Flatt, R. 11. Working Mechanism of Water Reducers and Superplasticizers. In *Science and Technology of Concrete Admixture*; 2016; pp 257–278.

(11) Marchon, D.; Boscaro, F.; Flatt, R. J. Cement and Concrete Research First Steps to the Molecular Structure Optimization of Polycarboxylate Ether Superplasticizers : Mastering Fluidity and Retardation. *Cem. Concr. Res.* **2019**, *115* (October 2018), 116–123.

(12) Lange, A.; Hirata, T.; Plank, J. Influence of the HLB Value of Polycarboxylate Superplasticizers on the Flow Behavior of Mortar and Concrete. *Cem. Concr. Res.* **2014**, *60*, 45–50.

(13) Ferrari, L.; Kaufmann, J.; Winnefeld, F.; Plank, J. Multi-Method Approach to Study Influence of Superplasticizers on Cement Suspensions. *Cem. Concr. Res.* **2011**, *41* (10), 1058–1066.

(14) Houst, Y. F.; Bowen, P.; Perche, F.; Kauppi, A.; Borget, P.; Galmiche, L.; Le Meins, J. F.; Lafuma, F.; Flatt, R. J.; Schober, I.; et al. Design and Function of Novel Superplasticizers for More Durable High Performance Concrete (Superplast Project). *Cem. Concr. Res.* **2008**, *38* (10), 1197–1209.

(15) Kirby, G. H.; Lewis, J. A. Comb Polymer Architecture Effects on the Rheological Property Evolution of Concentrated Cement Suspensions. *J. Am. Ceram. Soc.* **2004**, *87* (9), 1643–1652.

(16) Flatt, R.; Schober, I. *Superplasticizers and the Rheology of Concrete 7. Understanding the Rheology of Concrete*; Roussel, N., Ed.; Woodhead Publishing Limited: Oxford, 2011.

(17) Alonso, M. D. M.; Palacios, M.; Puertas, F. Effect of Polycarboxylate-Ether Admixtures on Calcium Aluminate Cement Pastes. Part 1: Compatibility Studies. *Ind. Eng. Chem. Res.* **2013**, *52* (49), 17323–17329.

(18) Flatt, R. J.; Houst, Y. F. A Simplified View on Chemical Effects Perturbing the Action of Superplasticizers. *Cem. Concr. Res.* **2001**, *31* (8), 1169–1176.

(19) Jolicoeur, C.; Simard, M. Chemical Admixture-Cement Interactions : Phenomenology and Physico-Chemical Concepts. *Cem. Concr. Res.* **1998**, *20*, 87–101.

(20) Uchikawa, H.; Hanehara, S.; Sawaki, D. Influence of Kind and Added Timing Organic Admixture on the Composition, Structure Nd Property of Fresh Cement Paste. *Cem. Concr. Res.* **1995**, *25* (2), 353–364.

(21) ASTM, I. ASTM C150 - Historiacal Standard Normalized Specification for Portland Cement. 1996, pp 1–14.

(22) *ASTM C 204 - Blaine Fineness*.

(23) Hirata, T.; Branicio, P.; Ye, J.; Zheng, J.; Tomike, Y.; Lange, A.; Plank, J.; Sullivan, M. Atomistic Dynamics Simulation to Solve Conformation of Model PCE Superplasticisers in Water and Cement Pore Solution. *Adv. Cem. Res.* **2017**, *29* (10), 418–428.

(24) Marchon, D.; Sulser, U.; Eberhardt, A.; Flatt, R. J. Molecular Design of Comb-Shaped Polycarboxylate Dispersants for Environmentally Friendly Concrete. *Soft Matter* **2013**, *9* (45), 10719.

(25) Sakai, E.; Yamada, K.; Ohta, A. Molecular Structure and Dispersion-Adsorption Mechanisms of Comb-Type Superplasticizers Used in Japan. *J. Adv. Concr. Technol.* **2003**, *1* (1), 16–25.

(26) Flatt, R. Interparticle Forces and Superplasticizers in Cement Suspensions, ÉCOLE POLYTECHNIQUE FÉDÉRALE DE LAUSANNE, 1999.

(27) Plank, J.; Hirsch, C. Impact of Zeta Potential of Early Cement Hydration Phases on Superplasticizer Adsorption. *Cem. Concr. Res.* **2007**, *37* (4), 537–542.

(28) Andersen, P. J.; Roy, D. M.; Gaidis, J. M.; W.R. Grace and Co. The Effects of Adsorption of Superplasticizers on the Surface of Cement. *Cem. Concr. Res.* **1987**, *17* (5), 805–813.

(29) Zingg, A.; Winnefeld, F.; Holzer, L.; Pakusch, J.; Becker, S.; Gauckler, L. Adsorption of Polyelectrolytes and Its Influence on the Rheology, Zeta Potential, and Microstructure of Various Cement and Hydrate Phases. *J. Colloid Interface Sci.* **2008**, *323* (2), 301–312.

(30) Plank, J.; Pöllmann, K.; Zouaoui, N.; Andres, P. R.; Schaefer, C. Synthesis and Performance of Methacrylic Ester Based Polycarboxylate Superplasticizers Possessing Hydroxy Terminated Poly (Ethylene Glycol) Side Chains. **2008**, *38*, 1210–1216.

(31) Winnefeld, F.; Becker, S.; Pakusch, J.; Götz, T. Effects of the Molecular Architecture of Comb-Shaped Superplasticizers on Their Performance in Cementitious Systems. *Cem. Concr. Compos.* **2007**, *29* (4), 251–262.

(32) Struble, L. J.; Lei, W. G. Rheological Changes Associated with Setting of Cement Paste. *Adv. Cem. Based Mater.* **1995**, *2* (6), 224–230.

(33) Taylor, H. F. W. *Cement Chemistry*, First Edit.; Thomas Telford Publishing LTD: New York, USA, 1990.

(34) Gartner, E. M.; Young, J. F.; Damidot, D. A.; Jawed, I. Hydration of Portland Cement. In *Structure and Performace of Cements*; CRC Press: London UK, 2001.

(35) Mollah, M. Y. A.; Adams, Ã. W. J.; Schennach, R.; Cocke, D. L. A Review of Cement Superplasticizer Interactions and Their Models. *Adv. Cem. Res.* **2000**, *12* (4), 153–161.

(36) Vollpracht, A.; Lothenbach, B.; Snellings, R.; Haufe, J. The Pore Solution of Blended Cements : A Review. *Mater. Struct.* **2016**, *49* (8), 3341–3367.

(37) Zhang, Y.; Kong, X. Correlations of the Dispersing Capability of NSF and PCE Types of Superplasticizer and Their Impacts on Cement Hydration with the Adsorption in Fresh Cement Pastes. *Cem. Concr. Res.* **2015**, *69*, 1–9.

(38) Yoshioka, K.; Tazawa, E. I.; Kawai, K.; Enohata, T. Adsorption Characteristics of Superplasticizers on Cement Component Minerals. *Cem. Concr. Res.* **2002**, *32* (10), 1507–1513.

(39) Meier, M. R.; Plank, J. Crystal Growth of [Ca3Al(OH)6·12H2O]2·(SO4)3·2H2O (Ettringite) under Microgravity: On the Impact of Anionicity of Polycarboxylate Comb Polymers. *J. Cryst. Growth* **2016**, *446*, 92–102.

Chapter 5: Effect of the Microstructure of the MPEG Superplasticizers on Different Crystalline Phases

5.1. Introduction

Ordinary Portland Cement is a heterogeneous material which, and as a general description, is composed mostly by clinker mixed with a small amount of gypsum or calcium sulphate compound. The clinker contains four major phases which are Alite (tricalcium silicate Ca_3SiO_5, C_3S), Belite (dicalcium silicate, Ca_2SiO_4, C_2S), Aluminate phase (tricalcium aluminate, $Ca_3Al_2O_6$, C_3A) and Ferrite phase (tetracalcium aluminoferrite (Ca_2AlFeO_5). Alite is tricalcium silicate and is the main phase present in OPC, which generally consist between 50-75% of the clinker and it is responsible of the production of CSH (Calcium Silicate Hydrate)[1]. Belite is dicalcium silicate and also forms CSH when reacting with water, but it has lower reactivity than alite and it appears in lower percentage in the clinker (15-30%). Also, it has been less studied because it does not affect the early properties of cement pastes and mostly contributes to the final properties of Portland cement[1]. Because its reaction time is much slower than in the case of alite it takes time for belite to harden. The aluminate phase is tricalcium aluminate and it is involved in the formation of ettringite ($Ca_6Al_2(SO_4)_3(OH)_{12}\cdot 26H_2O$) by reacting with gypsum present in cement on the first minutes of the hydration reaction. Ferrite phase (tetracalcium

aluminoferrite) is considered as one of the most reactive clinker phases present in ordinary Portland cement[2].

Knowing and understanding the interaction of the superplasticizers on each of the clinker phases is important because these interactions can help to understand their effect in Portland cements of different compositions[3]. Despite the fact that the use of PCEs on different cementitious systems has been investigated[3–7], there are certain aspects like how the microstructure affects each clinker phase that still remain unsolved. The complexity of the chemical processes involved in the hydration of the clinker phases makes it challenging to understand the most relevant processes.

Therefore, the aim of this chapter is to simplify this complexity by analyzing the effect of the synthesized PCEs on the pure crystalline phases that constitute the clinker. Specifically, the aim is to analyze the effect that different microstructural parameters of the MPEG type PCEs defined by Flatt et al.[8] (n parameter - backbone chain length, N parameter - charge density and P parameter - lateral chain length) have on three of the main clinker crystalline phases: C_2S, C_3S and C_3A and compare the effects with theoretical predictions developed by Marchon et al.[9].

For that, firstly, the clinker phases were characterized without admixture. Secondly, the physico-chemical properties of the pastes of the individual crystalline phases when the MPEG PCEs are added (admixture consumption, ζ-potential) were analyzed. Finally, the hydration kinetics monitored by calorimetry was studied and the effect of the microstructural properties of the PCEs on the hydration investigated.

5.2. Experimental Part

C_3S as well as C_3A were purchased from Chemical Bonds. They were stored under nitrogen and used as received. C_2S was synthesized in the laboratory according to the method developed by Link et al.[10]. The synthesis procedure is described in Appendix IV. However, it must be underlined that the C_2S phase is not a conventional phase as it was synthesized by a hydrothermal process based on the one developed by Link et al.[10] and it is more reactive than the conventional C_2S phase as it will be shown in the results and discussion section.

5.2.1. Characterization Methods

The methods described in chapter 4 were used here.

5.2.2. Characterization of the Pastes

As described for the OPC in chapter 4 the crystalline phases were mixed with water and the different PCEs. Due to the lower amount of material available for each phase, the water to cement ratio used in this chapter was different from the one used with OPC.

- ***Consumption of PCEs***

Consumption measurements were carried out by mixing 7 g of C_2S, C_3S or C_3A with 70 g of the aqueous solution (water + PCE) for 25 minutes (w/c: 10). Then, the aqueous solution was filtered with a Buchner funnel. The liquid phase extracted was then analyzed by Total Organic Carbon (TOC) analysis[11] at constant temperature. The total mass consumed was calculated subtracting the measured quantity by TOC to the total mass added. These analyses

were conducted by SGIker in the Faculty of the Science and Technology of the UPV/EHU in Leioa (Bizkaia-Spain).

- ***Zeta Potential measurements***

The Zeta Potential measurements were carried out using Acoustosizer IIs from Colloidal Dynamics. For the measurements, 30 g of crystalline phase and 160 g of water were mixed (w/c: 5.33 – water to cement ratio). An automatic titrator was used to add the PCE to the cement suspension and the dosages varied from 0-8 mg Pol/ g CEM[11].

- ***Sample Preparation for calorimetry***

Each material was prepared in a different way based on the quantity of the material available.

C_2S:

In this case, 25 g of the material were mixed with 31.25 g of water (w/c = 1.25). The dosage of the PCE was fixed to 3 mg PCE / g CEM. The mixing protocol to mix C_2S was different from the one used to mix OPC. The mixing procedure was the following:

1. 90 seconds mixing at 1500 rpm
2. Stop for 60 seconds
3. 90 seconds mixing at 1500 rpm

C_3S and C_3A:

In this case, due to the low quantity of material available, the mixing procedure was carried out by hand. The water to cement ratio was fixed to w/c = 0.5, 4 g of cement were mixed with 2 grams of aqueous solution that contain PCEs. The dosage of the PCE´s was fixed to 3 mg PCE/ g CEM.

- ***Hydration studies by calorimetry***

Hydration reactions were recorded in a TAM air conduction calorimeter at 25 ºC with water as reference material.

5.3. Results and Discussion

5.3.1. Characterization of the Crystalline Phases

All crystalline phases used in this section, C_3S, C_2S and C_3A where characterized by common characterization techniques to analyze their composition, morphology and physical properties such as density and surface area.

- **Sc*anning Electron Microscopy (SEM)***

The morphology of the individual clinker phases was analyzed by SEM and Figures 5.1-5.3 show that there is a difference on the shape and sizes of the different phases. Alite – C_3S (Figure 5.1), which is a commercial product, showed an irregular, but spherical-like morphology.

As it can be observed in Figure 5.1 generally all the particles presented a rounded shape and similar sizes although, some smaller particles were agglomerated forming bigger ones.

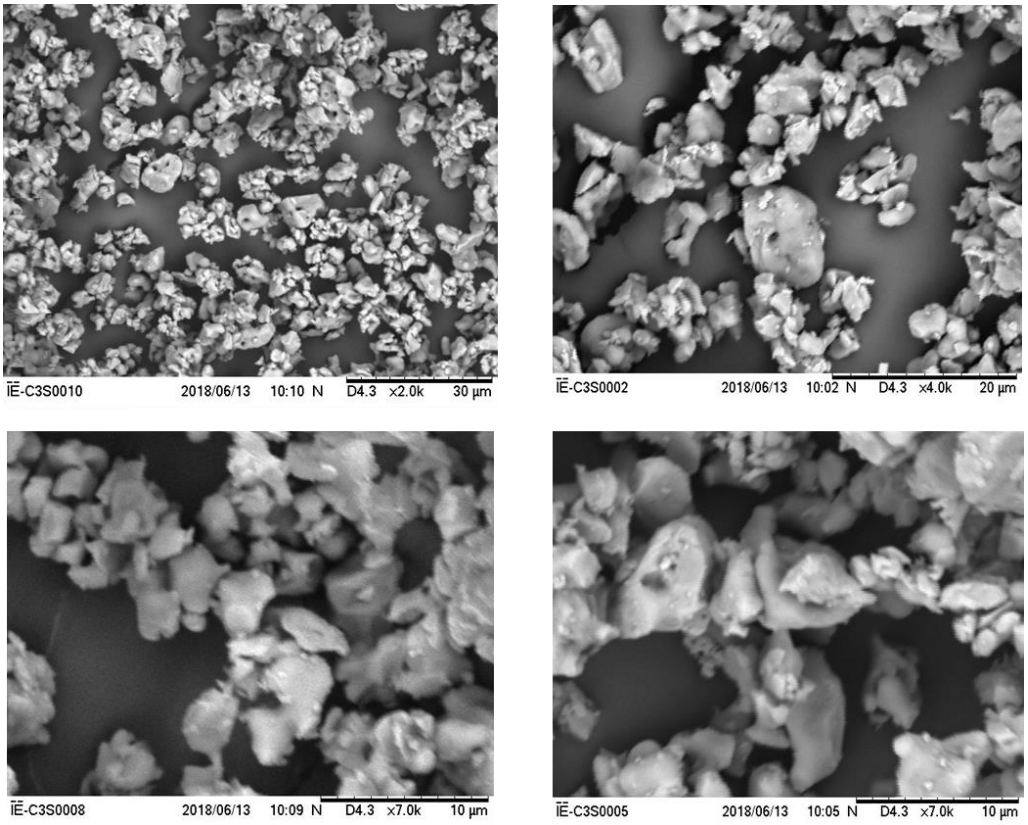

Figure 5.1: SEM images of the C_3S - Alite employed in this work.

On the other hand, C_2S-Belite (Figure 5.2), which was synthesized by a hydrothermal procedure (see Appendix IV), showed rectangular plate shape. Furthermore, agglomeration of the particles can be also observed, and coil type formations are present on top of the particles. The morphology of the particles coincided with the morphology reported by Link et al.[10].

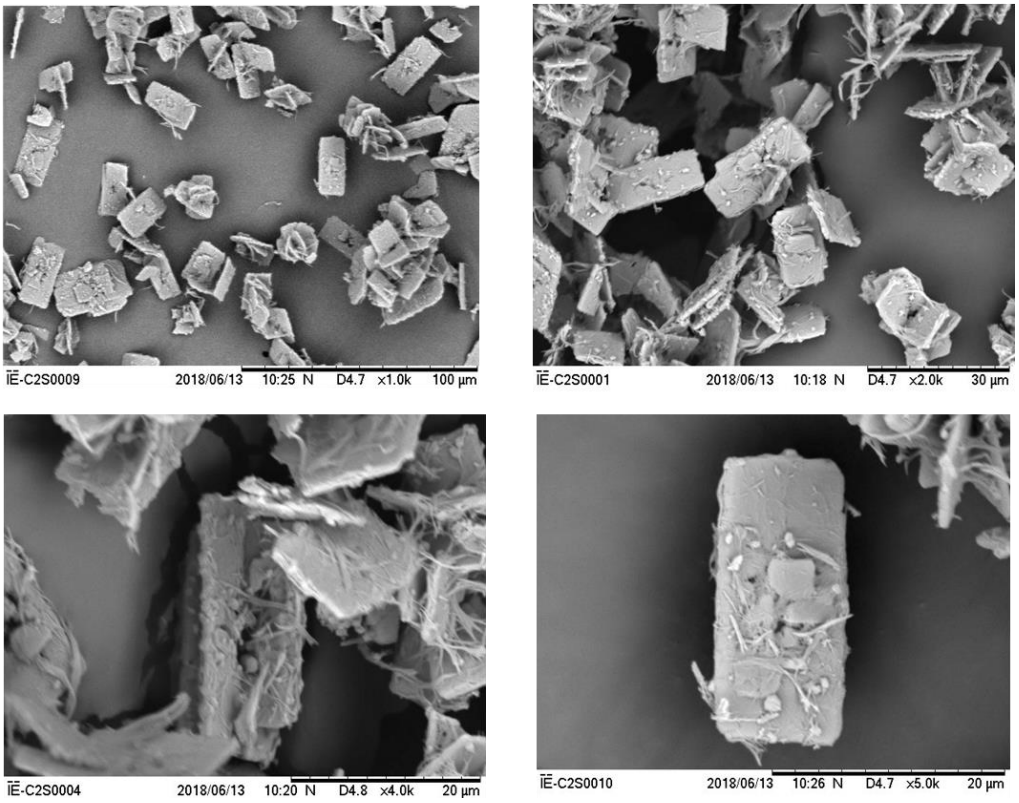

Figure 5.2: SEM images of the C_2S - Belite synthesized and employed in this work.

C_3A also showed a rounded morphology, but in this case broader distribution of sizes can be appreciated (Figure 5.3). There is substantial agglomeration of small particles on the surface of the bigger ones which makes the particles to have a granular type surface.

The three clinker phases present a different morphology and in comparison with OPC it can be said that alite presented the most similar morphology. However, in OPC particles with bigger sizes were observed (see Figure 4.3, chapter 4).

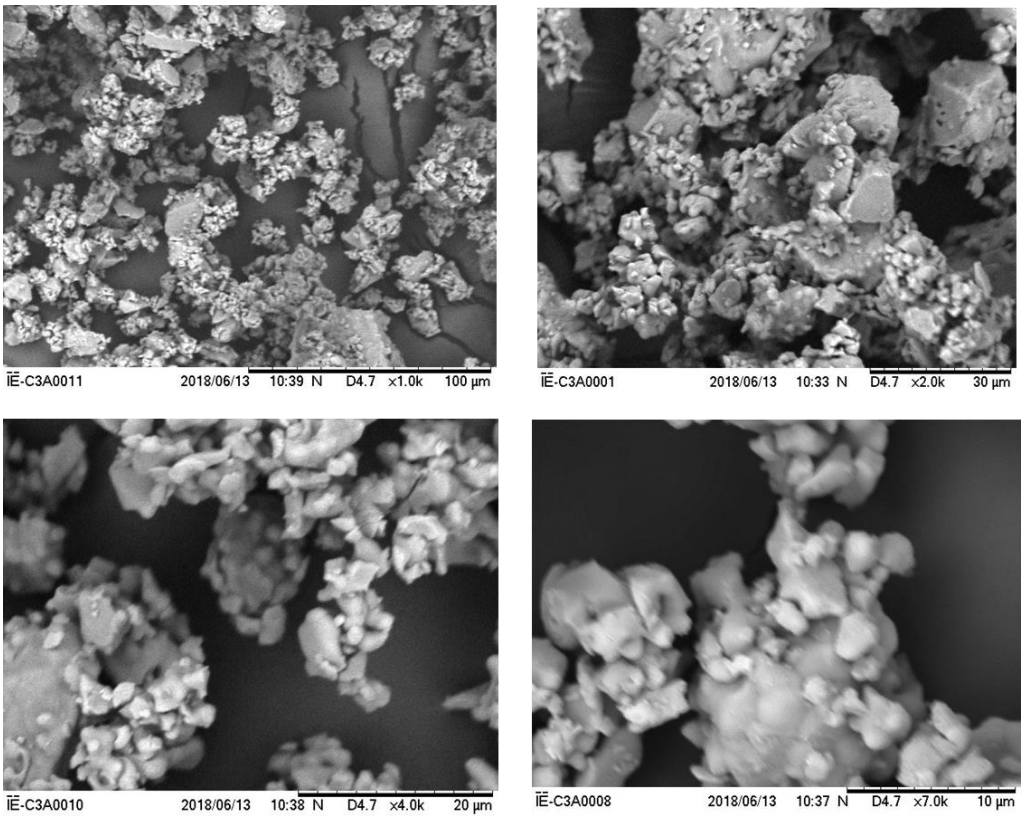

Figure 5.3: SEM images of C_3A - Aluminate employed in this work.

- ***X-ray diffraction XRD - Rietveld analysis– X-ray Fluorescence XRF***

X-ray diffraction measurements were carried out in order to characterize and confirm the composition of the materials used. Alite – C_3S (Figure 5.4) showed a clear XRD spectrum in which only calcium silicate and lime (in small proportion) are present.

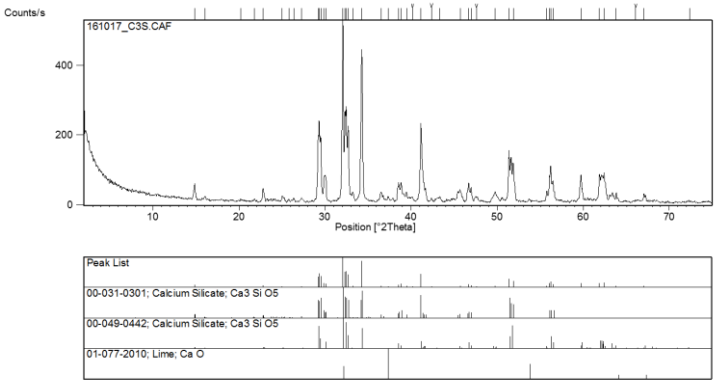

Figure 5.4: X-ray diffraction spectrum of the commercial C_3S-Alite.

C_2S-Belite showed heterogeneity on the qualitative analysis (Figure 5.5) as calcite ($CaCO_3$), dellaite ($Ca_6(SiO_4)(Si_2O_7)(OH)_2$ and portlandite ($Ca(OH)_2$) are present. Certain amount of hydrated phases can be expected because the C_2S is obtained by a mild calcination (450ºC) of a product (α-C_2SH) obtained by hydrothermal reaction. A quantification of the phases found in C_2S was done by the Rietveld method (Table 5.1).

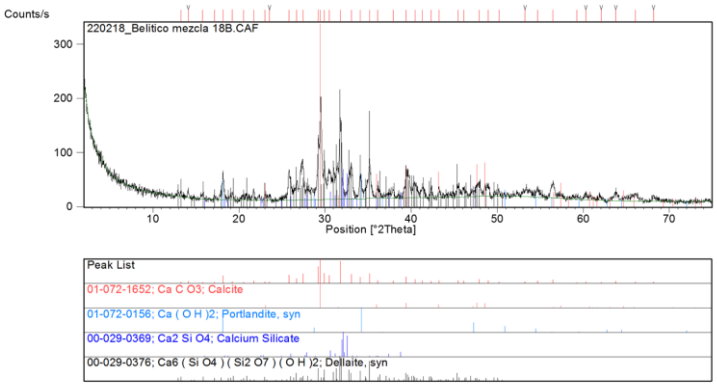

Figure 5.5: X-ray diffraction spectrum of the synthesized C_2S-Belite.

The different crystalline phases present in belite were quantified by Rietveld analysis. The main phase is the monoclinic C_2S (37.6%) followed by an amorphous phase which comprises the 27.2% of the total. The formation of this amorphous phase is due to the low annealing temperature[8] used. Furthermore, several hydrated phases are also present in the product which are Dellaite and Killalaite (see table 5.1). (Dellaite is a calcium silicate mineral ($Ca_6Si_3O_{11}(OH)_2$) which has around 4% of presence of water, so it is considered as hydrated compound[12]. Killalaite $Ca_{3+x}(H_{1-2x}Si_2O_7)(OH)$, with $x \approx 0{\cdot}2$, is the third most abundant compound in the Belite material, it is also a calcium silicate mineral with 3% of water[13]. Taking this into account, substantial amount of hydrated phases are present on Belite.

Table 5.1: Rietveld analysis of the C_2S – Belite employed in this work.

Rietveld Analysis	
Phases	***wt %***
Amorphous	27.2 ± 0.82
Porlandite	2.0 ± 0.08
Dellaite	9.9 ± 0.50
Calcite	1.1 ± 0.01
Brownmillerite	0.5
Ellestadite	1.1 ± 0.04
C_2S	37.6 ± 0.75
Xonotlite	4.8 ± 0.34
Killalaite	15.7 ± 0.31
Cristobalite	0.2

Aluminate – C_3A (Figure 5.6) also showed a clear XRD spectrum, where the majority of the material is tricalcium aluminate ($Ca_9Al_6O_{18}$) and there is also a small amount of calcium hydroxide present ($Ca(OH)_2$).

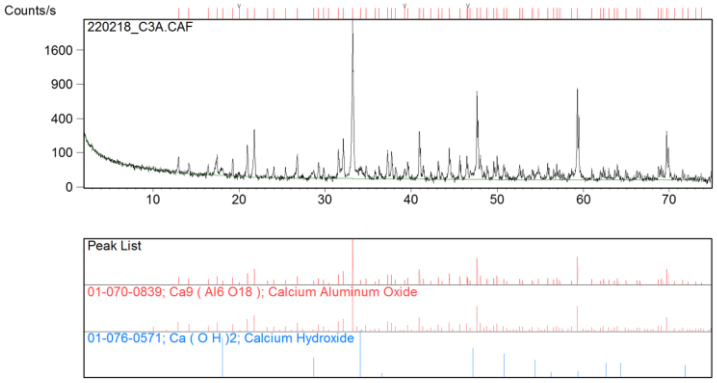

Figure 5.6: X-ray diffraction spectrum of the commercial C_3A-Aluminate.

X-ray fluorescence measurements was used to determine the elemental composition in oxides form of each of the materials. All the three materials showed expected elements. Calcium (in CaO form) is the most abundant element in the three materials followed by silicon in C_2S and C_3S and aluminum in C_3A.

Table 5.2: Composition of oxides of the different materials employed in this work.

C_3S – Alite		C_2S – Belite		C_3A – Aluminate	
Compound	*wt%*	*Compound*	*wt%*	*Compound*	*wt%*
CaO	70.79 ± 0.41	CaO	58.82 ± 0.34	CaO	60.16 ± 0.34
SiO_2	25.87 ± 0.22	SiO_2	33.03 ± 0.24	SiO_2	0.08 ± 0.01
F	1.12 ± 0.59	F	1.18 ± 0.53	F	1.20 ± 0.54
Al_2O_3	0.22 ± 0.02	Al_2O_3	-	Al_2O_3	35.23 ± 0.24
Na_2O	0.05 ± 0.01	Na_2O	0.87 ± 0.04	Na_2O	0.18 ± 0.02
MgO	0.03 ± 0.01	MgO	0.47 ± 0.02	MgO	0.11 ± 0.01
Fe_2O_3	0.03 ± 0.001	Fe_2O_3	0.14 ± 0.01	P_2O_5	0.21 ± 0.003

- ***Density measurements and surface area***

The characterization of the density of the material and the surface area will provide useful information at the time of understanding the interaction of the PCEs with the surface of these materials and also the surface area will have an effect on the rate at which these materials react with water. Density measurements were performed by Le Chatelieur flask method and surface areas by Blaine fineness.

Table 5.3 shows the calculated density and surface area of the different materials. As can be seen in Table 5.3 C_2S-Belite has the lowest density (2.5726 g/cm^3) and the value obtained is relatively lower than expected (3.280 g/cm^3)[2]. Ulm et al reported[14] that depending on the S/C ratio of the hydrate phase the density of the material can varied from 2.18 to 2.60 g/cm^3, in this case the density is 2.5726 g/cm^3, thus, this results could be due to the high amount of hydrated phases (amorphous) present in this material, like Dellaite and Killalaite. C_3S-Alite and C_3A-aluminate showed higher density and in both cases the experimental value obtained is close to the reported one[2]. Regarding the surface area, it can be observed that C_2S-Belite showed a much higher value than the other phases. The fact that the surface are is high will have considerable effect on the interaction of the PCEs as the higher the surface area the higher the interaction between substrate and the adsorbent.

Table 5.3: Density and Blaine fineness obtained for the different materials employed in this work.

Material	Density (g/cm^3)	Surface Area (cm^2/g)
C_3S – Alite	3.2292	3029
C_2S - Belite	2.5726	5360
C_3A - Aluminate	3.0313	2883

5.3.2. Characterization of Pastes Prepared with the Crystalline Phases

Figure 5.7 shows the time evolution of the zeta potential of the three different phases. In this case, all three phases presented positive zeta potential with C_2S presenting the lowest zeta potential (5-8 mV) and C_3S and C_3A presenting higher values in the range of 15-20 mV. Furthermore, the zeta potential of C_3A increased over time while the zeta potential of the other phases remained more or less constant.

In contrast with our results, in literature it has been observed that C_2S provided negative values[3,6]. In these cases, C_2S was also synthesized in the laboratory, however it was synthesize by rapid cooling after annealing it at temperatures above 1200 ºC. In our case, the synthesis process was hydrothermal and the different synthesis procedure provided a clinker phase with different morphology and characteristics

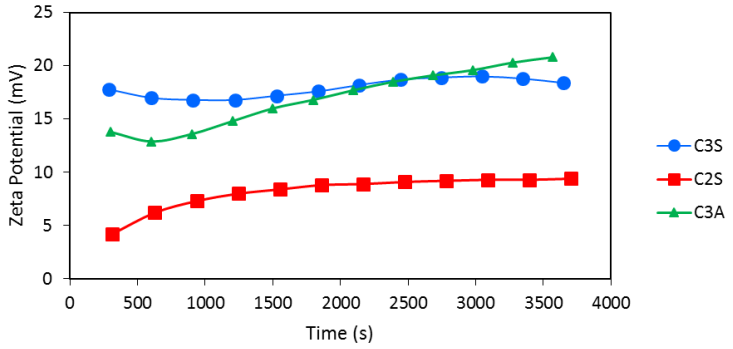

Figure 5.7: Time evolution of the zeta potential of the different phases without admixtures.

The different phases employed have different reactivities when reacting with water and with the aim of characterizing it, a comparison without admixture was performed. OPC was also

included for comparison purpose. As it can be seen in Figure 5.8, C_3S-Alite is the phase with the higher reactivity, while C_2S-Belite is a low reactive phase. As previously mentioned, C_2S was synthesized in the laboratory and the obtained phase is substantially more reactive than conventional C_2S[10] (see Apendix IV). On the other hand, Aluminate phase, in absence of calcium sulfate (Gypsum) reacts very fast. There is not induction period and setting is almost instanteneous[15].

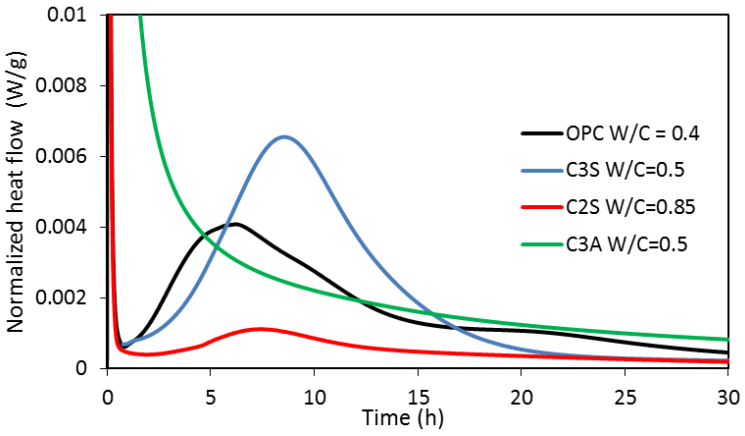

Figure 5.8: Time evolution of the normalized heat flow for the different materials employed.

5.3.3. Effect of Superplasticizers

In this part, the effect produced by the superplasticizers with each phase is analyzed. The superplasticizers were synthesized in chapters 2 and 3 with different characteristics. The effect of the n, N and P parameters (backbone length, charge density and side chain length) of the different superplasticizers is studied.

Firstly, consumption measurements and zeta potential measurements were carried out, afterwards the effect on the hydration kinetics was analyzed.

5.3.3.1. Effect of Superplasticizers with Short Side Chains (P=5)

5.3.3.1.a. Effect of n Parameter – Backbone Length

The superplasticizers employed to study the effect of n parameter on the different clinker phases were synthesized in chapter 2 (Series S) and they present low and fixed P value (P = 5, short side chains), fixed N value (N = 4, charge density) and variable n parameter (variable backbone lengths). Table 5.4 shows the main characteristics of the studied PCEs:

Table 5.4: Main characteristics of the synthesized SPs used on the analysis of the effect of n.

PCE	*Mw (kg/mol)*	*Đ*	*DP*	*n*	*P*	*N*
S1	88.0 ± 1.4	3.0	206	51.7	5	*4.0*
S4	51.4 ± 0.5	2.2	166	42.1	5	*3.9*
S5	40.8 ± 0.6	2.0	146	37.5	5	*3.9*
S6	32.8 ± 0.3	2.0	112	29.4	5	*3.8*

- ***Consumption of PCEs***

In Figure 5.9 the consumption of the PCEs from series S (short side chains, P=5) on the different phases are shown. The graphs presents the total mass consumed calculated from the difference of the added mass and the measured one by TOC on the filtration solution.

In the three materials, the effect of n on the consumption is very limited and differences are only appreciated at dosages around 6.0 mg PCE/ g CEM. As a general view it can be said that the behavior in all three cases is similar. However, some differences are appreciated when comparing the results with OPC. In OPC, when increasing the backbone length, n, of the PCE the consumption also increased slightly.

Previous studies revealed that the adsorption of PCEs mostly takes place in aluminate (C_3A) and ferrite (C_4AF) phases rather than in silicate phases[16]. Interestingly, we observed that adsorption is higher in aluminate phases, but substantial adsorption also occurs in C_2S and C_3S phases. This result is likely related to the positive zeta potential found for the three phases that favors the adsorption of macromolecules (PCEs) bearing negative charged in their backbone.

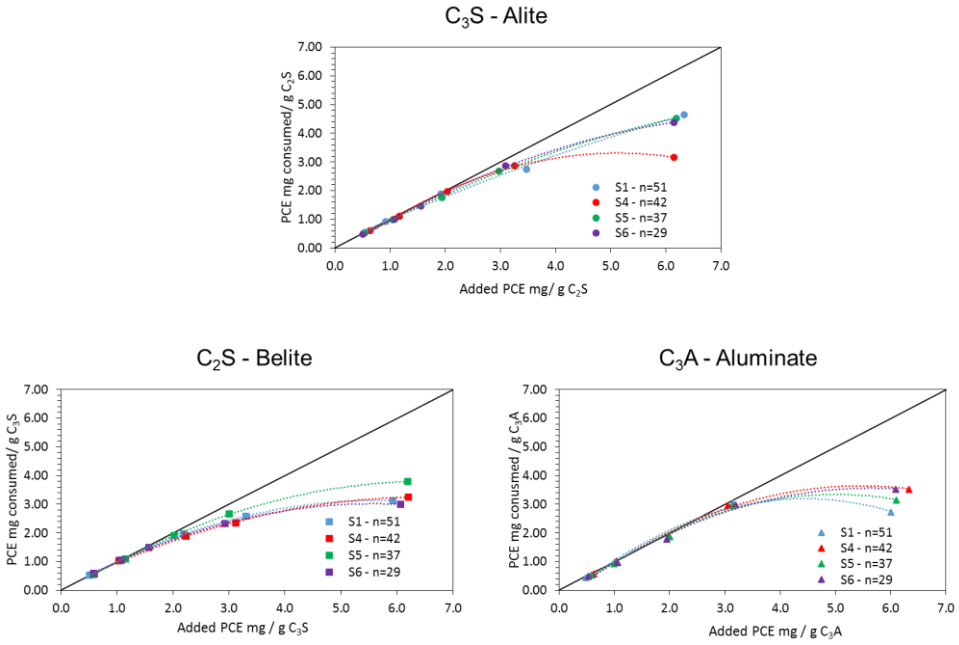

Figure 5.9: Consumption of PCE's with variable n parameter on C_3S, C_2S and C_3A.

Table 5.5 shows the consumed amount of PCEs by weight, extracted from Figure 5.9, by unit of area calculated using the surface area of the material (Table 5.3) and the consumed number of chains at 3 mg PCE addition / g CEM based on the Mn of the PCEs. The number of consumed chains per unit of are is higher in aluminate-C_3A than in Alite-C_3S and Belite-C_2S. Although the length of the backbone does not seem to have an effect on the consumed PCE amount per unit weight it does have an effect when calculated as the number of chains per unit area as also observed previously for OPC. The lower the n, the higher the number of chains consumed. This trend is maintained in all three crystalline phases.

Table 5.5: Adsorbed amount of the different PCEs in terms of unit weight, area and number of chains adsorbed per area[7].

Material	*Surface Area - Blaine Fineness (m^2/g)*	*PCE/ n*	*Consumed amount at (3 mg Pol/ g CEM)*		*Consumed number of PCE chains per unit area (chain/ 100 nm^2)*	K_A^* *Adsorption equilibrium constant*[9]*
			per unit weight (mg/g)	*per unit area (mg/m^2)*		
(C_3S)	0.3029	S1/ 51	2.35	7.76	5.30	S1 (n=51) – 414.7
		S4/ 42	2.35	7.75	9.07	
		S5/ 37	2.65	8.74	12.89	
		S6/ 29	2.35	7.76	14.24	S4 (n=42) – 499.9
(C_2S)	0.5360	S1/ 51	2.60	4.85	3.31	
		S4/ 42	2.65	4.94	5.79	
		S5/ 37	2.68	5.00	7.38	S5 (n=37) – 545.0
		S6/ 29	2.70	5.04	9.24	
(C_3A)	0.2883	S1/ 51	2.80	9.71	6.64	
		S4/ 42	2.80	9.71	11.37	S6 (n=26) – 666.2
		S5/ 37	2.70	9.37	13.82	
		S6/ 29	2.65	9.19	16.87	

This trend is in qualitative agreement with the theoretical adsorption constant defined by Marchon et al.[9] (equation 4.2 in chapter 4); namely increasing the backbone length the

adsorption constant decreases. Table 5.5 displays the values of K_A^* calculated with the theoretical expression for each of the PCEs studied here (the values of n, P and N presented in Table 5.4 were used). Note that the values of K_A^* are independent of the crystalline phase because the theoretical expression was calculated for a model substrate. In Figure 5.10 the theoretical adsorption constant and the experimentally determined consumed PCE chains per unit of area are shown. Table 5.6 presents the fitting of the experimental data to a potential function.

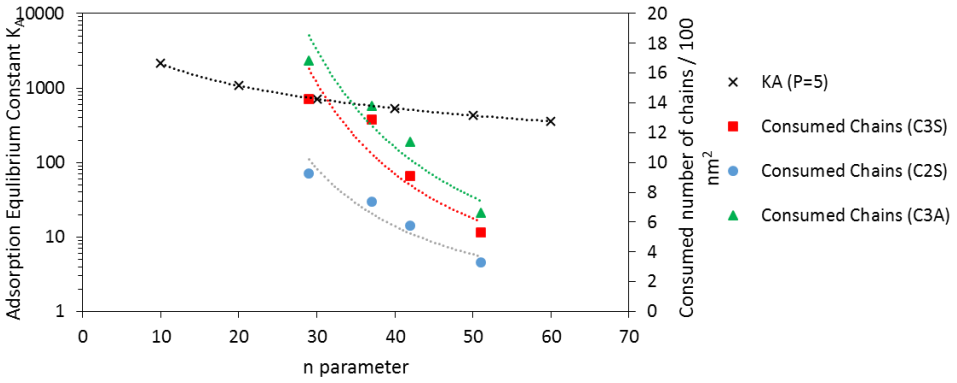

Figure 5.10: Comparison of theoretical prediction for K_A and the experimental data of the consumed chains per area for the different crystalline phases.

The consumed PCE chains per unit of area depends more strongly for all three materials on the backbone-chain length of the PCE's, n, than what theoretical equation predicts. For the three materials the experimental dependency is between a power of 1.6 and 1.8, whereas, in the theoretical equation the dependency is of the power of 1 (see table 5.6). Furthermore, it is worth mentioning that the experimental dependence observed in the three clinker phases is higher than

the observed in OPC (OPC – power of 1.12, clinker phases - power of 1.6-1.8). This effect might be because the clinker phases presented a different surface morphology.

Table 5.6: Dependencies obtained (theoretical K_A and experimental consumed chains) for the different PCEs in different crystalline phases.

PCE/ Phase	Equation
Series S (P=5)/ C_3S	Experimental Result: $Consumed\ Chains \propto 4270.1n^{-1.62}$
Series S (P=5)/ C_2S	Experimental Result: $Consumed\ Chains \propto 4253.2 \cdot n^{-1.79}$
Series S (P=5)/ C_3A	Experimental Result: $Consumed\ Chains \propto 4253.2 \cdot n^{-1.76}$
Theoretical $K_A^* \propto \frac{z^2(N-1)^2}{nP^{9/5}N^{3/5}} \cdot 10^5$	Theoretical Prediction: $K_A^* \propto 21442 \cdot n^{-1}$

- ***Zeta potential measurements***

Figure 5.11 shows the zeta potential evolution as a function of the PCE addition dosage for the three different crystalline phases analyzed.

Zeta-potentials are negative for Alite-C_3S and Belite-C_2S and remained positive for the Aluminate-C_3A although decreases notably from the initial value in absence of PCEs. In none of the crystalline phases the length of the backbone, n, show any significant effect which is in agreement with the results obtained in OPC with the same PCEs.

It is noteworthy that the Aluminate-C_3A phase presents positive charge when as shown by the consumption results is the phase that most PCEs consumed. However, it is worth recalling that the consumed PCE could not only be adsorbed on the surface of the crystalline phase, but it could also participate in the formation of organo-mineral phases.

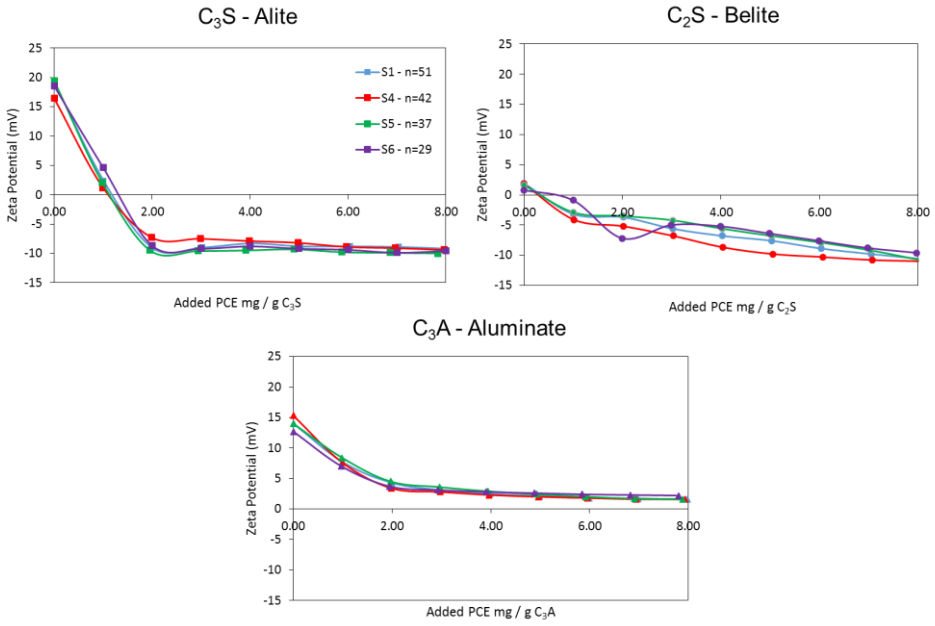

Figure 5.11: Evolution of the Zeta potential values over the added mg of PCE with variable n parameter in respect to grams of individual clinker phases.

- ***Hydration kinetics by calorimetry***

Aluminate phase, in absence of gypsum reacts very fast and the hydration reaction was kept unaltered with the addition of PCEs. Hence, the analysis of the hydration kinetics was not carried out with C_3A phase. In Figure 5.12A the time evolution of the hydration reactions of Alite-

C_3S with the different PCEs are presented. The hydration of C_3S is substantially delayed when PCEs are added, and the hydration peak is notably broadened. In this case, the main peak is retarded for about 10 hours. In general, it can be said that the n parameter (backbone length) of the PCEs did not affect the hydration of the C_3S, a result also reported by Marchon and Flatt[17,18].

Figure 5.12B shows the time evolution of the hydration reaction of C_2S. The addition of PCEs to C_2S changed the hydration curve of the material. The heat released curves are delayed and the peak is broader when PCEs are added. Regarding the backbone length only the PCE with n=42 shows a different effect in comparison to the others in the series. Both a higher delay and a broader peak are obtained, but admittedly we do not have an explanation for this behavior.

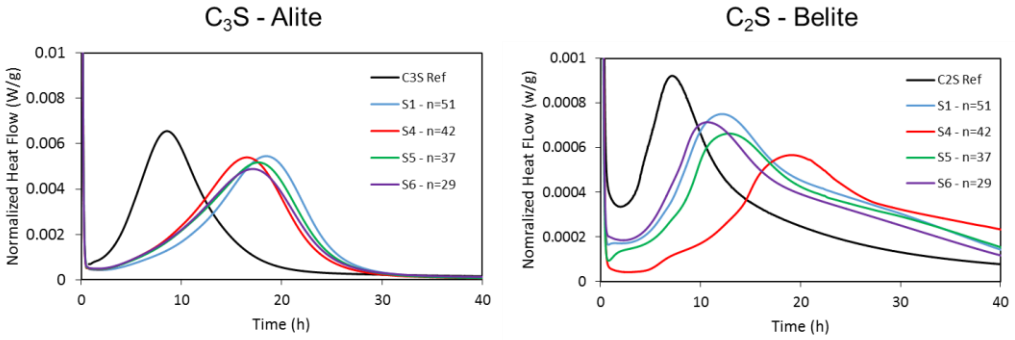

Figure 5.12: Time evolution of the normalized heat flow for A) C_3S-Alite and B) C_2S-Belite crystalline phases

Table 5.7 presents the obtained peak time, Δt with respect to the reference and normalized heat released for both crystalline phases, C_3S-Alite and C_2S-Belite.

Table 5.7: Peak time of the normalized heat flow, Δt of the peak with the reference and the normalized heat released at 40h of crystalline phases (C_3S-Alite and C_2S-Belite) with PCE's of different n parameter.

Crystalline Phase	*PCE/ n*	*Peak Time (h)*	*Δt (h)**	*Normalized heat 40h (J/g)*
C_3S-Alite	C_3S Ref	8.89	-	247.33
	S1/ 51	18.88	9.99	265.27
	S4/ 42	16.26	7.37	264.52
	S5/ 37	17.89	9.00	265.80
	S6/ 29	17.56	8.67	257.54
C_2S-Belite	C_2S Ref	7.53	-	66.25
	S1/ 51	12.25	4.72	68.67
	S4/ 42	19.10	11.57	59.74
	S5/ 37	13.03	5.50	59.48
	S6/ 29	11.01	3.48	61.72

* Δt is the difference of the main peaks time between the crystalline phase paste with PCE and the paste without without PCE

As previously mentioned, Marchon et al.[9] showed on the theoretical prediction for Δt that the retardation on the hydration was independent from n parameter (see eq. 4.5, chapter 4). That prediction was calculated for a model cement which contained a mixture of crystalline phases. In this case, where individual crystalline phases were used, it was also shown that n parameter has little effect on the retardation of the hydration. In Figure 5.13 a comparison between the model equation and the experimental values is presented. For the easiness of visualization the values are normalized taking the PCE S1 as reference. Except for S4, no significant differences are seen between the different PCEs. The experimental results obtained for these materials are in accordance with the obtained in OPC, where n parameter of the PCEs was independent of the hydration delay.

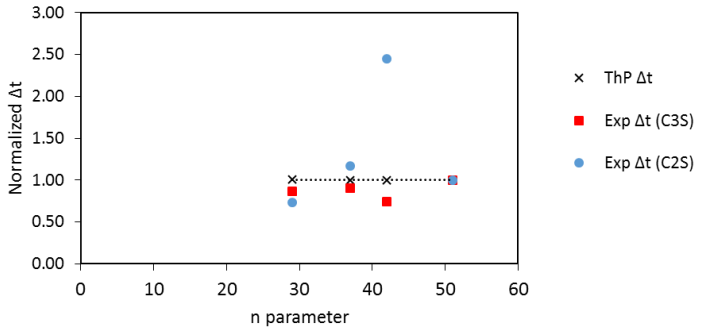

Figure 5.13: Retardation of the hydration of the Alite and Belite, Δt, as a function of the chain length, n, of the PCE's. All values have been normalized to S1

5.3.3.1.b. Effect of the MAA/PEGMA Ratio, N - Charge Density

The superplasticizers employed for the analysis of the N parameter (charge density) were synthesized in chapter 2 with low P value (P=5, short lateral chains). Unfortunately, the backbone chain length, was not controlled but as it has been shown in the previous section n has little effect and therefore, the effect (if any) observed in this section will be attributed to the charge density, N. Table 5.8 shows the main characteristics of these PCEs.

Table 5.8: Main characteristics of the PCEs used in the analysis of the N parameter.

PCE	*Mw (kg/mol)*	*Đ*	*DP*	*n*	*P*	*N*
S2	100.2 ± 0.7	3.0	211	71.5	5	*3.0*
S1	88.0 ± 1.4	3.0	206	51.7	5	*4.0*
S3	40.8 ± 0.6	2.0	156	31.2	5	*5.0*

- ***Consumption of PCEs***

Figure 5.14 shows the total mass consumed for PCE's with low P (P=5, short side chains) and variable N parameter (variable charge density) for the three different phases employed.

The consumption of PCEs is high in all three crystalline phases until the saturation point is reached. Especially, the high consumption of PCEs on Aluminate C_3A phase might be due to the formation of the organo-mineral phase as Flatt et al.[19] and Plank et al.[20] reported. Plank et al.[20] reported that anionic polymers which are applied as concrete admixtures can intercalate into the lamellar calcium aluminate hydrates and the ability of PCEs to intercalate increases with higher anionic charge density and shorter side chain. Over the saturation point, the consumption of the PCEs is stabilized even though in Belite-C_2S continued increasing.

There are not high differences when N of the PCE is varied, however, it seems that when N=3 (lowest N values used in the study) the consumption is lower especially in Alite-C_3S and Aluminate-C_3A. In Table 5.9 the consumed amount of PCE by mass per unit of weight and unit of area is presented. The number of consumed chains per unit of area is also included.

Table 5.9: Consumed amount of the different PCEs in terms of per unit weight, area and number of chains adsorbed per area[7].

Material	*Surface Area - Blaine Fineness (m^2/g)*	*PCE/ N*	*Consumed amount at (3 mg Pol/ g CEM)*		*Consumed number of PCE chains per unit area (chains/100 nm^2)*	K_A^* *Adsorption equilibrium constant*[9]
			per unit weight (mg/g)	*per unit area (mg/m^2)*		
Alite (C_3S)	0.3029	S2/ 3	2.00	6.60	3.97	S2 (N=3) – 153.3
		S1/ 4	2.35	7.75	5.30	
		S3/ 5	2.30	7.59	10.55	

Belite (C_2S)	0.5360	S2/ 3 S1/ 4 S3/ 5	2.75 2.60 2.85	5.13 4.85 5.31	3.08 3.31 7.38	S1 (N=4) – 414.7
Aluminate (C_3A)	0.2883	S2/ 3 S1/ 4 S3/ 5	2.60 2.80 2.80	9.01 9.71 9.71	5.41 6.64 13.50	S3 (N=5) – 1065.9

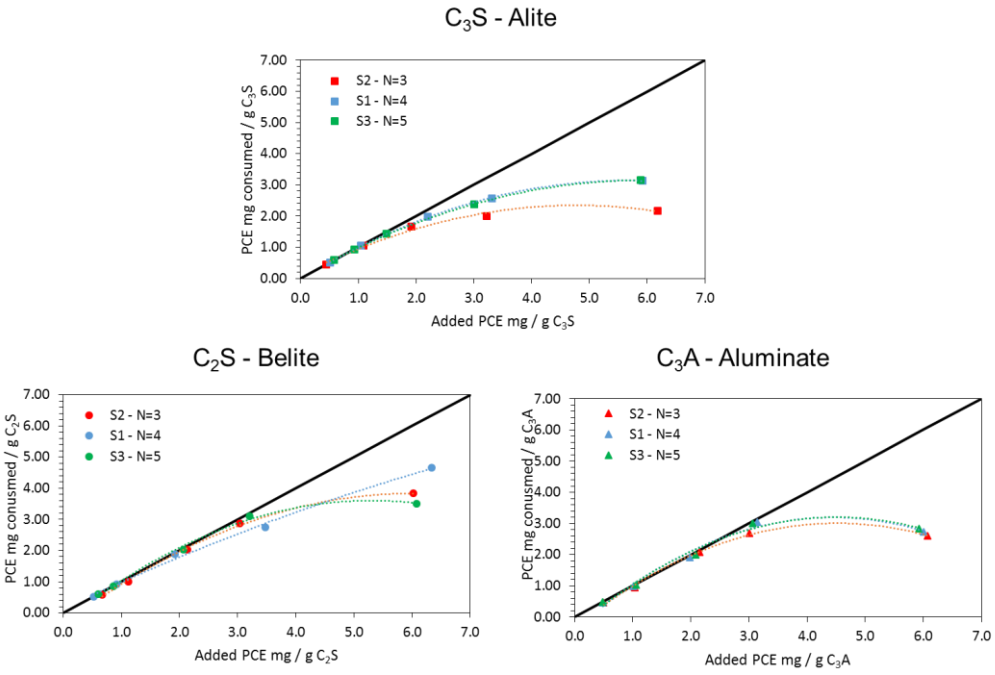

Figure 5.14: Consumption of PCEs with variable N. respect to added PCE.

The theoretical prediction of the adsorption constant K_A^* and experimental results of the number of PCE chains adsorbed per unit of area are plotted in Figure 5.15 to compare the trends. As in the case of OPC, in the case of crystalline phases the consumed PCE chains per unit of area increases with the ratio MAA/PEGMA (N) in agreement with the theoretical prediction, but

the power dependence calculated from the experimental results is slightly smaller (1.64-1.87 vs 2.14; see Table 5.10). This is likely due to the fact that the theoretical model considers 100% coverage of the surface and it does not consider that part of the PCE's can be consumed in OMP production. The experimental dependence with the variation of N is in agreement with the dependence obtained in OPC (1.75, see Table 4.11, chapter 4) hence, it can be said that the N parameter affects in a similar way to the consumption all the materials studied.

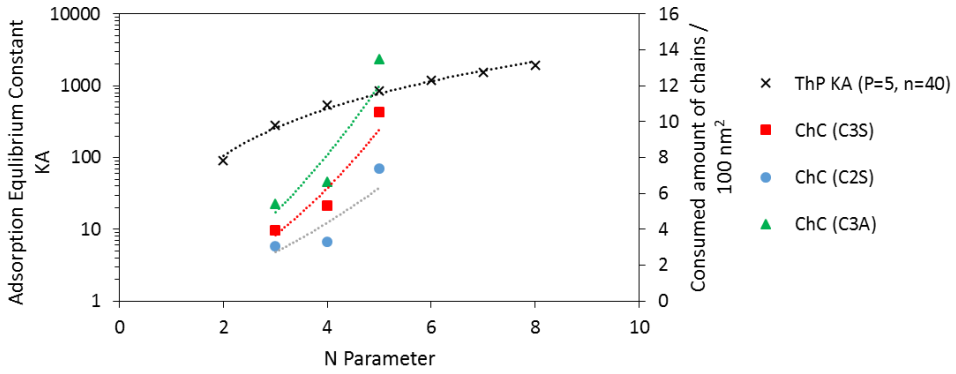

Figure 5.15: Comparison of theoretical prediction for K_A and the experimental data of the consumed chains per area for the different crystalline phases.

Table 5.10: Dependency relations obtained (theoretical K_A and experimental consumed chains) for the different PCEs with variable charge density, N, in different crystalline phases.

PCE/ Phase	Equation
Series S (P=5)/ C_3S	Experimental Result: $Consumed\ Chains \propto 0.4715 \cdot N^{1.87}$
Series S (P=5)/ C_2S	Experimental Result: $Consumed\ Chains \propto 0.4491 \cdot N^{1.64}$
Series S (P=5)/ C_3A	Experimental Result: $Consumed\ Chains \propto 0.7317 \cdot N^{1.74}$
Theoretical $K_A^* \propto \frac{z^2(N-1)^2}{nP^{9/5}N^{3/5}} \cdot 10^5$	Theoretical Prediction: $K_A^* \propto 23.632 \cdot N^{2.17}$

- ***Zeta potential measurements***

Figure 5.16 shows the evolution of the zeta potential with the addition of PCEs with variable N (variable charge density) to the different clinker phases used. The addition of the PCEs changed the zeta potential of the materials in all the three cases. In the case of C_2S and C_3S the zeta potential decreased up to -10 mV. This suggest that electrostatic forces are responsible for the dispersion of the particles as in the case of OPC. In the case of C_3A, the zeta potential decreased up to a slight positive value. Comparing the PCEs small differences are observed, even though S3 with the highest N value (N = 5, highest charge density) decreased slightly more the zeta potential of the materials.

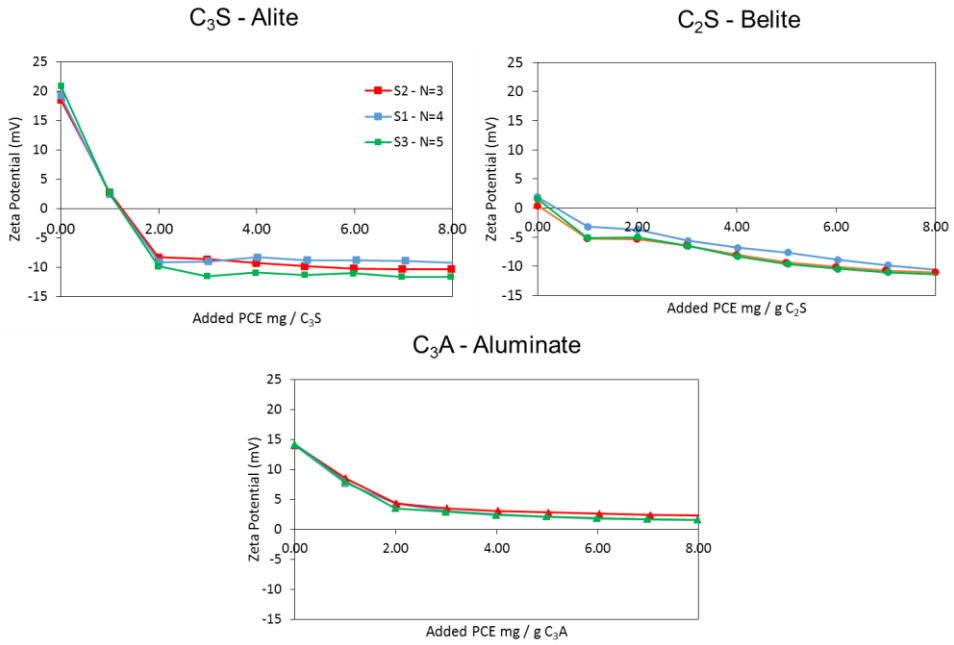

Figure 5.16: Evolution of the Zeta potential values over the added mg of PCE with variable N value in respect to grams of crystalline phase for the different clinker phases.

- ***Hydration kinetics by calorimetry***

Figure 5.17 shows the time evolution of the hydration reaction for both C_3S-Alite and C_2S-Belite crystalline phases. Table 5.11 shows the values of the peak time, Δt respect to the reference and the heat released at 40 h. In the case of C_3S-Alite, it can be observed that the retardation caused by the addition of PCEs is substantial, in all the cases (when PCEs are added) the peak time doubles the reference peak time. Furthermore, it is observed that the higher the N parameter (higher charge density) of the PCEs the higher the retardation produced. The addition of the PCEs generated a higher released of heat at 40h, so, it could be said that this type of PCEs enhance the hydration of C_3S. In the case of C_2S-Belite, the addition of PCEs cause

retardation on the hydration reaction but the charge density, N, does not cause any substantial changes on the hydration.

Table 5.11: Peak time, Δt with respect to the reference and normalized heat released at 40h for C_3S and C_2S with PCE's of different N parameter

Crystalline Phase	*PCE/ N*	*Peak Time (h)*	*Δt (h)*	*Normalized heat at 40h (J/g)*
C_3S-Alite	C_3S Ref	8.89	-	247.33
	S2/ 3	16.54	7.65	261.68
	S1/ 4	18.88	9.99	265.27
	S3/ 5	22.81	13.92	258.67
C_2S-Beite	C_2S Ref	7.53	-	66.25
	S2/ 3	11.68	4.15	58.92
	S1/ 4	12.25	4.72	68.67
	S3/ 5	13.13	5.60	62.72

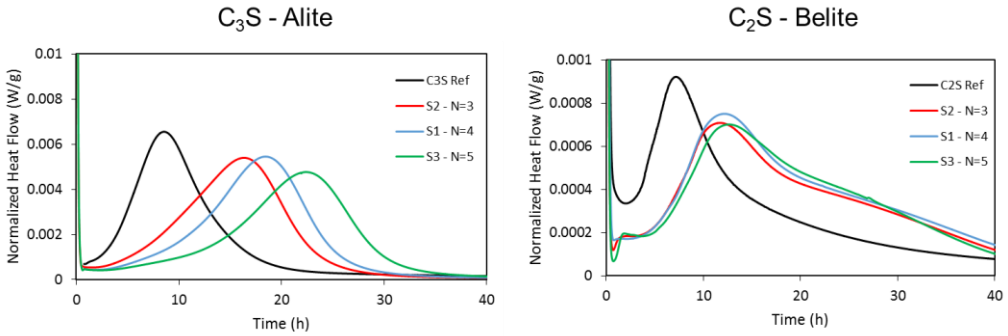

Figure 5.17: Time evolution of the normalized heat flow for A) C_3S-Alite and B) C_2S-Belite crystalline phases

As it is known and shown each crystalline phase produce different hydration reaction, and the PCEs do not affect all crystalline phases in the same manner. In this work, the comparison

of the theoretical prediction developed by Marchon et al.[9] with the experimental results was also assessed. As mentioned above, the theoretical prediction was developed for a model cement, therefore, one might expect some differences when compared with crystalline phases. Figure 5.18 presents the comparison of the normalized Δt predicted by the theoretical prediction and the experimental results obtained for both Alite and Belite. For easiness of visualization all values were normalized with respect to S3, the PCE with N=5. As observed, there is a substantial difference between theoretical prediction and the experimental results .The theoretical prediction is not sensitive to N in this range (3-5) and for PCE's with small lateral chain (P=5). However, the retardation of the hydration of the crystalline phases decreases as N decreases; the effect is more pronounced in C_3S than in C_2S. On the other hand, it is worth mentioning that the experimental results and theoretical prediction correlated for OPC material but not for C_3S and C_2S. An explanation for this behavior might be that other phases or constituents in OPC, like aluminate or gypsum, have influence on the hydration when PCEs are added.

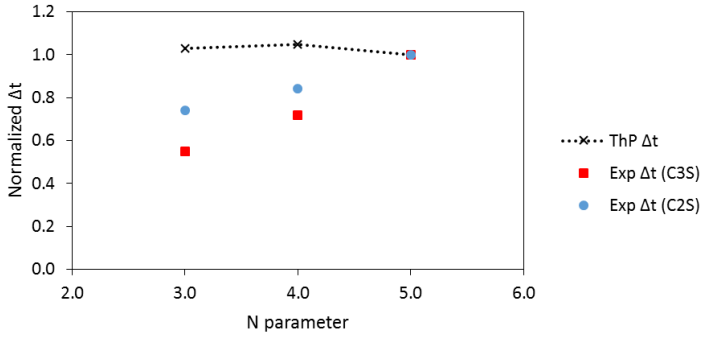

Figure 5.17: Comparison of theoretical prediction for normalized Δt and the experimental results for the different crystalline phases.

5.3.3.2. Effect of PCEs with Different Lateral Chain Length (P)

In order to study how the length of the side chains, P, affects the hydration of the clinker phases the PCEs listed in Table 5.12 were used (Series S was synthesized in chapter 2 and series M, L and XL were synthesized in chapter 3). The value of N (charge density) was fixed to N = 4 and the value of n (length of the backbone) was kept as similar as possible:

Table 5.12: Main characteristics of the SPs used in the analysis of P parameter (lateral chain length).

PCE	*Mw (kg/mol)*	*Đ*	*DP*	*n*	*P*	*N*
S6	32.8 ± 0.3	2.0	112	29.4	5	3.8
M1	46.2 ± 0.2	2.0	75	18.6	20	4.0
L2	184.7 ± 0.8	4.1	78	19.5	45	4.0
XL1	1303.5 ± 14.6	12.3	80	20	113	4.0

- ***Consumption of PCEs***

Figure 5.18 shows the consumption of PCEs with different P values (different lateral chain lengths). It can be observed that higher P value (longer the side chain length) the lower the consumption on all the different crystalline phases. As a general view, the PCE with the shortest side chains (P=5) gives a higher consumption than the rest and not substantial differences are observed between P=20 and 45 in none of the three phases. This effect has been previously observed in OPC and it was attributed to the decrease of the overall charge density when the length of the side chains (the value of P) is increased[21,22]. Also, the shrunk of the negative charges of the backbone by the long side chains could also affect to the interaction with the clinker phases. Nevertheless, the saturation point coincided for all PCEs in each phase.

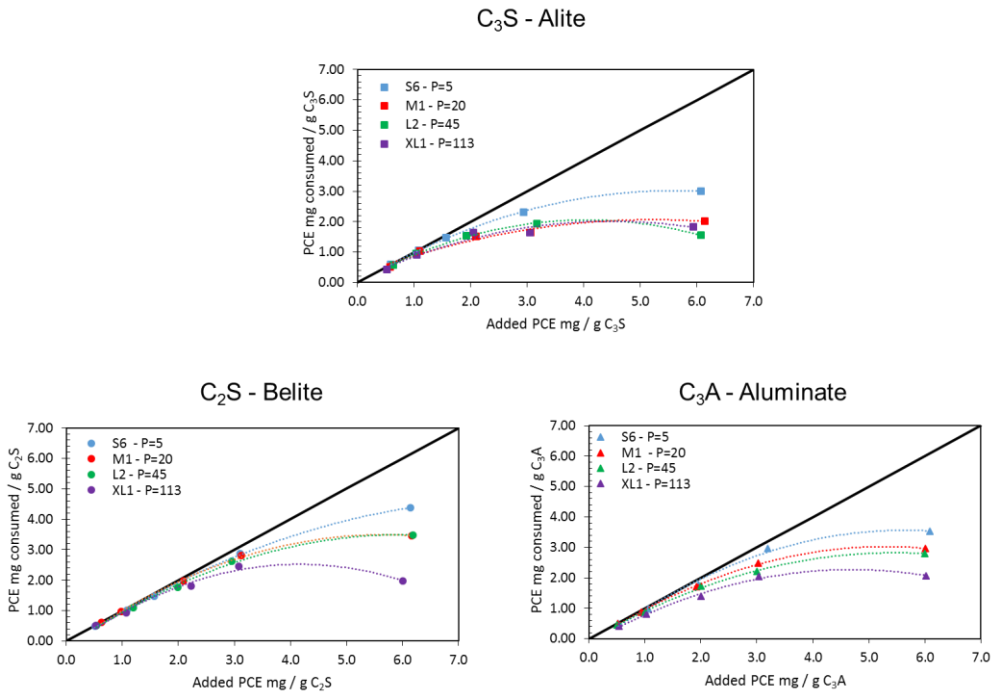

Figure 5.18: Consumption of PCEs with variable P respect to added PCE.

Table 5.13 shows the consumption amounts of the PCEs with variable P value. It can be observed that the number of chains consumed decreases as the P value increases.

Table 5.13: Consumed amount of the different PCEs in terms of per unit weight, area and number of chains consumed per area[7]

Material	*Surface Area - Blaine Fineness (m^2/g)*	*PCE/ P*	*Consumed amount at (3 mg Pol/ g CEM)*		*Consumed number of PCE chains per unit area (Chains/100 nm^2)*	K_A^* *Adsorption equilibrium constant*[9]
			per unit weight (mg/g)	*per unit area (mg/m^2)*		
Alite (C_3S)	0.3029	S6/ 5	2.35	7.76	14.24	S6 (P=5) – 666.2
		M1/ 20	1.70	5.61	7.31	
		L2/ 45	1.90	6.27	2.04	
		XL1/ 113	1.80	5.94	0.27	M1 (P=20) – 98.2
Belite (C_2S)	0.5360	S6/ 5	2.70	5.04	9.24	
		M1/ 20	2.65	4.94	6.44	
		L2/ 45	2.55	4.76	1.55	L2 (P=45) – 21.2
		XL1/ 113	2.30	4.29	0.20	
Aluminate (C_3A)	0.2883	S6/ 5	2.65	9.19	16.87	
		M1/ 20	2.40	8.32	10.84	
		L2/ 45	2.20	7.63	2.49	XL1 (P=113) – 3.9
		XL1/ 113	1.90	6.59	0.30	

As it was shown in the fourth chapter (eq. 4.2) the adsorption equilibrium constant is inversely proportional to the P parameter with a power dependence of 1.8. The experimental results showed that the number on consumed chains per unit of area are also inversely proportional to P with a power dependence in the range 1.21-1.28. Similar results have been obtained in the three crystalline phases. The experimental values obtained for the crystalline phases coincided with the value obtained for OPC. Thus, the length of the side chins affected in the same way the OPC and the crystalline phases. Figure 5.19 presents the effect of P on the theoretical adsorption constant K_A^* (calculated from eq. 4.2 and the values of the microstructural parameters of Table 5.12) predictions and the experimental values measured from the consumed PCE chains per unit of area. Table 5.14 displays the power dependencies of the fitted data.

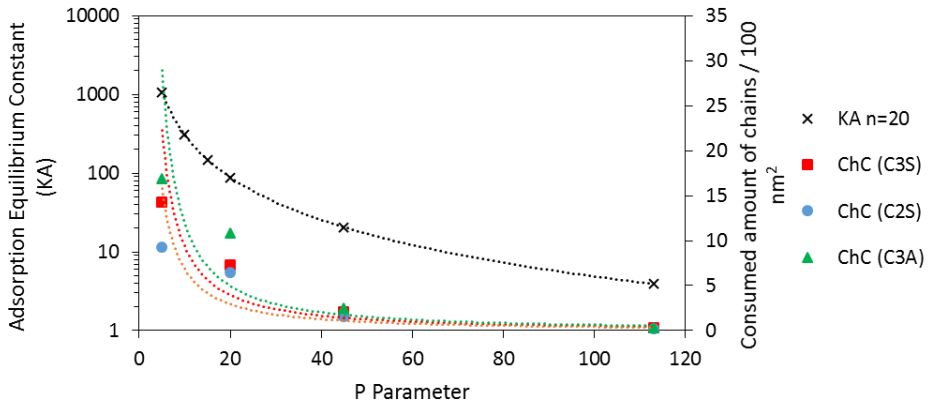

Figure 5.19: Comparison of theoretical prediction for K_A and the experimental data of the consumed chains per area.

Table 5.14: Dependencies obtained (theoretical K_A and experimental consumed chains) for the different PCEs with side chain length, P, in different crystalline phases.

PCE/ Phase	Equation
Variable P (n~20)/ C_3S	Experimental Result: $Consumed\ Chains \propto 165.7 \cdot P^{-1.25}$
Variable P (n~20)/ C_2S	Experimental Result: $Consumed\ Chains \propto 111.1 \cdot P^{-1.21}$
Variable P (n~20)/ C_3A	Experimental Result: $Consumed\ Chains \propto 225.0 \cdot P^{-1.28}$
Theoretical $K_A^* \propto \frac{z^2(N-1)^2}{nP^{9/5}N^{3/5}} \cdot 10^5$	Theoretical Prediction: $K_A^* \propto 19426 \cdot P^{-1.8}$

- ***Zeta potential measurements***

In Figure 5.20 the zeta potential results respect to dosage of the PCEs can be seen.

C_3S shows a sharp decrease of the zeta potential when PCEs are added. In this case, it can be observed that the PCE with the lowest P value (shortest side chains) decrease the zeta potential to negative values, probably due to the loop type conformation, while the other PCEs with longer side chains (P = 20, 45 and 113, series M, L and XL) decrease the zeta potential to close to the isoelectric point dispersing the particles by steric hindrance. As mentioned in chapter 4, these latter PCEs might be adsorbed in a train type conformation with the side chains dispersing the particles.

As mentioned before C_2S material showed slight positive zeta potential without any admixture. When PCEs are added a decrease on the zeta potential can be observed. Thus, for the PCE with P=5 the zeta potential is negative for all the dosages. For the longer side chain PCE's (P=20, 45 and 113) the zeta potential is at the isoelectric point till dosages of 3 mg PCE / g CEM and then the zeta potential goes into negative. However the zeta potential in the case of PCEs with longer side chains, higher P, are not as negative as for the PCEs with the smallest P. In the C_3S case, the decrease of the zeta potential towards the isoelectric point was attributed to a difference in conformation, from loop type (PCE with low P value, P = 5) to train type (PCEs with higher P values, P = 20, 45 and 113), however, in this case the PCE's with high P value also give a negative zeta potential which indicates that there should be other aspect rather than the conformation of the PCE's playing a roles on the zeta potential measured in belite phase. It has to be noted that the belite used in this study contains other compounds beside belite and they might also be interacting with the PCEs or have an effect in the zeta potential.

Finally, in the case of C_3A, all PCEs when added give a zeta potential close to the isoelectric point, but some differences are observed between PCEs. The PCEs with low P values (P = 5 and 20, series S and M) decrease more sharply the zeta potential at low dosages comparing to other PCEs. However, at higher dosages the addition of all the PCEs generate the same zeta potential result.

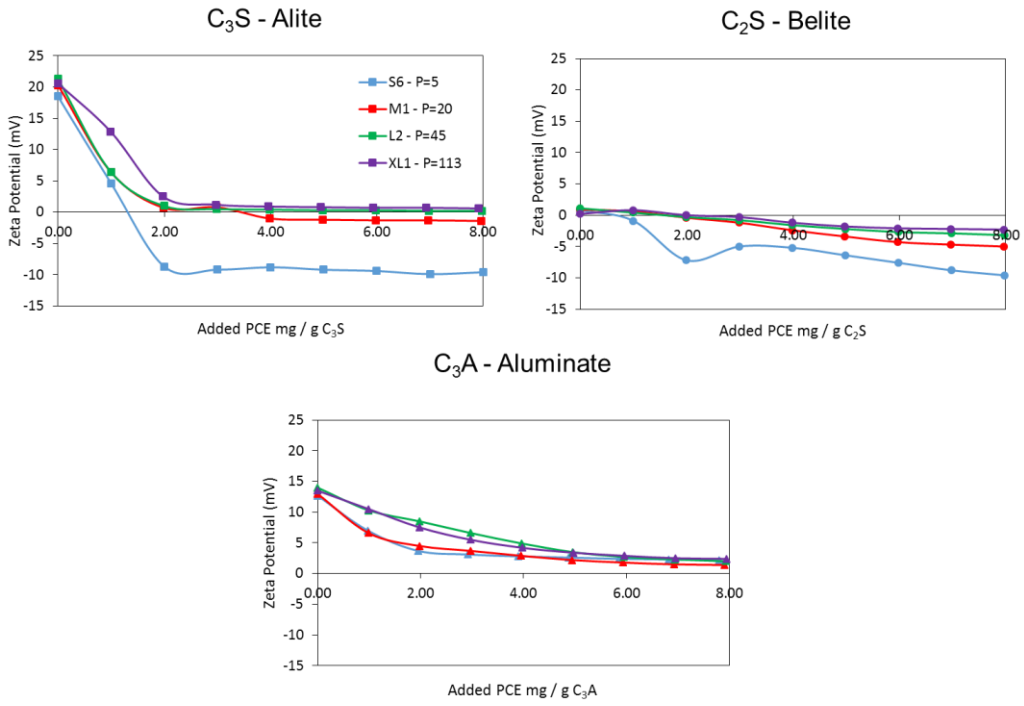

Figure 5.20: Evolution of the Zeta potential values over the added mg of PCE with variable P values respect to grams of cement for the different crystalline phases.

- ***Hydration kinetics***

Figure 5.21 shows the time evolution of the hydration reaction of C_3S and C_2S when PCE's with variable P are used. Table 5.15 shows the values of the delay the peak time respect to the reference peak time, Δt, and the heat released at 40 h.

In the case of C_3S the addition of PCEs produced a delay on hydration peak. The PCE with P = 5 retarded the most the hydration, followed by P = 45 and P = 20. The PCE with P = 113 retarded the least the hydration. In this case, it cannot be observed a tendency with the length of side chain or the P parameter.

In the case of C_2S, not all the PCEs retard the hydration of the materials, in fact, the PCE with the longest side chain (P = 113) accelerated the hydration. This behaviour is indeed strange and it was not expected. Furthermore, the PCE with P = 113 also released more heat than the reference sample at 40 h, so it also enhances the hydration. On the other hand, the rest of the PCEs retard the hydration, as a general trend it can be said that the lower the P value (shorter side chain) the longer the delay on the hydration. However, the PCE with P = 45 only delayed the hydration for one hour and the heat released during the hydration was also increased. The PCE's with low P values (P = 5 and 20, S6 and M1), are the ones which delayed the most the hydration and none of them increased the heat released in comparison with the reference.

An explanation for this behavior could be that PCEs with P = 45 and 113 did not adsorb on the surface but they were trapped between the plate-like particles. The consumption observed could be because they could have been consumed during the formation of an organo-mineral phase OMP. On the other hand, PCE with low P values (P = 5 and 20, S6 and M1) could have

been adsorbed onto the surface of the flake type particles and because of that they delayed the hydration of the material based on the mechanism that Mollah et al. reported[5].

- The PCEs are adsorbed onto the surface of the cement particles creating an impermeable coating and thus, retarding the dissolution of Ca^{2+} ions to the pore solution
- The PCEs present in the pore solution could form chelates with the Ca^{2+} ions and reduce the concentration of these ions in the aqueous solution retarding their precipitation.
- The dispersive action of the PCEs affects the kinetics of the process and changes the morphology of the hydrated phases.

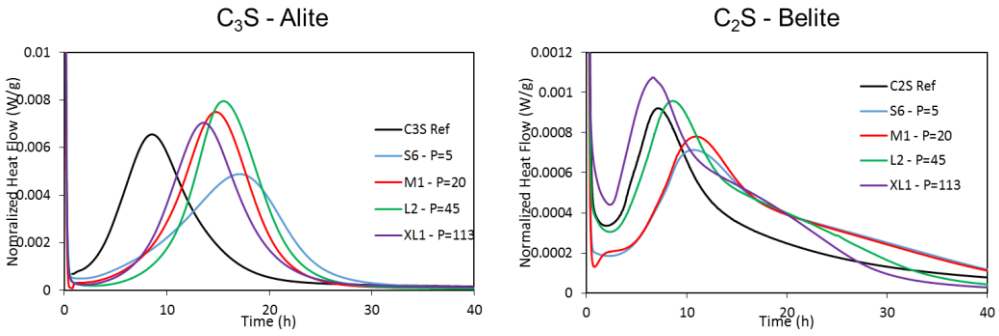

Figure 5.21: Hydration reaction of the crystalline phases C_3S and C_2S monitored by calorimetry.

Table 5.15: Start of the peak time, peak time on normalized heat flow and the normalized heat released at 40h of C_3S with PCE's of different P parameter.

PCE/ P	*Peak Time (h)*	*Δt (h)*	*Normalized heat 40h (J/g)*
C_3S Ref	8.89	-	247.33
S6/ 5	17.56	8.67	257.54
M1/ 20	14.76	5.87	268.75
L2/ 45	15.74	6.85	277.93
XL1/ 113	13.65	4.76	262.04
C_2S Ref	7.53	-	66.25
S6/ 5	11.01	3.48	61.72
M1/ 20	11.07	3.54	59.72
L2/ 45	8.76	1.23	67.29
XL1/ 113	7.01	-0.52	67.04

Figure 5.22 compares the theoretical prediction of the effect of P on the hydration delay (Δt) and the experimentally measured Δt for each crystalline phase. Although both theory and experiments indicate that Δt decreases when increasing the length of the side chain (for equal N and n) the experimental results present some differences.

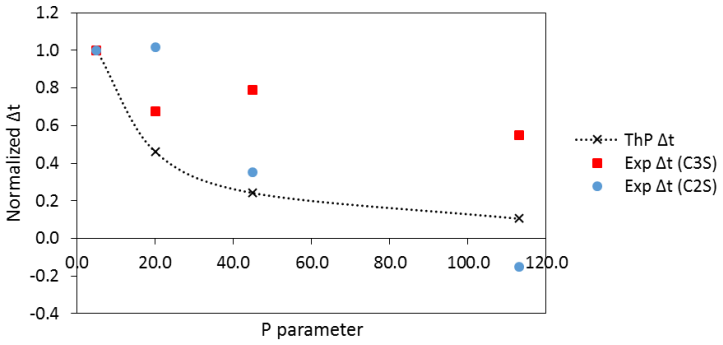

Figure 5.22: Comparison of theoretical prediction for normalized Δt and the experimental results for the different crystalline phases.

5.4. Conclusions

In the present chapter, substantially different cementitious materials were used in terms of morphology. C_2S, which was synthesized in the laboratory, presented rectangle regular plate like morphology. On the other hand, C_3S and C_3A, which are commercial materials, presented irregular shape type morphology with agglomeration of small particles onto bigger ones. The plate type morphology observed, had a high surface area, while the phases with rounded particles have smaller surface areas.

Furthermore, C_2S showed substantial heterogeneity in terms of composition. Due to the heterogeneity and the high concentration of hydrated phases, C_2S has a relatively low density, comparing to C_3S and C_3A.

The measurement of the zeta potential in absence of admixtures revealed that C_3A and C_3S have positive values. In terms of hydration, C_3A is the most reactive phase followed by C_3S, while C_2S is the least reactive phase.

In the case of Alite- C_3S the variation of n (backbone chain length) on the PCE's did not produce substantial changes on the consumption by mass, however, when decreasing n, higher amount of chains were consumed. The zeta potential and the hydration delay of Alite remained unaltered when varying n of PCEs. On the other hand, the variation of N (charge density) showed that PCE's with lower N were consumed in lower amounts, even though, the differences were not high. PCE's with higher N produced a higher decrease on the zeta potential and the higher the N, the higher the retardation of the hydration reaction of Alite. Finally, it was observed that PCEs with higher P (longer side chains) were consumed in lower amounts. Only the PCEs with

short side chains (P=5) decreased the zeta potential to negative values (-10mV) thus, these PCE's disperse Alite particles by electrostatic effect while the rest disperse the particles by steric hindrance. Analyzing the hydration reaction it cannot be said there is a tendency with P parameter in the case of Alite.

In the case of Belite-C_2S, following the trends observed in Alite, the variation of the n parameter showed that when n decreases, higher amount of chains are consumed. On the other hand, neither in zeta potential measurements nor in hydration reactions significant effects were observed. When analyzing the effect of the charge density (N) in this particular range (N= 3-5 and P=5), as a general view, it can be said that N parameter did not produced significant differences on the consumption by mass, the zeta potential or the hydration reaction of Belite crystalline phase. In the case of P, when increasing the length of the side chains, lower consumption of the PCEs was observed. All the PCEs when added to belite showed negative zeta potential above 3 mg / g C_2S dosage so, apart from the conformation other effects also affect to the zeta potential of the material. Interestingly, PCEs with long side chains (P=113) did not retard the hydration of C_2S and P=45 only retarded the hydration for one hour.

On Aluminate-C_3A phase, similar observation were obtained. The backbone lengths slightly affect the consumption by mass and zeta potential. The effect of charge density (N) was not significant and as in the previous crystalline phases, the longer the side chains of the PCEs lower consumption was observed.

The comparison between experimental results and theoretical predictions showed that reasonable agreement is observed on the tendencies between the adsorption equilibrium constant, K_A^*, and the consumed number of chains. However, the power dependencies showed

slight differences probably because theoretical models only considers surface adsorption of the PCEs. On the other hand, the theoretical predictions and the experimental result for the hydration delay, Δt, were only in accordance for n parameter. It was shown both theoretically and experimentally that Δt is independent from the backbone length. However, noticeable differences between theory and experiments on Δt were observed when N and P parameters of the PCEs were analyzed.

5.5. References

(1) Gartner, E. M.; Young, J. F.; Damidot, D. A.; Jawed, I. Hydration of Portland Cement. In *Structure and Performace of Cements*; CRC Press: London UK, 2001.

(2) Bye, G. C. *Portland Cement: Composition, Production and Properties*, Second Edi.; Thomas Telford Publishing LTD: London UK, 1999.

(3) Zingg, A.; Winnefeld, F.; Holzer, L.; Pakusch, J.; Becker, S.; Gauckler, L. Adsorption of Polyelectrolytes and Its Influence on the Rheology, Zeta Potential, and Microstructure of Various Cement and Hydrate Phases. *J. Colloid Interface Sci.* **2008**, *323* (2), 301–312.

(4) Uchikawa, H.; Hanehara, S.; Sawaki, D. The Role of Steric Repulsive Force in the Dispersion of Cement Particles in Fresh Paste Prepared with Organic Admixture. *Cem. Concr. Res.* **1997**, *27* (1), 37–50.

(5) Mollah, M. Y. A.; Adams, Ã. W. J.; Schennach, R.; Cocke, D. L. A Review of Cement Superplasticizer Interactions and Their Models. *Adv. Cem. Res.* **2000**, *12* (4), 153–161.

(6) Yoshioka, K.; Tazawa, E. I.; Kawai, K.; Enohata, T. Adsorption Characteristics of Superplasticizers on Cement Component Minerals. *Cem. Concr. Res.* **2002**, *32* (10), 1507–1513.

(7) Sakai, E.; Yamada, K.; Ohta, A. Molecular Structure and Dispersion-Adsorption Mechanisms of Comb-Type Superplasticizers Used in Japan. *J. Adv. Concr. Technol.* **2003**, *1* (1), 16–25.

(8) Flatt, R. J.; Schober, I.; Raphael, E.; Plassard, C.; Lesniewska, E. Conformation of Adsorbed Comb Copolymer Dispersants. *Langmuir* **2009**, *25* (2), 845–855.

(9) Marchon, D.; Boscaro, F.; Flatt, R. J. Cement and Concrete Research First Steps to the Molecular Structure Optimization of Polycarboxylate Ether Superplasticizers : Mastering Fluidity and Retardation. *Cem. Concr. Res.* **2019**, *115* (October 2018), 116–123.

(10) Link, T.; Bellmann, F.; Ludwig, H. M.; Ben Haha, M. Reactivity and Phase Composition of Ca2SiO4 Binders Made by Annealing of Alpha-Dicalcium Silicate Hydrate. *Cem. Concr. Res.* **2015**, *67*, 131–137.

(11) Alonso, M. D. M.; Palacios, M.; Puertas, F. Effect of Polycarboxylate-Ether Admixtures on Calcium Aluminate Cement Pastes. Part 1: Compatibility Studies. *Ind. Eng. Chem. Res.* **2013**, *52* (49), 17323–17329.

(12) Ganiev, R. M.; Ilyukhin, V. V.; Belov, N. V. Crystalline Structure of the Y=Ca6[Si2O7][SiO4](OH)2 Phase. *Dokl. Akad. Nauk SSSR* **1970**, *190* (4), 831–834.

(13) Taylor, H. The Crystal Structure of Killalaite. *Mineral. Mag.* **1977**, *41* (319), 363–369.

(14) Pellenq, R. J.; Kushima, A.; Shahsavari, R.; Vliet, K. J. Van; Buehler, M. J.; Yip, S.; Ulm, F. A Realistic Molecular Model of Cement Hydrates. *PNAS* **2009**, *106* (30), 16102–16107.

(15) Bullard, J. W.; Jennings, H. M.; Livingston, R. A.; Nonat, A.; Scherer, G. W.; Schweitzer, J. S.; Scrivener, K. L.; Thomas, J. J. Mechanisms of Cement Hydration. *Cem. Concr. Res.* **2011**, *41*, 1208–1223.

(16) Plank, J.; Hirsch, C. Impact of Zeta Potential of Early Cement Hydration Phases on Superplasticizer Adsorption. *Cem. Concr. Res.* **2007**, *37* (4), 537–542.

(17) Gelardi, G.; Sanson, N.; Nagy, G.; Flatt, R. J. Characterization of Comb-Shaped Copolymers by Multidetection SEC, DLS and SANS. *Polymers (Basel).* **2017**, *9* (2).

(18) Marchon, D.; Juilland, P.; Gallucci, E.; Frunz, L.; Flatt, R. J. Molecular and Submolecular Scale Effects of Comb-Copolymers on Tri-Calcium Silicate Reactivity: Toward Molecular Design. *J. Am. Ceram. Soc.* **2017**, *100* (3), 817–841.

(19) Flatt, R. J.; Houst, Y. F. A Simplified View on Chemical Effects Perturbing the Action of Superplasticizers. *Cem. Concr. Res.* **2001**, *31* (8), 1169–1176.

(20) Habbaba, A.; Dai, Z.; Plank, J. Cement and Concrete Research Formation of Organo-Mineral Phases at Early Addition of Superplasticizers : The Role of Alkali Sulfates and C 3 A Content. *Cem. Concr. Res.* **2014**, *59*, 112–117.

(21) Kirby, G. H.; Lewis, J. A. Comb Polymer Architecture Effects on the Rheological Property Evolution of Concentrated Cement Suspensions. *J. Am. Ceram. Soc.* **2004**, *87* (9), 1643–1652.

(22) Winnefeld, F.; Becker, S.; Pakusch, J.; Götz, T. Effects of the Molecular Architecture of Comb-Shaped Superplasticizers on Their Performance in Cementitious Systems. *Cem. Concr. Compos.* **2007**, *29* (4), 251–262.

Chapter 6: Conclusions and Future Perspectives

The synthesis of hydrophilic copolymers (MAA-co-PEGMA) with comb structure and their interaction with cementitious materials was investigated in this thesis. These copolymers can be synthesized by several forms, and in this work, the aqueous phase free-radical solution copolymerization was used and studied. Despite the extensive use in construction of these copolymers, also known as Superplasticizers or PCEs, their interaction with cement and its individual crystalline phases is not totally understood yet. This thesis has been an attempt to shed light on the effect of microstructure of the MPEG-PCEs on the interaction with cementitious materials.

Firstly, MPEG-type PCEs with short lateral chains (MAA-co-PEGMA5) were synthesized, by semibatch aqueous free-radical copolymerization in alkaline media. Alkaline conditions were necessary because the copolymers precipitated in acidic conditions. Thus, the reactivity ratios of the MAA and PEGMA comonomers in alkali conditions were estimated and turned out that they were widely different and hence batch copolymerization yield very heterogeneous copolymers. Therefore, for obtaining homogenous copolymers in terms of composition starved semibatch strategies were assessed which required high polymerization rates that were achieved by employing 30% solids content, high initiator concentrations and long feeding rates (8 hours). However, this method did not provide completely homogeneous copolymers (20% of the total amount of chains presented some composition drift), hence advanced open loop strategies were employed. To use this methods a mathematical model of the aqueous phase

copolymerization was developed taking into account all the kinetics parameters that take part in the copolymerization. Employing this truly homogeneous copolymers assessed by measuring, the monomer sequence distribution were successfully synthesized. Furthermore, copolymers were obtained in substantially shorter times than with the conventional starved semibatch method.

The synthesis homogenenous of MAA-co-PEGMA copolymers with longer side chain lengths (PEGMA of 20, 45 and 113 EGu) was accomplished by using monomer starved feed semibatch process. In this case, the synthesis was performed in acidic conditions because of the higher hydrophilicity of the PEGMA macromonomers and the copolymers. Furthermore, in acidic conditions the reactivity ratios of both monomer is close to the unit, therefore, totally homogenous copolymers were obtained. This was demonstrated by using NMR techniques (^{1}H-NMR and ^{13}C-NMR). On the other hand, the longer the PEGMA macromonomer used, the more complicate was to control the viscosity of the medium and hence, lower solids contents and higher concentration of CTA were needed in order to obtain manageable viscosities.

The conformation of the synthesized copolymers in a good solvent was estimated following the theoretical approach described by Gay and Raphael and Flatt et al. The conformation of the synthesized copolymers fits into the so-called Flexible Backbone Worm (FBW) based on the structural characteristics of the comb-copolymers n, P and N determined by SEC/MALS, ^{1}H and ^{13}C-NMR and MALDI-TOF. Only the copolymer XL1, produced with the PEGMA with 113 EG groups in the lateral chain, falls in the conformation called Stretched Backbone Worm (SBW) and some PCEs of series S are in the borderline between decorated chain (DC) and FBW conformation.

In addition, the experimentally determined structural characteristics of the comb-copolymers PCEs were used to validate the power law model for the prediction of the radius of gyration developed by Gay and Raphael and adapted by Flatt et al. for FBW type of PCEs. It was found that for the PCEs synthesized with the long PEGMAs the model captured well the power law dependencies on molecular structure parameters of solution conformation. However, as also found by Gelardi et al. the numerical prefactor is not accurate, which means that, although the relative effect of changes in molecular structure can be well predicted, the absolute values are not.

When applying the synthesized copolymers on ordinary Portland cement several effects were observed. Firstly the effect of n parameter (length of the backbone) was analyzed using PCE's with different P parameter (P = 5, 20 and 45, series S, M and L respectively). When PCEs of P = 5 (series S) were used it was observed that the n parameter have slight effects on different properties. In the case of consumption, it was observed that PCEs with higher n, were consumed in higher amounts by mass. The zeta potential of the cement paste remained unaltered when varying the n parameter of the PCEs. The decrease on the viscosity was similar for all the PCEs with variable n, although, the workability of the pastes was lengthen when PCEs of higher n were used. On the other hand, the hydration reaction retardation, Δt, was not altered by the variation of the n parameter .The setting time of the pastes was only slightly increased if the n parameter was decreased. Analyzing the n parameter of PCEs with medium side chains (P = 20 and 45, series M and L) it was observed that the variation on the n parameter did not provide substantial differences, the findings are in accordance with the effects observed for PCEs of P = 5 with variable n parameter.

The variation of the side chain length (varying P parameter) substantial changes were

observed. Regarding the consumption of the superplasticizers it can be said that PCEs with lower P value (P=5, short side chains) were consumed to a higher extent than the rest of PCEs with longer side chains (P=20, 45 and 113). By zeta potential measurements it was observed that PCEs with short side chains dispersed the particles by an electrostatic force while the PCEs with long side chains (P>20) produced a steric hindrance. This was attributed to the variation of the adsorption conformation from loop type (P=5) to train type (P>20). From rheological analyses it was concluded that possessing medium side chain length (P = 20-45 EGu) could be the most beneficial because of the higher reduction of the viscosity and longer workability retention. From the hydration kinetics, it was observed that the delay is higher when PCEs with shorter side chain are used (comparing P = 20, 45 and 113, series M, L and XL). However, PCE's with P = 5 (series S) did not follow this trend, most probably because of the different dispersion mechanism. Setting times studies correlated with the observed behavior at hydration kinetics. Also, it was observed that PCEs with short side chains (P = 5) produced narrower setting times than PCEs with medium and long side chains (P = 20, 45 and 113).

The effect of the backbone charge density or MAA/PEGMA ratio, was analyzed for the PCEs with the short lateral chain (P=5). It was found that PCEs higher N value were adsorbed to higher amounts. Zeta potential measurements did not show a clear trend with the N parameter of the PCEs. The decrease in the viscosity produced by the PCEs was similar and a trend was not observed. On the other hand, when N parameter was increased the workability retention was lengthen. The hydration kinetics of the cement pastes, did not follow a trends in respect with N but, it was observed an increase on the peaks of the monosulphates, thus, the PCEs with higher N promoted the hydration of this material. Higher N values (higher charge density) provided narrower setting time of the cement pastes.

The comparison between the theoretical predictions developed by Marchon et al. for the equilibrium adsorption constant and the experimental results of the consumption of PCE chains showed that there is a reasonable good correlation in the case of the variation of n parameter for PCEs with different P (P=5 and P=45). In both cases, the experimental results depend more strongly on the backbone chain length than the theoretical prediction. When the P parameter is varied the correlation is also reasonably good but in this case, the theoretical prediction have stronger dependency on the P parameter. There is also a good agreement between theoretical models and experimental results when the N (charge density) is varied but the potential factors are higher for the theoretical predictions.

Marchon et al. also attempted to predict the Δt of OPC in respect to the microstructural parameter of the PCEs. Taking their prediction into account the retardation should be independent of n, as it was observed in the experimental results. However the absolute values did not agree. The analysis of P showed that there was good correlation between theory and experimental results but the accuracy was lost at low P values (P=5). Finally, reasonable good correlation was observed in respect of N.

As the ordinary Portland cement is a multiphasic material the effect of the superplasticizers on individual clinker phases was also analyzed. The individual phases chosen, C_3S, C_2S and C_3A, presented substantially different morphologies that affected to the interaction of the PCEs because of their different surface areas and zeta potentials.

When PCEs with different backbone lengths, n, and short side chains (P = 5) are added to the individual phases it was observed that the consumption was not sensitive to n. Similarly, the zeta potential measurements were not affected by the n parameter of the PCEs. C_2S and

C_3S presented negative values when PCEs were added whereas, the zeta potential of C_3A was remained at slightly positive values. Hydration studies showed that the backbone length of the PCEs did not have substantial effect on the delay of the hydration kinetics on the phases C_2S and C_3S.

The effect of the charge density of the backbone or the ratio MAA/PEGMA (N parameter) was analyzed for MPEG-type PCEs with shor lateral side chains (P=5) and similar backone length. It was observed that the higher the N the higher the amount of chains consumed for al crystalline phases. The hydration was also affected by the MAA/PEGMA ratio. The higher the N value, the higher the delay for both C_2S and C_3S, although it was more noticeable for C_3S.

The variation of the side chain length of the PCEs, P, showed that higher P values (longer side chains) provoked lower consumption in all three materials. From the zeta potential measurements, it could be understood that PCE's with high P values (series M, L and XL) disperse the particle by a steric hindrance while PCE's with low P (P = 5, series S) disperse the particle by electrostatic effect, as it was also observed for ordinary Portland cement. Finally in terms of hydration, substantial differences were observed. PCE's with long side chains (series L and XL, P = 45 and 113) especially enhance the hydration of C_2S and they did not delay the hydration while in C_3S, all the PCEs delay the hydration. In the case of C_3S, the PCE's with P = 45 (L series) are the ones which enhanced the most the hydration.

The theoretical model developed by Marchon et al. were also compared with the experimental results obtained for the individual clinker phases. The consumed PCE chains per unit of area depends more strongly for all three materials on the backbone-chain length of the PCE's, n, than the theoretical prediction for the adsorption equilibrium constant. Also, when the

charge density, N, of the PCEs was varied, the experimental results fitted reasonably well with theoretical predictions. The results obtained when varying the length of the side chains of the PCEs maintained the tendency predicted by the model even though the predictions over-estimate the dependency. The analysis of the hydration retardation showed that the independency observed on the hydration retardation with respect to n was also predicted by the theoretical model. However, when the charge density of the PCEs, N, was varied the tendencies on the hydration retardation did not correlate with the theoretical predictions. This observation could be attributed to the effect produced by other crystalline phases like ettringite, gypsum or ferrite on the addition of PCEs. Finally, the theoretical predictions of the hydration did not correlate neither with the experimental results obtained when varying the side chain length, P, of the PCEs.

Overall, it can be said that the n parameter of the PCEs had little effect on the dispersing effect of the cementitious materials. On the other hand, the variation on the N parameter (charge density) showed that higher N values allow to higher consumptions, and higher delay on the hydration but with narrower setting time. This, was also observed on individual clinker phases. Finally, it can be said that medium P values ($20 < P < 45$) are generally the most beneficial on decreasing the viscosity and lengthen the workability window, but however broaden the setting times.

- ***Further consideration and future perspectives:***

Note that this PhD thesis has been the first project in the frame of the BASKRETE initiative where the Polymerization Processes Group of POLYMAT (UPV/EHU) and the Materials Group of Sustainable Construction Division from TECNALIA R&I have jointly participated. In this work,

the bases of the investigation and development in the field of cement and polymeric admixtures were established and the first topic was the “Synthesis of Hydrophillic Polymers with Comb Structure for Cementitious Formulations”. Therefore, from this first project several ideas that could be pursued in the future have been indentified.

Regarding the synthesis of the macromolecules it was observed during this project that the polydispersity of the MWD of the copolymers was always above 2 because FRP was used. Even though, it was observed that the length of the backbones did not provide substantial effect on the hydration and rheology of cementitious systems, if controlled free radical copolymerization (CFRP) is employed (using RAFT agents, Reversible Addition-Fragmentation chain Transfer polymerization) copolymers with narrower dispersities can be obtained and in that way the length of the backbones of the copolymers can be studied in more detail. Furthermore, with this copolymerization technique, different microstructures can be obtained (block copolymers, gradient like chains etc.) and therefore study the effect of PCE’s microstructure on cementitious materials. The study of the specific synthesis procedures by employing the esterification of PEG groups onto PMAA backbones could results in another alternative project.

Also, it was observed that the charge density of the backbone provided different effects on the cementitious materials. However, in this work only PCEs with short side chains and with variable charge density were analyzed. Designing PCE’s with variable charge densities with longer side chains will provide the opportunity to analyze if the trends observed in this work are maintained in PCE’s with longer side chains.

On the same line, the PCE industry is seeking for new chemistries which show improvements on very specific applications. Some interesting research line could be developed

for copolymers in which both their backbone and their side chains present negative charges and in such way obtain stronger adsorption capabilities. Other possibilities can be the incorporation into the backbone of functional monomers with the contribution of two carboxylic groups which may enhance the adsorption and the interactions. The variation of the macromonomer could offer also the development of new products with probably better resistance against the hydrolysis at high pHs.

As it is known from the literature, PCEs can be categorized into different conformation like DC, FBW, SBW, FBS and SBS. Generally, in most of the cases PCEs offer a FBW conformation as it was shown in this work. Tailoring the synthesis and obtaining copolymer with all the different conformation could also lead to some interesting projects.

In this project it was observed that ordinary Portland cement present a wide distribution of particle sizes. The different sizes of the particles could results into different reactivities and also produce different interactions with admixtures. If the particles are differentiated regarding their size it could possibly be investigated how this affects to different cement properties.

Despite individual phases of cement were employed to carry out some studies with the PCEs, unfortunately, not all the individual phases could be used in this study. Literature reports have stated that especially Ettringite is one of the most affecting phases, Ferrite phases are also prone to interact with the PCEs. Furthermore, new investigation and developments are showing that new mineral admixture are being used in order to increase the hydration reactions like the CSH seeds. Furthermore, the interaction of PCEs with additional cementitious materials like sand, gravel, clays etc. can also result in different research lines. Also, the appearance of new cements like the geopolymers that showed low CO_2 emmisions, together with the use of

superplasticizers could led to high performance cements that fulfill the latest sustainable requirements.

It is obvious that the chemistry of construction materials is continuously developing as cement is one of the most employed materials in the world. In these lines it was shown some of the research and development projects that could fit into the polymer and cement line that was started with the conduction of this thesis project. Of course, apart from the mentioned ones many other projects could be develop taking into account which are the necessities from the industrial and academic sector.

Laburpena eta Ondorioak

Hormigoia eraikuntzaren munduan dagoen materialik erabiliena da eta urez, areaz, legarrez eta zementuz osatuta dago. Zementua material hauen aglutinatzailea da eta lehengaien errekuntzaren bitartez sortzen da. Zementua fase ezberdinez osatuta dago eta urarekin erreakzionatu eta gero denborarekin gogortu egiten da. Zementuak duen arrakasta eraikuntzaren munduan propietate honek ematen dio.

Askotan zementua ez da bakarrik erabiltzen eta beste gehigarri batzuk gehitzen zaizkio bere propietateak hobetzeko edo aldatzeko. Gehigarrien artean PCE superplastifikatzaileak aurkitzen ditugu, zeintzuk orokorrean polimero hidrofilikoak diren. Hauek zementuaren biskositatea jaisten dute maneiukortasun hobeagoak lortzeko, edo beste modura, ura/zementua erlazioa gutxitzen dute eta horrela propietate mekaniko altuagoak lortu daitezke ere. Nahiz eta PCE superplastifikatzaileak urte askotan erabili izan diren, 1980 garren hamarkadan aurkitu ziren, superplastifikatzaileen eta zementuaren arteko interakzioak ez dira guztiz ulertzen gaur egun.

Tesi honen helburu nagusia PCE superplastifikatzaileen eta zementuaren arteko interakzioaren ikerketa fundamentala egitea da. Horretarako, tesia bi zatitan banatu da. Lehengo zatian PCE-n sintesi kontrolatua eta makromolekulen karakterizazioari buruz aritzen da. Makromolekula hauen mikroestruktura enborraren luzeraren, enborrean dauden karga

negatiboen (karga dentsitatearen) eta albo kateen luzeraren menpekotasuna izango du.

Bigarren zatia PCE superplastifikatzaileen eta zementuaren eta zementua osatzen duten faseen arteko interakzioak aztertzean eta ikertzean datza, PCE superplastifitzaileen mikroestrukturak duen efektua ikus dadin.

Esan bezala, PCE superplastifikatzileak ikertu dira tesi honetan zehar. PCE-ak orrazi moduko kopolimero hidrofilikoak dira (MAA-co-PEGMA) eta hauen mikroestruktura MAA/PEGMA erlazioa aldatuta, PEGMA makromonomero ezberdinak erabilita eta sintesi parametro ezberdinak erabilita eraldatu daitezke. Nahiz eta mikroestruktura ezberdinak erabili nahi izan diren, kasu guztietan mikroestruktura homogeneoko kopolimeroak lortu nahi dira.

Lehendabizi, MAA-co-PEGMA5, kopolimeroak sintetizatu ziren ur fasean erradikal askeko polimerizazio bitartez kondizio basikoetan. Monomeroen arteko erreaktibitateak oso ezberdinak zirela ikusita, errektibitate erlazioen estimazioa egin zen algoritmoen estimazio parametroak erabilita. PEGMA monomeroaren erreaktibitatea MAA-rena baino askoz handiagoa zela egoera basikoean ikusi zen, gainera erreaktibitate erlazioak solido edukiarekin eta monomero kontzentrazioarekin menpekotasuna zutela egiaztatu zen. Beraz, konposizio homogeneozko kopolimeroak lortzeko erreaktore ez-jarraiak gose balditzetan erabili behar izan ziren, zeintzuk polimerizazio abiadura altuak behar dituzten. Horretarako, %30-eko solido edukia, haztarazle kontzentrazio altuak (%2 monomeroaren pisuarekiko) eta elikadura luzeak (8 ordu) erabili ziren. Dena den, modu honek ez zuen konposizioz guztiz homogeneoak diren kopolimeroak sortzen (kateen %20-a konposizio aldaketa erakusten zuten) beraz “open loop” deituriko estrategiak erabili behar izan ziren. Azken estrategia hauek modelo matematiko baten

beharra dute, eta estrategiak hauek erabilita konposizio guztiz homogeneoko kopolimeroak lortu ziren. Kopolimero hauen konposizioa homogeneoa zela monomero sekuentziaren bidez egiaztatu zen, RMN-ren bitartez. Gainera, kopolimero hauek gose balditzen prestatutakoak baino denbora laburragoan prestatu ziren.

Albo kate luzeko MAA-co-PEGMA (PEGMA 20, 45 eta 113 EGu) kopolimeroen sintesia erreaktore ez-jarraietan gose baldintzetan egin zen. Kasu honetan, sintesia baldintza azidoetan egin zen eta monomeroen arteko erreaktibitate erlazioak unitatearen hurbil zeudenez konposizio homogeneoko kopolimeroak lortu ziren. Konposizioa homogeneoaren egiaztapena ^{1}H-RMN eta ^{13}C-RMN bitartez egin zen. Bestalde, PEGMA makromonomero luzeak erabiltzerako orduan soluzioaren biskositatearen kontrola zailagoa zen eta CTA-en erabilpena derrigorrezkoa izan zen.

Sintetizatutako kopolimero guztien konformazioa estimatu zen literaturan aurkitutako Gay eta Raphael-en eta Flatt-en modelo desberdinak erabilita. Modelo hauek kopolimeroen mikroestruktura hiru parametro desberdinen arabera (n, N eta P) definitzen dute. Gainera, kopolimero guztiak FBW konformazioaren barruan kokatzen dira, oso albo kate luzeak dituenak izan ezik (PEGMA 113). Bestalde, albo kate motzak dituzten kopolimeroak nahiz eta FBW konformazioan egon DC konformazioaren ertzean kokatu daitezke.

Gainera, esperimentalki determinatutako parametroak erabili ziren Flatt-ek garatutako biratze erradioaren aurreikuspen modeloaren balidazioa egiteko. Modeloak ondo aurreikusten zituen PEGMA luzeagoko mikroestrukturaren konformazioaren dependentzia. Hala eta guztiz ere, faktore aurre-esponentziala ez zen guztiz zehatza, beraz, nahiz eta aldaketa erlatiboak ondo

aurreikusten diren, balore absolutuak ezin dira aurreikusi.

Sintetizatutako kopolimeroak erabiltzerako orduan efektu desberdinak ikusi ziren zementu material ezberdinetan. Lehendabizi, n parametroaren efektua ikertu zen, P ezberdineko PCE-ak erabilita. P baxua duten PCEak erabiltzen direnean, PCE-n n parametroa igotzerakoan PCE-ak gehiago kontsumitzen dira. Bestalde, zementu pasten zeta potentziala aldatu gabe mantentzen da PCE-n n parametroa aldatuta. Pastaren biskositatea aldatu gabe mantentzen da n parametroarekin baina zementuaren maneiukortasuna denbora luzeagoz mantentzen da n parametroa handituta. Hidratazio denborak ere ez zuten aldaketarik sufritu n parametroaren aldaketarekin. Bestalde, n txikitzerakoan gogortze denbora murriztu egiten da. P ertaina (P = 20 eta 45) duten PCE-ak erabilita ikusitako joerak P txikiak (P=5) ikusitakoekin alderatu daitezke.

Albo kateen luzera aztertzen (PCE-en P parametroa) bada efektu nabarmenak ikusi dira. P parametro baxuak (P=5) duten PCE-ak (albo kate motzak) P parametro altuak (P = 20, 45 eta 113, albo kate ertainak eta luzeak) dituztenak baino gehiago adsorbatzen dira. Gainera, P baxuko PCE-ak “loop” erako adsortzio konformazioa erakusten dute, P altuko PCE-ak “train” moduko adsortzio konformazioa duten bitartean. Beraz, zementu partikulak dispertsatzeko modua ezberdina da. Hau zeta potentzialaren neurketen bitartez ondorioztatu zen. Erreologiaren aldetik esan daiteke P parametro ertainak izanda (P = 20 eta 45) zementuaren biskositatearen jaitsiera handiagoa sortzen dutela eta zementuaren maneiukortasuna denbora luzeagoz mantentzen dutela. Zementuaren hidratazioa aztertzerakoan gero eta P baxuagoa izanda, zementuaren hidratazioa moteltzen dutela esan daiteke (P = 20, 45 eta 113 duten PCE-ak aztertuta). Hala ere, P = 5 duten PCEak, ez dute joera hau jarraitzen beraien adsortzio konformazioa eta partikulak sakabanatzeko modua desberdina delako.

Kopolimeroen karga dentsitatea edo MAA/PEGMA erlazioa (N parametroa) ere aztertu da albo kate motzak dituzten PCE-entzako (P=5), N igotzerakoan PCE-ak gehiago adsorbatzen zirela ikusi zen. Bestalde, zeta potentzialaren neurketak ez zuten ondorio garbirik erakutsi. Biskositatea eta erreologiaren neurketetan, N parametroa igotzerakoan ez zen joera garbirik ikusi baina mainukortasuna denbora luzeagoz mantentzen zen. Zementatuaren hidratazio denboran ez zen joera garbirik ikusi baina monosulfato fasearen hidratazioa asko handitzen zen PCE-en N parametroa igota. Gainera, N parametro altuagoak dituzten PCE-ak gogortze denbora estuagoak sortzen zituzten.

Marchonek garatutako modelo teorikoen eta datu esperimentalen arteko egindako konparaketak zentzuzko korrelazioak irudikatu zituen n parametro ezberdineko PCE-ak erabilita. Kasu honetan, datu esperimentalak n parametroan dependentzia altuagoa daukate modelo teorikoak baino. PCE-en P parametroa aztertuta, korrelazioa ere zentzukoa zen baina kasu honetan, modelo teorikoaren dependentzia P parametroan altuagoa zen. N parametroa alderatzerakoan modelo teorikoak ere dependentzia altuagoa erakusten du.

Superplastifitzaileek zementua osatzen duten fase kristalinoetan (C_2S, C_3S eta C_3A) sortzen duten efektua ere aztertu da. Fase hauen morfologiak nahiko ezberdinak dira eta superplasfitzaileekin izan dezaketen interakzioa alda daiteke.

Enbor luzera ezberdineko (n parametro ezberdina eta P parametro baxua P = 5) PCE-ak erabiltzerakoan fase ezberdinetan n parametroak ez duela efektu handirik, kontsumizio neurketetan, zeta potentzialean eta hidratazio zinetiketan ikusi zen. Aldiz, N ezberdineko PCE-ak gehitzerakoan, N altuko PCE-ak kontsumizio altuagoak izaten zituzten fase guztietan.

Gainera, faseen hidratazioa moteltzen da N altuko PCE-ak erabilita, batez ere C_3S fasean. Albo kateen aldaketa, P parametroaren aldaketa aztertuta, efektu ezberdinak ikusi dira. P altuko PCE-ak (P = 20, 45 eta 113) kontsumo baxuak ematen dituzte P baxuko (P = 5) PCE-ekin konparatuz. Zeta potentzialen bitartez partikulak sakabanatzeko modua ere ezberdina dutela ondorioztatu da, OPC zementuan bezala. Hidratazioari dagokionez, ezberdintasun nabarmenak ikusi dira. P altuko PCE-ak (P = 45 eta 113) ez dute C_2S-ren hidratazioa moteltzen, azkartu baizik., C_3S fasean PCE guztiak hidratazioa moteltzen duten bitartean.

Fase kristalinoetan lortutako emaitzak Marchon-ek garatutako modeloarekin alderatuta dira. Kontsumitutako kateen kantitatea eta modelo teorikoak bat egiten dute baina datu esperimentaletan ikusitako dependentziak altuagoak dira modelo teorikoan baino. Kate nagusiaren karga dentsitatea aztertzerako orduan datu esperimentalak ondo bate-egiten dute modelo teorikoekin. Albo kateen luzera aldatuta ere, datu esperimentalak eta datu teorikoak bat egiten dute. Bestalde, hidratazioaren atzerapena aurreikusten duen modelo teorikoak ondo korrelazionatzen da lortutako datu esperimentalekin n parametroa aztertzerako orduan, baina albo kateen luzera (P) eta karga dentsitatea (N) aztertzerakoan modelo teorikoak ez du aurreikusten lortutako emaitzak.

Orokorrean esan daiteke n parametroak efektu txikia duela zementuaren eta faseen propietateetan. Bestalde, N parametroaren aldaketak eragin handiago sortzen dut. Azkenik, esan daiteke P ertaineko balioak dituzten PCE-ak eragin handiena sortzen dutenak direla, batez ere, biskositatea eta maneiakortasuna hobetzerako orduan.

Appendix I. Polymeric Materials, Processes and Characterization Methods

I.1. Materials

The monomers methacrylic acid MAA (99%, with 250 ppm hydroquininone monomethyl ether MEHQ as inhibitor) and polyethylene glycol methyl ether methacrylate PEGMA 5/20 (Mn = 300 g/mol and Mn = 950 g/mol, with 100 ppm MEHQ and 300 ppm butylated hydroxyl toluene BHT), were purchased from Sigma-Aldrich and used as received. Metoxypolyethylene glycol methacrylate (Mn = 2000 g/mol and Mn = 5000 g/mol) 50 wt % in water called Visiomer MPEG 2005 and 5005 MA W were kindly supplied by Evonik Industries. The structure of these monomers can be seen in Figure AI.1:

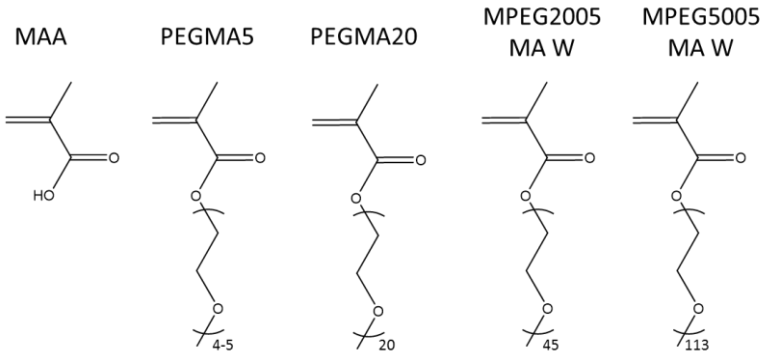

Figure AI.1: Structure of the monomers used through this work.

The initiator potassium persulfate (KPS > 99%) was purchased from Sigma-Aldrich and used as received. The chain transfer agent 3-mercaptopropionic acid (3-MPA 99% purity) from Sigma-Aldrich was also used as received.

Sodium hydroxide (NaOH), sodium nitrate ($NaNO_3$) and sodium bicarbonate ($NaHCO_3$), high purity compounds, were purchased from Sigma-Aldrich. Deionized water was used through the thesis conducted as solvent for the reactions. Mili-Q quality water was used to prepare the eluent of the molar mass measurements. N-N-dimethylformamide (DMF) chromatography GPC grade purchased from Fisher-Scientific was used as internal reference in ^{1}H-NMR experiments and deuterium oxide (D_2O) >99.9% was purchased from Euriso-Top and used as co-solvent for ^{1}H-NMR and ^{13}C-NMR experiments.

I.2. Copolymerization Reactions

I.2.1. Batch Aqueous Solution Copolymerizations

Aqueous solution batch copolymerization reactions were carried out in 500 ml glass jacketed reactors with mechanical stirring of 250 rpm. The reactor in this case was additionally equipped with a condenser, sampling device and nitrogen inlet. Several reaction were carried for the purpose of assessment of starved condition and obtaining homogeneous copolymers. These consisted of reactions at low solids content (SC: 5, 10 wt%) with low initiator concentration (I_2: 1 wt% bwom) and at 70 ºC. Other reactions were carried out with the purpose of estimating different kinetics parameters in order to use them in the mathematical model developed (see Appendix III). The conditions of these reactions were relatively high solids content (SC: 20, 30 wt%) high initiator concentration (I_2: 2 wt% bwom) and high temperatures, 90 ºC.

I.2.2. Semibatch Aqueous Solution Copolymerizations

The aqueous solution polymerization reactions were carried out semibatchwise in a 1L glass jacketed reactor with a mechanical stirrer rotating at 250 rpm. The reactor was equipped with a condenser, a pH-meter, two feeding inlets and nitrogen bubbling which was also used as sampling device. A scheme of the reactor can be observed in the Figure AI.2.

The solids content was fixed to 30 wt%. Part of the solvent (20 wt%) was initially charged in the reactor before increasing the temperature to 90 ºC, during the reactions the reactor was purged under nitrogen flow at 15 ml/min. A monomer solution which was previously neutralized with NaOH to pH=7 and the initiator solution were fed into the reactor in two separate streams for 8 hours, the reaction was left one more hour for post-polymerization in order to minimize the unreacted monomer.

Different comonomer ratios (2/1, 3/1, and 4/1) were employed in order to obtain copolymers with different number of carboxylic monomer units in the chains (different charge density). In order to analyze the effect of the length of the backbone, copolymers with different degree of polymerization were synthesized by reactions with different chain transfer agent concentration (0%, 0.5%, 1% and 1.5% by mol of monomer “bmom”). The CTA chosen for this purpose is 3-mercaptopropionic acid (3-MPA) which is water soluble. All reactions were initiated by a water soluble thermal initiator KPS, the concentration of the initiator in all cases was 2% by weight of monomer. All the reactions were carried out at 90 ºC and at neutral pH (pH=7). Sampling time was varied along the reaction, withdrawing samples at shorter times (20 minutes) at the begging of the reaction, and leaving longer times at the end (2 hours). Tables AI.1 and AI.2 summarize the compositions of the synthesized copolymers.

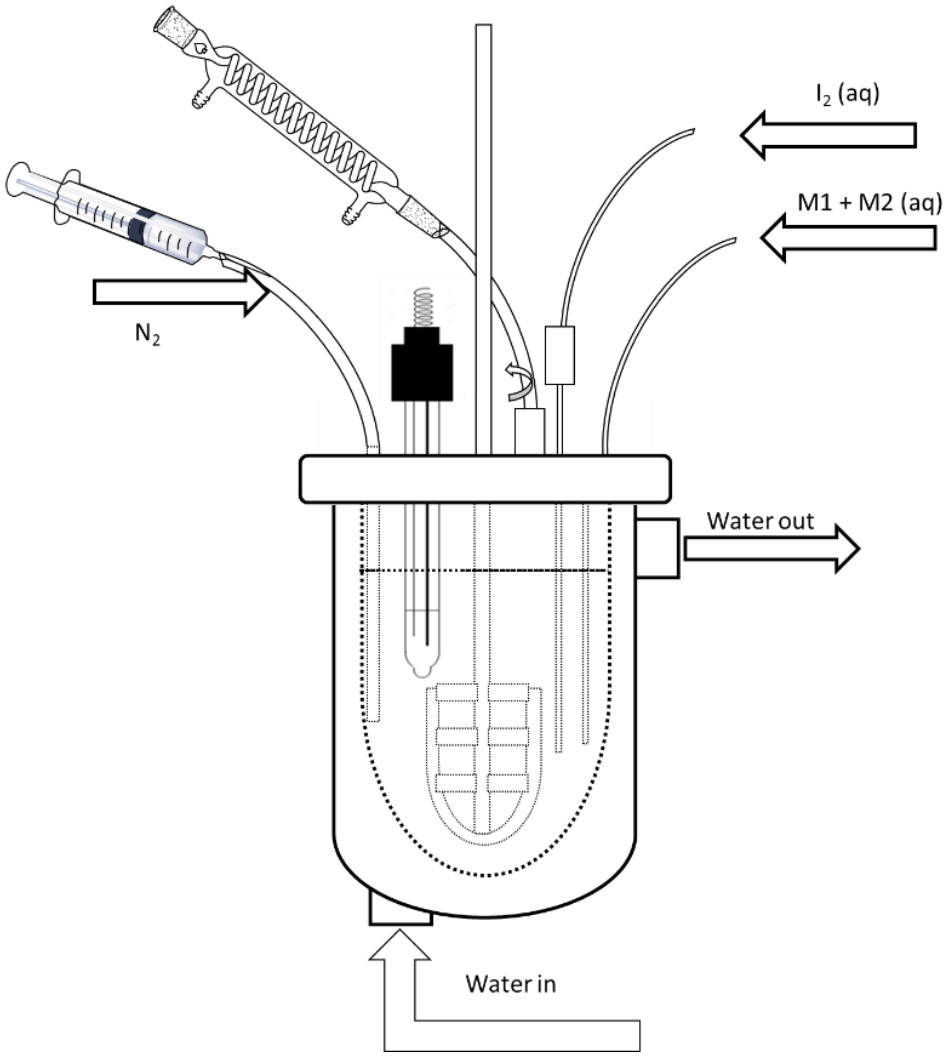

Figure AI.2: Scheme of the reactor employed during the starved semibatch reactions carried out during this work.

Table AI.1: Formulation to prepare MAA/PEGMA5 copolymers with variable comonomer ratios by semicontinuous aqueous solution polymerization.

Comonomer Ratio	**2/1**		**3/1**		**4/1**	
Ingredients	**IC* wt %**	**F** wt %**	**I C wt %**	**F wt %**	**IC wt %**	**F wt %**
MAA	0.00	10.79	0.00	13.91	0.00	15.78
PEGMA	0.00	18.78	0.00	16.15	0.00	13.71
$NaHCO_3$	0.00	0.18	0.00	0.18	0.00	0.18
NaOH	0.00	4.30	0.00	5.45	0.00	6.27
H_2O	20.06	45.29	20.07	43.64	20.02	43.44
KPS	0.00	0.60	0.00	0.60	0.00	0.60

IC*: Initial Charge F**: Feed.

Table AI.2: Formulation to prepare MAA/PEGMA5 copolymers (MAA/PEGMA: 3/1) with variable CTA concentrations by semicontinious aqueous solution polymerization.

CTA Content	**0% bmom**		**0.5% bmom**		**1% bmom**		**1.5% bmom**	
Ingredients	**IC wt%**	**F wt%**	**IC wt%**	**F wt%**	**IC wt%**	**F wt%**	**IC wt%**	**F wt%**
MAA	0.00	13.91	0.00	13.88	0.00	13.77	0.00	13.74
PEGMA	0.00	16.15	0.00	16.13	0.00	16.00	0.00	15.98
NaHCO3	0.00	0.18	0.00	0.19	0.00	0.18	0.00	0.18
NaOH	0.00	5.45	0.00	5.60	0.00	5.48	0.00	5.47
3-MPA	0.00	0.00	0.00	0.11	0.00	0.22	0.00	0.34
H2O	20.07	43.64	20.09	43.40	20.08	43.67	20.06	43.63
KPS	0.00	0.60	0.00	0.60	0.00	0.60	0.00	0.60

I.2.3. ^{1}H-NMR in Situ Reactions

Aqueous-phase (mixture of H_2O/D_2O) free-radical copolymerization reactions of MAA and PEGMA5 were carried out in NMR tubes and the copolymerization reactions were in situ monitored. Comonomer solutions were prepared at different solids contents (5–20 wt %) with different monomer molar ratios (MAA/PEGMA5: 3/1, 2/1, 1/1) Comonomer mixture solutions were neutralized with a 30% NaOH solution and kept at a pH between 7 and 9, ensuring total ionization of the carboxylic monomer in all cases. $NaHCO_3$ was used as buffer at 1/1 mol ratio with respect to the initiator. All reactions were initiated with a water-soluble thermal initiator KPS at a concentration of 1 wt % based on monomer. Note that the monomer molar ratios expressed here are the nominal values; the actual monomer molar ratios were calculated from the vinyl peak areas of each monomer before starting the reaction (t0 in the NMR tube). The liquid ^{1}H-NMR spectra were recorded on a Bruker 500 AVANCE (500 MHz) equipped with a Z gradient Broadband observe (BBO) probe. The kinetic study of the reaction was conducted at 343 K using ^{1}H spectra with suppress of the solvent using WATERGATE sequence. The spectrum was recorded every 2 min during the first 16 min and then every 10 or 15 min for 3 h. In the following section how the conversion was determined is explained.

I.3. Monomer Conversion by ^{1}H-NMR (Proton Nuclear Magnetic Resonance)

Approximately 2 mL of the copolymer solution were withdrawn from the reactor during the polymerization process, placed in a pre-weighed glass vial were couple of drops N,N-dimethyl formamide DMF (for semibatch experiments) and 1 wt % hydroquinine HQ have been previously

placed and weighted. 500 µl of the solution plus 100 µl of D_2O were then transferred to a NMR tube.

Conversions were measured by ^{1}H-NMR technique with the suppress of the solvent by employing watergate sequence in a Bruker AVANCE 400 MHz equipment. Conversion of MAA and PEGMA was calculated on the evolution of the peaks corresponding to the vinyl protons of MAA (δ, 5.60, 5.25 ppm) and PEGMA (δ, 6.10, 5.70 ppm). In batch experiments the peak corresponding to the metoxy group of PEGMA (δ, 3.30 ppm) was used as internal reference. In the case of the semibatch experiments, DMF (δ, 7.80 ppm) was added to the samples withdrawn and the used as internal reference.

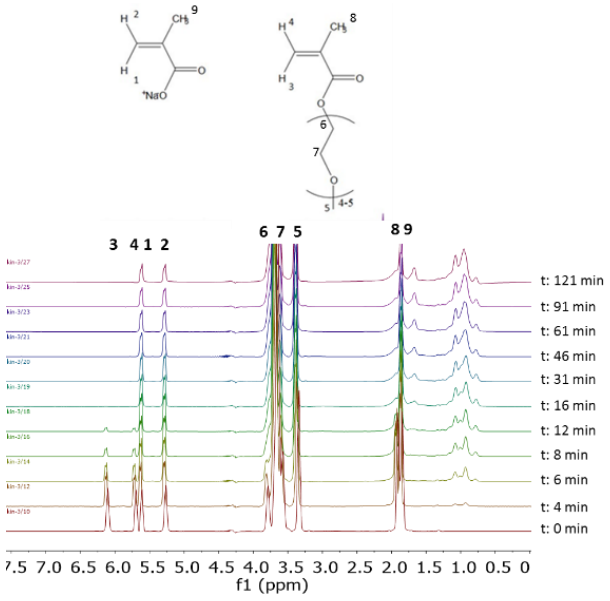

Figure AI.3: Time evolution of the proton nuclear magnetic resonance (^{1}H-NMR) spectra of the aqueous-solution copolymerization of MAA and PEGMA5 carried out at 70 ºC (SC = 10 wt % MAA/PEGMA5 = 1/1).

I.4. Microstructure Characterization by ^{13}C-NMR

The microstructure of the copolymers synthesized in chapters 2 and 3 was determined by a Lorentzian deconvolution of the carboxylate and ester peak obtained from ^{13}C-NMR spectroscopy. The measurements were carried out in a Bruker AVANCE 500 MHz equipment. 500 µl of the final sample of the copolymers was added into the NMR tubes with 100 µl of D_2O. The adquisition time of the experiments was 9h with 7000 scans. In the case of the copolymers with medium and long lateral chains, due to the high intensity of the ethylene glycol (EG) peak the spectra was recorded with a selected pulse from 170 – 200 ppm. In this way, the intensity of this region is intensified.

The carbonyl signal of MAA-co-PEGMA copolymers appear in the region of 190-175 ppm and actually it displays two different signals, one attributed to the acid comonomer and the other attributed to the ester monomer. Due to the higher concentration of acid comonomer in the mixture the intensity of this signal is more intense so the deconvolution was carried based on the acid signal. As the spectrum was sufficiently well resolved not only to perform the deconvolution into triads but also to pentads. The intensities of triads were evaluated by the sum of the intensities of the pentads, A letter refers to the carboxylic monomer and B letter represent the ester monomer[1]: Figure AI.4 shows the signal of the carbonyl area where the deconvolution into pentads was performed.

- (AAA) = (AAAAA) + (AAAAB) + (BAAAB)
- (AAB) = (AAABA) + (AAABB) + (BAABA) + (BAABB)
- (BAB) = (ABABA) + (BBABA) + (BBABB)

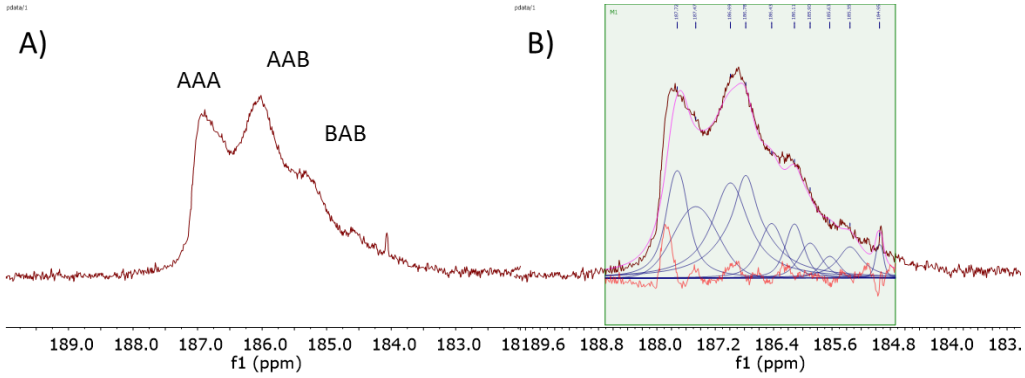

Figure AI.4: A) 13C-NMR pattern of the carboxylate area of a synthesized copolymer (S1). B) Lorentzian deconvolution into triad of the carboxylate area.

The theoretical values are calculated based on the Bernouillian distribution[2] which are based on the experimental copolymer cumulative composition. The comparison of the experimental and theoretical values provided an illustration of how homogenous in terms of composition were the synthesized copolymers. Following, the equation employed for the calculation of each triad are shown, where Y_{MAA} is the cumulative composition of the copolymers in respect to MAA.

$$(AAA) = Y_{MAA}^3 \qquad \text{Eq: (AI.1)}$$

$$(AAB) = Y_{MAA}^2 \cdot (1-Y_{MAA}) \qquad \text{Eq: (AI.1)}$$

$$(BAB) = (1-Y_{MAA})^2 \cdot Y_{MAA} \qquad \text{Eq: (AI.1)}$$

I.5. Determination of the Molar Mass by Aqueous SEC-MALS/RI

The molar mass and the root-mean square radius of the polymers were analyzed by SEC/MALS/RI. The equipment was composed by a LC20 pump (Shimadzu) coupled to a miniDAWN Treos multiangle (3 angles) light scattering laser photometer equipped with an He-Ne laser (l¼658 nm) and an Optilab T-Rex differential refractometer (l¼658 nm) (all from Wyatt Technology Corp., USA). Separation was carried out using three columns in series (Ultrahydrogel 120, 250, and 2000 with pore sizes of 120, 250, and 2000 A°, respectively, Waters, Barcelona, Spain). The analyses were carried out at 35ºC and a $NaNO_3$ 0.1M pH=12 (NaOH was added as base) aqueous solution was used as eluent at a flow rate of 0.6 mL min. The copolymers were dissolved in the eluent at 5.0 mg/mL concentration and afterward there were filtered and injected (100 µL) into the equipment. The SEC/MALS/RI data was analyzed by using the ASTRA software version 6.1. (Wyatt technology, USA). The absolute molar mass and the radius of gyration were calculated from the MALS/RI data using the Debye plot (with first-order Zimm formalism).

In literature[3], the dn/dc values of PEG (dn/dc=0.135 ml/g) has been generally used to obtain the absolute molar mas of this type of copolymers. In this work, the dn/dc value for each copolymer was determined using the refraction index instrument.

I.6. Viscosity Measurements

Apparent viscosity of MAA/PEGMA aqueous solutions was measured using a TA Instruments-AR1500ex rheometer. Flow procedures using a 60 mm diameter steel plate as geometry were carried out at 25 ºC. Several steps were set for carrying the experiments: A

conditioning step of two minutes in which the temperature is set, a first continuous ramp from 0.01 to 1000 s^{-1} and a second continuous ramp from 1000 s^{-1} to 0.01.

I.7. References

(1) Borget, P.; Galmiche, L.; Le Meins, J. F.; Lafuma, F. Microstructural Characterisation and Behaviour in Different Salt Solutions of Sodium Polymethacrylate-g-PEO Comb Copolymers. *Colloids Surfaces A Physicochem. Eng. Asp.* **2005**, *260* (1–3), 173–182.

(2) C. Booth, C. Prince, G. A. *Compresive Polymer Science*, Vol. 1.; Pergamon Press: Oxford, UK, 1989.

(3) Plank, J.; Pöllmann, K.; Zouaoui, N.; Andres, P. R.; Schaefer, C. Synthesis and Performance of Methacrylic Ester Based Polycarboxylate Superplasticizers Possessing Hydroxy Terminated Poly(Ethylene Glycol) Side Chains. *Cem. Concr. Res.* **2008**, *38* (10), 1210–1216.

Appendix II. Estimation of Reactivity Ratios of Water Soluble Monomers MAA/PEGMA 5

II.1. Method Development

The reactivity ratios are estimated based on the evolution of the copolymer cumulative composition. Note that the estimated values are apparent values, meaning the concentration of monomer around the propagating radical is the same to the average concentration of monomer in the reactor.

In free radical polymerization the monomer distribution along the chains is exclusively based on kinetics factors. Generally, in free radical copolymerization it is assumed that the radical activity is based on the terminal unit of the propagating chains[1]. Furthermore, it is considered that the copolymer chains are sufficiently long to consider the effect of the initiation and termination in respect to propagation negligible.

The reactivity ratios were estimated using experimental data of the evolution of the cumulative copolymer composition over the overall conversion, based on the method developed by De la Cal et al.[2]. The method is summarized below:

MAA and PEGMA will be represented with letter A and B respectively. The material balances for each of the monomers in batch reactor, considering that terminal model kinetics is applied, can be written as:

$$\frac{d[A]}{dt} = -R_{pA} = -(k_{pAA}P_A + k_{pBA}P_B)[A][R^*] \quad \text{(eq: AII.1)}$$

$$\frac{d[B]}{dt} = -R_{pB} = -(k_{pAB}P_A + k_{pBB}P_B)[B][R^*] \quad \text{(eq: AII.2)}$$

In equations 1 and 2 [*i*] is concentration of monomer *i* (mol/L), R_{pi}, the polymerization rate of monomer *i* (mol/L·s), k_{pij}, the propagation rate constant of radicals of terminal unit *i* with monomer *j* (L/mol·s), P_i the probability of finding active chain with ultimate unit of type *i* and *R** is the total concentration of radicals (mol/L).

Assuming the Queasy-Steady-State Assumption (QSSA) is fulfilled, the probabilities are defined as follows:

$$P_A = \frac{k_{pBA}[A]}{k_{pBA}[A] + k_{pAB}[B]} \quad \text{(eq: AII.3)}$$

$$P_B = 1 - P_A \quad \text{(eq: AII.4)}$$

MAA conversion and overall conversion are defined as:

$$X_A = \frac{[A]_0 - [A]}{[A]_0} \quad \text{(eq: AII.5)}$$

$$X_T = \frac{([A]_0 - [A]) + ([B]_0 - [B])}{[A]_0 + [B]_0} \quad \text{(eq: AII.6)}$$

where $[A]_0$ and $[B]_0$ are initial concentration of MAA and PEGMA, respectively. Thus:

$$dX_A = -\frac{d[A]}{[A]_0} \quad \text{(eq: AII.7)}$$

$$dX_T = \frac{-d[A] - d[B]}{[A]_0 + [B]_0} \quad \text{(eq: AII.8)}$$

$$\frac{dX_A}{dX_T} = \frac{[A]_0 + [B]_0}{[A]_0} \frac{R_{pA}}{R_{pA} + R_{pB}} = \frac{[A]_0 + [B]_0}{[A]_0} \left(\frac{1 + r_A \frac{[A]}{[B]}}{2 + r_A \frac{[A]}{[B]} + r_B \frac{[B]}{[A]}} \right) \quad \text{(eq: AII.9)}$$

where r_A and r_B are the reactivities of MAA and PEGMA defined as:

$$r_A = \frac{k_{pAA}}{k_{pAB}} \quad \text{(eq: AII.10)}$$

$$r_B = \frac{k_{pBB}}{k_{pBA}} \quad \text{(eq: AII.11)}$$

To integrate equation AII.9, concentrations can be expressed as a function of X_A and X_T employing equation 5 and 6:

$$\frac{[A]}{[B]} = \frac{[A]_0(1 - X_A)}{[B]_0 - X_T([A]_0 + [B]_0) + [A]_0 X_A} \quad \text{(eq: AII.12)}$$

The cumulative composition can be determined as a function of the individual conversion of MAA, X_A, and the overall conversion as follow:

$$Y_A = \frac{[A]_0 X_A}{([A]_0 + [B]_0) X_T} \quad \text{(eq: AII.13)}$$

The reactivity ratios r_A and r_B can be estimated using a parameter estimation algorithm that minimizes the objective function of equation AII.14 where Y_{Aexp} is the experimentally measured cumulative composition referred to MAA determined by in-situ ^{1}H-NMR, and Y_{Acal} is the theoretically determined cumulative composition calculated using the set of equations AII.9-13 and the initial concentrations of the comonomers. The subscript *i* makes reference to the experiment and subscript *j* to the sample number of each of the experiments used in the estimation procedure. The only parameters of the model are the reactivity ratios.

$$J = \left[\sum_{i=1}^{N}\sum_{j=1}^{Pi}\left(Y_{Aexp} - Y_{Acal}\right)^2\right] \qquad \text{(eq: AII.14)}$$

Parameter estimation was carried out using a direct search estimation algorithm employing subroutine DBCPOL and the subroutine for solving ordinary differential equations DIVPRK from IMSL library.

II.2. Individual Conversions and Kinetics of In-situ NMR Monitored Reactions

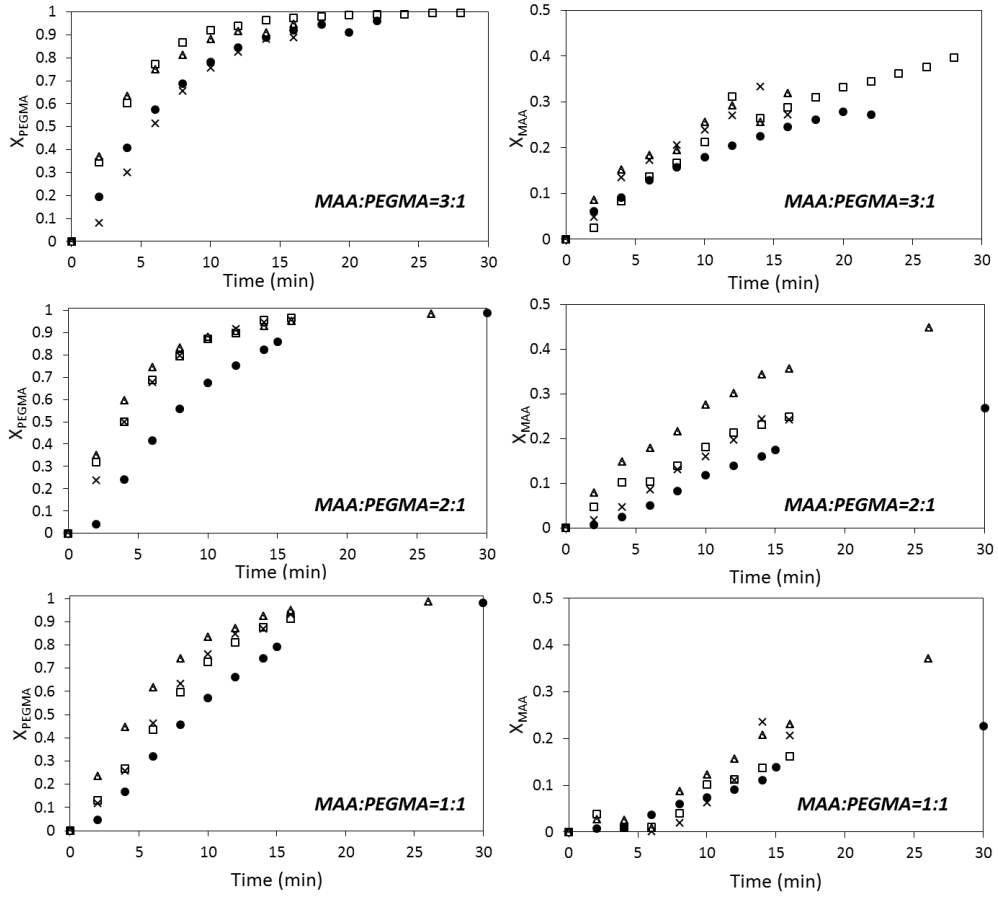

Figure AII.1: Time evolution of the conversion of MAA and PEGMA 5 for different monomer ratios (MAA/PEGMA as indicated in the figures) at different solids content (SC): ● – 5 wt%; □ – 10 wt%; x – 15 wt%; Δ - 20 wt %.

Figure AII.1 shows that the conversion of both monomers increase with the solids content and that PEGMA is more reactive that MAA at fully ionized conditions. The effect observed in the conversion with solids content indicates that the dependence of the polymerization rate on the monomer conversion is not of first order for none of the monomers. Those findings were observed by Buback et al. in the literature[3–7]. Also, it was found that the reactivity ratios of the system MAA-co-PEGMA have similar features of variation with solids content that were observed for the system AA-co-AM[8–10].

The results of the estimation are included in Chapter 2, where the influence of the solids content on the reactivity ratios is shown.

II.3. References

(1) Mayo, F. R.; Lewis, F. M. Copolymerization I. A Basis for Comparing the Behavior of Monomers in Copolymerization. The Copolymerization of Styrene and Methyl Methacryate. *J. Am. Chem. Soc.* **1944**, *66* (9), 1594–1601.

(2) De La Cal, J.C., Leiza, J.R., Asúa, J. M. Estimation of Reactivity Ratios Using Emulsion Copolymerization Data. Journal of Polymer Science: Part A: Polymer Chemistry 1991, pp 155–167.

(3) Beuermann, S.; Buback, M.; Hesse, P.; Lacík, I. Free-Radical Propagation Rate Coefficient of Nonionized Methacrylic Acid in Aqueous Solution from Low Monomer Concentrations to Bulk Polymerization. *Macromolecules* **2006**, *39* (1), 184–193.

(4) Beuermann, S.; Buback, M.; Hesse, P.; Kukućková, S.; Lacík, I. Propagation Rate Coefficient of Non-Ionized Methacrylic Acid Radical Polymerization in Aqueous Solution. The Effect of Monomer Conversion. *Macromol. Symp.* **2007**, *248*, 41–49.

(5) Buback, M.; Hesse, P.; Hutchinson, R. A.; Lacík, I.; Kasák, P.; Stach, M.; Utz, I. Kinetics and Modeling of Free-Radical Batch Poymerization of Nonionized Methacrylic Acid in Aqueous Solution. *Ind. Eng. Chem.* **2008**, *47* (21), 8197–8204.

(6) Beuermann, S.; Buback, M.; Hesse, P.; Kukuc, S.; Lacik, I.; Hutchinson, R. A. Termination Kinetics of the Free-Radical Polymerization of Nonionized Methacrylic Acid in Aqueous Solution Termination Kinetics of the Free-Radical Polymerization of Nonionized Methacrylic Acid in Aqueous Solution. *Macromolecules* **2008**, *41* (10), 3513–3520.

(7) Smolne, S.; Weber, S.; Buback, M. Propagation and Termination Kinetics of Poly(Ethylene Glycol) Methyl Ether Methacrylate in Aqueous Solution. *Macromol. Chem. Phys.* **2016**, *217* (21), 2391–2401.

(8) Preusser, C.; Ezenwajiaku, I. H.; Hutchinson, R. A. The Combined Influence of Monomer Concentration and Ionization on Acrylamide/Acrylic Acid Composition in Aqueous Solution Radical Batch Copolymerization. *Macromolecules* **2016**, *49* (13), 4746–4756.

(9) Paril, A.; Alb, A. M.; Giz, A. T.; Çatagil-Giz, H. Effect of Medium PH on the Reactivity Ratios in Acrylamide Acrylic Acid Copolymerization. *J. Appl. Polym. Sci.* **2007**, *103*, 968–974.

(10) Riahinezhad, M.; Mcmanus, N.; Penlidis, A. Effect of Monomer Concentration and PH on Reaction Kinetics and Copolymer Microstructure of Acrylamide/Acrylic Acid Copolymer. *Macromol. React. Eng.* **2015**, *9* (2), 100–113.

Appendix III. Modelling of the Kinetics of MAA-co-PEGMA5 Aqueous Phase Copolymerization

III.1. Introduction

In this section, the aim is to develop a mathematical model which predicts the kinetics of the copolymerization between MAA and PEGMA5. It has to be mentioned that predictive models for water soluble copolymers deal with a substantial complexity because of the variation of different kinetic parameters such as, propagation rate coefficients, termination rate coefficient and reactivity ratios among others. Despite several groups have analyzed the variations of the kinetic parameters of the water soluble monomers, still there is a lack of detailed mathematical model with full knowledge on the kinetics of the copolymerization of MAA and PEGMA5 as water soluble monomers. Reported coefficients were taken from the literature but some coefficients are not available and hence were estimated based on experimental data. Furthermore, the model was validated based on experiments reported in Chapter 2. Once the model was validated, then it was used to develop optimal monomer addition strategies (see Chapter 2)

A full kinetic model of the copolymerization of MAA/PEGMA 5 was implemented in the commercial software Predici®. The model includes all the variation for the propagation rate constant (*kp)* of water soluble monomers found in the literature and the reactivity ratios estimated previously in this work (see Chapter 2 and Appendix II).

III.2. Model Description and Kinetics

The most common water soluble monomers (acrylic acid AA [1–4], acrylamide AM [5,6], N-vinyl pyrrolidone NVP [7], N-vinyl formamide NVF [8,9]) have been extensively studied by several groups in terms of propagation rate constants "*kp*" in the last decades. All these studies shared a common finding that the *kp* of these monomers decreases with the increase of the concentration.

In the case of MAA, both propagation and termination rate coefficients have been analyzed for the non-ionized form, finding that concentration of monomer affects to the *kp*. In these works, it was also found that the presence of polyMAA units do not contribute to the change of the *kp* because it does not become of the solvent environment. This finding has high influence when modelling the kinetics of MAA at different monomer conversion and concentrations[10–12]. The effect of ionization was also analyzed finding that the ionized forms of MAA behave in an opposite way comparing to the non-ionized forms. Non-ionized or partially ionized forms used to increase the *kp* when decreasing the concentration, obtaining the highest values at dilute conditions. On the other hand, fully-ionized forms increased the values of *kp* with the concentration, however the highest values of the *kp* at fully ionized conditions is not as high as the values obtained at partially and non-ionized conditions[13] (see Figure AIII.1). Recently, a new study has analyzed the effect of the electrolyte concentration on the polymerization rate and kinetic behavior of fully-ionized MAA[14] (see Figure AIII.2).

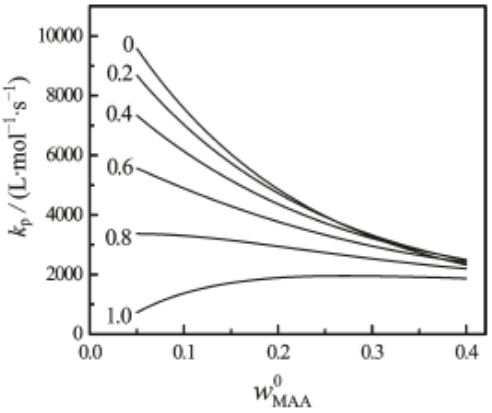

Figure AIII.1: *kp* values estimated by Lacik et al.[13] for various α (ionization degree) values and initial weight fractions of MAA in water, w^o_{MAA}, at 50ºC.

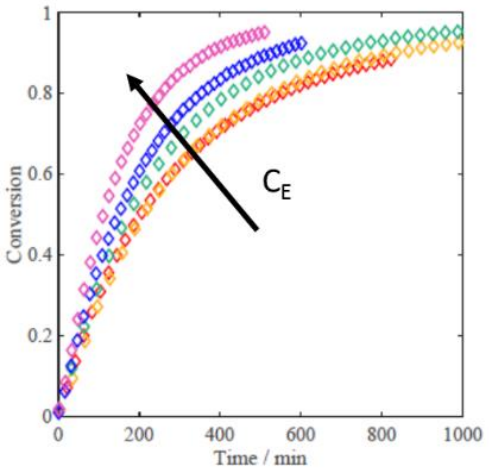

Figure AIII.2: Monomer conversion vs time of fully ionized MAA at 50 ºC with increasing electrolyte concentration (C_E) in the system[14].

The propagation rate coefficient of PEGMA has been recently studied and a similar finding was obtained. In this case, it was demonstrated that the *kp* decreases by a factor of seven between highly diluted aqueous solution to bulk polymerization attributed to the change of the pre-exponential factor[15,16].

Based on the literature data a detailed mathematical model was developed based on the kinetic scheme of the copolymerization of MAA and PEGMA presented in Scheme 1 using Predici® commercial software[17]. The kinetics scheme contains the conventional steps for free radical copolymerization: initiation, propagation chain transfer to monomer and termination reactions.

Scheme AIII.1: Kinetic mechanism of the copolymerization of MAA/PEGMA. M_1: MAA monomer; M_2: PEGMA monomer; I: Initiator; $R_{i,1}$: Chain end radical of monomer 1 with length i; $R_{i,2}$: Chain end radical of monomer 2 with length i; Pi: Dead polymer with length i; f: Initiator efficiency.

Initiation:

$$I \xrightarrow{k_d} 2fR_0$$

$$R_0 + M_1 \xrightarrow{k_{i1}} R_1$$

$$R_0 + M_2 \xrightarrow{k_{i2}} R_2$$

Propagation:

$$R_{i,1} + M_1 \xrightarrow{kp_{11}} R_{i+1,1}$$

$$R_{i,2} + M_2 \xrightarrow{kp_{22}} R_{i+2,2}$$

$$R_{i,1} + M_2 \xrightarrow{kp_{12}} R_{i+1,2}$$

$$R_{i,2} + M_1 \xrightarrow{kp_{21}} R_{i+2,1}$$

Chain Transfer to Monomer:

$$R_{i,1} + M_1 \xrightarrow{ktrm_{11}} R_{i+1,1}$$

$$R_{i,2} + M_2 \xrightarrow{ktrm_{22}} R_{i+2,2}$$

$$R_{i,1} + M_2 \xrightarrow{ktrm_{12}} R_{i+1,2}$$

$$R_{i,2} + M_1 \xrightarrow{ktrm_{21}} R_{i+2,1}$$

Termination by Disproportionation:

$$R_{i,1} + R_{j,1} \xrightarrow{cd*kt_{11}} P_i + P_j$$

$$R_{i,2} + R_{j,2} \xrightarrow{cd*kt_{22}} P_i + P_j$$

$$R_{i,1} + R_{j,2} \xrightarrow{cd*kt_{12}} P_i + P_j$$

$$R_{i,2} + R_{j,1} \xrightarrow{cd*kt_{21}} P_i + P_j$$

Termination by Combination:

$$R_{i,1} + R_{j,1} \xrightarrow{(1-cd)*kt_{11}} P_{i+j}$$

$$R_{i,2} + R_{j,2} \xrightarrow{(1-cd)*kt_{22}} P_{i+j}$$

$$R_{i,1} + R_{j,2} \xrightarrow{(1-cd)*kt_{12}} P_{i+j}$$

$$R_{i,2} + R_{j,1} \xrightarrow{(1-cd)*kt_{21}} P_{i+j}$$

The kinetic parameters taken from the literature, used in the model, are presented in Table AIII.1. As it is previously mentioned, the kinetics of the water soluble monomers are presenting more complexities and are dependent on the reaction medium properties such as pH,

monomer weight fraction. Beuermann et al.[12] based on pulsed laser polymerization (PLP) measurements proposed an expression for the propagation rate coefficient of MAA as a function of reaction temperature, monomer concentration, pressure and conversion. It was found that the activation energy was almost constant for a wide range of concentrations. Later, Lacik et al [13] improved the previous expression by incorporating the ionization degree of the MAA. However, none of the expressions were applicable for low monomer concentration conditions (below 5 wt%) and they did not take into account the ionic strength of the medium. Cucatto et al.[14] proposed a propagation rate coefficient for a fully ionized system composed of the intrinsic kinetic term and a diffusion term. The expression has two differentiated parts: a non-electrostatic dependence of the monomer concentration and a second part in which the electrolyte concentration is taken into account**:**

$$kp_1 = \left(\frac{1}{k_{p,i}^0 \exp\left(-Bw_{M,MAA}\right)} + \frac{1}{K_D C_E^{\beta}}\right) \qquad \text{(eq: AIII.1)}$$

where B, β, k_D are fitting parameters, and C_E is the electrolyte concentration in mol/kg which is in function of $w_{M,MAA}$. kp^0_i is the intrinsic propagation kinetic rate coefficient of fully ionized MAA (without any electrostatic interaction effect). This value was estimated at 50°C in the work carried out by Cucatto et al.[14]. Using the estimated intrinsic propagation rate coefficient at 50° and the activation energy from the work performed by Buback et al.[11] , the exponential expression of kp^0_i was obtained.

The kinetics of the PEGMA5 monomer similar to other water-soluble monomers is a function of monomer concentration[16] the increase of the *kp* when decreasing the concentration is due to the effect of the fluidification of the aqueous environment, which at the same time increases the prexponential factor.

Below expression was considered for termination rate coefficient following the work of Buback et al.[18] and the more recent work of Beuermann et al.[15] on the termination of PEGylated methacrylates:

$$\boldsymbol{kt} = \frac{\mathbf{1}}{\frac{\mathbf{1}}{\boldsymbol{k_{SD}}} + \frac{\boldsymbol{\eta_r}}{\boldsymbol{k^0_{TD}}}} \qquad \text{(eq: AIII.2)}$$

where k_{SD} representing *kt* under segmental diffusion control and $\boldsymbol{k^0_{TD}}$ the theoretical value of *kt* under diffusion control at negligible conversion and $\eta r = exp(C\eta \cdot X)$ where *x* is the weight fraction of the monomer. For $\boldsymbol{k^0_{TD}}$ a typical value of 1 x 10^9 was taken from literature[18] k_{SD} and $C\eta$ were estimated in this work.

The reactivity ratio for this pair of monomer has been recently estimated[19] (see Appendix II and Chapter 2). In that work, we observed the reactivity ratios were dependent on the solids content and constant over the whole process. However, in this work this simplification is not taken into account and the dependency of the reactivity ratios on the monomer weight fraction was considered and thus, the parameters were unknown.

Table AIII.1: Arrhenius parameters for the rate coefficient used in the simulation of the MAA/PEGMA5 copolymerization. 1 refers to MAA and 2 refers to PEGMA. The pre-exponential factor is in s^{-1} or in $L \cdot mol^{-1} \cdot s^{-1}$

Rate Coefficient	Reference
$kd = 8.0\ x\ 10^{15} exp^{(-\frac{135.0}{RT})}$ $f = 0.6$	20

$$kp_1 = \left(\frac{1}{k_{p,i}^0 \exp\left(-Bw_{M,MAA}\right)} + \frac{1}{K_D C_E^{\beta}}\right) \quad 14$$

$$C_E = 2\left(\frac{w_{NaOH}}{MW_{NaOH}} + \frac{w_{NaHCO3}}{MW_{NaHCO3}} + \frac{w_{M,MAA}}{MW_{MAA}}\right)$$

$$k_{p,i}^0 = 2.5 \times 10^5 \exp(-1880.0/\mathrm{T})$$

$$B = 1.92$$

$$\beta = 2.18$$

$$K_D = 201$$

$$kp_2 = exp^{\left(16.58 - \frac{2.1\ x\ 10^4}{8.3144T} - 1.86\ x\ 10^{-2} W_{\%PEGMA}\right)} \quad 16$$

$$kp_{12} = \frac{kp_{11}}{r_{12}} \quad 19$$

$$r_{12} = 0.07 + b_1 \cdot W_M$$

$$kp_{21} = \frac{kp_{22}}{r_{21}}$$

$$r_{21} = 9.89 + 117.21 \cdot W_M$$

$$ktrm_{11} = 0.353\ at\ 50℃\ for\ non\ ionized\ MAA \quad 11$$

$$ktrm_{22} = 2.0\ x\ 10^{15} exp^{\left(-\frac{46.1}{RT}\right)}\ for\ MMA \quad 21$$

$$ktrm_{12} = ktrm_{21} = \sqrt{ktrm_{11} x\ ktrm_{22}} \quad \text{This Work}$$

$$kt_{11} = kt22 = \frac{1}{\frac{1}{k_{SD}} + \frac{\eta_r}{k_{TD}^0}} \quad 15$$

$$\eta_r = exp^{(C_\eta x)}\ x: weight\ fraction\ of\ polymer$$

$$cd = 0.8$$

$$k_{TD}^{0} = 1 \times 10^{9}$$

$$kt_{12} = kt_{21} = \sqrt{kt_{11}x\ kt_{22}} \qquad \text{This Work}$$

III.3. Estimation of Model Parameters and Model Validation

To estimate model parameters batch reaction experimental kinetic data was used. It is worth mentioning that for the parameter estimation only batch experiment individual conversion data were used, as the semibatch experiments were done in a substantial starved condition in which the rate of polymerization is controlled by the feeding rate. In this condition, the kinetics of the copolymerization is mostly controlled by the feeding flow rate rather than the kinetic parameters. However, later semibatch starved reactions were used to validate the model.

The above developed mathematical model was used to estimate the unknown kinetic parameters by fitting the experimental data obtained from the batch aqueous solution copolymerization of MAA and PEGMA5 with SC: 20 and 30 wt%. For that, the fractional conversion of the comonomers were considered only in the first 500 seconds (8.33 minutes), where the copolymerization reaction took place. Over this time only homopolymerization of MAA occurs due to total consumption of the PEGMA5 monomer which is the more reactive one.

The unknown parameters were estimated using the parameter estimation algorithm of Predici® Commercial Software. In this algorithm, the relative total residual is:

$$r_{rel} = \frac{1}{\sqrt{N}}\sqrt{SS_E} \qquad \text{(eq: AIII.3)}$$

where, N is the total number of data and SS_E is the weighted residual sum of squares. It

As mentioned before, two unknown parameters of the termination rate coefficient under gel effect and the dependency parameters of the reactivity to the actual weight fraction of the monomer (a1 and b1) were the most uncertain parameters to be estimated. However sensitivity analysis of these parameters showed that the two parameters of the termination rate coefficient and the dependency factor of the reactivity ratio of the MAA monomer (b1) are the sensitive parameters and though the dependency factor of the reactivity ratio of PEGMA5 monomer was taken as the reported value in the reference[19].

Table AIII.2. presents the estimated parameters. Figure AIII.3 shows the comparison of the experimental results and the simulation using the estimated parameters for batch solution copolymerization of MAA/PEGMA5 at different solids contents.

Table AIII.2: Estimated parameters from this work.

Parameter	Units
k_{SD} = 9.1·105 ± 4.3·105	$L \cdot mol^{-1} \cdot s^{-1}$
Cη = 19.24 ± 65.55	
b_1 = 12.07 ± 7.37	

Figure AIII.3 shows the comparison of the experimental data with the model prediction. It can be seen that the model fits reasonably well the experiments data although the fitting is not perfect. The high uncertainty of K_{SD} and Cη reflects the fact that these parameters are highly

coupled with each other. High uncertainty of these parameters were also previously reported in the estimation of these parameters in batch polymerization of non-ionized MAA[11]. The uncertainty of the reactivity ratio parameter relates to the high difference between reactivity ratios of the monomers.

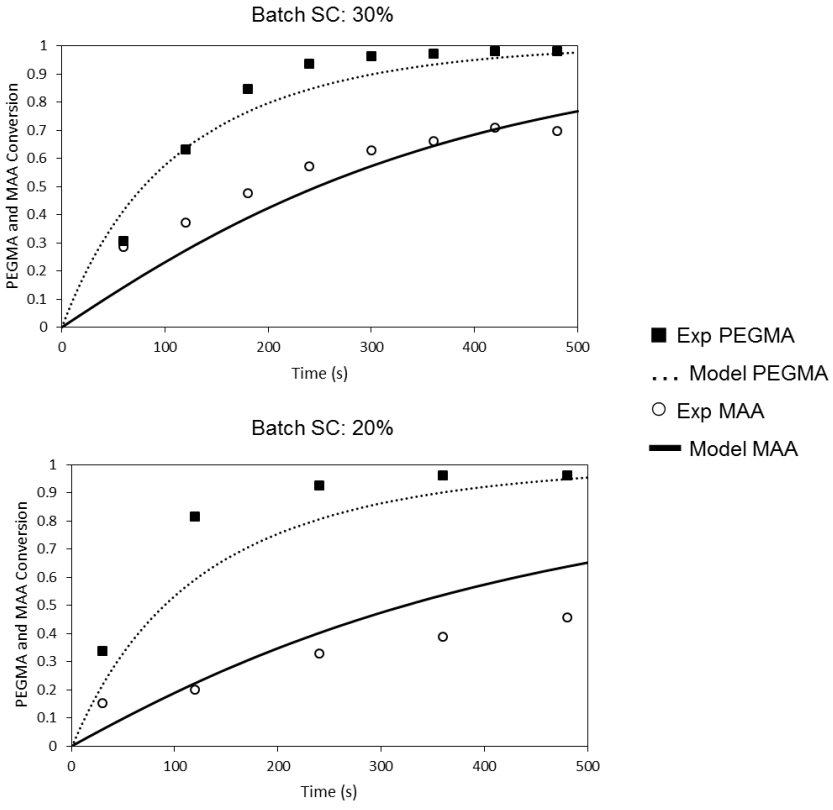

Figure AIII.3: Conversion evolution of MAA and PEGMA monomers of batch experiments at different solids content (20 and 30% SC) comparing experimental data a model predictions.

The mathematical model with the estimated parameters were also used to predict the starved semibatch experiments (see Figure AIII.4). The model predicted well the partial conversion of both monomer even though some mismatch can be observed at short time of reactions with the conversion of PEGMA5, especially at 3/1 and 4/1 comonomer ratios. In the case of MAA, the model predicted a behavior in the conversion that is between the experimental results for most part of the reaction, even though at low reaction times, the model is slightly slower that the experimental results. The model also predicted well the cumulative composition obtained in the semibatch reactions. As can be seen, for the reactions with high MAA content (3/1 and 4/1 comonomer ratios) model prediction are very close to the obtained experimental data. (Figure AIII.5). As it has been previously mentioned in Chapter 2, this starved semibatch addition is very time-consuming (8h of feeding) and in addition the copolymer composition has a significant drift in almost 20% of the polymer conversion.

From model verification it can be concluded that remarkable accuracy has been obtained for the model. Furthermore, satisfactory results were obtained when employing optimal addition strategies to obtain homogeneous copolymers in terms of cumulative copolymer composition when employing the developed model (see Chapter 2).

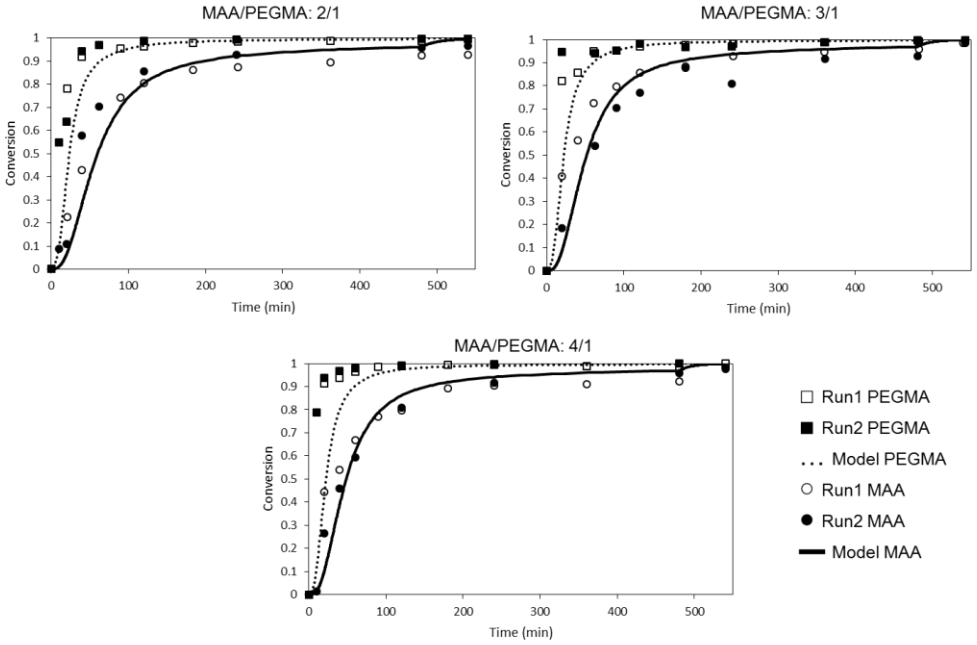

Figure AIII.4: Instantaneous conversion evolution of MAA and PEGMA monomers of semibatch experiments comparing experimental data and model predictions.

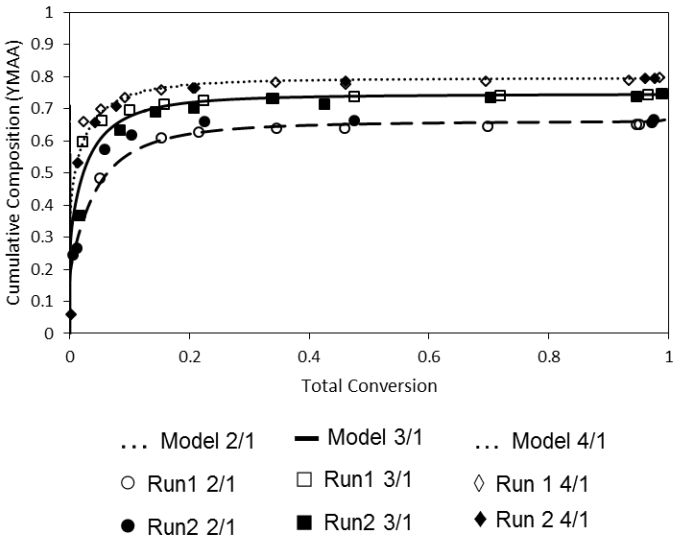

.

Figure AIII.4: Cumulative composition of the semibatch experiments performed at different comonomer ratios compared with the model predictions.

III.4. References

(1) Lacík, I.; Beuermann, S.; Buback, M. PLP-SEC Study into Free-Radical Propagation Rate of Nonionized Acrylic Acid in Aqueous Solution. *Macromolecules* **2003**, *36* (25), 9355–9363.

(2) Lacík, I.; Beuermann, S.; Buback, M. Aqueous Phase Size-Exclusion-Chromatography Used for PLP-SEC Studies into Free-Radical Propagation Rate of Acrylic Acid in Aqueous Solution. *Macromolecules* **2001**, *34* (18), 6224–6228.

(3) Lacik, I.; Beuermann, S.; Buback, M. PLP-SEC Study into the Free-Radical Propagation Rate Coefficients of Partially and Fully Ionized Acrylic Acid in Aqueous Solution. *Macromol. Chem. Phys.* **2004**, *205* (8), 1080–1087.

(4) Cutie, S. S.; Smith, P. B.; Henton, D. E.; Staples, T. L.; Powell, C. Acrylic Acid Polymerization Kinetics. *J. Polym. Sci. Part A Polym. Chem.* **1997**, *35*, 2029–2047.

(5) Lacík, I.; Chovancova, A.; Uhelsk, L.; Preusser, C.; Hutchinson, R. A.; Buback, M. PLP-SEC Studies into the Propagation Rate Coefficient of Acrylamide Radical Polymerization in Aqueous Solution. *Macromolecules* **2016**, *49* (9), 3244–3253.

(6) Seabrook, S. A.; Tonge, M. P.; Gilbert, R. G. Pulsed Laser Polymerization Study of the Propagation Kinetics of Acrylamide in Water. *J. Polym. Sci. Part A Polym. Chem.* **2005**, *43* (7), 1357–1368.

(7) Stach, M.; Lacík, I.; Chorvát, D.; Buback, M.; Hesse, P.; Hutchinson, R. A.; Tang, L. Propagation Rate Coefficient for Radical Polymerization of N -Vinyl Pyrrolidone in Aqueous Solution Obtained by PLP−SEC. *Macromolecules* **2008**, *41* (14), 5174–5185.

(8) Stach, M.; Lacík, I.; Kasák, P.; Chorvát, D.; Saunders, A. J.; Santanakrishnan, S.; Hutchinson, R. A. Free-Radical Propagation Kinetics of N-Vinyl Formamide in Aqueous Solution Studied by PLP-SEC. *Macromol. Chem. Phys.* **2010**, *211* (5), 580–593.

(9) Santanakrishnan, S.; Hutchinson, R. A.; Učňová, L.; Stach, M.; Lacík, I.; Buback, M. Polymerization Kinetics of Water-Soluble N-Vinyl Monomers in Aqueous and Organic Solution. *Macromol. Symp.* **2011**, *302* (1), 216–223.

(10) Beuermann, S.; Buback, M.; Hesse, P.; Kukućková, S.; Lacík, I. Propagation Rate Coefficient of Non-Ionized Methacrylic Acid Radical Polymerization in Aqueous Solution. The Effect of Monomer Conversion. *Macromol. Symp.* **2007**, *248*, 41–49.

(11) Buback, M.; Hesse, P.; Hutchinson, R. A.; Lacík, I.; Kasák, P.; Stach, M.; Utz, I. Kinetics and Modeling of Free-Radical Batch Poymerization of Nonionized Methacrylic Acid in Aqueous Solution. *Ind. Eng. Chem. Res.* **2008**, *47* (21), 8197–8204.

(12) Beuermann, S.; Buback, M.; Hesse, P.; Kukuc, S.; Lacik, I.; Hutchinson, R. A. Termination Kinetics of the Free-Radical Polymerization of Nonionized Methacrylic Acid in Aqueous Solution Termination Kinetics of the Free-Radical Polymerization of Nonionized Methacrylic Acid in Aqueous Solution. *Macromolecules* **2008**, *41* (10), 3513–3520.

(13) Lacık, I.; Lucia, U.; Beuermann, S. Propagation Rate Coefficient of Free-Radical Polymerization of Partially and Fully Ionized Methacrylic Acid in Aqueous Solution. *Macromolecules* **2009**, *42* (20), 7753–7761.

(14) Fischer, E. J.; Storti, G.; Cuccato, D. Aqueous Free-Radical Polymerization of Non-Ionized and Fully Ionized Methacrylic Acid. *Processes* **2017**, *5*, 23.

(15) Beuermann, S.; Siegmann, R.; Jelic, A. Propagation and Termination Kinetics of PEGylated Methacrylate Radical Polymerizations A. *Macromol. Chem. Phys.* **2010**, *211* (5), 546–562.

(16) Smolne, S.; Weber, S.; Buback, M. Propagation and Termination Kinetics of Poly(Ethylene Glycol) Methyl Ether Methacrylate in Aqueous Solution. *Macromol. Chem. Phys.* **2016**, *217* (21), 2391–2401.

(17) Wulkow, M. Computer Aided Modeling of Polymer Reaction Engineering-The Status of Predici, I-Simulation. *Macromol. React. Eng.* **2008**, *2* (6), 461–494.

(18) Buback, M. Free-Radical Polymerization up to High Conversion. A General Kinetic Treatment. *Die Makromol. Chemie* **1990**, *191* (7), 1575–1587.

(19) Emaldi, I.; Hamzehlou, S.; Sanchez-dolado, J.; Leiza, J. R. Kinetics of the Aqueous-Phase Copolymerization of Monomer Concentration and Side Chain Length. *Processes* **2017**, *5*, 19.

(20) Lansalot, M.; Davis, T. P.; Heuts, J. P. A. RAFT Miniemulsion Polymerization : Influence of the Structure of the RAFT Agent. *Macromolecules* **2002**, *35* (20), 7582–7591.

(21) Sangster, D. F.; Feldthusen, J.; Strauch, J.; Fellows, C. M. Measurement of Transfer Coefficients to Monomer for N-Butyl Methacrylate by Molecular Weight Distributions from Emulsion Polymerization. *Macromol. Chem. Phys.* **2008**, *209* (15), 1612–1627.

Appendix IV. Cementitious Materials and Characterization Methods

IV.1. Materials

The Ordinary Portland Cement type I 52.5R used in this work was kindly supplied to Tecnalia Research & Innovation by Cementos Lemona S.A. This cement was characterized and verified that fulfills the requirements of a common cement Type I 52.5R.

To carry out this project, individual crystalline phases that compose the OPCs were also used. C_2S (Dicalcium silicate – Belite) was synthesized in a two-step process and following used. C_3S (Tricalcium silicate – Alite) and C_3A (Tricalcium Aluminate) were purchased from Bonding Chemicals. Both compounds were of high purity (> 98%) based on supplier.

IV.2. Synthesis of Dicalcium Silicate – Belite C_2S

The synthesis of Belite-C_2S was carried out in a two-step process, firstly an autoclave reactor was employed and after this reaction, an annealing process was done.

Firstly, CaO (1.33 mol), SiO2 (0.688 mol), and NaOH (0.11 mol) were mixed in 1200 ml of deionized water. The autoclaved reaction was carried out at 225 ºC for 18h. During the process

the pressure inside the reactor should reach to 18 bar. Once the reaction is finished the materials are extracted from the reactor and are filtered in a Buchner type funnel. The obtained solid is (considered as α-C_2SH) weighted and dried in an oven at 70 ºC overnight. Once the product is dried a XDR of the white powder is performed for the sake of the characterization of the product.

The second step of the synthesis is the annealing of the product at a high temperature oven. Based on the literature[1], different annealing temperatures provide products with different reactivities. For this work a high reactivity of the product is sought, in that way the effect of the addition of the superplasticizers is expected to be seen in a clearer way. In this work, four annealing temperatures were programmed: 800 ºC, 600 ºC, 500 ºC, and 400 ºC. For all the temperatures the annealing time was of 1 hour.

In order to characterize the reactivity of the different annealing temperatures, the hydration kinetics were monitored by calorimetry. For that, the annealed phases were mixed by hand on a water to cement ratio of 0.5 (W/C = 0.5). Figure AIV.1 shows the hydration kinetics of the synthesized C_2S phase annealed at different temperature. It is clearly observable that the high annealing temperatures (600 ºC and 800 ºC) lead to very low reactivitites. On the other hand, 500 ºC leads to a very reactive phase, while 400 ºC provide a lower induction period (400 ºC 2h of induction period, 500ºC 3h of induction period) with a clear lower reactivity. Therefore, for the analysis of the effects of the superplasticizers the annealing temperature chosen was 450 ºC based on the results obtained.

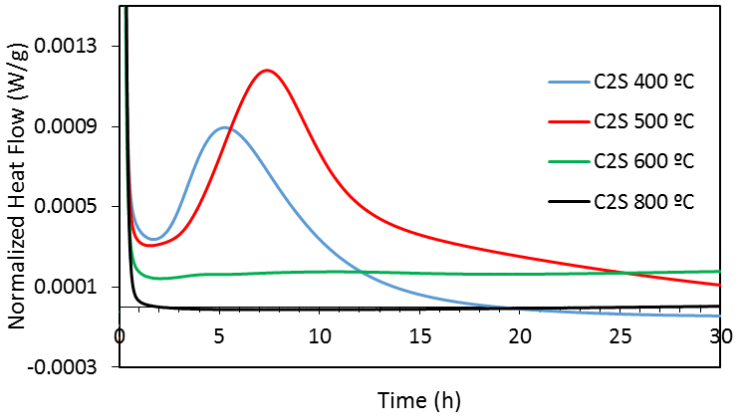

Figure AIV.1: Hydration kinetics of the different annealing temperature for C_2S phase.

IV.3. Cement Characterization

IV.3.1 Scanning Electron Microscopy (SEM)

In order to observe the particle morphology and shape the Scanning Electron Microscope was used to characterize the Ordinary Portland Cement and the individual crystalline phases employed in this work.

The surface morphology of the cementitious materials was examined using a scanning electron microscope: a Hitachi TM3030 table top model at an accelerating voltage of 15 kV after the samples had been coated with a gold thin layer and a FEI Quanta 250 FEG model with low field detector (LFD) at an accelerating voltage of 10 kV under low- or high vacuum mode with standard detectors.

IV.3.2. X-Ray Diffraction

The diffractometer used for this study is the model X-Pert Pro from Philips. This apparatus uses the method of the powder, or of Debye Scherrer, in which the samples are ground to a fine powder and then compressed into pellets. Despite XRD allow the quantification of the different constituents of the cement based materials within this work this techniques was used to their identification. To do so, the analysis software counts with a Powder Diffraction File (PDF) database consisting on a list of the d-values and relative intensities of the diffraction lines of a great number of known substances. This file is released and annually updated by the International Centre for Diffraction Data[2]. Comparing the obtained spectra with the database allow the identification of the mayor constituents, however the heterogeneity of the cementitious materials and the low crystallnity of some parts complicate this process, so it is common the use of more precise quantitative techniques for such process.

IV.3.3. X-Ray Diffraction – Rietveld Technique

Rietveld technique is one of the alternative to quantify the constituents present in Ordinary Portland Cements. Its main advantage is the reproducibility and repeatability of the measurements compared to previous analysis methods like the Bogue calculations[3].

The refinement of the crystalline structure by Rietveld method consists of minimizing the difference between the experimental difractogram and the calculated one. In order to obtain the calculated diffractogram, it employed an approximate structural model and some parameter which allow to distribute the intensities in the diffractogram. This method does not use the intensities of the peaks, it employs the whole diffractogram though, and it this way the

overlapping problem is solved. Furthermore, this methods allow to obtain the maximum information possible[4].

The analyses were carried out by the Servicios Centralizados de Apoyo a la Investigación (SCAI) of the University of Málaga. The measurements were carried out using radiation MoKα1 in a BRUKER diffractogram D8 Advance with autosampler. The sample receives monochromatic light produced by the optic system of the equipment. The detection system is LYNXeye XE. The measurements were carried out from 3º to 40º (2θ) for 3h. The tube worked at 50 kV and 50 Ma and the sample was turned around in order to increase the statistic of the particles. The quantification was carried out employing the Rietveld method using TOPAS 4.2 software from BRUKER.

IV.3.4. X-Ray Fluorescence

The X-ray fluorescence was used for the semi quantitative analysis of the different cementitious materials. This technique is based on the emitting of the secondary radiation after the sample has been irradiated by X-rays. Each element present a specific frequency of emission and the intensity of the emitted radiation corresponds to the abundance of this element in the sample. This techniques is broadly used in the elemental analysis of crystalline materials[5]. These analyses were carried out by the Servicios Centralizados de Apoyo a la Investigación (SCAI) of the University of Málaga.

IV.3.5. Density and Blaine Fineness

Density measurements were perfomed employing Le Chatelieur flaks method. The measurements are generally performed employing standard liquids such as kerosene or naphta even though other liquids can also be employed. For the measurements the temperature has to be controlled.

Firstly, the liquid is poured inside the flask until it reaches to the meniscus. Then, the material to be measured is added and the difference in volume of the meniscus is measured. Based on the difference of the volume and mass of material the density is determined. These measurements were carried out by Tecnalia's operators.

The Blaine fineness can also be defined as the surface are of the cement particles. It is generally measured following the standard method ASTM C 204 which consist of the measurement of the surface are by air permeability. The instrument measures the time for a set of volume of air to pass through a packed bed of powder particles.

The surface area is calculated using the following equation:

$$S = (52.43 \cdot K \cdot t^{\frac{1}{2}})/\rho \qquad \text{(eq: AIV.1)}$$

where: S is the surface area, *K* is the constant of the apparatus (26.69), *t* is the time required for air to pass through and *ρ* is the density of cement measured with the Le Chatelieur flask method.

These measurements were also carried out by Tecnalia's operators.

IV.4. Characterization of Cement Pastes

IV.4.1. Consumption Measurements by Total Organic Carbon

For consumption measurements, the cementitous materials were mixed with PCE dilute aqueous solutions with different concentrations (ranging from 0 to 6 mg of PCE/ g of cement, based on dry weight of PCE), for 25 minutes in two different W/C ratios (w/c = 2 for OPC, w/c = 10 for individual clinker phases). After, they were filtered in a Buchner funnel. The liquid phase extracted was then analyzed by Total Organic Carbon (TOC) analysis[6]. These analyses were conducted by SGIker in the Faculty of the Science and Technology of the UPV/EHU in Leioa (Bizkaia).

The TOC equipment employed in these measurements is the TOC-L Analyzer from Shidmazu. It allows the measurement of total carbon TC, inorganic carbon IC, total organic carbon TOC and non-volatile organic carbon NPOC employing the catalytic combustion at 680 ºC. The range of measurements is extremely wide from 4 µg/l up to 30000 mg/l. It also contains automatic sampler with acidification and sparging with an auto-sample with capacity for 93 vials of 24 ml.

IV.4.2. Zeta Potential Measurements by Acoustosizer

The values of the zeta potential of this work were conducted in an AcoustoSizer IIs from Colloidal Dynamics Inc. 30 grams of binder with 160 g of water were mixed for 15 minutes and by using an automatic titrator the aqueous PCE solutions were added into the colloidal system. The suspension was mixed at 300 rpm rotating speed of the stirrer while the titration was being performed. The titration dosages varies from 0 to 8 mg of PCE / g Cement.

The electroacoustic technique employed by the AcoustoSizer II for determining particle size and zeta potential can be applied to concentrated suspensions because it involves the measurement of sound waves generated by the particles present in the suspension. To generate these sound waves a high frequency electric field is applied to the colloidal system, and this causes the charged colloidal particles to move. The sound has the same frequency as the applied field which is usually in MHz range, this phenomenon is known as the ESA effect (elektrokinetic sonic amplitude). In the equipment the ESA measurement is made by applying a voltage pulse across the colloid. From the ESA measurements the amplitude and phase of the particle velocity can be determined, both parameters are employed then to determine the dynamic mobility. The calculation of this dynamic mobility is the first step in the calculation of the zeta potential and particle size.

IV.4.3. Hydration Studies by Calorimetry

The hydration reaction of cement pastes was measured by isothermal calorimetry employing the TAM Air instruments from TA Instruments. The equipments consists of 8 channels were the sample and the reference are places in ampoules up to 20 mL of capacity. In this work, 6 grams of materials were used for the sample and reference (water).

IV.4.4. Rheological Measurements

Apparent viscosity of cement pastes was measured using a TA Instruments-Discovery Hybrid Rheometer HR-3. Flow procedures using a 40 mm diameter steel peltier plate with grainy surface to avoid slipping of the sample as geometry were carried out at 25 ºC. Tha gap employed

for the measurements was of 1000 μm. The measurements were carried out in a continuous ramp from 1 to 1000 s^{-1}.

In order to measure the evolution of the apparent viscosity with time flow peak hold experiments were carried out in the same rheometer. For this case, the special geometry (helix) with the cylinders was employed using a gap of 4.5 mm and a constant shear rate of 0.01 s^{-1} at 25 ºC.

IV.4.5. Setting Studies by Vicat Needles

Setting studies of OPC cement pastes were performed with the Autovicat equipment from Ibertest. The equipment follows the rule ASTM C191. For the test the equipment was programmed to perform perforations every 30 minutes when the penetration of the needle is over 25 mm (P > 25 mm, 30 minutes/point). When the penetration decreases the record of point is done at shorter times, 15 minutes. (P < 25 mm, 15 minutes/point).

IV.5. References

(1) Link, T.; Bellmann, F.; Ludwig, H. M.; Ben Haha, M. Reactivity and Phase Composition of Ca2SiO4 Binders Made by Annealing of Alpha-Dicalcium Silicate Hydrate. *Cem. Concr. Res.* **2015**, *67*, 131–137.

(2) Gaitero, J. J. PhD Thesis - Multi-Scale Study of the Fibre-Matrix Interface and Calcium Leaching in High Performance Concrete ., UPV/EHU, 2008.

(3) Le Saoût, G.; Kocaba, V.; Scrivener, K. Application of the Rietveld Method to the Analysis of Anhydrous Cement. *Cem. Concr. Res.* **2011**, *41* (2), 133–148.

(4) García, M. A.; Cabeza, A.; de la Torre, A. G. *El Método de Rietveld*; Cano, V. J. E., Ed.; Biblioteca Universitat Jaume Primero: Castelló de la Plana, 2006.

(5) Moir, G. *Advanced Concrete Technology*; Newman, J., Choo, B. S., Eds.; Elsevier Ltd: Burlington, MA, USA, 2003.

(6) Alonso, M. D. M.; Palacios, M.; Puertas, F. Effect of Polycarboxylate-Ether Admixtures on Calcium Aluminate Cement Pastes. Part 1: Compatibility Studies. *Ind. Eng. Chem. Res.* **2013**, *52* (49), 17323–17329.